R&D 5295-MS-01

(1)

AD-A214 160

DTIC FILE COPY

TECHNISCHE UNIVERSITY, INSTITUTE OF APPLIED AND TECHNICAL PHYSICS, VIENNA, AUSTRIA

ANISOTROPY AND MICROSTRUCTURE OF HIGH COERCIVITY RARE EARTH IRON PERMANENT MAGNETS. LIST OF PAPERS PUBLISHED

1986 - 1989

Contract No.: DAJA45-86-C-0010
Report No.: R/D-5295-MS-01

Best available copy per the Originator

LIST OF PAPERS PUBLISHED UNDER ERO SPONSORSHIP DURING THIS REPORTING PERIOD 1986-1989

Contract No.: DAJA 45-86-C-0010

(1) R.Grössinger, X.K Sun, R.Eibler, K.H.J.Buschow, H.R. Kirchmayr
"Temperature Dependence of Anisotropy Fields and Initial Susceptibility in $R_2Fe_{14}B$ Compounds"
JMMM 58 (1986) 55.

(2) G.Hilscher, R.Grössinger, S.Heiss, H.Sassik, G.Wiesinger
"Magnetic and Anisotropy Studies of Nd-Fe-B Based Permanent Magnets", JMMM 54 (1986) 577.

(3) R.Grössinger, R.Krewenka, H.R.Kirchmayr, J.Omerod, K.H.J.Buschow
"The Hard Magnetic Properties of Sintered Nd-Fe-B Permanent Magnets", J. Less. Common Met. 118 (1986) 167.

(4) R.Grössinger, R.Krewenka, X.K.Sun, K.H.J.Buschow, R.Eibler, H. R. Kirchmayr
"Magnetic Phase Transitions and Magnetic Anisotropy in $Nd_2Fe_{(14-x)}Co_xB$ Compounds", J. Less. Com. Met. 124 (1986) 165.

(5) R.Grössinger, R.Krewenka, K.S.V.L.Narasimhan, H.R.Kirchmayr
"Investigation of the hysteresis loop and the magnetic anisotropy of Nd-Fe-B based permanent magnets", IEEE Trans. on Magn. MAG-22 (1986) 760.

(6) R.Grössinger, R.Krewenka, H.R.Kirchmayr, S.Sinnema, Yang-Fu-ming, Huang Ying-kai, F.R. de Boer, K.H.J.Buschow
"Magnetic anisotropy in $Pr_2(Fe_{1-x}Co_x)_{14}B$ compounds"
J. Less. Com. Met. 132 (1987) 265.

(7) R.Grössinger, R.Krewenka, H.R.Kirchmayr, P.Naastepad, K.H.J.Buschow
"Note on the coercivity in Nd-Fe-B magnets"
J. Less. Com. Met. 134 (1987) L17-L21.

(8) R.Grössinger, H.Harada, A.Keresztes, H.R.Kirchmayr, M. Tokunaga
"Anisotropy and hysteresis studies of highly substituted Nd-Fe-B based permanent magnets"
IEEE Trans. on Magn. MAG-23 (1987) 2117.

(9) R.Grössinger, R.Krewenka, F.Haslinger, M.Sagawa, H.R.Kirchmayr
"Temperature dependence of the coercivity and the anisotropy of Nd-Fe-B based magnets"
IEEE Trans. on Magn. MAG-23 (1987) 2114.

(10) R.Grössinger, A.Kereszte, H.Harada, Z.Shougong "The coercivity and anisotropy of (Nd,X)-(Fe,Y)-B (X=Dy and Y=Co,Al) based permanent magnets", Proc. of 9th Int. Workshop on rare earth magnets, Bad Soden (1987) Vol.I, 593.

(11) A.Handstein, J.Schneider, U.Heinecke, R.Grössinger, Z. Shougong "Magnetic properties of sintered $Nd_{16}(Fe_{100-x}Al_x)_{76}B_8$ magnets", Proc. of 9th Int. Workshop on rare earth magnets Bad Soden (1987) Vol. I, 601.

(12) R.Grössinger "Does a Co substitution really improve the temperature dependence of Nd-Fe-B based permanent magnets", Proc. of 9th Int. Workshop on rare earth magnets Bad Soden (1987) Vol. II, 15.

(13) R.Grössinger, H.R.Kirchmayr, K.H.J.Buschow "Magnetic anisotropy in the system $La_2Fe_{14-x}Co_xB$ and its relation to the system $Nd_2Fe_{14-x}Co_xB$", J. Less. Com. Met. 136 (1987) 367.

(14) R.Grössinger, F.Haslinger, Z.Shougong, R.Eibler, L.Yinglie, J.Schneider, A.Handstein, H.R.Kirchmayr "The effect of substitution of Al on the magnetic properties of $Nd_{15}Fe_{78}B_7$ permanent magnets", IEEE Trans.on Magn. MAG-24 (1988) 1629.

(15) R.Grössinger, X.C.Chou, R.Krewenka, G.Wiesinger, R.Eibler, X.K.Sun, Y.C.Chuang "The effect of substitution in $Nd_2Fe_{14-x}Z_x$ B (Z=Al,Si,Co, Ga) compounds", J. de Physique 49 (1988) C8-599.

(16) R.Grössinger, R.Krewenka, H.Buchner, H.Harada "A new analysis of Nd-Fe-B based permanent magnets" J. de Physique 49 (1988) C8-659.

(17) R.Grössinger "Improvements of Nd-Fe-B Magnets", Proc. of ERA-Technol. Conf. June (1989) (London), in press.

(18) J.Fidler and P.Skalicky, "New developments in the field of permanent magnetic materials", Radex-Rundschau 2/3, 63, (1986).

(19) S.H.F.Parker, P.J.Grundy and J.Fidler, "Electron microscope study of precipitation in a niobium containing (Nd,Dy)-Fe-B sintered magnet", J.Magn.Magn.Mat., 66, 74, (1987).

(20) M.H. Ghandehari and J.Fidler, "Microstructural evidence for the magnetic surface hardening of Dy_2O_3-doped $N_{15}Fe_{77}B_8$ magnets", Materials Letters, 5, 285, (1987).

(21) Josef Fidler, "On the role of the Nd-rich phases in sintered Nd-Fe-B magnets", IEEE Trans.Magn.,Vol. MAG-23, 2106, (1987).

(22) Josef Fidler, J.Bernardi and P.Skalicky,
"Analytical electron microscope study of high- and low-coercivity SmCo 2:17 magnets", Materials Research Society Symposium Proceedings, Vol.96, 1987 (ed.S.G. Sankar, J.F. Herbst and N.C. Koon), Pittsburgh, PA, USA, p.181.

(23) M.H. Ghandehari and J. Fidler,
"Microstructural studies of high coercivity Nd15Fe77B8 sintered magnets", Materials Research Society Symposium Proceedings, Vol.96, 1987 (ed.S.G. Sankar, J.F. Herbst and N.C. Koon), Pittsburgh, PA, USA,p.193.

(24) J.Fidler and P.Skalicky,
"Metallurgical factors determining the magnetic hardness of sintered Nd-Fe-B permanent magnets", Mikrochimica Acta, [Wien], I, 115, (1987).

(25) Josef Fidler,
"The role of the microstructure on the coercivity of Nd-Fe-B sintered magnets", Proc. V. Int. Symposium on magnetic Anisotropy and Coercivity in Rare Earth-Transition Metal Alloys, Bad Soden, FRG, Sept. 1987,(proceedings Book by: Deutsche Physikalische Gesellschaft e.V., D-5340 Bad Honef 1, FRG), Vol.2, p. 363.

(26) J.Fidler and Y.Tawara,
"TEM-Study of the precipitation of iron in Nd-Fe-B sintered magnets", IEEE Trans.Magn., 24, 1951, (1988).

(27) Josef Fidler,
"Electron microscopy in the development of new magnetic materials", Proceedings IX. European Congress on Electron Microscopy (EUREM), York, England, September 1988, Inst.Phys.Conf.Ser.No.93,Vol.2,(1988),p.211.

(28) J.Fidler, K.G.Knoch, H.Kronmüller and G.Schneider,
"Analytical TEM-study of Al-doped, two-phase Nd-Fe-B sintered magnets", J. Mater. Res., in press.

(29) J.Fidler and K.G.Knoch,
"Electron microscopy of Nd-Fe-B based magnets", J.Magn.Magn.Mat., in press.

(30) Josef Fidler,
"On the role of microstructure on coercivity of rare earth permanent magnets", Proceedings of VII. Int. Seminar on Magnetism, Dreseden, DDR, April 1989, in press.

(31) J.Fidler and K.G.Knoch,
"The influence of dopants on microstructure and coercivity of Nd-Fe-B sintered magnets", Proceedings of X. Int. Workshop on rare earth magnets and their applications, Kyoto, Japan, May 1989, (proceedings Book by: The Society of Non-Traditional Technology, Toranomon Kotohira-kaikan Bldg. 3F, 1-2-8 Toranomon, Minatu-Ku. Tokyo 105, Japan), Vol.2, p. 283.

Pages 62, 63, 64, 65 + 66 - Best available from the Originator DTIC 8 Nov 89

(32) K.G.Knoch, G.Schneider, J.Fidler, E.-Th. Henig, H.Kronmüller, "Al-doped Nd-Fe-B permanent magnets: wetting and microstructural investigations", IEEE Trans.Magn., in press.
(33) K.G.Knoch, E.Bischoff, E.Th.Henig and J.Fidler, "Analytical TEM-study of cast Nd80-Fe15-B5 alloys", J.Mat.Lett., submitted.
(34) K.G. Knoch, E.-Th. Henig and J.Fidler, "Correlation between Al addition and microstructural changes in Nd-Fe-B magnets", Proc. EMMA '89 Conf., Rimini, Italy, submitted.

1

Journal of Magnetism and Magnetic Materials 58 (1986) 55-60
North-Holland, Amsterdam

TEMPERATURE DEPENDENCE OF ANISOTROPY FIELDS AND INITIAL SUSCEPTIBILITIES IN $R_2Fe_{14}B$ COMPOUNDS

R. GRÖSSINGER *, X.K. SUN *, R. EIBLER *, K.H.J. BUSCHOW + and H.R. KIRCHMAYR *

* *Institute for Experimental Physics, Technical University of Vienna, Austria*
+ *Philips Research Laboratories, 5600 JA Eindhoven, The Netherlands*

Received 5 August 1985

The temperature dependence of the anisotropy field was determined in various $R_2Fe_{14}B$ compounds (R = Y, La, Ce, Pr, Nd, Gd, Ho, Lu and Th). The magneto-crystalline anisotropy in materials where the R component has an orbital moment consists of two different contributions that have an opposite temperature dependence. At temperatures well below the Curie temperature the 4f sublattice anisotropy decreases with temperature while the 3d lattice anisotropy increases with temperature. We measured the temperature dependence of the initial susceptibility of all $R_2Fe_{14}B$ compounds mentioned, including the compounds with R = Sm, Dy, Er and Tm in the range from 4.2 to 300 K. Indications for the presence of a spin reorientation were found in $Pr_2Fe_{14}B$, $Nd_2Fe_{14}B$ and $Ho_2Fe_{14}B$.

1. Introduction

In a previous investigation we briefly reported on the temperature dependence of the anisotropy field (H_A) in various ternary intermetallic compounds of the type $R_2Fe_{14}B$ (R = rare earth or Th) studied by means of the singular point detection (SPD) technique at temperatures ranging from 4.2 K to the corresponding Curie temperatures [1]. The SPD method is useful in particular for investigating compounds that have a uniaxial magnetic anisotropy with an easy magnetization direction parallel to the c-axis ($K_1 > 0$). In the SPD method the anisotropy field at a given temperature is revealed as a singularity when d^2M/dH^2 is plotted versus H, M representing the magnetization [2]. Closer analysis of the SPD data showed that in some compounds changes in the easy magnetization direction occur upon a decrease of temperature [1]. For instance, in $Nd_2Fe_{14}B$ such changes were observed near 135 K, which closely agrees with observations made on a single crystal by Givord et al. [3]. In order to have a better understanding of the magnetic behaviour of the various $R_2Fe_{14}B$ compounds we have measured the temperature dependence of their ac susceptibility. The results of these measurements will be discussed in conjunction with the SPD data obtained previously.

2. Experimental

The samples were prepared from 99.9% pure starting materials by means of arc melting in purified argon gas. After arc melting the samples were wrapped in Ta foil, sealed into an evacuated quartz tube and vacuum-annealed at 900°C for a period of two weeks. X-ray diffraction was performed on powdered samples with a standard powder diffractometer equipped with a graphite crystal monochromator using CuK_α radiation. In order to study magnetic phase transitions a.c. susceptibility measurements were performed between 4.2 and 300 K. The ac field was approximately 10^{-4} T peak to peak using a frequency of 82 Hz. All the samples were given a spherical shape in order to have the same demagnetizing factors.

The anisotropy field was measured using the SPD (Singular Point Detection) technique [1]. The theory of this method predicts a singularity in the second derivative of the magnetization ($d^2M/$

0304-8853/86/$03.50

4

dH^2) at the anisotropy field H_A if the external field is applied parallel to the hard plane ($K_1 > 0$). From the fact that this method samples the properties of only the correctly oriented grains (H_{ext} parallel to the hard axis), it follows that H_A can be measured on aligned powder samples but also on polycrystalline samples. This method is well suited for easy axis materials. If the anisotropy of a material having an easy plane of magnetization has to be measured, the theory predicts that the third derivative (d^3M/dH^3) will show a singularity at $H = H_A$. Unfortunately, owing to experimental difficulties, measurements of d^3M/dH^3 are virtually impossible. Our anisotropy studies were therefore restricted to $R_2Fe_{14}B$ compounds of easy axis magnetic anisotropy.

3. Results and discussion

The temperature dependence of the anisotropy fields in $R_2Fe_{14}B$ compounds in which the easy magnetization direction is parallel to the c direction [4] is shown in fig. 1. Although $Tb_2Fe_{14}B$ and $Dy_2Fe_{14}B$ have the same type of easy magnetization direction, their values of the anisotropy fields appeared to be too high to be determined with our pulsed field equipment. Inspection of the results given in fig. 1 shows that at low temperatures the anisotropy field in the $R_2Fe_{14}B$ compounds where the R atoms have an orbital moment (top part of fig. 1) is about an order of magnitude larger than in the remaining $R_2Fe_{14}B$ compounds. The strong temperature dependence of H_A in these materials can be explained as follows. In the case where the anisotropy is determined exclusively by the R sublattice magnetization one may describe its temperature dependence by means of the reduced hyperbolic Bessel function $\hat{I}_{5/2}\ m(T)$ of degree $l = 2$, where $m_R(T)$ is the reduced 4f-sublattice magnetization [5]. This leads to a temperature dependence of H_A which can be represented by the expression

$$H_A(T) = \frac{2K_1(T)}{M(T)} = \text{constant}\frac{\hat{I}_{5/2}[m_R(T)]}{M(T)}, \quad (1)$$

where M is the total magnetization. Using a mean field model and assuming that $\hat{I}_{5/2} m_R(T)$ varies as $m_R^2(T)$ for temperatures close to T_c, one expects that $H_A(T)$ will vary as $M_{Fe}\ [T(T-c)]^{-1}$ in this temperature range, the constant c depending on the strength of the 4f–3d coupling. It is likely therefore that H_A is mainly due to the Fe sublattice at temperatures close to T_c. At lower temperatures H_A of the R sublattice becomes dominant, the more so since it varies even more strongly with decreasing T, owing to the fact that $\hat{I}_{5/2}\ m_R(T)$ behaves as $m_R^3(T)$ at temperatures $T < T_c$.

A much more modest temperature dependence of H_A is observed for the $R_2Fe_{14}B$ compounds in which R is nonmagnetic (R = Y, La, Lu, Ce, Th). Here $H_A(T)$ is seen to decrease with decreasing temperature ($T \ll T_c$). These results suggest that the Fe atoms at the different crystallographic Fe sites will contribute differently to H_A and that the temperature dependence of these contributions will not be the same either. A similar situation was assumed to exist in Y_2Co_{17} [6]. Attempts were made to describe the 3d sublattice anisotropy in uniaxial Co-base intermetallic compounds in terms of the second-order crystal field parameter B_2^0 [7]. In this model one expects a correlation between the anisotropy energy and the factor $1 - \frac{3}{8}(c/a)^2$,

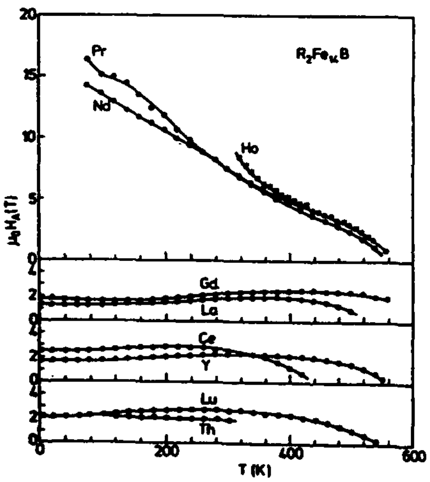


Fig. 1. Temperature dependence of the anisotropy field $\mu_0 H_A$ in various $R_2Fe_{14}B$ compounds.

Table 1
Comparison between the values of $1-\frac{3}{8}(c/a)^2$ derived from the lattice constants a and c and the values of the anisotropy field (H_A) or anisotropy energy (H_AM). The room temperature magnetic induction M used in the latter product was obtained by means of the room temperature magnetization (σ_s) measured on aligned powder particles

Compound	$1-\frac{3}{8}(c/a)^2$	μ_0H_A (T)	σ_s (Am^2/kg)	M (T)	μ_0H_AM (T^2)
$Lu_2Fe_{14}B$	0.302	2.64	111	1.17	3.1
$Y_2Fe_{14}B$	0.293	2.35	154	1.35	3.2
$La_2Fe_{14}B$	0.167	1.97	149	1.38	2.7
$Ce_2Fe_{14}B$	0.284	2.64	119	1.16	3.1
$Th_2Fe_{14}B$	0.278	2.03	115	1.29	2.6

where a and c are the lattice constants. The values of H_A obtained in the course of the present investigation are compared with values of the factor $1-\frac{3}{8}(c/a)^2$ in table 1, using data for a and c reported elsewhere [8]. Since the factor $1-\frac{3}{8}(c/a)^2$ is expected to scale to the anisotropy energy rather than to the anisotropy field, it is more appropriate to compare the values of this factor with the corresponding product μ_0H_AM, where M is the magnetization induction determined from the density and the saturation magnetization σ_s measured on aligned powder particles. Comparison of the values listed in the second and the last column of table 1 shows that only a rather weak correlation of the type mentioned seems to be present in both types of materials (R is trivalent in the cases Lu, Y, La and tetravalent in the cases Ce and Th).

Results of the measurements of the temperature dependence of the ac susceptibility (χ_i) are shown in fig. 2 for various $R_2Fe_{14}B$ compounds in which R is nonmagnetic (R = La, Th, Y, Ce, Lu) or where the 4f moment consists exclusively of a spin moment (R = Gd). In all these cases the values of χ_i are seen to show only little variation with temperature. Considerably more variation with temperature has been observed in the $\chi_i(T)$ curves of the compounds $Pr_2Fe_{14}B$ and $Nd_2Fe_{14}B$ (fig. 3) and $Ho_2Fe_{14}B$ (fig. 4) whereas in $Tb_2Fe_{14}B$ and $Dy_2Fe_{14}B$ the variation of χ_i with T is rather slight. In all the compounds mentioned above, X-ray diffraction on aligned powder particles had shown the easy magnetization direction to be parallel to the c-axis at room temperature. Results for compounds with an easy plane magnetization ($Sm_2Fe_{14}B$, $Er_2Fe_{14}B$ and $Tm_2Fe_{14}B$) are shown in fig. 5.

The initial susceptibility χ_i is defined as follows:

$$\chi_i = \lim_{\Delta H_i \to 0} \left(\frac{\Delta M}{\Delta H_i} \right) \Bigg|_{H_i = 0}, \qquad (2)$$

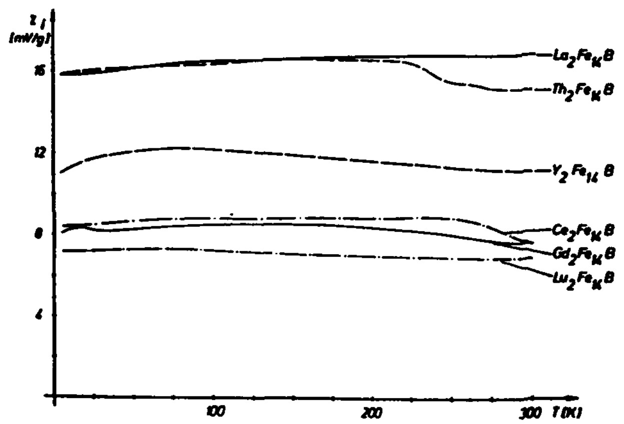


Fig. 2. Temperature dependence of the initial susceptibility (χ_i) in various $R_2Fe_{14}B$ compounds (R = La, Th, Y, Ce, Gd, Lu).

6

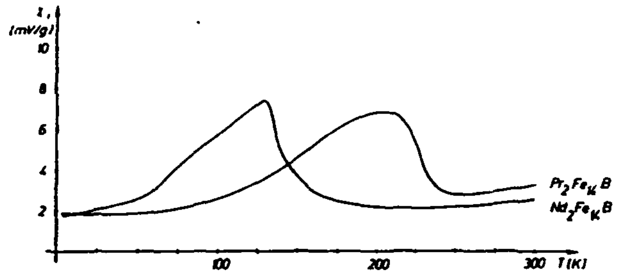


Fig. 3. Temperature dependence of the initial susceptibility (χ_i) in the compounds $Pr_2Fe_{14}B$ and $Nd_2Fe_{14}B$.

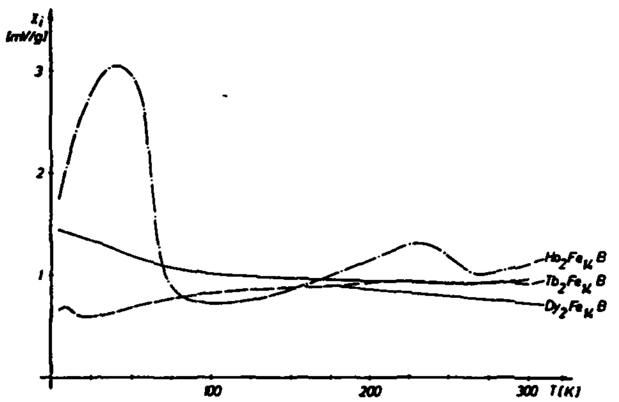


Fig. 4. Temperature dependence of the initial susceptibility (χ_i) in various $R_2Fe_{14}B$ compounds (R = Ho, Dy, Tb).

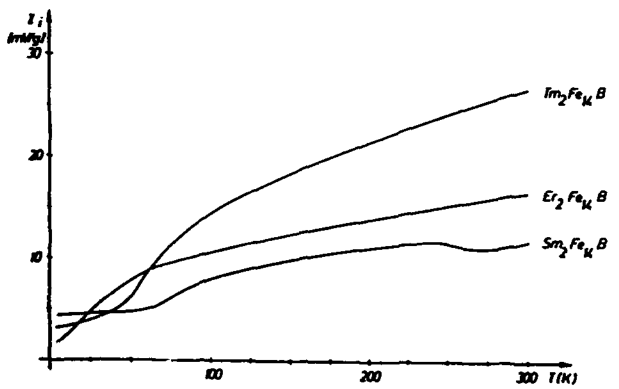


Fig. 5. Temperature dependence of the initial susceptibility (χ_i) in various $R_2Fe_{14}B$ compounds (R = Tm, Er, Sm).

where M is t
field. Owing
field (demag
measured ini

$\chi_i^{eff} = [1/\chi_i -$

The internal
the material h
or a large m
$D \ll \chi_i'$ and t

A crude es
of easy magn
by assuming
solely due to
case one may

$\chi_i = \frac{M_s^2}{3K_1 + \frac{9}{2}\lambda}$

$\chi_i = \frac{}{6(K_1 + 2}$

$\chi_i = \frac{}{(2K_1 + 3}$

where F is de

$F(\eta) = (5 + 6$

and where λ a
and the intern

Inspection
having an eas
that the tempe
reflect the tem
magnetization
constant K_1.
which the ani
sublattice mag
Lu) one sees f
with tempera
(4.2–300 K). S
and disregard
pects the initia
ature as $\chi_i =$
increase sligh
from 4.2 to 30
show a pro

where M is the magnetization and H_i the internal field. Owing to the presence of demagnetizing fields (demagnetizing factor D) the experimentally measured initial susceptibility χ_i^{eff} takes the form

$$\chi_i^{eff} = [1/\chi_i + D]^{-1}. \tag{3}$$

The internal initial susceptibility χ_i^i is small when the material has either a large magnetic anisotropy or a large magnetoelastic energy. In such cases $D \ll \chi_i^i$ and the effect of D can be neglected.

A crude estimate of χ_i for three different cases of easy magnetization directions can be obtained by assuming that changes in magnetization are solely due to rotation of the moments [9]. In that case one may write;

$$\chi_i = \frac{M_s^2}{3K_1 + \frac{9}{2}\lambda\sigma} \quad \text{(easy axis)}, \tag{4}$$

$$\chi_i = \frac{M_s^2}{6(K_1 + 2K_2) + 9\lambda\sigma} \quad \text{(easy plane)}, \tag{5}$$

$$\chi_i = \frac{M_s^2}{(2K_1 + 3\lambda\sigma - 2K_1 F(\eta))} \quad \text{(easy cone)}, \tag{6}$$

where F is defined as follows:

$$F(\eta) = (5 + 6\eta)/(1 + 2\eta), \quad \eta = K_2/K_1,$$

and where λ and σ represent the magnetostriction and the internal stress, respectively.

Inspection of eq. (4) shows that in materials having an easy axis magnetization one may expect that the temperature dependence of χ_i will strongly reflect the temperature dependence of the squared magnetization (M_s^2) and the reciprocal anisotropy constant K_1. Concentrating on the compounds in which the anisotropy is exclusively due to the 3d sublattice magnetization (R = La, Th, Y, Ce, Gd, Lu) one sees from fig. 1 that H_A increases slightly with temperature in the range considered here (4.2–300 K). Substituting $H_A = 2K_1/M_s$ in eq. (3) and disregarding magnetoelastic effects, one expects the initial susceptibility to vary with temperature as $\chi_i = M_s/H_A$. Since both M_s and H_A increase slightly with temperature in the range from 4.2 to 300 K, this means that χ_i should not show a pronounced temperature dependence, which is in satisfactory agreement with the results shown in fig. 2.

The anisotropy behaviour in $R_2Fe_{14}B$ compounds where the R sublattice also contributes to the anisotropy is fairly complicated since a decreasing temperature may lead to an easy magnetization direction different from that found at room temperature (see below) [3,9]. Nevertheless, for those compounds where the easy magnetization direction at room temperature is parallel to the c-axis it is possible to compare the values observed for χ_i with values calculated by means of eq. (4) on the basis of the data available for M_s and $K_1 = 2H_A/M_s$. We have compiled in table 2 experimental values of M_s, $\mu_0 H_A$ and χ_i for all materials having an easy magnetization direction parallel to the c-axis. Included in the table are values of χ_i calculated by means of eq. (4), neglecting magnetoelastic contributions and demagnetizing effects. Owing to these latter effects in particular, the uncertainties in the χ_i values may become rather large and reach values as high as 30% in the worst case. In order to exclude the effect of these uncertainties as far as possible we have normalized both sets of χ_i values to the corresponding values of $Y_2Fe_{14}B$. These normalized values are given in the last two columns of the table, and are indicated as $\bar{\chi}_i^{exp}$ and $\bar{\chi}_i^{calc}$, respectively. Inspection of these data shows that, with the exception of $La_2Fe_{14}B$, there is satisfactory agreement between experimental and calcu-

Table 2
Saturation magnetization (σ_s) anisotropy field ($\mu_0 H_A$) and initial susceptibility (χ_i^{exp}) for various $R_2Fe_{14}B$ compounds at room temperature. The values listed as χ_i^{calc} were calculated on the basis of eq. (4) and are given in arbitrary units. The values $\bar{\chi}_i^{exp}$ and $\bar{\chi}_i^{calc}$ are normalized to the χ_i values of $Y_2Fe_{14}B$

Compound	σ_s (Am^2/kg)	$\mu_0 H_A$ (T)	χ_i^{exp} (mV/g)	χ_i^{calc} (a.u.)	$\bar{\chi}_i^{exp}$	$\bar{\chi}_i^{calc}$
$Y_2Fe_{14}B$	154	2.35	11.1	4.36	1	1
$La_2Fe_{14}B$	149	1.97	16.8	5.06	1.51	1.16
$Ce_2Fe_{14}B$	119	2.64	8	2.99	0.72	0.68
$Pr_2Fe_{14}B$	150	7.5	3.2	1.34	0.28	0.31
$Nd_2Fe_{14}B$	147	7.5	2.5	1.30	0.23	0.30
$Gd_2Fe_{14}B$	84	2.36	7.6	2.38	0.68	0.54
$Ho_2Fe_{14}B$	83	9.2	1.1	0.60	0.10	0.15
$Lu_2Fe_{14}B$	111	2.64	6.9	2.80	0.62	0.64

lated values, implying that the simple model description of the susceptibility data is basically correct.

It can be seen from the results in figs. 3 and 4 that the compounds $R_2Fe_{14}B$ with R = Pr, Nd and Ho show marked anomalies in their $\chi_i(T)$ curves. Studies on a single crystal of $Nd_2Fe_{14}B$ had revealed that this compound undergoes a spin reorientation when cooling from room temperature to below 135 K[3]. At room temperature the easy magnetization direction is parallel to the c-axis but below 135 K the easy magnetization direction corresponds to a cone, the corresponding tilting angle being equal to about 30°. It follows from eqs. (4) and (6) that χ_i passes through a maximum when going from a situation corresponding to an easy axis to one corresponding to an easy cone. Taking account of the demagnetizing factor, the initial susceptibility at the transition temperature is proportional to $\chi_{i,max} \propto M_s^2/(3\lambda\sigma + D)$.

While the temperature dependence of χ_i observed by us for $Nd_2Fe_{14}B$ is in agreement with the change in easy magnetization direction observed on a single crystal of this compound, there are no such single crystal data available for $Pr_2Fe_{14}B$ and $Ho_2Fe_{14}B$. Our $\chi_i(T)$ data then suggest that similar changes in the easy magnetization direction might also occur in the latter two compounds, whereas no such changes are expected to be present in $Dy_2Fe_{14}B$ and $Tb_2Fe_{14}B$ (see fig. 4). In $Dy_2Fe_{14}B$ and $Tb_2Fe_{14}B$ the values of χ_i are particularly low. The reason for this is the relatively low value of M_s in eq. (4), which is due to the antiparallel coupling between the 3d and 4f sublattice magnetizations. Furthermore, the SPD measurements had shown that H_A in these materials is comparatively high.

Low values of M_s are also expected for the $R_2Fe_{14}B$ compounds shown in fig. 5. In $Er_2Fe_{14}B$ and $Tm_2Fe_{14}B$ one has again an antiparallel coupling between the R and Fe sublattices, while in $Sm_2Fe_{14}B$ the R sublattice magnetization is only very small. The reason why these compounds have nevertheless quite appreciable values of χ_i stems from the fact that the easy magnetization direction in these materials is perpendicular to the c-axis and the concomitant mobility of the magnetization vector is relatively large. The values of M_s decrease with decreasing temperature in all three compounds, which is reflected in the temperature dependence of $\chi_i(T)$.

4. Concluding remarks

We have shown that the magnetocrystalline anisotropy in tetragonal $R_2Fe_{14}B$ phases consists of two contributions that have a different temperature dependence. The crystal-field-induced anisotropy prevails in materials in which the R component has an orbital moment and this contribution decreases strongly with temperature, particularly at temperatures well below T_c. The anisotropy contributed by the Fe sublattice magnetization is much weaker. But at temperatures well below T_c this anisotropy increases with temperature.

We found that a weak correlation exists between the magnetic anisotropy energy and the factor $1 - \frac{3}{4}(c/a)^2$, suggesting that the Fe sublattice anisotropy originates, too, from crystal field effects. Inherent in such a description is the presence of an orbital moment on the Fe atoms, which would agree with the observation of a non-negligible magnetization anisotropy in $La_2Fe_{14}B$ and $Y_2Fe_{14}B$ [8].

The initial susceptibility of the $R_2Fe_{14}B$ compounds studied appears to be mainly governed by the corresponding magnetocrystalline anisotropy. Pronounced variations of the initial susceptibility with temperature were observed in $R_2Fe_{14}B$ compounds with R = Pr, Nd or Ho. These changes point to changes in easy magnetization direction at the corresponding temperature.

References

[1] R. Grössinger, X.K. Sun, R. Eibler, K.H.J. Buschow and H.R. Kirchmayr, J. de Phys. 46 (1985) C6–221.
[2] G. Asti and S. Rinaldi, J. Appl. Phys. 45 (1974) 3600.
[3] P. Givord, H.S. Li, J.M. Moreau, R. Perrier de la Bâthie and E. du Trémolet de Lacheisserie, Physica 130B (1985) 323.
[4] M. Sagawa, S. Fujimura, H. Yamamoto, Y. Matsuura and K. Hiraga, IEEE Trans. Magn. MAG-20 (1984) 1584.
[5] E. Callen, Physica 114B (1982) 71.
[6] K. Inomata, Japan. J. Appl. Phys. 15 (1976) 821.
[7] B. Szpunar and P.A. Lindgård, J. Phys. F9 (1979) L55.
[8] S. Sinnema, R.H. Radwanski, J.J.M. Franse, D.B. de Mooij and K.H.J. Buschow, J. Magn. Magn. Mat. 44 (1984) 333.
[9] X.K. Sun, Thesis (1985) Austria.

9

2

Journal of Magnetism and Magnetic Materials 54–57 (1986) 577–578

MAGNETIC AND ANISOTROPY STUDIES OF Nd–Fe–B BASED PERMANENT MAGNETS

G. HILSCHER, R. GRÖSSINGER, S. HEISZ, H. SASSIK and G. WIESINGER

Institute for Experimental Physics, Technical University Vienna, A-1040 Vienna, Karlsplatz 13, Austria

Magnetocrystalline anisotropy and coercivity of sintered and rapidly solidified Nd–Fe–B magnets are compared. The coercivity for melt-spun ribbons with optimum cooling rate appears to be dominated by domain wall pinning, while for sintered Nd–Fe–B the coercivity is mainly controlled by nucleation of reverse domains.

The development of an outstanding hard magnetic material rich in Fe based on Co-free R–Fe–B-alloys was successfully demonstrated by: rapidly quenched ribbons [1], by sintered magnets [2] and recently by a ternary diffusion path [3]. The principle sources of the hard magnetic properties in Nd–Fe–B are the intrinsic properties of the tetragonal $Nd_2Fe_{14}B$ phase as the high uniaxial crystal anisotropy and the high saturation magnetisation ($H_A \approx 7.5$ T, $\mu_0 M_s \approx 1.6$ T) at room temperature, but also the metallurgical possibility for the formation of small crystallites of the $Nd_2Fe_{14}B$ phase with a size near to monodomain particles giving rise to a high coercivity $_IH_C$. The aim of this paper is to compare the anisotropy and coercivity mechanisms in samples prepared by three different production technologies.

The permanent magnets have been prepared by applying three different techniques: i) rapidly quenching using the melt spinning technique [1]; ii) the conventional sintering procedure with the main steps: melting, crushing and milling, pressing and magnetically aligning in a die, sintering and a post-sintering heat treatment under vacuum [2]; iii) reaction of elemental Fe and Nd powder in combination with a master alloy of Fe_2B along a ternary diffusion path according to Stadelmaier [3]. The magnetic measurements have been performed in static fields up to 5 T at 300 K and in pulsed fields up to 25 T in the range 77–600 K. The anisotropy field was measured in the range 77–600 K using the SPD (Singular Point Detection) technique.

The anisotropy and coercivity of melt spun alloys is shown for two compositions in fig. 1 as function of the wheel velocity. For $Nd_{15}Fe_{77}B_8$ we obtain $_IH_C$ values exceeding 2 T while for $Nd_{14}Fe_{81}B_5$ the maximum of $\mu_{0I}H_C$ is about 1.4 T. The pulsed field measurements of $_IH_C$ performed on 10 to 15 pieces of the ribbons glued together are found to agree well with static measurements on ribbons ground to powder and pressed with Scotch Cast 260. The anisotropy measurements at room temperature show that for wheel velocities larger than 13 m/s the anisotropy field H_A remains independent of the cooling rate within the experimental accuracy and equals (7.5 ± 0.2) T. Only for underquenched samples ($v \leqslant 13$ m/s), a sharp decrease of H_A was observed [4], while for overquenched samples ($v < 19$ m/s), contrary to the reduced $_IH_C$, H_A is still of the order of 7.5 T. The same H_A value (7.5 T) at 300 K was obtained for various sintered Nd–Fe–B-magnets and also for samples produced by the 3rd method, the ternary diffusion process according to Stadelmaier [3].

It was shown recently that the easy axis of magnetization changes from the *c*-axis at $T > 135$ K to an easy cone below 135 K [5]. This gives rise to a jump of the anisotropy field which is observed for both the sintered [6] and the melt-spun material. In fig. 2 the anomaly at H_A and $_IH_C$ is shown for a melt-spun sample occurring between 150 and 200 K and slightly depending on the cooling rate. Furthermore, we note that the variation of the Nd–Fe–B composition hardly influences both the absolute value of H_A and its temperature dependence.

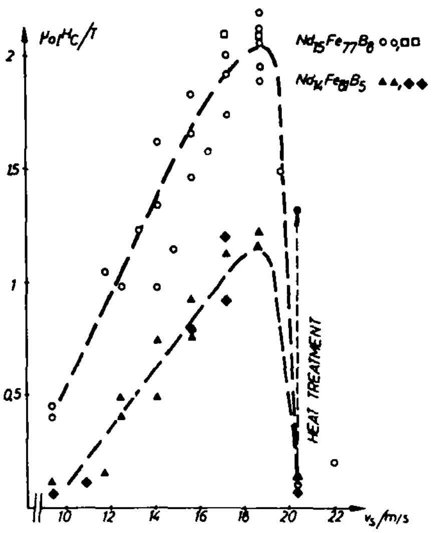


Fig. 1. The dependence of $_IH_C$ of melt-spun ribbons upon the wheel velocity. Static measurements $Nd_{15}Fe_{77}B_8$ (○), $Nd_{14}Fe_{81}B_5$ (▲), pulsed field measurements (□, ◆).

10

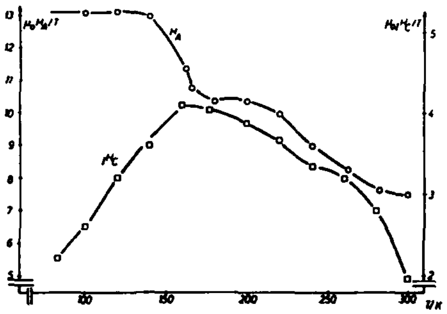


Fig. 2. Temperature dependence of the anisotropy field (O) and coercivity (□) of a melt-spun ribbon $v = 15$ m/s.

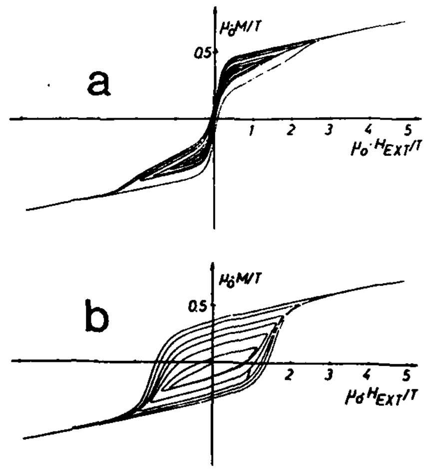


Fig. 3. Comparison of successive hysteresis loops of an overquenched sample before (a) and after annealing (b).

Their change, however, can be achieved by substituting Nd partly by heavy rare earths as Dy or Tb. From these anisotropy measurements we conclude that H_A is an intrinsic property of $Nd_2Fe_{14}B$ and is not influenced by the 3 different metallurgical processes.

In contrast to H_A, ${}_IH_C$ depends strongly on the metallurgy, which is demonstrated in fig. 1 where ${}_IH_C$ of melt-spun alloys depends on both the cooling rate and the Nd–Fe–B composition. As shown by ref. [7] the coercivity of overquenched melt-spun samples with low ${}_IH_C$ can be enhanced by a factor of more than 10 by an additional heat treatment at 700°C (see also fig. 1). From the analysis of the Mössbauer-spectra of under- and overquenched ribbons we conclude, that free α-Fe is present, coming presumably from $8j_2$-places of the $Nd_2Fe_{14}B$ lattice. No free Fe can be detected with the Mössbauer effect in high coercive ribbons quenched with a wheel velocity 15 m/s $\leq v \leq$ 19 m/s. The hysteresis loops of under- and overquenched ribbons exhibit a pronounced dip in the second quadrand which according to Becker [8] arises from a soft magnetic phase (fig. 3a). This finding is in accordance with the Mössbauer analysis. After heat treating the overquenched samples at 700°C, the pronounced dip in the second quadrant has diminished and the shape of the minor loops has changed from a typical nucleation type behaviour to a wall pinning behaviour (fig. 3b). Both metallurgical processes, namely diffusion of α-Fe into the $Nd_2Fe_{14}B$ lattice and a grain growth are the origin for the ${}_IH_C$ enhancement and the predominant wall pinning behaviour of the overquenched, heat treated melt-spun samples.

For sintered $Nd_{15}Fe_{77}B_8$ magnets ${}_IH_C$ values from 0.7 T up to 1.2 T were obtained depending upon the post-sintering heat treatment. From the shape of the minor loops of these magnets (0.7 T $\leq \mu_{0I}H_C \leq$ 1.2 T) and magnets produced by the ternary diffusion path ($\mu_{0I}H_C \approx 0.7$ T) we deduce that the coercivity mechanism is mainly controlled by the nucleation process which can be changed into a wall pinning behaviour, if Nd is replaced either by Pr or partly by heavy rare earth elements as Dy or Tb.

[1] J.J. Croat, J.F. Herbst, R.W. Lee and F.E. Pinkerton, J. Appl. Phys. 55 (1984) 2078.
[2] M. Sagawa, S. Fujimura, N. Togawa, H. Yamamoto and Y. Matsuura, J. Appl. Phys. (1984) 2083.
[3] H.H. Stadelmaier, N.A. El Masry and S.R. Stallard, J. Appl. Phys. 57 (1985) 4149.
[4] R. Grössinger, G. Hilscher, H. Kirchmayr, H. Sassik, R. Strnat and G. Wiesinger, Physica 130B (1985) 307.
[5] D. Givord, H.S. Li, J.M. Moreau, R. Perrier de la Bâthie and E. du Tremolet de Lacheisserie, Physica 130B (1985) 323.
[6] R. Grössinger, H. Kirchmayr, R. Krewenka, K.S.V.L. Narashimhan and M. Sagawa, Proc. 8th Workshop on Rare Earth Magnets, ed. K. Strnat (Dayton, 1985) p. 565.
[7] G.C. Hadjipanayis, R.C. Hazelton and K.R. Lawless, J. Appl. Phys. 43 (1983) 797.
[8] J.J. Becker, IEEE Trans. on Magn. MAG-18 (1982) 1451.

3

13441

Journal of the Less-Common Metals, 118 (1986) 167 - 172

THE HARD MAGNETIC PROPERTIES OF SINTERED Nd–Fe–B PERMANENT MAGNETS

R. GRÖSSINGER, R. KREWENKA, R. EIBLER and H. R. KIRCHMAYR

Institute for Experimental Physics, Technical University of Vienna, A-1040 Vienna (Austria)

J. ORMEROD

Mullard Magnetic Components, Southport (Gt. Britain)

K. H. J. BUSCHOW

Philips Research Laboratories, 5600 JA Eindhoven (The Netherlands)

(Received September 5, 1985)

Summary

A permanent magnet based on Nd–Fe–B was prepared by liquid phase sintering ($(BH)_{max}$ = 290 kJ m^{-3}, $_JH_c$ = 593 kA m^{-1}, B_r = 1.24 T). The temperature dependence of the coercive force was compared with the temperature dependence of the anisotropy field, the anisotropy energy, the ratio between wall energy and magnetization and the nucleation field for reversed magnetic domains. It was found that the coercive force is neither purely pinning controlled nor purely nucleation controlled.

1. Introduction

Permanent magnet materials obtained by the sintering of powders of Nd–Fe–B alloys have been shown to possess outstanding magnetic properties [1, 2]. A drawback of these materials is their limited corrosion resistance and the relatively high negative temperature coefficient of the coercive force. In this paper we report an investigation in which we have studied the temperature dependence of the coercive force $_JH_c$ in more detail. We include in this investigation the temperature dependences of the anisotropy field H_A, the anisotropy energy K_1 and the domain wall energy γ in an attempt to determine in how far the temperature dependence of $_JH_c$ is related to that of H_A, K_1 or γ.

2. Materials and methods

The sintered magnet body used was made from an Nd–Fe–B alloy close in composition to $Nd_2Fe_{14}B$. The various steps involved were particle

0022-5088/86/$3.50

12

alignment, pressing, sintering and heat treatments. These have been described in more detail elsewhere [3]. The measurements of $_JH_c$ were made in a pulsed-field system. For the measurements of H_A we used the singular point detection (SPD) method [4]. The temperature dependence of the saturation magnetization σ was measured on a conventional σ–T apparatus based on the Faraday method. The performance of the magnet body at room temperature can be specified by the following parameters: $(BH)_{max}$ = 290 kJ m^{-3}, $_JH_c$ = 593 kA m^{-1} and B_r = 1.24 T.

3. Results and discussion

The temperature dependence of the anisotropy field H_A is shown in Fig. 1. The strong rise in H_A with decreasing temperature has a small discontinuity below about 250 K for which we have no explanation at the moment. The small structure near 250 K in the $H_A(T)$ curve is probably of minor importance since the overall behaviour of the $H_A(T)$ curve of the sintered magnet body is much the same as the $H_A(T)$ curve measured on a piece of an arc-cast alloy of the composition $Nd_2Fe_{14}B$ after homogenizing at 900 °C for 3 weeks [5].

The temperature dependence of $_JH_c$ and J_s is shown in Fig. 2. Separate measurements showed that the Curie temperature is close to 585 K.

An important parameter for describing the coercive fields in hard magnetic materials is the domain wall energy γ. The room temperature value of

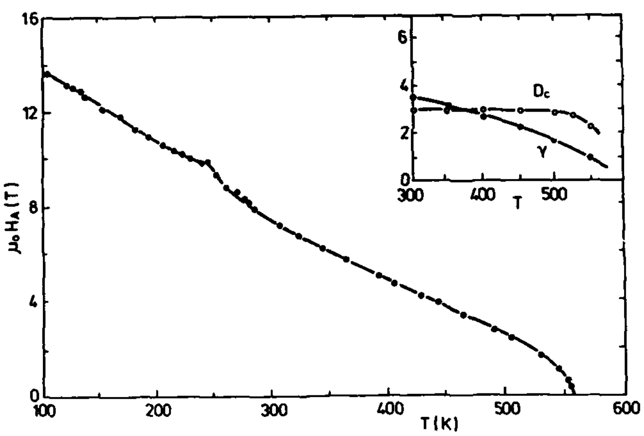


Fig. 1. Temperature dependence of the anisotropy field $\mu_0 H_A$ for a sintered permanent magnet body based on Nd–Fe–B. The inset shows the temperature dependence of the single-domain particle diameter D_c (in units of 100 μm) and the temperature dependence of the domain wall surface energy γ (in units of 10^{-2} J m^{-3}).

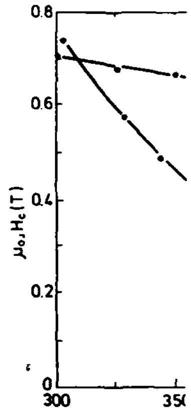


Fig. 2. Temperature
temperature depend
sintered permanent n

this quantity was
3.5 × 10^{-2} J m^{-2}.
dence by means o

$$\gamma = \left(\frac{2kT_cK_1}{d}\right)^{1/2}$$

$$K_1 = \tfrac{1}{2}H_AJ_s$$

where the tempe
and 2. In eqn. (1
between the mag
this way is show
is the single-dom
isolated sphere b
ferred to two-do
J_s^{-2} Livingston [6
0.3 μm at room t
from the temper
and 2). As can b
eter shows virtua
At all temperatu
than the grain dia

In Fig. 3 v
terms of various

13

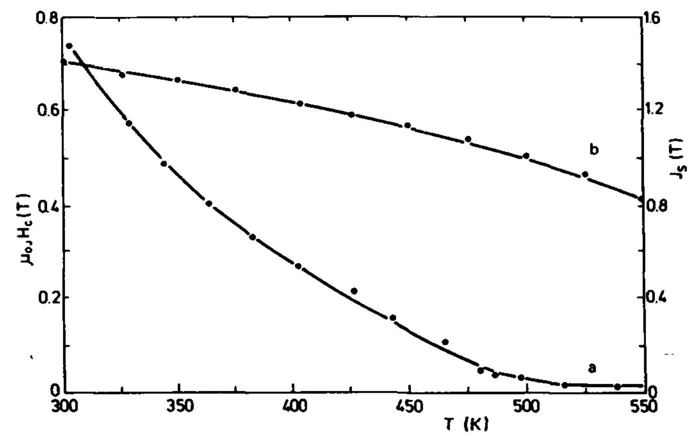


Fig. 2. Temperature dependence of the coercive field $\mu_0 {}_J H_c$ (curve a, left scale) and temperature dependence of the saturation magnetization J_s (curve b, right scale) for a sintered permanent magnet based on Nd–Fe–B.

this quantity was determined recently by Livingston [6], who reports $\gamma = 3.5 \times 10^{-2}$ J m^{-2}. We used this value and determined its temperature dependence by means of the relations

$$\gamma = \left(\frac{2kT_c K_1}{d}\right)^{1/2} \tag{1}$$

$$K_1 = \tfrac{1}{2} H_A J_s \tag{2}$$

where the temperature dependences of H_A and J_s were taken from Figs. 1 and 2. In eqn. (1) k represents the Boltzmann constant and d is the distance between the magnetic atoms. The temperature dependence of γ obtained in this way is shown in the inset of Fig. 1. An important parameter related to γ is the single-domain particle diameter D_c, representing the diameter of an isolated sphere below which single-domain structures are energetically preferred to two-domain structures in zero applied field. Using $D_c = 1.4(4\pi)^2 J_s^{-2}$ Livingston [6] found that in Nd–Fe–B permanent magnets D_c is about 0.3 μm at room temperature. The temperature dependence of D_c was derived from the temperature of γ and the temperature dependence of J_s (Figs. 1 and 2). As can be seen in the inset of Fig. 1, the single-domain particle diameter shows virtually no temperature dependence in the region below 500 K. At all temperatures we may expect, therefore, that D_c will be much smaller than the grain diameter, being typically 10 μm.

In Fig. 3 we have analysed the temperature dependence of ${}_J H_c$ in terms of various models relating ${}_J H_c$ to one or more of the other magnetic

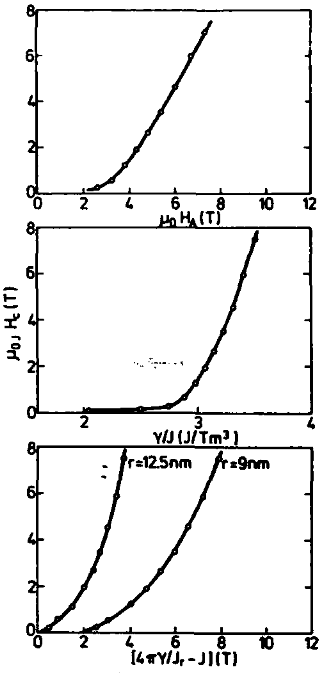


Fig. 3. Plots of the coercive force $\mu_{0J}H_c$ *vs.* the anisotropy field $\mu_0 H_A$ (top part), the ratio of wall energy and magnetization γ/J (middle part) and the nucleation field $4\pi\gamma/Jr - J$ (bottom part). The quantity r in the bottom part represents the defect radius. For more details, see text.

parameters considered in this report. Inspection of the results in the top and middle parts of Fig. 3 shows that the coercive force is not proportional to the anisotropy field, as was proposed by for uniform pinning on extended planar defects by Kütterer *et al.* [7]. Zijlstra [8] considered discrete pinning and showed that if the coercive force originates from wall pinning at discrete sites one may expect $_JH_c$ to be proportional to γ/J. As shown in the middle part of Fig. 3, this proportionality is not found in the permanent magnet material investigated. Livingston [6] studied various Nd–Fe–B permanent magnet materials by means of microscopic investigations using the Kerr effect. He found indications that the coercive force in these materials is nucleation controlled rather than pinning controlled. For spherical defects of radius r the internal nucleation field was estimated by that author to be $H_n = 4\pi\gamma/Jr - NJ$, where NJ represents the demagnetizing field. Taking the temperature dependence of γ shown in the inset of Fig. 1 together with the

temperature
have calculat
ous values o
$_JH_c$ and the
of $_JH_c$ *versus*
Surprisi
ture depende

$_JH_c \propto \left(\frac{K_1}{J_s}\right)^{5.}$

proposed by
volume pinni
et al. [7] suc
coercive force
of $SmCo_5$. Ho
case was appr
lower than th
bility of this
therefore dou

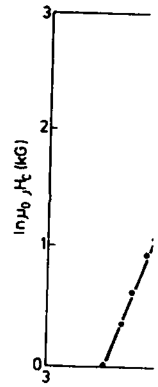


Fig. 4. Double log

4. Conclusions

Our study
the temperature
manent Nd–Fe

15

temperature dependence of J given in Fig. 2 and taking N equal to unity we have calculated the temperature dependence of this nucleation field for various values of r. In none of these cases did we find a proportionality between ${}_JH_c$ and the nucleation field H_n. Two representative examples of such plots of ${}_JH_c$ *versus* H_n are shown in the bottom part of Fig. 3.

Surprisingly enough we found a satisfactory description of the temperature dependence of the coercive force (Fig. 4) when using the relation

$$ {}_JH_c \propto \left(\frac{K_1}{J_s}\right)^{5/2} \propto H_A{}^{5/2} \qquad (3)$$

proposed by Kütterer *et al.* [7] for the case when ${}_JH_c$ is determined by volume pinning associated with the presence of atomic disorder. Kütterer *et al.* [7] successfully applied their model to the description of the intrinsic coercive force caused by pinning of narrow domain walls in a single crystal of $SmCo_5$. However, the magnitude of the coercive forces considered in this case was approximately 10^{-3} T, which is more than three orders of magnitude lower than the coercive forces considered in the present study. The applicability of this model to the Nd–Fe–B permanent magnet material seems therefore doubtful.

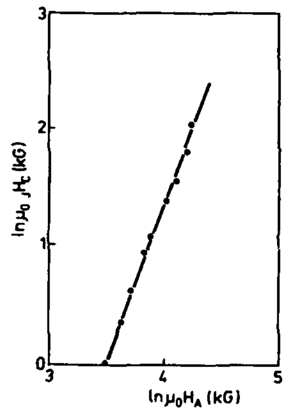


Fig. 4. Double logarithmic plot of the coercive field ${}_JH_c$ *vs.* the anisotropy field H_A.

4. Conclusions

Our study of the temperature dependence of the coercive force ${}_JH_c$ and the temperature dependence of the anisotropy field H_A for a sintered permanent Nd–Fe–B magnet revealed that the coercive force decreases more

16

strongly with temperature than the anisotropy field. We found that a satisfactory description of the strong temperature dependence of the coercivity cannot be given in terms of current models in which this quantity is taken is be either pinning controlled or nucleation controlled. It is not unlikely that the underlying mechanism of $_JH_c$ itself depends on the temperature.

References

1 M. Sagawa, S. Fujimura, H. Yamamoto, Y. Matsuura and S. Hirosawa, *J. Appl. Phys.*, *57* (1985) 4094.
2 K. S. V. L. Narasimhan, *J. Appl. Phys.*, *57* (1985) 4081.
3 J. Ormerod, *J. Less-Common Met.*, *111* (1985) 49.
4 G. Asti and S. Rinaldi, *J. Appl. Phys.*, *45* (1974) 3600.
5 R. Grössinger, X. K. Sun, R. Eibler, K. H. J. Buschow and H. R. Kirchmayr, *J. Phys. (Paris)*, *46* (1985) C6 - 221.
6 J. D. Livingston, *Proc. 8th Int. Workshop on Rare Earth Magnets, Dayton, Ohio, May 1985.*
7 R. Kütterer, H. R. Hilzinger and H. Kronmüller, *J. Magn. Magn. Mater.*, *4* (1977) 1.
8 H. Zijlstra, in E. P. Wohlfarth (ed.), *Ferromagnetic Materials, Vol. 3*, North Holland, Amsterdam, 1982, p. 37.

17

4

Journal of the Less-Common Metals, *124* (1986) 165 - 172

MAGNETIC PHASE TRANSITIONS AND MAGNETIC ANISOTROPY IN $Nd_2Fe_{14-x}Co_xB$ COMPOUNDS

R. GRÖSSINGER, R. KREWENKA, X. K. SUN, R. EIBLER and H. R. KIRCHMAYR
Institut für Experimentalphysik, Technische Universität Wien, A-1040 (Austria)
K. H. J. BUSCHOW
Philips Research Laboratories, P.O. Box 80.000, 5600 JA Eindhoven (The Netherlands)
(Received March 10, 1986)

Summary

The temperature dependence of the anisotropy field of $Nd_2Fe_{14-x}Co_xB$ has been measured between 77 K and the Curie temperature, using the singular point detection (SPD) technique. The anisotropy field at room temperature is found to decrease with increasing cobalt content. Measurements of the temperature dependence of the initial susceptibility show that at a temperature T_1, which is below room temperature, the easy magnetization direction changes. The origin of the change is attributed to the neodymium-sublattice anisotropy. For the cobalt-rich samples ($x > 5$) it is found that at temperatures T_2 higher than ambient temperatures a second spin reorientation takes place, which is attributed to the competing effect of the neodymium sublattice anisotropy and the 3d sublattice anisotropy.

1. Introduction

The compound $Nd_2Fe_{14}B$ is the basic material for the production of high quality permanent magnets [1, 2]. It crystallizes [3] in a tetragonal structure (space group $P4_2/mnm$) and combines a high saturation magnetization ($4\pi M_s = 1.6$ T) with a high uniaxial anisotropy at room temperature ($\mu_0 H_A = 7$ T). The magnetic structure of $Nd_2Fe_{14}B$ is not the same at all temperatures. Below 135 K a spin reorientation takes place from an easy magnetization along the *c* axis to an easy magnetization direction in the (110) plane [4]. Investigations of the mixed crystal series $(Nd_xR_{1-x})_{15}Fe_{77}B_8$ ($R \equiv$ Y, Ce, La) showed that this anomaly is mainly due to the temperature dependence of the neodymium sublattice anisotropy [5].

A major disadvantage of the Nd–Fe–B magnets is their rather low Curie temperature ($T_c = 580$ K) [6]. Substitution of cobalt for iron leads to an increase of T_c [7]. However, a further requirement for the attainment of high coercivity magnets is the presence of a high anisotropy. In

0022-5088/86/$3.50

18

the present work we have concentrated therefore mainly on changes in the anisotropy caused by cobalt substitution in $Nd_2Fe_{14}B$.

2. Experimental details

The $Nd_2Fe_{14-x}Co_xB$ samples were prepared by arc melting under purified argon gas from starting materials of at least 99.9% purity. X-ray diffraction showed that arc-casting did not result in single-phase samples. For this reason all samples were vacuum annealed for 3 weeks at about 900 °C. After this treatment the samples were found to be approximately single phase, remnants of the impurity phases being of the order of a few per cent.

In order to determine the Curie temperature of the various compounds we measured the temperature dependence of the magnetization σ above room temperature by the Faraday method. The values of T_c were obtained by plotting σ^2 *versus* T and extrapolating to $\sigma^2 \rightarrow 0$.

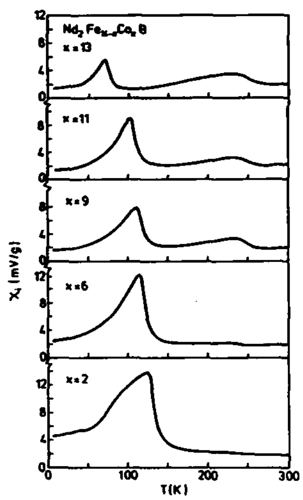
The anisotropy field H_A was measured in a pulsed field system from 77 K up to the Curie temperature using the singular point detection (SPD) technique [8]. This method leads to a singularity at $H = H_A$ in experimental curves of d^2M/dt^2 *versus* H (M is the magnetization) if the c axis is the easy magnetization direction. As already mentioned, in $Nd_2Fe_{14}B$ a spin reorientation from an easy c axis to an easy cone was found to occur near $T_1 = 135$ K. Assuming the usual series expansion of the anisotropy energy, $E_a = K_1 \sin^2\theta + K_2 \sin^4\theta$, a necessary condition for such a spin reorientation is a change in sign of K_1 from positive to negative. Consequently there exists a temperature range above T_1 where K_1 becomes small and where higher order anisotropy constants determine the shape of the anisotropy energy surface. Such behaviour was indeed found in $Nd_2Fe_{14}B$ below 200 K by Yang Fu-Ming *et al.* [9] who studied the temperature dependence of K_1 and K_2 over an extended temperature range. The change in relative magnitude of the anisotropy constants leads to the occurrence of additional relative minima in E_a. The magnetization vector can no longer rotate smoothly in this temperature range and jumps in $M(H)$ can appear. This phenomenon is commonly referred to as the first order magnetization process (FOMP). A theoretical description of it was given by Asti and Bolzoni [10]. Such a FOMP was not only found in $Nd_2Fe_{14}B$ [11], but also in various $(R, Nd)_2Fe_{14}B$ compounds [5] as well as in Nd–Fe–B permanent magnets [12]. We recall that the critical field H_{cr}, for which such a FOMP is observed, is not equal to H_A ($H_{cr} < H_A$). This can be derived from measurements made on Nd–Fe–B magnets where it had been possible to measure simultaneously $H_A(T)$ and $H_{cr}(T)$ in the temperature range of interest, $135\text{ K} < T < 200\text{ K}$ [13]. Therefore the change in shape of the d^2M/dt^2 *versus* H curves found below 200 K in most of the samples studied in the course of the present investigation was taken to be indicative of such a FOMP anomaly.

19

A more accurate determination of the spin reorientation temperature can be obtained from measurements of the temperature dependence of the initial susceptibility $\chi_i(T)$. Measurements of $\chi_i(T)$ were made in the temperature range between 4.2 and 300 K by using a lock-in technique and employing a small a.c. field of frequency 83 Hz. In a previous investigation [14] we showed that χ_i can be taken to be proportional to $M_s/(K_1 + F)$, where F is a function of the higher order constants K_2, K_3 etc. Since K_1 is expected to change its sign at the spin reorientation temperature (and hence $K_1 \rightarrow 0$) one expects a maximum to occur in the $\chi_i(T)$ curve near the same temperature.

3. Results and discussion

Examples of measurements of the temperature dependence of the initial susceptibilities are shown in Fig. 1. It appears from our measurements that the phenomenon of spin reorientation is present in the whole concentration range of the $NdFe_{14-x}Co_xB$ series. The spin reorientation temperatures T_1 derived from these measurements have been plotted as a function of cobalt concentration in Fig. 2. It can be seen from Fig. 2 that the spin reorientation temperature shows a comparatively low concentration



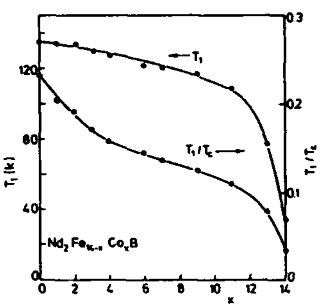


Fig. 1. Temperature dependence of the initial susceptibility in various $Nd_2Fe_{14-x}Co_xB$ compounds.

Fig. 2. Concentration dependence of the low-temperature spin reorientation temperature (T_1) in $Nd_2Fe_{14-x}Co_xB$ compounds.

dependence for all but the highest cobalt concentrations. For cobalt concentrations higher than that corresponding to the approximate formula composition $Nd_2Fe_2Co_{12}B$ there is a strong decrease.

Results of measurements of the temperature dependence of the anisotropy field H_A are shown for the two extreme compositions in Fig. 3. It may be seen from this figure that the decrease in H_A with T is much stronger in $Nd_2Co_{14}B$ than in $Nd_2Fe_{14}B$. Owing to the proximity of the spin reorientation in $Nd_2Fe_{14}B$ at temperatures below 200 K, measurements of H_A by the SPD method are somewhat difficult [11], which implies that the actual H_A values in this temperature range may be somewhat higher. In any case, static measurements made in high magnetic fields on magnetically aligned powders showed that the H_A values of both materials at 4.2 K are approximately the same, which means that both curves shown in Fig. 2 will eventually reach the same end point at low temperature.

In order to facilitate the comparison of the $H_A(T)$ curves obtained for the various compounds of the series $NdFe_{14-x}Co_xB$ we have plotted in Figs. 4 and 5 the reduced values of $H_A(T)$ *versus* the corresponding reduced temperatures. The reduced temperatures are defined as T/T_c. The reduced values of H_A are defined as $H_A(T)/H_A(4.2\ K)$, where we have used $\mu_0 H_A(4.2\ K) = 31$ T, being the mean value between $\mu_0 H_A = 32$ T found for $Nd_2Co_{14}B$ and $\mu_0 H_A = 30$ T found for $Nd_2Fe_{14}B$ [6, 15]. Inspection of the results shown in Figs. 4 and 5 makes it clear that the reduced anisotropy fields behave in a systematic way when the cobalt concentration is increased in $Nd_2Fe_{14-x}Co_xB$. It is interesting to note that the T_c value of $Nd_2Co_{14}B$ (1005 K) is considerably higher than that of $Nd_2Fe_{14}B$ (585 K). Whereas $H_A(T)$ in the iron-rich compounds tends to become zero at temperatures close to T_c, one may notice in Fig. 5 that $H_A(T)$ of the cobalt-rich compounds, as measured by the SPD method, tends to become zero at a temperature far below T_c.

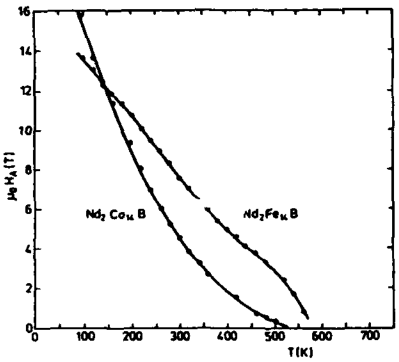
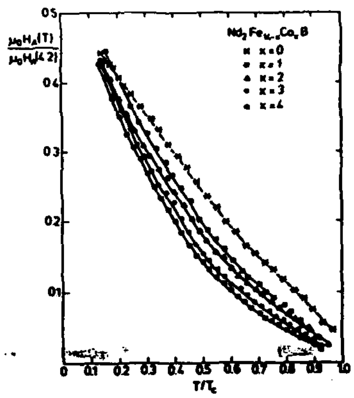


Fig. 3. Comparison of the temperature dependence of the anisotropy field $\mu_0 H_A$ in ○, $Nd_2Co_{14}B$ and ●, $Nd_2Fe_{14}B$.



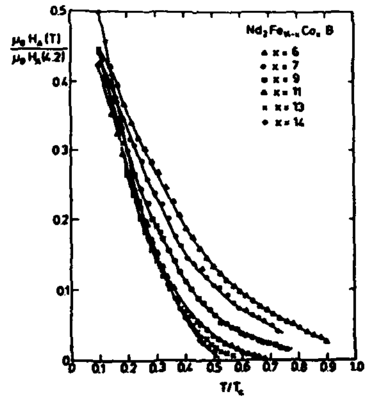


Fig. 4. Reduced anisotropy fields *vs.* reduced temperature in iron-rich $Nd_2Fe_{14-x}Co_xB$ compounds.

Fig. 5. Reduced anisotropy fields *vs.* reduced temperature in cobalt-rich $Nd_2Fe_{14-x}Co_xB$ compounds.

The concentration dependence of H_A at room temperature is shown in Fig. 6. H_A decreases from more than 7 T in $Nd_2Fe_{14}B$ to less than 5 T in $Nd_2Co_{14}B$. We have included in Fig. 6 the $H_A(x)$ values derived from the data published by Sagawa *et al.* [16]. It is obvious that the agreement for the iron-rich compounds is satisfactory, but a discrepancy between the

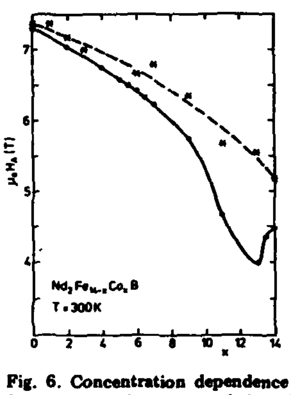


Fig. 6. Concentration dependence of H_A at room temperature in $Nd_2Fe_{14-x}Co_xB$: ●, data obtained by means of the SPD method in the course of the present investigation; *, H_A values corresponding to $2K_1/J_s$ from ref. 16.

22

two $H_A(x)$ curves is manifest for the compound of relatively high cobalt concentration. The reason for this discrepancy might be the following. The H_A values measured by means of the SPD technique represent the physically relevant anisotropy field, including all anisotropy constants (independent of the chosen series expansion of the anisotropy energy). The H_A values obtained from the K_1 data of ref. 16 were calculated by means of the formula $H_A = 2K_1/J_s$. It is interesting to note that this difference starts to become appreciable for those concentrations where a spin reorientation from the *c* axis to the basal plane occurs at higher temperatures (see below). This means that negative contributions to H_A become relatively important for increasing cobalt concentration, which are less easily taken into account by considering only K_1.

Detailed measurements of the temperature dependence of the magnetization on a $Nd_2Co_{14}B$ single crystal were made by Le Roux *et al.* [17]. These authors found a cusp in $M(T)$ of this compound at the very temperature (T_2) where $H_A(T)$ tends to vanish in our measurements. This coincidence may be explained by assuming that at this temperature, T_2, a second spin reorientation takes place. X-ray diffraction studies made on magnetically aligned powders of various $R_2Co_{14}B$ compounds had made it clear that the easy magnetization direction is parallel to the *c* direction in $Nd_2Co_{14}B$ at room temperature. However, it was found that the easy direction is perpendicular to the *c* axis in compounds in which the *R* component does not contribute to the anisotropy. Consequently one expects that in $Nd_2Co_{14}B$, too, the easy magnetization direction will become perpendicular to the *c* direction when the temperature is sufficiently raised to make the contribution of the strongly temperature-dependent neodymium sublattice anisotropy negligibly small. However, no such second spin reorientation is

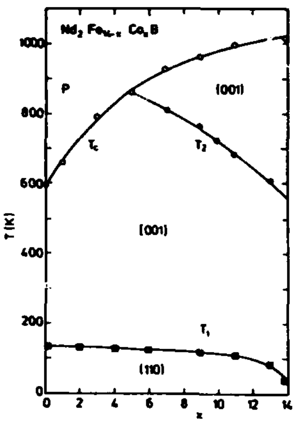


Fig. 7. Magnetic phase diagram of the $Nd_2Fe_{14-x}Co_xB$ system.

expected in $Nd_2Fe_{14}B$ since the iron sublattice anisotropy favours the same easy magnetization direction (parallel to the *c* axis) as the neodymium sublattice anisotropy. From the fact that the 3d sublattice anisotropy is of opposite character in the iron and cobalt compounds one may expect that T_2 will increase with increasing iron concentration in $Nd_2Fe_{14-x}Co_xB$, as is found experimentally. The magnetic phase diagram, showing the concentration dependence of T_2, together with the corresponding concentration dependence of T_1 and T_c, is given in Fig. 7.

4. Concluding remarks

In order to improve the unfavourably large temperature coefficient of the magnetization of Nd–Fe–B base permanent magnets, various pseudo-ternary alloys were considered in which part of the iron was replaced by cobalt [7]. As a result of this replacement, the Curie temperature of these alloys rose substantially and the concomitant room temperature coefficient of magnetization was considerably lowered. However, the beneficial influence of the cobalt substitution with regard to the temperature coefficient of the magnetization was found to be accompanied by an unfavourable lowering of the room temperature coercive forces attainable in these materials. This behaviour is rather unexpected since the strength of the maximum coercive field is commonly considered to be related to the magnitude of the anisotropy field, and since the latter quantity was found to be almost equal in both materials at 4.2 K [6, 16]. The results presented in the previous section make it clear, that the temperature dependence of H_A is much stronger in $Nd_2Co_{14}B$ than in $Nd_2Fe_{14}B$, leading to a room temperature value of H_A which is 40% lower in $Nd_2Co_{14}B$ than in $Nd_2Fe_{14}B$ (see Fig. 3). This lowering of H_A seems less strong than the lowering of the coercive force, which is equal to 7.3 kOe in $Nd_{15}Fe_{77}B_8$ but only 0.8 kOe in $Nd_{15}Fe_{17}Co_{60}B_8$ [7]. This suggests that, apart from the change of H_A, changes in the microstructure of the alloys also take place, leading to changes in the nucleation or pinning centres. This is not unexpected since the ternary Nd–Co–B phase diagram contains considerably more ternary compounds than the Nd–Fe–B phase diagram.

We have shown that the low-temperature spin reorientation temperature T_1 in $Nd_2Fe_{14-x}Co_xB$ has a peculiar concentration dependence, being relatively insensitive to cobalt substitution up to $x \approx 12$, then decreasing strongly with x. The low-temperature spin reorientation is due primarily to the neodymium sublattice anisotropy and it was proposed on several occasions that its origin is due to the contribution anisotropy constants of higher order than K_1, which become important at low temperatures [18, 19]. The concentration dependence of these higher-order anisotropy constants is still unknown at present. From the magnetic phase diagram proposed by us (Fig. 5) it follows that for compounds with relatively high cobalt content there is a second spin reorientation transition (T_2) at higher

temperatures. In contrast with the transition at T_1, this high-temperature transition depends not only on the neodymium sublattice anisotropy but also on the 3d sublattice anisotropy. It can be seen from the magnetic phase diagram that neither of these phase transitions will have any bearing on the possible application of these compounds as starting materials for permanent magnets.

Acknowledgement

The part of the work performed at the Technical University of Vienna was supported by the European Office of the U.S. Army (Contract Number DAJA-45-84-C-0010).

References

1 J. J. Croat, J. F. Herbst, R. W. Lee and F. E. Pinkerton, *J. Appl. Phys.*, *55* (1984) 2078.
2 M. Sagawa, S. Fujimura, N. Togawa, H. Yamamoto and Y. Matsuura, *J. Appl. Phys.*, *55* (1984) 2083.
3 J. F. Herbst, J. J. Croat, F. E. Pinkerton and W. P. Yelon, *Phys. Rev. B*, *29* (1984) 4176.
4 D. Givord, H. S. Li, J. M. Moreau, R. Perrier de la Bâthie and E. du Trémolet de Lacheisserie, *Physica B*, *130* (1985) 323.
5 R. Grössinger, X. K. Sun, R. Eibler and H. R. Kirchmayr, in K. Strnat (ed.), *Proc. 8th Int. Workshop on Rare-Earth Magnets*, Dayton University Press, 1985, p. 553.
6 S. Sinnema, R. J. Radwanski, J. J. M. Franse, D. B. De Mooij and K. H. J. Buschow, *J. Magn. Magn. Mater.*, *44* (1984) 333.
7 S. Fujimura, M. Sagawa, Y. Matsuura, Y. Hitoshi and N. Togawa, *European Patent 0 134 304 A1* (1983).
8 G. Asti and S. Rinaldi, *J. Appl. Phys.*, *45* (1974) 3600.
9 Yang Fu-Ming, Zhao Xi-Chao, Zhao Ru-Wen, Yu Zhi-Hong and Zhang Shou-Gong, in K. Strnat (ed.), *Proc. 8th Workshop on Rare Earth Magnets*, Dayton University Press, 1985, p. 529.
10 G. Asti and F. Bolzoni, *J. Magn. Magn. Mater.*, *15 - 18* (1980) 29.
11 R. Grössinger, X. K. Sun, R. Eibler, K. H. J. Buschow and H. R. Kirchmayr, *J. Phys. (Paris)*, *46* (1985) C6 - 221.
12 R. Grössinger, R. Krewenka, K. S. V. L. Narasimhan and M. Sagawa, *J. Magn. Magn. Mater.*, *15* (1980) 160.
13 R. Grössinger, R. Krewenka, M. Sagawa and H. R. Kirchmayr, to be published.
14 R. Grössinger, X. K. Sun, R. Eibler, K. H. J. Buschow and H. R. Kirchmayr, *J. Magn. Magn. Mater.*, *58* (1986) 55.
15 K. H. J. Buschow, D. B. de Mooij, S. Sinnema, R. J. Radwanski and J. J. M. Franse, *J. Magn. Magn. Mater.*, *51* (1985) 211.
16 M. Sagawa, Y. Matsuura, S. Fujimura, H. Yamamoto and S. Hirosawa, *IEEE Trans. Magn. Jpn.*, *1* (1985) 48.
17 D. Le Roux, H. Vincent, P. L'Heritier and R. Fruchart, *J. Phys. (Paris)*, *46* (1985) C6 - 243.
18 H. Szymczak, *J. Phys. (Paris)*, *46* (1985) C6 - 225.
19 E. B. Boltich and W. E. Wallace, *Solid State Commun.*, *55* (1985) 6.

25

INVESTIGATION OF THE HYSTERESIS LOOP AND THE MAGNETIC ANISOTROPY OF Nd-Fe-B BASED PERMANENT MAGNETS

R.Grössinger, R.Krewenka, K.S.V.L.Narasimhan [+], H.R.Kirchmayr

Institut für Experimentalphysik; Techn. Univ. Vienna, Austria.
+)*Crucible Research Center*; Colt Industries.

Abstract

The anisotropy field as well as the coercivity of technical, sintered permanent magnets based on Nd-Fe-B was measured from 80K up to the Curie temperature using a pulsed field system. It was tried to correlate the temperature dependence of the coercivity with that of the anisotropy. A general correlation of the type: $_IH_c$ prop. $(H_A)^k$ was found, where the power "k" lies between 1.5 and 3. The power "k" decreases with decreasing temperature showing either a temperature induced change of the coercivity-mechanism or the influence of K_2.

Introduction

High quality permanent magnets are generally based on Rare Earth 3d-metal (Fe,Co) intermetallic compounds. There exist three technically used magnet families:

i) $SmCo_5$ based magnets.
ii) Sm_2Co_{17}, especially $Sm(Co,Fe,Cu,Zr)_{7.5}$ magnets.
iii) $Nd_2Fe_{14}B$ based magnets.

These materials exhibit the following important properties at room temperature (see table 1).

Table 1: Survey of the magnetic properties of Rare Earth 3d-metal magnets.

Material	$4\pi M_s$(kG)	$\mu_0 H_A$(T)	T_c (K)	$\mu_0\, {_IH_c}$(T)
$SmCo_5$	11.2	29	1020	2-2.5
Sm_2Co_{17}	12.8	6.5	1195	1-1.5
$Nd_2Fe_{14}B$	16	7.5	580	1-2

It is obvious that the hard magnetic properties of the Sm-Co permanent magnets are excellent, however the high costs of the raw materials are prohibitiv for large scale applications. A possible solution of this economical problem may be found by the development of the new Nd-Fe-B magnets (1,2). The hard magnetic properties of these new magnets are based on the high uniaxial magnetic anisotropy of the $Nd_2Fe_{14}B$ compound. $Nd_2Fe_{14}B$ has at room temperature an easy c-axis, but below 135K the easy axis lies in a cone (3). Due to this spinreorientation K_1 (first order anisotropy constant) changes its sign. Therefore between 200K and 135K the higher order anisotropy constants become important, as visible regarding the $K_1(T)$ and $K_2(T)$ measurements performed on $Nd_{15}Fe_{77}B_8$(4). This can cause additional relative minima in the anisotropy energy surface, which can lead to jumps in the M(H) curve. This effect was theoretically analysed (5,6) and is called a FOMP (First Order Magnetization Process). Below 200K the occurence of such a FOMP was indeed observed in Nd-Fe-B samples (7,8). The magnetic anisotropy is an intrinsic property which is in technical permanent Nd-Fe-B magnets mainly given by the $Nd_2Fe_{14}B$ grains (8). The coercivity however is strongly influenced by the metallurgy of the magnet (e. g. heat treatment, grain size). The aim of the present paper is to try to correlate the magnetic anisotropy with the coercivity of various Nd-Fe-B based magnets.

Experimental

The following samples of technical permanent magnets supplied by Colt Industries based on Nd-Fe-B were available: "Colt1", which was one of the first produced sintered magnets, Crumax 30A, Crumax 35 and Crumax 40. All materials were aligned sintered magnets.
The magnetic investigations were performed in a pulsed field system (pulse duration sin half wave 5ms, maximum field μ_0H=28T), which can be operated between 4.2K and 800K. The anisotropy fields were determined using the SPD-technique (9). With this method the anisotropy field H_A of a polycrystalline sample can be measured. If a sample is not single phased (which is surely the case in permanent magnets) this technique pickes out only the anisotropy of that grains where the easy axis of magnetization lies in the c-axis (hard magnetic matrix); *additionally only* that grains contribute to the signal where these axes are orientated perpendicular to the external field. The field was calibrated using the anisotropy field of well known samples as for instance ferrites, YCo_5 and $PrCo_5$. The absolute accuracy of H is better then 3% (mainly determined by the reliability of the available anisotropy data), the relative accuracy is better then 1%.

Results and Discussion

Fig.1 shows the temperature dependence of the anisotropy field H_A. Below 200K an anisotropy anomaly, similar as mentioned above, was observed for all specimen. Arrows indicate this critical temperature, where a field induced first order magnetic phase transition begins to appear. The theoretical explanation is the same as that given for pure $Nd_2Fe_{14}B$ (7). It should be noted that below this critical temperature the meaning of H_A is no longer that of usual anisotropy field, because there H_A is the critical field which is caused by the occurence of relative minima in the anisotropy energy surface; therefore $H_{cr} < H_A$ is valid. Above 200K, however, the anisotropy field as measured by the SPD-technique is in fact the real physically relevent anisotropy field. The most widely applied method for determining H_A of hard magnetic materials is the magnetization measurement parallel and perpendicular to the preferential axis. Extrapolating $M_\perp(H)$ to the saturation value should deliver H_A. *Beside the problems of* misorientation and of having not monodomainic grains, this technique suffers under the generally to small external fields (e.g. the field of a conventional electro-magnet is 2T, whereas the anisotropy fields of the here interesting rare earth-3d compounds are much larger (see table 1)). All these difficulties combined with the often discussed uncertainties defining H_A (the definition depends naturally on the type of the choosen series expansion of the anisotropy energy) causes troubles comparing H_A data which were obtained using different methods. It is a great advantage of the SPD- method that it

0018-9464/86/0900-0760$01.00©1986 IEEE

26

determines the real anisotropy field (for a uniaxial material that field which is necessary to rotate the magnetization vector from the c-axis into the hard plane) independent of any mathematical definition.

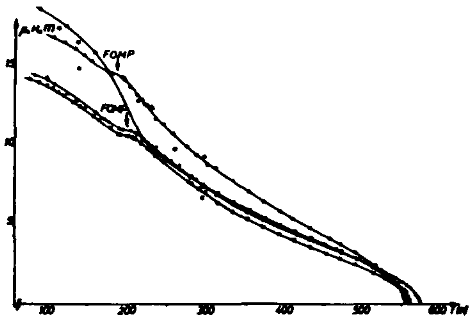


Fig.1: Temperature dependence of the anisotropy field of the samples: "Colt 1" (□), Crumax 30A (o), Crumax 35 (x), Crumax 40 (Δ).

Between 200K and the Curie temperature the $H_A(T)$ curves of all samples except that of the Crumax 30A are very similar with respect to the magnitude as well as to the character. The Crumax 30A material exhibits remarkable higher values of H_A (e.g. at room temperature $\mu_0 H_A$=9T) indicating a substitution of the Nd by a heavy rare earth element.

A similar result was obtained for the temperature dependence of the coercivity $_IH_c$ (see Fig. 2). Also there the $_IH_c(T)$ values of Crumax 30A are much higher than that of all other samples. It should be noted that the spinreorientation causes no anomaly in $_IH_c(T)$. Only if the external field is applied perpendicular to the preferential axis a down-turn below 200K is detected (8) (see the dotted curve in Fig. 2).

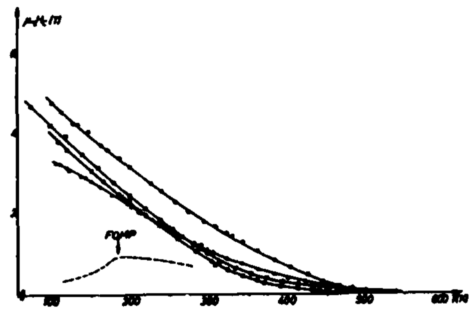


Fig.2: Temperature dependence of the coercivity of the samples:"Colt 1" (□) Crumax 30A (o), Crumax 35 (x), Crumax 40 (Δ). The dotted curve represents $_IH_c(T)$ of the "Colt 1" magnet applying the external field perpendicular to the preferential axis (8).

It is well known that a high uniaxial anisotropy is a necessary condition for the formation of a high coercivity in a permanent magnet. In the case of an ideal monodomainic single particle magnet the coercivity is equal to the anisotropy field. The critical diameter of single domain particles is:

$$D_c = 1.4\gamma/M_s^2 \qquad (1)$$

using the relation for γ (10):

$$\gamma = 2\sqrt{AK}\,\{1+[(1+\eta)/\eta^{1/2}]\sin^{-1}(\eta/\eta+1)^{1/2}\} \qquad (2)$$

A...average exchange constant; $\eta = K_2/K_1$.

In the case of the here interesting $Nd_{15}Fe_{77}B_8$ according to (11) the room temperature values are: $A=7.7\times10^{-12}$J/m , D_c =0.2µm. The average grain size of a sintered Nd-Fe-B magnet is between 5 and 10µm (12). This means that such a magnet cannot be treated as a single particle material. However there exists theoretical predictions for the temperature dependence of the coercivity of technical Sm-Co magnets (13). The most important idea of this work is trying to correlate the coercivity field with the nucleation field which can be caused by various sources. The mathematical expression of this nucleation field is K_1/M_s, which is same as that of the anisotropy field neglecting higher order anisotropy constants. This encourages to look if any correlation can be found between $_IH_c$ and H_A. The general mathematical onset used for this purpose is of the type:

$$_IH_c(T) \text{ prop } H_A(T)^k \qquad (3)$$

The above described experimental techniques allows us to determine $_IH_c$ as well as H_A on the same sample. This gives the chance testing theoretical models in a direct manner as it was not yet possible. According the fact that in the above mentioned work (13) various powers, depending on the special assumptions which are made for these calculations, are predicted, a plot of $\ln(_IH_c(T)/_IH_c(T=300K))$ divided by $\ln(H_A(T)/H_A(T=300K))$ versus the temperature was made (see Fig. 3).

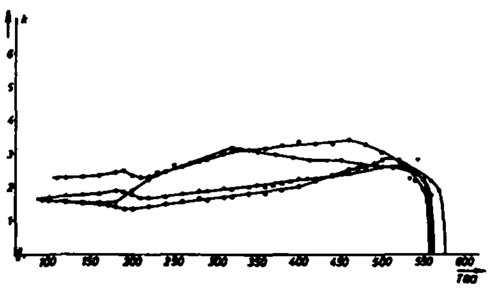


Fig.3: Temperature dependence of $k=\ln(_IH_c(T)/_IH_c(T=300K))/\ln(H_A(T)/H_A(T=300K))$ of the samples: "Colt 1" (∇), Crumax 30A (•), Crumax 35 (o), Crumax 40 (Δ).

Kronmüller and Hilzinger (14) have shown that in the case of incoherent nucleation the coercivity field is determined either by the nucleation of reversed domains in the magnetically soft phase or by the expansion of these reversed domains into the magnetically hard matrix. In both cases $_IH_c(T)$ is approximately given by

$$_IH_c(T) \sim K_1/M_s \qquad (4)$$

In the first case, however, we have to insert into equation (4) the anisotropy of the perturbed region, whereas in the second case

K_1 means the anisotropy constant of the hard magnetic matrix. Another possibility is that the coercive force is caused by a pinning of domain walls at grain boundaries. It is expedient to distinguish two cases corresponding to the thickness G of the grain boundaries with respect to the wall width d_w. Additionally it have to be assumed that the ratios of the exchange- and the anisotropy energies at the grain boundaries are temperature independent. This leads to:

$$_I H_c(T) \sim (K_1/M_s)^{3/2} \quad (G<d_w) \qquad (5)$$

$$_I H_c(T) \sim K_1/M_s \quad (G>d_w) \qquad (6)$$

According to an electron microscopy study the grain boundary phase of a sintered $Nd_{15}Fe_{77}B_8$ magnet are after the heat treatment between 2 and 3nm (15). The average domain wall width of such a magnet is about 4nm (11). Consequently a relation close to (5) may be valid.

If narrow domain walls exist atomic defects act as effective pinning centres. Nearly all permanent magnets deviate from the exact stochiometry, therefore the existence of such defects can be assumed. The temperature dependence of $_I H_c$ following from a pinning of domain walls by atomic disorder is due to (16)

$$_I H_c(T) \sim M_s^2 (K_1/M_s)^{5/4} \qquad (7)$$

In materials with not so high coercivity fields it was assumed that $_I H_c$ is determined by volume pinning. The pinning forces are supposed to originate from statistically distributed defects. Due to the larger wall area the statistical fluctuations of the defect density are less important. Assuming that the interaction energy of the walls with the defects is mainly determined by the anisotropy, leads to a temperature dependence of $_I H_c$:

$$_I H_c(T) \sim (K_1/M_s)^{5/2} \qquad (8)$$

In summary all these relations show that for some simple cases a correlation between $_I H_c$ and the anisotropy field H_A can be expected. Fig.3 shows that the coercivity mechanism changes with temperature, however not as clear as described by the above given formulas. Below 200K "k" values between 3/2 and 5/2 were obtained. However in this temperature range the analysis is not so reliable because of the occurence of a FOMP ($H_{cr}<H_A$; but the temperature dependence of H_{cr} is approximately the same as that of H_A). Additionally another model might be valid at low temperatures. Recently it was shown that K_2 changes for Nd-Fe-B magnets the nucleation field H_n remarkable below room temperature ($H_n<H_A$) (17). This effect may also explain the temperature variation of "k". Above 200K the curves k(T) of the samples Crumax 40 and 30A are looking similar, independent of the fact that the sample "30A" is a heavy rare earth substituted Nd-Fe-B magnet. The k(T) of the two other magnets (Colt1 and Crumax 35) are lying at higher values. A mean value for k is approximately 5/2, which corresponds the power law as predicted by formula (8). A possible interpretation of the k(T) behaviour might be that either the coercivity mechanism changes from a pinning of the domain walls at grain boundaries at low temperatures to a volume pinning of extended domain walls at higher temperatures or that the reduction of "k" at low temperatures is caused by the increasing influence of K_2. The there interesting fact is that in all cases the anisotropy of the hard magnetic matrix seems to be of major importance for the coercivity of various Nd-Fe-B magnets. Fig.3 demonstrates that for k(T) the substitution of the Nd (Crumax 30A) is of minor importance, the different metallurgy (e. g. grain size, heat treatment) seems to influence $_I H_c(T)$ and consequently k(T). Concluding this discussion shows that, the experimental possibilty of measuring $_I H_c(T)$ as well as $H_A(T)$ on the same sample, gives for the first time the chance to find a correlation between these two magnet parameters. In order to test these models $_I H_c(T)$ and $H_A(T)$ studies on various permanent magnets, representing different coercivity mechanisms, (e.g. rapidly quenched Nd-Fe-B magnets, Sm-Co based materials but also ferrites) are therefore in progress.

Acknowledgement: This work was supported by the European Office of the U.S. Army Contract number: DAJA-45-84-C-0010.

Literature:

1) M.Sagawa,S.Fujimura,M.Togawa,H.Yamamoto, Y.Matsuura
J. Applied Phys. 55 (1984) 2083
2) J.J.Croat,J.F.Herbst,R.W.Lee,F.E.Pinkerton
J. Applied Phys. 55 (1984) 2078
3) P.Givord,H.S.Li,J.M.Moreau,R.Perrier de la Bathie,E. du Tremolet de Lacheisserie
Physica 130B (1985) 323
4) Yang Fu-Ming,Zhao Xi-Chao,Zhao Ru-Wen,Yu Zhi-Hong,Zhang Shou-Gong,Zhou Xi-Jian,Sun Tian-Duo
Proc. of eight Int. Workshop on rare-earth magnets. Dayton (USA) (1985) 529
5) G.Asti,F.Bolzoni
JMMM 15-18 (1980) 29
6) X.K.Sun
Thesis (1985) Techn. Univ. Vienna
7) R.Grössinger,X.K.Sun,R.Eibler,H.R.Kirchmayr
Proc. of eight Int. Workshop on rare-earth magnets. Dayton (USA) (1985) 553
8) R.Grössinger,H.R.Kirchmayr,R.Krewenka, K.S.V.L.Narasimhan,M.Sagawa
Proc. of eight Int. Workshop on rare-earth magnets. Dayton (USA) (1985) 565
9) G.Asti,S.Rinaldi
J. Applied Phys. 45 (1974) 3600
10)H.Träuble,O.Boser,H.Kronmüller,A.Seeger
phys. stat. sol. 10 (1965) 283
11)K.D.Durst,H.Kronmüller
JMMM (1986) in print
12)J.D.Livingston
Proc. of eigth Int. Workshop on rare-earth magnets. Dayton (USA) (1985) 423
13)R.Kütterer,H.R.Hilzinger,H.Kronmüller
JMMM 4 (1977) 1
14)H.Kromüller,H.R.Hilzinger
JMMM 2 (1976) 3
15)K.Hiraga,M.Hirabayashi,M.Sagawa,Y.Matsuura
Jap. Journ. of Applied Phys. 24 (1985) L30
16)H.Kronmüller,H.R.Hilzinger
JMMM 5 (1973) 27
17)G.Herzer,W.Fernengel,E.Adler
JMMM 58 (1986) 48

6

Journal of the Less-Common Metals, 132 (1987) 265 - 272

MAGNETIC ANISOTROPY IN $Pr_2(Fe_{1-x}Co_x)_{14}B$ COMPOUNDS

R. GRÖSSINGER, R. KREWENKA and H. R. KIRCHMAYR
Institut für Experimentalphysik, Technische Universität Wien, Wien A-1040 (Austria)
S. SINNEMA, YANG FU-MING*, HUANG YING-KAI† and F. R. DE BOER
Natuurkundig Laboratorium, University of Amsterdam, 1018 XE Amsterdam (The Netherlands)
K. H. J. BUSCHOW
Philips Research Laboratories, P.O. Box 80.000, 5600 JA Eindhoven (The Netherlands)

Summary

We have measured the concentration dependence of the Curie temperature, magnetization, anisotropy field and lattice parameters in $Pr_2(Fe_{1-x}Co_x)_{14}B$ for $0 < x < 1$. The Curie temperature strongly increases with x. The saturation magnetization at 4.2 K decreases with x after remaining approximately concentration independent up to $x = 0.2$. The room temperature anisotropy field first decreases with x but after passing through a minimum at about $x = 0.7$ strongly increases with x. The experimental results are compared with results obtained previously for $Nd_2(Fe_{1-x}Co_x)_{14}B$ and are discussed in terms of crystal-field effects.

1. Introduction

Compounds of the type $R_2Fe_{14}B$ (where R represents neodymium or praseodymium) are basic materials for the production of high quality permanent magnets [1, 2]. Both compounds crystallize in a tetragonal structure (space group $P4_2/mnm$) and combine a high saturation magnetization with a high uniaxial anisotropy at room temperature [3, 4]. A major disadvantage of the R–Fe–B magnets is their rather low Curie temperature ($T_c = 600$ K) [5]. Substitution of cobalt for iron leads to an increase in T_c. However, a further requirement for the attainment of high coercivity magnets is the presence of a high anisotropy. Recently we have investigated at room temperature the changes of the anisotropy field B_A caused by

*Permanent address: Institute of Physics, Academica Sinica, P.O. Box 603, Beijing, China.

†Permanent address: Institute of Metal Research, Academica Sinica, Wenhua Road, Shenyang, China.

0022-5088/87/$3.50

29

cobalt substitution in $Nd_2Fe_{14}B$ [6]. We found that B_A in $Nd(Fe_{1-x}Co_x)_{14}B$ exhibits a minimum near $x = 0.9$.

The purpose of the present study is to investigate whether similar features are also present in the concentration dependence of B_A in the series $Pr_2(Fe_{1-x}Co_x)_{14}B$.

2. Experimental results and discussion

The $Pr_2(Fe_{1-x}Co_x)_{14}B$ samples were prepared by arc melting under purified argon gas from starting materials with a purity of at least 99.9%. All samples were vacuum annealed for three weeks at about 900 °C. After this treatment the samples were found to be approximately single phase, remnants of the impurity phases being of the order of a few per cent. The composition dependence of the lattice constant is shown in Fig. 1.

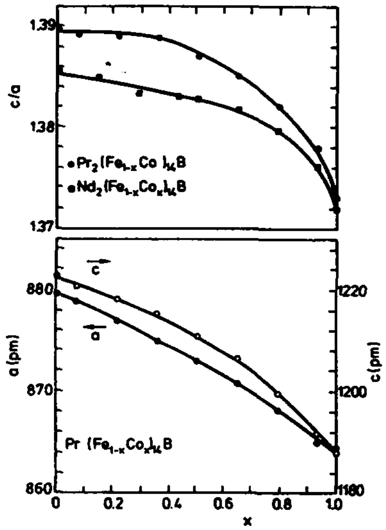


Fig. 1. Concentration dependence of the lattice constants in $Pr_2(Fe_{1-x}Co_x)_{14}B$ and $Nd_2(Fe_{1-x}Co_x)_{14}B$ compounds.

The high field magnetization measurements with B up to 35 T were performed at 4.2 K in the high field magnet at the University of Amsterdam [7]. For all measurements we used powdered samples after aligning the powder particles in a magnetic field and fixing their direction with epoxy resin. High field isotherms were recorded with the external field either

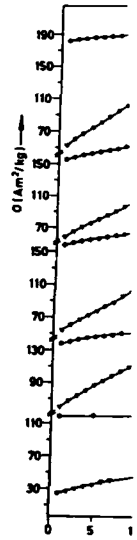
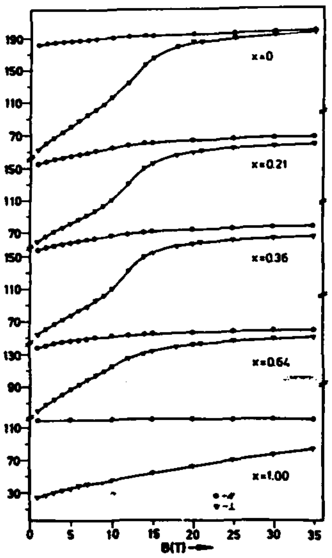


Fig. 2. Magneti pounds with th tion.

Fig. 3. Concentr 4.2 K.

parallel ($\sigma_\parallel$) examples of m tion magnetiz curves by ext $Pr_2(Fe_{1-x}Co_x$

It can be contents, the field applied the magnetiza This phenome process (FOMI and for the (N FOMP shows neglected in th these compou anisotropy-ene



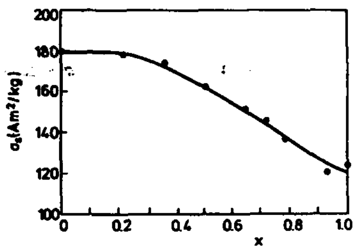


Fig. 2. Magnetization curves at 4.2 K of magnetically aligned $Pr_2(Fe_{1-x}Co_x)_{14}B$ compounds with the magnetic field applied parallel or perpendicular to the alignment direction.

Fig. 3. Concentration dependence of the saturation magnetization in $Pr_2(Fe_{1-x}Co_x)_{14}B$ at 4.2 K.

parallel ($\sigma_\parallel$) or perpendicular ($\sigma_\perp$) to the alignment field. In Fig. 2 some examples of measured magnetization curves are shown. Values for the saturation magnetization σ_s were derived from the high field part of the $\sigma(B)$ curves by extrapolating to $B = 0$. The concentration dependence of σ_s for $Pr_2(Fe_{1-x}Co_x)_{14}B$ at 4.2 K is shown in Fig. 3.

It can be seen in Fig. 2, that for the compounds with the higher iron contents, the high field magnetization curves, measured with the magnetic field applied perpendicular to the alignment direction, display a "jump" in the magnetization at a transition field which depends on the composition. This phenomenon can be understood in terms of a first-order magnetization process (FOMP), which has been observed for $Nd_2Fe_{14}B$ by Pareti *et al.* [8] and for the $(Nd, Pr)_2Fe_{14}B$ system by Huang *et al.* [9]. The existence of this FOMP shows that the sixth-order anisotropy constant K_3 cannot be neglected in the expression of the uniaxial magnetocrystalline anisotropy for these compounds. We have calculated the magnetization curves using an anisotropy-energy expression including K_3, but neglecting the in-plane

anisotropy. From the observation (in Fig. 2) that the perpendicular magnetization curves have a large intercept with the magnetization axis we can conclude that there is a substantial misalignment of the grains in the samples. This misalignment has been taken into account in the calculation of the magnetization curves. A gaussian distribution of the *c* axes of the grains around the alignment direction has been assumed. The neglect of the in-plane anisotropy is in disagreement with the observed different magnetization curves for $Nd_2Fe_{14}B$ in the [100] and [110] directions [10]. However, incorporation of the in-plane anisotropy in the calculations would lead to too many fitting parameters. For this reason the values of the anisotropy constants, as found in the performed analysis, must be considered as corresponding to values averaged over the basal plane. It can be seen from Fig. 4 that there is satisfactory agreement between the calculations and the experimental data. In Fig. 5 the composition dependence of the anisotropy constants at 4.2 K as obtained from this analysis are shown.

The Curie temperatures of the various compounds were determined by measuring the temperature dependence of the magnetization σ above room temperature by means of the Faraday method. The values of T_c were

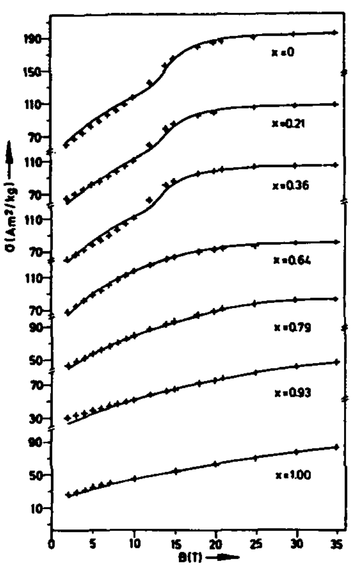


Fig. 4. Calculated (full lines) and experimental (plus signs) magnetization curves at 4.2 K of $Pr_2(Fe_{1-x}Co_x)_{14}B$ compounds with the field perpendicular to the alignment direction.

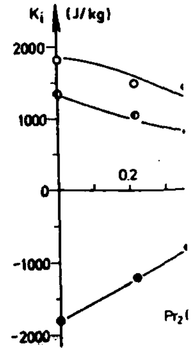


Fig. 5. Composition
4.2 K.

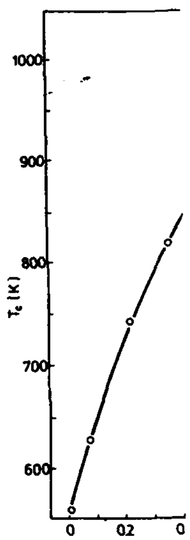


Fig. 6. Concentratio
pounds.

obtained by plotti
in Fig. 6. The con
temperature was c

ır mag-
we can
amples.
of the
grains
of the
metiza-
owever,
lead to
otropy
as cor-
n from
and the
otropy

rmined
above
T_c were

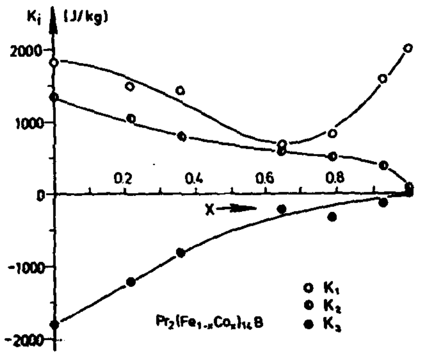


Fig. 5. Composition dependences of K_1, K_2 and K_3 in the $Pr_2(Fe_{1-x}Co_x)_{14}B$ system at 4.2 K.

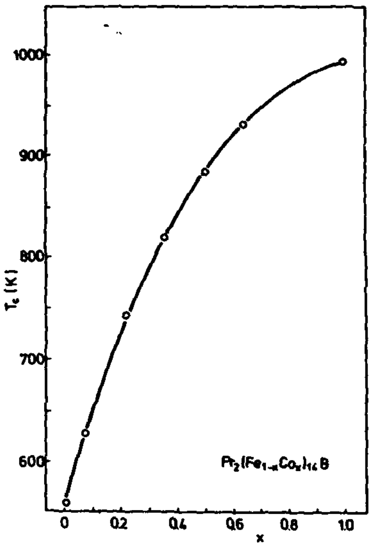


Fig. 6. Concentration dependence of the Curie temperature in $Pr_2(Fe_{1-x}Co_x)_{14}B$ compounds.

curves at
lignment

obtained by plotting σ^2 *vs.* T and extrapolating to $\sigma^2 \to 0$. Results are shown in Fig. 6. The concentration dependence of the anisotropy field B_A at room temperature was determined in a pulsed field system using the singular point

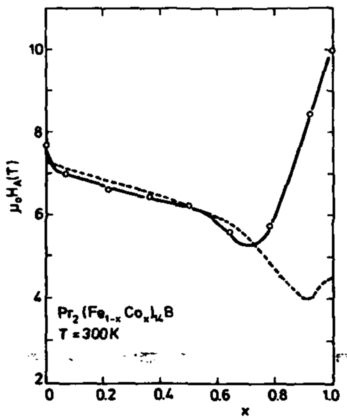


Fig. 7. Comparison of the room temperature anisotropy field $\mu_0 H_A$ in $Pr_2(Fe_{1-x}Co_x)_{14}B$ (full line) and $Nd_2(Fe_{1-x}Co_x)_{14}B$ (broken line).

detection (SPD) technique [11]. This method leads to a singularity at $B = B_A$ in experimental curves of d^2M/dt^2 *vs.* B (M is the magnetization) if the c axis is the easy magnetization direction. Such a situation is expected for the system $Pr_2(Fe_{1-x}Co_x)_{14}B$. The concentration dependence of B_A at room temperature is shown in Fig. 7. B_A decreases from more than 7 T for $x = 0$ to about 5 T for $x = 0.7$. At higher x values B_A is seen to increase strongly.

We have included in Fig. 7 the $B_A(x)$ values derived from the data published earlier for $Nd_2(Fe_{1-x}Co_x)_{14}B$ [6]. It is obvious that the concentration dependence of B_A for the iron-rich compounds is almost similar in both cases. However, a discrepancy between the two $B_A(x)$ curves is manifest for the compounds of relatively high cobalt concentration. Nevertheless the trend is evidently the same in both cases. The decrease in $B_A(x)$ observed for small x values is followed by an increase in $B_A(x)$ for high x values, the main difference being the location of the minimum of $B_A(x)$.

This minimum in the concentration dependence of the anisotropy field seems difficult to explain. It follows from the results of many previous investigations that the magnetocrystalline anisotropy in these materials is mainly determined by the single-ion crystal-field anisotropy of the rare earth component [12]. The minimum of B_A would then be indicative of a pronounced concentration-dependent change in one (or more) of the crystal-field parameters that determine the anisotropy. When attempting to relate the $B_A(x)$ behaviour to the corresponding changes in crystallographic properties it is well to recall that the increase of B_A in $Nd_2(Fe_{1-x}Co_x)_{14}B$ for $x > 0.9$ is accompanied by a strong reduction in the spin reorientation temperature (by about a factor of two) [6]. This suggests that it is primarily the

increase of K_1
(a shift of K_1
K_1 passes thro
Thus, if we ta
centrations at
sponding valu
second-order c
approximation
is expected to
B_2^0 also depen
increase mainl
mately consta
x while for h
moderately or
precisely the
$Pr_2(Fe_{1-x}Co_x)$
centration dep
charge conside
of Mössbauer
materials by c
of these sites
course, may
To exclude su
binary compo
lower in its ir
opposite beha
point charge c

3. Concluding

It follow
tion of cobalt
lographic and
minimum in
occurrence of
$Pr_2(Fe_{1-x}Co_x)$
the $B_A(x)$ curv
of this behavio
In the c
substitution in
temperature.
ture coefficien
small decrease
attainable in t

34

increase of K_1 which causes $B_A(x)$ to increase in this concentration range (a shift of K_1 towards more positive values lowers the temperature at which K_1 passes through zero and hence lowers the spin reorientation temperature). Thus, if we take it for granted that the increase in $B_A(x)$ for high cobalt concentrations at room temperature originates from an increase of the corresponding values of K_1 we may restrict ourselves to considering only the second-order crystal-field parameters, since $K_1 \propto 3B_2^0 - B_2^2$. In a point charge approximation the decrease in the lattice parameters with x shown in Fig. 1 is expected to lead to a general increase in both parameters. However, since B_2^0 also depends on the c/a ratio, this quantity will benefit from the general increase mainly at the beginning of the series, where the c/a ratio is approximately constant. For low x values one expects, therefore, K_1 to increase with x while for higher cobalt concentrations one expects K_1 to increase only moderately or even to decrease with x. Such a concentration dependence is precisely the opposite of that observed for B_A in $Nd_2(Fe_{1-x}Co_x)_{14}B$ and $Pr_2(Fe_{1-x}Co_x)_{14}B$ (Fig. 7). It seems therefore that explanations of the concentration dependence of the anisotropy in $R_2(Fe_{1-x}Co_x)_{14}B$ based on point charge considerations are unsatisfactory. Recently, it was shown by means of Mössbauer spectroscopy that the occupation of the 3d sites in the above materials by cobalt and iron is not a random occupation but that several of these sites are occupied preferentially by cobalt (iron) [13]. This, of course, may lead to a rather unusual concentration dependence of B_A. To exclude such short-range ordering effects we will concentrate on the pure binary compounds ($x = 0$ and $x = 1$). Then one finds that B_A in $Nd_2Co_{14}B$ is lower in its iron counterpart while the praseodymium compounds show the opposite behaviour (see Fig. 7). This still remains unexpected on the basis of point charge considerations.

3. Concluding remarks

It follows from the results shown in the preceding section that substitution of cobalt for iron in $Pr_2Fe_{14}B$ leads to gradual changes of the crystallographic and magnetic properties, the most prominent feature being the minimum in the concentration dependence of the anisotropy field. The occurrence of a minimum in the concentration dependence of B_A in $Pr_2(Fe_{1-x}Co_x)_{14}B$ is paralleled by the occurrence of a similar minimum in the $B_A(x)$ curve of $Nd_2(Fe_{1-x}Co_x)_{14}B$, but we are unable to trace the origin of this behaviour.

In the concentration range of practical interest ($0 < x < 0.2$) cobalt substitution in $R_2Fe_{14}B$ leads to a fairly strong enhancement of the Curie temperature. While this might have a beneficial influence on the temperature coefficient of the magnetization, it is unfortunately accompanied by a small decrease of the anisotropy, which might lower the coercive force attainable in these materials.

Acknowledgment

The investigations reported in this paper have been partly supported by the Concerted European Action on Magnets (CEAM). The part of the work performed at the Technical University of Vienna was supported by the European Office of the U.S. Army (Contract DAJA-45-86-C-0010). The work in Amsterdam was carried out within the scientific exchange programme between China and the Netherlands.

References

1 J. J. Croat, J. F. Herbst, R. W. Lee and F. E. Pinkerton, *J. Appl. Phys., 55* (1984) 2078.
2 M. Sagawa, S. Fujimura, N. Togawa, H. Yamamoto and Y. Matsuura, *J. Appl. Phys., 55* (1984) 2083.
3 J. F. Herbst, J. J. Croat, F. E. Pinkerton and W. P. Yelon, *Phys. Rev. B, 29* (1984) 4176.
4 D. Givord, H. S. Li, J. M. Moreau, R. Perrier de la Bâthie and E. du Trémolet de Lacheisserie, *Physica B, 130* (1985) 323.
5 S. Sinnema, R. J. Radwanski, J. J. M. Franse, D. B. de Mooij and K. H. J. Buschow, *J. Magn. Magn. Mater., 44* (1984) 333.
6 R. Grössinger, R. Krewenka, K. H. J. Buschow, X. K. Sun, R. Eibler and H. R. Kirchmayr, *J. Less-Common Met., 124* (1986) 165.
7 R. Gersdorf, F. R. de Boer, J. C. Wolfrat, F. A. Muller and L. W. Roeland, in M. Date (ed.), *High Field Magnetism*, North-Holland, Amsterdam, 1983, p. 277.
8 L. Pareti, F. Bolzoni and O. Moze, *Phys. Rev. B, 32* (1985) 7604.
9 Y.-K. Huang, F.-M. Yang and F. R. de Boer, to be published.
10 J. P. Gavigan, D. Givord, H. S. Li, P. Tenaud and T. Viadieau, *Proc. 3rd Int. Conf. on Physics of Magnetic Materials, Szczyrk-Bita, 1986.*
11 G. Asti and S. Rinaldi, *J. Appl. Phys., 45* (1974) 3600.
12 K. H. J. Buschow, *Materials Research Reps., 1* (1986).
13 H. M. van Noort and K. H. J. Buschow, *J. Less-Common Met., 113* (1985) L9.

36

7

Journal of the Less-Common Metals, *134* (1987) L17 - L21

Letter

137 16

Note on the coercivity in Nd–Fe–B magnets

R. GRÖSSINGER, R. KREWENKA and H. R. KIRCHMAYR
Institut für Experimentalphysik, Technische Universität, Wien, A-1040 (Austria)
P. NAASTEPAD
Philips Metalware Factories PMF, 5600 JA Eindhoven (The Netherlands)
K. H. J. BUSCHOW
Philips Research Laboratories, 5600 JA Eindhoven (The Netherlands)

(Received March 10, 1987)

In a previous study we addressed the problem of the origin of the coercive force in permanent magnets based on Nd–Fe–B. We showed that simple nucleation-controlled or pinning-controlled models are inadequate in explaining the temperature dependence of the coercive force over the whole temperature range considered [1]. The same problem was addressed recently by Durst and Kronmüller [2] who compared the temperature dependence of the coercive force (${}_JH_c$) with the temperature dependence of the anisotropy constant K_1, experimental values for K_1 (and K_2) being obtained on a sintered magnet body by means of the Sucksmith–Thompson method. From the linear relationship between ${}_JH_c$ and $2K_1/J_s$ (J_s is the saturation induction) observed in the range from about 280 K to 370 K, the conclusion reached by these authors was the applicability of a nucleation-controlled coercivity mechanism, changing to a pinning-controlled mechanism for temperatures in excess of 370 K [3].

Since the temperature range in which the linear relationship between ${}_JH_c$ and $2K_1/J_s$ (or between ${}_JH_c$ and the anisotropy field H_A) was observed to be valid is somewhat restricted, we have extended our measurements to lower temperatures. Apart from the Nd–Fe–B magnet studied previously we have included a magnet based on (Nd, Dy)–Fe–B in the present study.

The (Nd, Dy)–Fe–B magnet body was prepared as follows. Firstly, the constituent elements were melted together, the approximate formula composition being $Nd_{13.5}Dy_{1.5}Fe_{77}B_8$. Subsequently, fine powder particles were obtained by milling under freon. The particles were aligned in a magnetic field and compacted in a die. Liquid-phase sintering was performed in a protective atmosphere for 1 h at 1050 °C. A post-sintering treatment consisted of heating for 1 h at 630 °C. After magnetizing, the following characteristic room temperature values were obtained: coercive force ${}_JH_c$ = 1312 kA m^{-1} ($\mu_{0J}H_c$ = 1.64 T), remanence B_r = 1.04 T.

0022-5088/87/$3.50

The values of the Nd–Fe–B magnet without dysprosium addition, studied previously, were $_{J}H_c$ = 593 kA m^{-1}, B_r = 1.24 T. The coercive forces and the anisotropy fields H_A were measured in a pulsed field system from 77 K up to the Curie temperature. We used the singular point detection (SPD) technique [4] to obtain the latter values. Results for the two magnets studied are shown in Fig. 1. Here we recall that the SPD method leads to a singularity at $H = H_A$ in experimental curves of d^2M/dt^2 *vs.* H (M is the magnetization) if the c axis is the easy magnetization direction. However, it is well known that a spin reorientation from an easy c axis to an easy cone was found to occur in $Nd_2Fe_{14}B$ near T_s = 135 K [5]. If the anisotropy energy

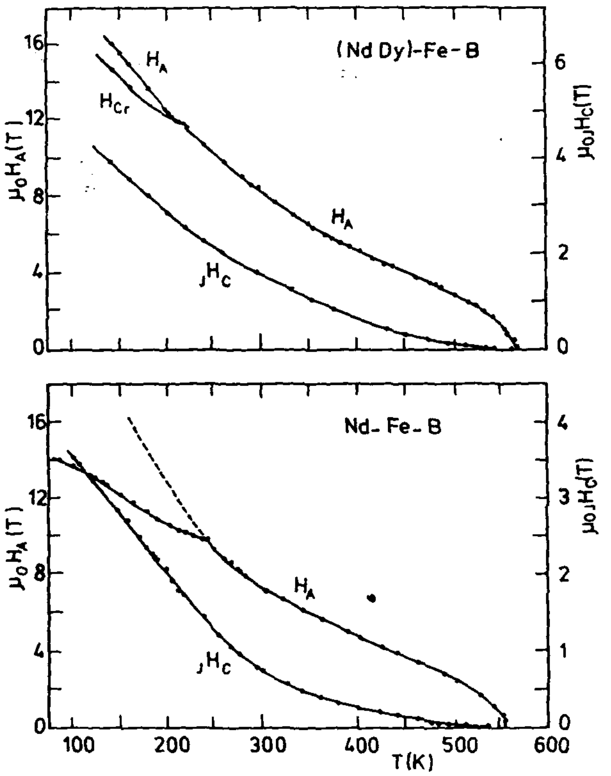


Fig. 1. Temperature dependence of the coercive field $_{J}H_c$, the anisotropy field H_A and the critical field for FOMP transitions H_{cr} in an (Nd, Dy)–Fe–B magnet (top part) and in an Nd–Fe–B magnet (bottom part).

can be writte
spin reorienta
Consequently
small and wh
the anisotrop
200 K [2,
constants lea
magnetizatio
range and j
referred to
description c
SPD data ob
1) made it
longer refle
values of th
magnet mat
neously the
200 K (see
In ord
Fe–B over
temperatur
mentioned
temperatur
H_A. This i
$Nd_2Fe_{14}B$
field depe
jump in th
16 T. Ext
value at 4
ature regi
extrapola
(broken l
H_A for N
obtained
extrapola
Sinnema
the valu
magnets
range ex
Plo
In both
the relat

$_{J}H_c$ = s

Here H,
the lin

can be written as $E_a = K_1\sin^2\theta + K_2\sin^4\theta$, a necessary condition for such a *spin reorientation* implies a change in sign of K_1 from positive to negative. Consequently there exists a temperature range above T_s where K_1 becomes small and where higher-order anisotropy constants determine the shape of the anisotropy energy surface. Such a situation is found in $Nd_2Fe_{14}B$ below 200 K [2, 6, 7]. The change in relative magnitude of the anisotropy constants leads to the occurrence of additional relative minima in E_a. The magnetization vector can no longer rotate smoothly in this temperature range and jumps in $M(H)$ can appear. This phenomenon is commonly referred to as a first-order magnetization process (FOMP). A theoretical description of it was given by Asti and Bolzoni [7]. A closer analysis of the SPD data obtained by us for the Nd–Fe–B magnet (see bottom part of Fig. 1) made it clear that the cusps in the dM^2/dt^2 curves of this material no longer reflect the value of H_A below about 250 K, but rather reflect the values of the critical field H_{cr} associated with the FOMP transition. For the magnet material based on (Nd, Dy)–Fe–B we were able to measure simultaneously the values of H_{cr} and H_A in a limited temperature range below about 200 K (see top part of Fig. 1).

In order to be able to analyse both the data of (Nd, Dy)–Fe–B and Nd–Fe–B over an extended temperature range it is necessary to first discuss the temperature dependence of H_A in the latter material below 250 K. It was mentioned above that the data points obtained by the SPD methods in this temperature range reflect the temperature dependence of H_{cr} rather than of H_A. This interpretation of the SPD data agrees with the data obtained on a $Nd_2Fe_{14}B$ single crystal by Cadogan *et al.* [8]. These authors measured the field dependence of the magnetization in the [100] direction and found a jump in the *M vs. H* curve which at 4.2 K occurs at a critical field of about 16 T. Extrapolation of the lower branch of our SPD curve leads to the same value at 4.2 K. Therefore, to obtain an estimate of H_A in the lower temperature region we have to use the higher branch of the SPD curve obtained by extrapolation of the curve found above $T \approx 250$ K to lower temperatures (broken line in the bottom part of Fig. 1). The temperature dependence of H_A for Nd–Fe–B represented by the broken line is consistent with H_A values obtained by static measurements reported in the literature. The broken line extrapolates to within 5% from the value $H_A = 30.5$ T at 4.2 K reported by Sinnema *et al.* [9] while the value of H_A at 190 K is also within 5% of the the value $H_A \approx 13$ T reported by Pareti *et al.* [10]. For both types of magnets we are now able to compare ${}_JH_c(T)$ with $H_A(T)$ in a temperature range extending over more than 400 K.

Plots of ${}_JH_c(T)$ *vs.* $H_A(T)$ for both magnet materials are given in Fig. 2. In both materials these plots can be characterized by extended regions where the relationship between both quantities is linear:

$$ {}_JH_c = s\,H_A + H_{eff} \qquad (1) $$

Here H_{eff} represents the intercept with the horizontal axis and s the slope of the linear part of the curve. The field H_{eff} can be regarded as an effective

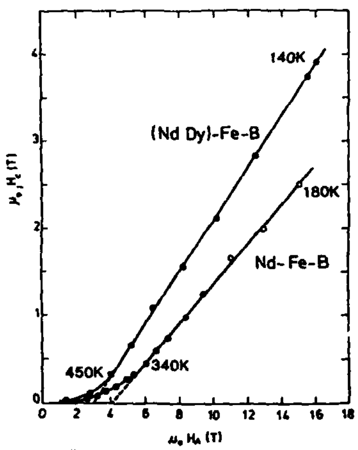


Fig. 2. Dependence of coercive field ${}_JH_c$ on anisotropy field H_A in an Nd–Fe–B magnet and an (Nd, Dy)–Fe–B magnet.

demagnetizing field which depends on the magnetization and which decreases with increasing temperature. This implies that the linear region extends to much higher temperatures when ${}_JH_c$ *vs.* $sH_A + H_{eff}$ is plotted and H_{eff} is taken to be proportional to the magnetization. The results described above are reminiscent of an approach for describing the temperature of ${}_JH_c$ proposed by Durst and Kronmüller [2, 3]. They considered the existence of magnetically less hard regions within the $Nd_2Fe_{14}B$ grains or at the grain boundaries which might serve as nucleation centres for reversed domains. These imperfect regions are taken largely to determine the coercive field, which in turn is determined by the nucleation field H_n. The results presented in Fig. 2 are somewhat surprising since they show that a perfectly linear behaviour extends for both types of materials to temperatures appreciably below room temperature. In fact, the linear behaviour between coercive force and anisotropy field seems to be valid even at 4.2 K. When using the relation $\mu_{0J}H_c = 0.23\ \mu_0 H_A - 4.1$ derived for Nd–Fe–B from the plot shown in Fig. 2, in conjunction with the value $\mu_0 H_A = 30.5$ T found by Sinnema *et al.* [9] at 4.2 K, one finds $\mu_{0J}H_c = 6.1$ T. This value is in satisfactory agreement with $\mu_{0J}H_c = 5.9$ T reported by Kuntze *et al.* [11] for the same temperature.

In conclusion, experimental results obtained from measurements of the temperature dependence of the anisotropy field and the coercivity together with experimental results reported in the literature for Nd–Fe–B base magnets show that the coercivity depends linearly on the anisotropy field in

a very br
temperatu
linear re
affected
Our data
force dep
in which
and K_3,
become l

1 R. Grö
Busch
2 K. D.
3 K. D.
4 G. Ast
5 D. Gi
Lache
6 F. M.
Proc.
Dayt
7 G. As
8 J. M.
Physi
9 S. Si
J. Ma
10 L. Pa
11 K. K
(198

a very broad temperature range. The latter range seems to extend from temperatures well above room temperature to 4.2 K, meaning that the linear relationship between these two experimental quantities is not affected by spin reorientation phenomena occurring below about 130 K. Our data speak in favour of a coercivity mechanism in which the coercive force depends linearly on the measured value of the anisotropy field, and in which the individual contributions of the anisotropy constants K_1, K_2 and K_3, which may have temperature dependences of opposing signs, become less directly apparent.

1 R. Grössinger, R. Krewenka, R. Eibler, H. R. Kirchmayr, J. Ormerod and K. H. J. Buschow, *J. Less-Common Met.*, *118* (1986) 167.
2 K. D. Durst and H. Kronmüller, *J. Magn. Magn. Mater.*, *59* (1986) 86.
3 K. D. Durst and H. Kronmüller, *J. Magn. Magn. Mater.*, to be published.
4 G. Asti and S. Rinaldi, *J. Appl. Phys.*, *45* (1974) 3600.
5 D. Givord, H. S. Li, J. M. Moreau, R. Perrier de la Bâthie and E. du Trémolet de Lacheisserie, *Physica B*, *130* (1985) 323.
6 F. M. Yang, X. C. Zhao, R. W. Zhao, Z. H. Yu and S. G. Zhang, in K. Strnat (ed.), *Proc. 8th Workshop on Rare Earth Magnets, Dayton, OH*, Dayton University Press, Dayton, 1985, p. 529.
7 G. Asti and F. Bolzoni, *J. Magn. Magn. Mater.*, *15 - 18* (1980) 29.
8 J. M. Cadogan, J. P. Gavigan, D. Givord and H. S. Li, *Proc. 3rd Int. Conf. on Physics of Magnetic Materials*, Sczyrk-Bila, Poland, 1986.
9 S. Sinnema, R. J. Radwanski, J. J. M. Franse, D. B. De Mooij and K. H. J. Buschow, *J. Magn. Magn. Mater.*, *44* (1984) 333.
10 L. Pareti, F. Bolzoni and O. Moze, *Phys. Rev. B*, *32* (1985) 7604.
11 K. Kuntze, D. Kohake, R. Beranek, S. Stieler and C. Heiden, *J. Phys. (Paris)*, *46* (1985)C6 - C253.

Nd–Fe–B magnet

ion and which
he linear region
$_{eff}$ is plotted and
results described
nperature of $_JH_c$
l the existence of
s or at the grain
eversed domains.
he coercive field,
results presented
a perfectly linear
atures appreciably
between coercive
K. When using the
B from the plot
30.5 T found by
is value is in satis-
e *et al.* [11] for the

easurements of the
coercivity together
for Nd–Fe–B base
e anisotropy field in

41

IEEE TRANSACTIONS ON MAGNETICS, VOL. MAG-23, NO. 5, SEPTEMBER 1987

8

ANISOTROPY AND HYSTERESIS STUDIES OF HIGHLY SUBSTITUTED Nd-Fe-B BASED PERMANENT MAGNETS

R.Grössinger, H.Harada *), A.Keresztes, H.R.Kirchmayr, M.Tokunaga*)

Inst. f. Experimentalphysik; Techn. Univ. Vienna A-1040 Karlsplatz 13; AUSTRIA
*) Hitachi Metals Ltd. Japan

ABSTRACT

Sintered Nd-Fe-B based permanent magnets where either the Nd was partly substituted by Dy or the Fe by Co or both (Dy and Co) were studied with respect to their anisotropy field H_A and their hysteresis loop between 100K and the Curie temperature. Dy increases H_A and consequently the coercivity $_IH_C$. Co reduces H_A only slightly, however $_IH_C$ decreases strongly. Substituting Dy and Co delivers a magnet with a temperature behaviour comparabel to a pure Nd-Fe-B magnet.

INTRODUCTION

Nd-Fe-B based materials exhibit excellent hard magnetic properties at room temperature. Due to the rather low Curie temperature of 589K the behaviour above room temperature is not yet sufficient. For this purpose attempts were undertaken to improve the magnet parameters at elevated temperature. The main problems arise from the strong decrease of the coercivity $_IH_C$ with increasing temperature (1,2). There exist two different strategies to enhance $_IH_C(T)$:

i) Partial substitution of the Nd by a heavy rare earth element like Dy or Tb. Such a substitution increases generally the anisotropy field H_A and consequently $_IH_C$ (3), which might improve $_IH_C$ at e.g. 100 °C also.
ii) Partial substitution of the Fe by Co. A Co substitution increases the Curie temeprature (4) and therefore a better temperature behaviour is expected. Below 50% Co the reduction of H_A is small; from this point of view only a minor decrease of $_IH_C$ is expected. Nevertheless a large decrease of $_IH_C$ due to the Co substitution was found (3) which can only be explained by assuming a different microstructure compared with the pure Nd-Fe-B magnets.

In order to study the responsible coercivity mechanism in more detail a set of sintered magnet samples with different heat treatments, but also with various substitutions (Dy and/or Co), which might improve the magnet parameters, were manufactured. As shown in table1 from each composition exist three different heat treatments. The first aim of the present study was to investigate the influence of a partial Dy and/or Co substitution on the magnet parameters like the coercivity and the remanence but also on the intrinsic magnetic anisotropy. Additionally the effect of the usual heat treatment should be investigated in order to test its influence on the coercivity mechanism.

EXPERIMENTAL

A series of orientated sintered permanent magnets of the composition (Nd,X)-(Fe,Y)-B with X=Dy and Y=Co was produced by Hitachi Metals Ltd. varying the heat treatment as well as the concentration as described in table1.

Table1: Sample concentration and heat treatment pattern of all magnets.

Samples	Alloy
A1-j	$Nd(Fe_{0.92}B_{0.08})_{5.5}$
A2-j	$(Nd_{0.9}Dy_{0.1})(Fe_{0.92}B_{0.08})_{5.5}$
A3-j	$(Nd_{0.8}Dy_{0.2})(Fe_{0.92}B_{0.08})_{5.5}$
A4-j	$(Nd_{0.7}Dy_{0.3})(Fe_{0.92}B_{0.08})_{5.5}$
B2-j	$Nd(Fe_{0.874}Co_{0.046}B_{0.08})_{5.5}$
B2-j	$Nd(Fe_{0.828}Co_{0.092}B_{0.08})_{5.5}$
B4-j	$Nd(Fe_{0.736}Co_{0.184}B_{0.08})_{5.5}$
C1-j	$(Nd_{0.8}Dy_{0.2})(Fe_{0.828}Co_{0.092}B_{0.08})_{5.5}$
C2-j	$(Nd_{0.8}Dy_{0.2})(Fe_{0.736}Co_{0.184}B_{0.08})_{5.5}$

Heat treatment pattern:
- j=1 as sintered (1090°C 2 hours)
- j=2 1090°C 2h and 900°C 2h then cooling at 1.3°C/min
- j=3 1090°C 2h and 900°C 2h then cooling with 1.3°C/min down to 600°C then quenched in water

From these samples the hysteresis loop and also the anisotropy field was measured between 77K and the Curie temperature using a pulsed field system ($\mu_0 H_{max}$=28T; pulse duration of a sin half wave 5ms). From the hysteresis loop the remanence and the coercivity field was determined. The anisotropy field was measured using the SPD (Singular Point Detection) technique (5).
The magnetization was calibrated using Fe powder (grain size 10µm) which was fixed in epoxy in order to avoid eddy current troubles. It should be mentioned that the accuracy of magnetization measurements depends strongly on the shape of the sample. Therefore for comparitive studies the sample geometry should be always identical.
The field calibration was performed by measuring $_IH_C$ of well known samples (e.g. barium ferrite and a YCo_5 single crystal). The absolute accuracy for the magnetization as well as for the field measurements is approximately 5% (worst case) the relative accuracy is 1%.

RESULTS

From Fig.1 with increasing Dy content increasing anisotropy is obvious. The ordering temperature is naturally not affected by the Dy substitution. Fig.2 shows the influence of a partial Co substitution. It is evident that small amounts of Co are of negligible influence on $H_A(T)$ below approximately 400K however the temperature where H_A disappears increases drastically due to the Co substitution -indicating that Co really enters into the 2/14/1 lattice. These results are in agreement with an anisotropy study of the mixed crystal series $Nd_2Fe_{14-x}Co_xB$ (6). From the above given data we know that Dy increases H_A but Co increases the Curie temperature. It would be interesting to combine these two

0018-9464/87/0900-2117$01.00©1987 IEEE

42

Best available Page

substitutions as was done in the samples C1-1,2,3 and C2-1,2,3. In Fig.3 $H_A(T)$ of the (Nd,Dy)-(Fe,B) is compared with that of corresponding Co substituted magnets. The result is similar as that shown in Fig.2; below 400K $H_A(T)$ is independent of such small Co substitutions but the Curie temperature rises due to the Co.

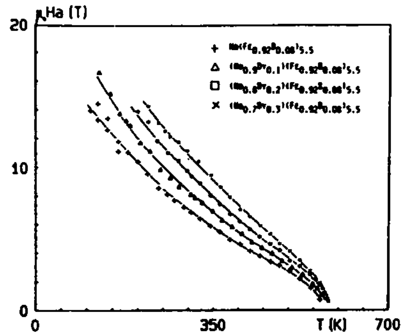


Fig.1: Temperature dependence of the anisotropy field of the samples A1-j (+), A2-j (Δ), A3-j (□) and A4-j (x) (j=1,2,3).

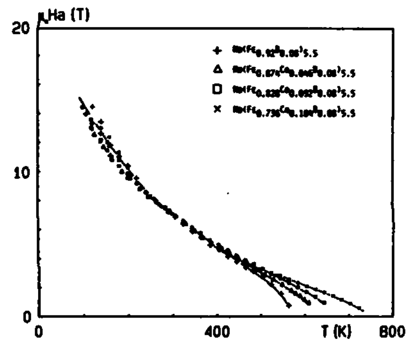


Fig.2: Temperature dependence of the anisotropy field of the samples A1-j (+), B2-j (Δ), B3-j (□) and B4-j (x) (j=1,2,3).

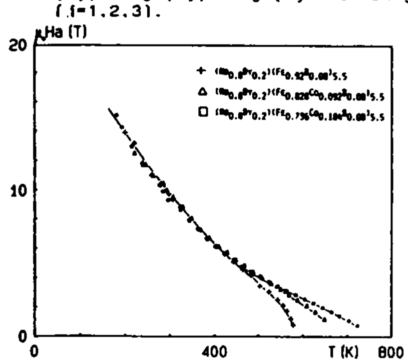


Fig.3: Temperature dependence of the anisotropy field of the samples A3-j (+), C1-j (Δ) and C2-j (□) (j=1,2,3).

Fig.1,2 and 3 show the temperature dependence of the anisotropy fields of all samples. Careful comparing studies demonstrated that for all magnets of the same composition but with varying heat treatments $H_A(T)$ was identical over the whole temperature range. This is not a trivial result because similar investigations performed on $SmCo_5$ based magnets showed strong variations of $H_A(T)$ with the heat treatment (7). The above given results are in general agreement with stochiometry studies of Nd-Fe-B based series, which gave also $H_A(T)$ curves which were independent of such variations (8). It should be mentioned that all Nd containing samples showed below 180K an anisotropy anomaly which is generally called a FOMP (First Order Magnetic Phase) transition. The physical origin of such a transition is that higher order anisotropy constants can influence the shape of the anisotropy energy in a manner that additional relative minima occurs which causes jumps in the M(H) curve. In $Nd_2Fe_{14}B$ below 135K a spinreorientation from the c-axis to an easy cone was found (9). This causes a change of sign of K_1 (first order anisotropy constant) and consequently rises the importance of K_2 and K_3. At 4.2K a jump of M(H) in the basal plane of a single crystal of $Nd_2Fe_{14}B$ was recently detected (10). A similar study performed on a sintered $Nd_{16}Fe_{77}B_8$ permanent magnet gave also such a jump at μ_0H_{cr}=16.3T at 4.2K (11). Therefore between 135K and 180K a change of the shape of the "SPD-singularity" indicates the appearence of such a FOMP transition below 180K, as was shown in more detail in (1). Sometimes both "singularities", that of the FOMP transition (H_{cr}) and that of the real anisotropy field (H_A) could be observed. Generally H_{cr} must be smaller than H_A; with decreasing temperature the difference between H_{cr} and H_A increases. Summarising the above described measurement demonstrates that H_A increases due to the Dy substitution strongly but it is nearly independent of the Co substitution.
However the Co enhances the Curie temperature which might be important for the temperature behaviour of the magnetization.
As mentioned previously the hysteresis loops as a function of temperature were also measured. From these measurements the remanence $M_r(T)$ and the coercivity $_IH_c(T)$ was deduced. Fig.4 shows $_IH_c(T)$ of the samples A1-3, A2-3, A3-3 and A4-3. The coercivity increases with increasing Dy amount drastically. In this case a correlation between the $_IH_c$ and H_A behaviour can be assumed. The remanence $M_r(T)$ is reduced due to the Dy substitution, as could be expected. In Fig.5 the corresponding curves for the magnets A1-3, B2-3, B3-3 and B4-3 are drawn. The remanence below 400K is nearly independent of the Co substitution but at higher temperatures the influence of the Co is obvious. Therefore $M_r(T)$ reflects a real improvement due to the Co substitution. However regarding $_IH_c$ (T) a reduction due to the Co substitution is evident, but this reduction is larger as could be expected according to H_A (T). The $_IH_c$ (T) curves of the Co containing magnets can be subdivided into two regions- one below room temperature with a large d_IH_c/dT and one above room temperature with a very small d_IH_c /dT. The slope d_IH_c /dT generally decreases with increasing Co substitution.
Fig.6 shows $_IH_c(T)$ of the samples A3-3, C1-3 and C2-3.

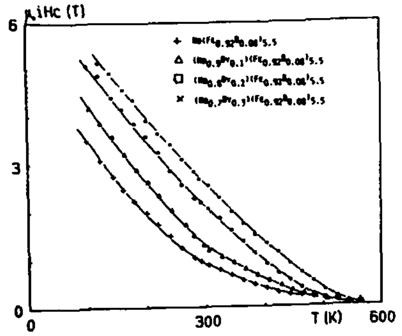


Fig.4: Temperature dependence of the coercivity field of the samples Ak-3 (k=1 (+),2 (Δ),3 (□),4 (x)).

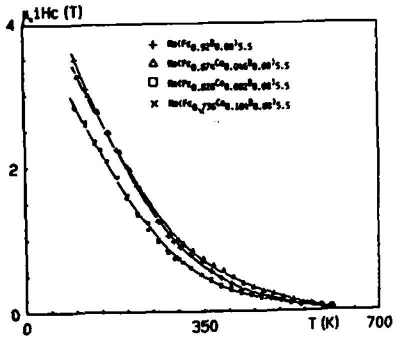


Fig.5: Temperature dependence of the coercivity of the samples A1-3 (+), B2-3 (Δ), B3-3 (□) and B4-3 (x).

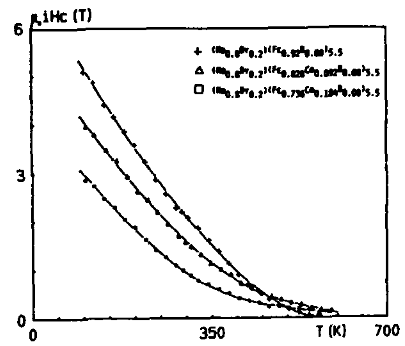


Fig.6: Temperature dependence of the coercivity of the samples A3-3 (+), C1-3 (Δ) and C2-3 (□).

Below approximately 400K $M_r(T)$ changes only slightly due to the Co, at elevated temperatures the Co influence is obvious. The reducing effect of Co on $_IH_C$ is in the Dy containing magnets more pronounced than in the pure Nd-Fe-B samples. It is worth to note that these highly substituted samples exhibit a temperature behaviour of the magnet parameters, which is comparable with that of a pure Nd-Fe-B magnet. Assuming a simple correlation between $_IH_C$ and H_A as demonstated in many coercivity models (12,13) such a drastic reduction of $_IH_C$ was not expected regarding H_A of these materials. Therefore the microstructure of Co substituted magnets must be much more unfavourable than in "normal" Nd-Fe-B magnets. A solution of the problem of "bad Co effect" seems only possible by searching for in Co adequate heat treatment or to find additives which cause a useful microstructure.

It should be mentioned that not only the hysteresis of the samples with the best heat treatment were studied but also the materials which were only sintered A,B,Ck-1 as well as the material with an intermediate heat treatment charecterised by the numbers A,B,Ck-2. The temperature behaviour of $_IH_C$ changes as a function of the heat treatment but also as a function of the sample composition. This might be an indication of a changed coercivity mechanism. A detailed analysis of all data presented here will be given in another work.

LITERATURE

1) R.Grössinger, R.Krewenka, K.S.V.L.Narasimhan, M.Sagawa JMMM 51 (1985) 160
2) D.Li, H.F.Mildrum, K.J.Strnat J. Appl. Phys. 57 (1985) 4140
3) M.Sagawa, S.Fujimura, H.Yamamoto, Y.Matsuura, K.Hiraga IEEE Trans. on Magn. MAG-20 (1984) 1584
4) Zhang Maocai, Ma Deqing, Jiang Xiuling, Liu Shiqiang Proc. of 8th Int. workshop on rare earth magnets Dayton (USA) (1985) 541
5) G.Asti, S.Rinaldi J. Appl. Phys. 45 (1974) 3600
6) R.Grössinger, R.Krewenka, X.K.Sun, K.H.J.Buschow, R.Eibler, H.R.Kirchmayr J. Less Com. Met. 124 (1986) 165
7) R.Grössinger, P.Obitsch, H.Kirchmayr, F.Rothwarf IEEE Trans. on Magn. MAG-20 (1984) 1575
8) R.Grössinger, X.K.Sun, R.Eibler, H.R.Kirchmayr Proc. of 8th Int. workshop on rare earth magnets Dayton (USA) (1985) 553
9) P.Givord, H.S.Li, J.M.Moreau, R.Perrier de la Bathie E. du Tremolet de Lacheisserie Physica 130B (1985) 323
10) J.P.Gavigan, D.Givord, H.S.Li, P.Tenaud, T.Viadieu Proc. of 3rd Int. Conf. on Physics of Magn. Mat. Szczyrk-Bila (Poland) (1986)
11) R.Grössinger et al. to be published
12) R.Kütterer, H.R.Hilzinger, H.Kronmüller JMMM 4 (1977) 1
13) G.Herzer, W.Fernengel, E.Adler JMMM 58 (1986) 48

TEMPERATURE DEPENDENCE OF THE COERCIVITY AND THE ANISOTROPY OF Nd-Fe-B BASED MAGNETS

R.Grössinger, R.Krewenko, F.Hoslinger, M.Sagawa*), H.R.Kirchmayr

Inst. f. Experimentalphysik, Techn. Univ. Vienna, A-1040 Karlsplatz 13; Austria
*) Sumitomo Special Metals Ltd.

ABSTRACT

The temperature dependence of the coercivity $_IH_C$ and the anisotropy field H_A from Nd-Fe-B based sintered permanent magnets was measured from 100K up to the Curie temperature. A $Pr_{15}Fe_{77}B_8$ magnet and a series of the compositions $Nd_{14.5}Dy_{1.5}(Fe_{77.5-x}Co_x)B_7$ (x=0,10,20) were studied in order to achieve improvements of the temperature characteristic above room temperature. The Co substitution increases naturally the Curie temperature but it chances H_A at room temperature only slightly. The coercivity however is reduced so drastically, that the temperature behaviour of the sample with x=20 is comparabel to that of a pure Nd-Fe-B magnet. The best results in this respect were achieved with a heavy rare earth substituted material (x=0) and with the $Pr_{15}Fe_{77}B_8$ sample. Additionally it was tried to correlate $_IH_C(T)$ and $H_A(T)$ using two different models in order to get information about the coercivity mechanism. The results thus obtained are in general agreement with the usual picture of the coercivity mechanism valid in Nd-Fe-B based magnets.

INTRODUCTION

Magnets based on Nd-Fe-B have reached a standard, which is beyond that of Sm-Co materials. At room temperature a high remanent induction of more than 12 kG is combined with coercivity fields between 10 and 20 kOe. Consequently magnets with energy products higher than 40 MGOe were achieved (see e.g. (1)). The main restriction of Nd-Fe-B magnets comes from the rather low Curie temperature of 570K, which is responsible for the strong temperature dependence of the coercivity $_IH_C$ and the remanence at elevated temperatures (see e.g. 2,3). The temperature behaviour of the remanence can be described by a Brillouin function similar as that of the saturation magnetization M_s. For the temperature dependence of the coercivity up to now no physically reasonable analytical description exists. However in any model description of the coercivity field a rough correlation between the anisotropy and $_IH_C$ is assumed (4). Additional influences (as e.g. the grain size, the occurence of impurity phases etc.) depending on the metallurgical process of the magnet (as e.g. the heat treatment) determine the coercivity mechanism and consequently the real type of the correlation between $_IH_C$ and the anisotropy.

The aim of the present work is to investigate the temperature dependence of the coercivity and the anisotropy field of Nd-Fe-B based magnets in order to test possible correlations between these properties over an entire temperature range. Additionally the highly substituted samples should be tested with respect to possible improvements, especially concerning the behaviour of the magnetic parameters above room temperature.

EXPERIMENTAL

The following orientated, sintered magnet samples, supplied by Sumitomo Corp., were studied: a pure Nd-Fe-B magnet ("sum 1"), a heavy rare earth substituted material (Neomax 30H) and a pure $Pr_{15}Fe_{77}B_8$ magnet. Additionally a set of samples with the composition $Nd_{14.5}Dy_{1.5}(Fe_{77.5-x}Co_x)B_7$ (x=0,10,20) was available. The hysteresis loops (from which the remanence M_r and the coercivity $_IH_C$ were determined) and H_A were measured between 100K and the Curie temperature using a pulsed field system (μ_0H_{max} =28T; pulse duration of a sin half wave is 5ms). The anisotropy was measured using the SPD (Singular Point Detection) technique (5). The calibration procedure is described in (6).

RESULTS AND DISCUSSION

Fig.1 shows $H_A(T)$ of the first series of Nd-Fe-B based magnets. $H_A(T)$ of the heavy rare

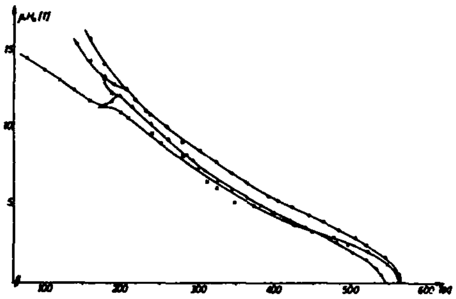


Fig.1 Temperature dependence of the anisotropy field of the Sumitomo-magnets: "sum 1" (x), 30H (o) and $Pr_{15}Fe_{77}B_8$ (▲).

earth substituted magnet (30H) lies above the other $H_A(T)$ curves, whereas $H_A(T)$ of the $Pr_{15}Fe_{77}B_8$ magnet is only slightly different from that of the pure Nd-Fe-B sample. At lower temperatures (T<200K) $H_A(T)$ of the pure as well as of the 30H magnet splits up into two branches. The upper branch represents the usual anisotropy field. The lower branch is the critical field due to a first order magnetization process (FOMP) as it has been observed for all compounds (R,Nd)-Fe-B (R=Y,La, Ce) containing Nd (7). The theoretical background of such a transition was explained in (8). Below 135K a change of the easy axis from the c-axis to an easy cone occurs in all Nd containing samples, as was found for a $Nd_2Fe_{14}B$ single crystal too (9). In a $Pr_2Fe_{14}B$ sample a FOMP anomaly was detected in pulsed field measurements (10) but not believed regarding the first anisotropy studies. Nevertheless it was recently found at 4.2K

0018-9464/87/0900-2114$01.00©1987 IEEE

(11) in static high field results also. Fig.2 shows the temperature dependence of $_IH_c$ of the above described samples. $_IH_c(T)$ of the heavy rare earth substituted magnet (30H) lies due to the larger H_A values above $_IH_c(T)$ of the pure Nd-Fe-B sample.
It is worthwhile to note that the coercivity of the $Pr_{15}Fe_{77}B_8$ magnet is 16kOe at room temperature, a value which corresponds nearly to that of the 30H specimen, inspite of the

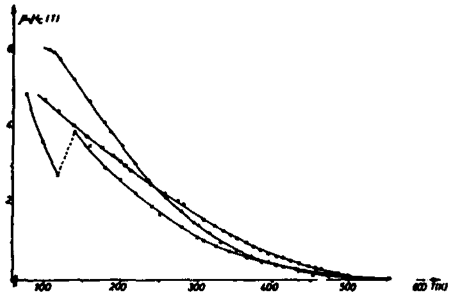


Fig.2 Temperature dependence of the coercivity field of the Sumitomo-magnets: "sum 1" (x), 30H (o) and $Pr_{15}Fe_{77}B_8$ (Δ).

fact that H_A(T=300K) of $Pr_{15}Fe_{77}B_8$ is only slightly larger than that of the pure Nd-Fe-B magnet (see Fig.1).
For improving the temperature behaviour of $_IH_c$, substituted magnets of the composition $Nd_{14.5}Dy_{1.5}(Fe_{77.5-x}Co_x)B_7$ were produced. In Fig.3 the temperature dependence of the anisotropy fields is drawn. At low temperatures all curves show a splitting into two branches. The situation is similar to that discussed for the Nd-Fe-B magnets above. Generally $H_A(T)$ decreases due to the Co substitution slightly as was found in the mixed crystal series $Nd_2Fe_{14-x}Co_xB$ for the Fe-rich side too (12). Consequently at room temperature the anisotropy field is (within 3kOe) the same for all these samples. Fig.4 shows the temperature dependence of the coercivity of these samples. It is evident that $_IH_c(T)$ decreases with increasing Co substitution. At room temperature $_IH_c$ decreases from 19.5 kOe (x=0) to 15 kOe (x=10) and finally to 12 kOe (x=20). This value is approximately the same as that of a pure Nd-Fe-B magnet. Additionally, inspite of the increase of the temperature where H_A vanishes (x=0: T=554K; x=10: T=675K; x=20: T=766K), $_IH_c$ disappears always at approximately 580K independent of the Co substitution. The reason why $H_A(T)$ behaves near the Curie temperature different from $_IH_c(T)$ is not yet clear. It is evident that $_IH_c(T)$ could not be improved by these substitutions.
Summarising, it can be concluded that attempts to improve the temperature behaviour by substituting Nd partly by Dy and by substituting Fe partly by Co were not successfull. The reducing effect of Co on $_IH_c(T)$ is so drastic, that the resulting material is as good as a pure Nd-Fe-B magnet. Consequently this highly substituted compound does not solve the above mentioned problems. As mentioned previously, $_IH_c$ can be improved either by using Pr instead of Nd or by substituting Nd partly by Dy. Unfortunately

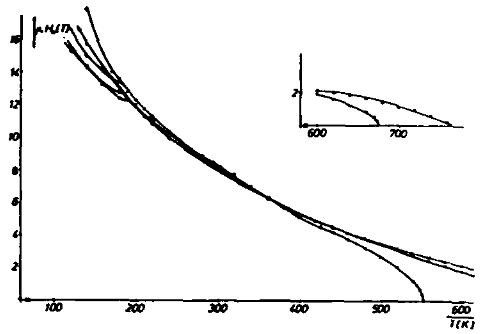


Fig.3 Temperature dependence of the anisotropy field of the $Nd_{14.5}Dy_{1.5}(Fe_{77.5-x}Co_x)B_7$ magnets: x=0 (x), x=10 (o), x=20 (Δ).

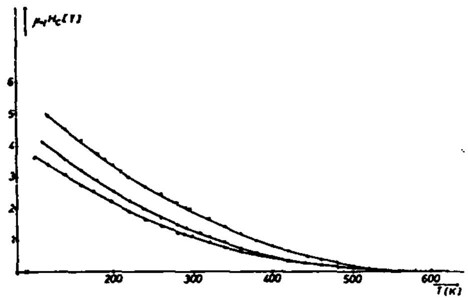


Fig.4 Temperature dependence of the coercivity field of the $Nd_{14.5}Dy_{1.5}(Fe_{77.5-x}Co_x)B_7$ magnets: x=0 (x), x=10 (o), x=20 (Δ).

this does not lead to the high temperature, high quality magnet.

ANALYSIS

As mentioned previously in any model the coercivity is related to the magneto-crystalline anisotropy. A first approach starts with a formula of the type (4):

$$_IH_c(T) \text{ proportional to } (H_n(T))^k \quad (1)$$

According to the fact that the nucleation field H_n can be written as $2K_1/M_s$ we replaced H_n by the anisotropy field H_A, which we can really measure. The power factor "k" can be 1/2, 1, 3/2 and 5/2 depending on the responsible coercivity mechanism. Consequently by plotting $\ln(_IH_c(T)/_IH_c(T=300K))$ divided by $\ln(H_A(T)/H_A(T=300K))$ vs the temperature T describes k(T) which is correlated to the coercivity mechanism and its temperature behaviour. If such a procedure is performed on the samples described here a k(T) is obtained, which is nearly independent of the sample composition. k(T) starts at low temperatures at approximately 3/2 and increases with increasing temperature approaching a value of 5/2 above room temperature. A similar behaviour was found for a series of Nd-Fe-B based magnets from Colt Industries (13), but also for the second series of magnets with the composition $Nd_{14.5}Dy_{1.5}(Fe_{77.5-x}Co_x)B_7$. k=3/2

was theoretically obtained by assuming a pinning of the domain walls (thickness d) at planar defects or grain boundaries (thickness D) where D<d must be valid (4). From electron microscopy studies contraversal values for D were determined which are either 2-3nm according to (14) or 10 and 50 nm according to (15), whereas the domain wall width is approximately 5 nm (16). This means that D<d but also D>d is possible. k=5/2 was obtained for low coercivity magnets assuming that broader domain walls are pinned at statistical distributed defects ("volume pinning") (4). Additionally it should be mentioned that the influence of K_2, which is not negligible at low temperatures, makes the validity of a model which uses $H_n = H_A = 2K_1/M_s$ doubtfull.
Recently a more detailed model describing the coercivity of Nd-Fe-B magnets appeared (17). This model starts with a formula of the type:

$$_iH_c) = c(H_n) - nM_s \qquad (2)$$

H_n is the nucleation field, however it was calculated taking the influence of K_2 (K_2 ...second order anisotropy constant) also into account. If $K_2 > 0.4K_1$ H_n is always smaller than the anisotropy field $H_A = (2K_1 + 2K_2)/M_s$, which is valid especially for Nd-Fe-B magnets below room temperature. Above room temperature H_n can be replaced by H_A . The constant "c" describes the exchange interaction across the grain boundaries. For ideally isolated grains c should approach to 1, whereas if exchange coupling of neighbouring grains is dominant c=0 is assumed. The term "$-nM_s$" represents the local stray field at the grain boundaries. We tried to combine the two above given model and used a formula of the type:

$$_iH_c(T) = c(H_A(T))^k - nM_s \qquad (3)$$

The parameters c,k and the term "$-nM_s$ " were determined by plotting $_iH_c(T)$ vs $H_A(T)$, taking all possible values of "k" (1/2, 1, 3/2, 5/2). In table 1 the best suited parameters are summarised.

Table 1: "k", "c" and "$-nM_s$" of the studied magnets.

Sample	k	c	$-nM_s$ (T)
sum1	5/2	0.12	0.4
30H	1	0.31	1.0
$Pr_{15}Fe_{77}B_8$	3/2	0.21	0.53
$Nd_{14.5}Dy_{1.5}(Fe_{77.0-x}Co_x)B_7$			
x=0	1	0.36	1.09
x=10	1	0.28	1.50
x=20	1	0.30	1.26

This new analysis gives a mean, temperature independent power factor "k" which is in four of the studied samples equal to 1. According to (4) k=1 can be obtained assuming two different coercivity mechanisms:

i) nucleation of reverse domains in the magnetically soft phase
ii) pinning of domain walls (thickness d) at planar defects or at grain boundaries (thickness D) if D>d is valid.

For Nd-Fe-B based magnets the first explanation is more probable. The coefficient "c" is always close to 0.3 indicating a strong exchange coupling between neighbouring grains. The demagnetizing field "$-nM_s$" is rather large (1T) which points to irregulary shaped grains.

It is clear that these attempts to analyse $_iH_c(T)$ and $H_A(T)$ are only first steps to get a better understanding of these properties. Additionally it should be pointed out that all three models (formula 1, 2 and 3) are only attempts to find a correlation between $_iH_c$ and H_A. Up to now we believe that a fit procedure where the measured $_iH_c(T)$, $H_A(T)$ and $M_s(T)$ is approached using formula 3 (c,k, and n are free fit parameters) would be the best procedure. Such an analysis is in progress. The meaning of k values unequal to one should be subject of further theoretical considerations.

ACKNOWLEDGEMENT

This work was supported by the European Office of the U.S. Army Contract number DAJA-45-86-C-0010.

LITERATURE

1) J.D.Livingston
Proc. of 8th Int. workshop on rare-earth magnets Dayton (USA) (1985) 423
2) R.Grössinger, R.Krewenka, K.S.V.L.Narasimhan, M.Sagawa
JMMM 51 (1985) 160
3) K.S.V.L.Narasimhan
J. Applied Phys. 57 (1985) 4081
4) R.Kütterer, H.R.Hilzinger, H.Kronmüller
JMMM 4 (1977) 1
5) G.Asti, S.Rinaldi
J. Applied Phys. 45 (1974) 3600
6) R.Grössinger, H.Harada, A.Keresztes, H.R.Kirchmayr, M.Tokunaga
IEEE Trans. on Magn. (1987) same issue
7) R.Grössimger, X.K.Sun, R.Eibler, H.R.Kirchmayr
Proc. of 8th Int. workshop on rare-earth magnets Dayton (USA) (1985) 553
8) G.Asti, F.Bolzoni
JMMM 15-18 (1980) 29
9) D.Givord, H.S.Li, J.M.Moreau, R.Perrier de la Bathie, E du Tremolet de Lacheisserie
Physica 130B (1985) 323
10) R.Grössinger, X.K.Sun, R.Eibler, K.H.J.Buschow, H.R.Kirchmayr
J. de Physique Tome 46 (1985) C6-221
11) R.Grössinger, R.Krewenka, H.R.Kirchmayr, S.Sinnema, Yang Fu-Ming, Huang Ying-Kai, F.R. de Boer, K.H.J.Buschow
J. Less Com. Met. (1986) submitted
12) R.Grössinger, R.Krewenka, X.K.Sun, R.Eibler, H.R.Kirchmayr, K.H.J.Buschow
J. Less Com. Met. 124 (1986) 165
13) R.Grössinger, R.Krewenka, K.S.V.L.Narasimhan, H.R.Kirchmayr
IEEE Trans. on Magn. MAG-22 (1986) 760
14) K.Hiraga, M.Hirabayashi, M.Sagawa, Y.Matsuura
Jap. J. of Applied Phys. 24 (1985) L30
15) M.Tokunaga, M.Tobise, N.Meguro, H.Harada
Proc. of Intermag (1986) Phoenix (USA)
16) H.Szymczak, E.Burzo, W.E.Wallace
J. de Physique Tome 46 (1985) C6-309
17) G.Herzer, W.Fernengel, E.Adler
JMMM 58 (1986) 48

J. Magnetism a. Magn. Mat. 4 (1977) 1

/8/ R. Grössinger, R. Krewenka, F. Haslinger, M. Sagawa, H.R. Kirchmayr
Proc. of Intermag (1987) Tokyo

/9/ M. Sagawa, S. Hirosawa, K. Tokuhara, H. Yamamoto, S. Fujimura, Y. Tsubokawa, R.Shimizu
J. Applied Physics 61(8) (1987) 3559

10/ M. Sagawa, S. Fujimura, H. Yamamoto, K. Hiraga
IEEE Trans. on Magn. MAG-20 (1984) 1584

/11/ R. Grossinger, R. Krewenka, K.S.V.L. Narasimhan, M. Sagawa
J. Magnetism a. Magn. Mat. 51 (1985) 160

/12/ M. Sagawa, Y. Matsuura, S. Fujimura, H. Yamamoto, S. Hirosawa
IEEE Trans. on Magn. MAG-1 (1985) 48

/13/ Zhang Maocai, Ma Deqing, Jiang Xiuling, Liu Shiqiang
Proc. of 8th Int. workshop on rare earth magnets (Ed. K.J. Strnat) Univ Dayton (1985) p. 541

/14/ M. Jurczyk
J. Magnetism a. Magn. Mat. 67 (1987) 187

/15/ G. Asti, S. Rinaldi
J. Applied Physics 45 (1974) 3600

/16/ R. Grössinger, H. Harada, A Keresztes, H.R. Kirchmayr, M. Tokunaga
Proc. of Intermag (1987) Tokyo

/17/ Y. Matsuura, S. Hirosawa, S. Fujimura, M. Sagawa
Applied Physics Letters 46 (1985) 308

/18/ K. Hiraga, M. Hirabayashi, M. Sagawa, Y. Matsuura
Japanese J. of Applied Physics 24(1) (1985) L30

/19/ A. Handstein, J. Schneider, U. Heinecke, R. Grössinger, Zhang Shougong
this conference

/20/ M. Endoh, M. Tokunaga, H. Harada
Proc. of Intermag (1987) Tokyo

/21/ G. Herzer, W. Fernengel, E. Adler
J. Magnetism a. Magn. Mat. 58 (1986) 48

/22/ R. Grössinger, R. Krewenka, R. Eibler, H.R. Kirchmayr, J. Ormerod, K.H.J. Buschow
J. Less Common Metals 118 (1986) 167

48

MAGNETIC PROPERTIES OF SINTERED $Nd_{16}(Fe_{100-x}Al_x)_{78}B_6$ MAGNETS

A. Handstein[+], J. Schneider[+], U. Heinecke[++], R. Grössinger[+++], and Zhang Shougong[++++]

+ Zentralinstitut für Festkörperphysik und Werkstofforschung der AdW der DDR, Dresden, GDR
++ Hochschule für Verkehrswesen, Wissenschaftsbereich Physik, Dresden, GDR
+++ Institut für Experimentalphysik, TU Wien, Vienna, Austria
++++ Institute of Physics, Cinese Academy of Sciences, Beijing, China

ABSTRACT

The effects of substitution of Fe by Al on the saturation magnetisation J_s, intrinsic coercive force $_JH_c$, anisotropy field H_A as well as on the character of the hysteresis loops in $Nd_{16}(Fe_{100-x}Al_x)_{78}B_6$ sintered magnets with x = 0, 2, 4, 6, 8, and 10 were investigated in the temperature range from 100 K to 295 K. The phase constitution and microstructure were studied by X-ray diffraction and electron probe microanalysis. It is found that the magnetic reversal behaviour remains a nucleation dominated one. While H_A decreases with x the coercive field of the hard magnetic phase increases. The substitution of Fe by Al in $Nd_{16}(Fe_{100-x}Al_x)_{78}B_6$ seems to deteriorate the hard magnetic properties at a lower Al-content than in $Nd_{16}(Fe_{100-x}Al_x)_{76}B_8$.

INTRODUCTION

The NdFeB permanent magnets posses certain disadvantages such a low Curie temperature T_c, insufficiently high values of the coercive fields $_JH_c$, and high temperature coefficients of remanence B_r and $_JH_c$. Substituting Nd by heavy rare-earth elements like Dy or Tb an increase of the anisotropy field H_A as well as an increase of $_JH_c$ was observed /1, 2/. However, the temperature coefficients of $_JH_c$ and B_r are still high.

* * * * * * * * *

Paper no. WP8.12 at the 9th International Workshop on Rare-Earth Magnets and Their Applications, Bad Soden, FRG, August 31 - September 2, 1987 (Proceedings Book by: Deutsche Physikalische Gesellschaft e.V., D-5340 Bad Honnef 1, FRG).

Adress inquiries to: A. Handstein, ZFW, AdW der DDR, Postfach, Dresden, DDR-8027, GDR.

An improvement of the temperature coefficient of $_JH_c$ was found by substituting of Co for Fe, which give rise to an increase of the Curie temperature T_c /3 to 5/. On the other hand the addition of Co lowers $_JH_c$.

Recently it has been found that the substitution of Fe by Al in $Nd_{16}Fe_{76}B_8$ results in a remarkable increase of $_JH_c$ /6/. The decrease of B_r and of the energy product $(B \cdot H)_{max}$ with increasing Al-content is smaller than the observed variation of $_JH_c$. Besides the changes of B_r and $_JH_c$ also the changes of the character of the demagnetisation curves by additions of Al have to be analysed to clarify the effect of Al in improvement the magnetic properties of NdFeB permanent magnets. Furthermore the influence of Al on the value of H_A and on the microstructure have to be studied to understand the underlying mechanism for the increase of $_JH_c$.

In this paper the effect of the substitution of Fe by Al in $Nd_{16}(Fe_{100-x}Al_x)_{78}B_6$ on $_JH_c$, J_s, H_A, and the magnetisation processes has been investigated.

EXPERIMENTAL

The specimens used in the present study were prepared by the standard powder metallurgy methods. The nominal compositions of the magnets are $Nd_{16}(Fe_{100-x}Al_x)_{78}B_6$ with x = 0, 2, 4, 6, 8, and 10. The hysteresis loops of the sintered magnets were measured on cylindrical samples (diameter 2.9 mm, height 6.0 mm) by a ballistic method in the temperature range from 100 K to 293 K and in applied static fields up to $\mu_0 H_i$ = 6.7 T. The demagnetisation of the samples was done by thermal treatment. In addition the superconducting coil was demagnetised by an ac-current with decreasing amplitudes before the measurement of the virgin curves. The anisotropy field H_A was determined from pulse field measurements up to $\mu_0 H$ = 25 T applying the SPD-technique (Singular Point Detection) /7/.

The phase constitution and microstructure were studied by X-ray diffraction and electron probe microanalysis.

RESULTS AND DISCUSSION

Table I summarises the experimentally observed values of $_JH_c$, H_A and J_s at room temperature (RT) for $Nd_{16}(Fe_{100-x}Al_x)_{78}B_6$. The values of T_c are also included. The observed decrease of T_c with x may be correlated with the observed increase of the lattice parameter c (see Table I). The X-ray diffraction analysis indicates that the lattice parameter a remains constant with increasing x (a = 0.882 nm) /8/.

Figure 1 shows the virgin magnetisation curves of the $Nd_{16}(Fe_{100-x}Al_x)_{78}B_6$ samples after thermal demagnetisation. The steep increase of magnetisation of all samples points to easy

movable domain walls at low fields. The shape of the observed virgin magnetisation and demagnetisation curves characterizes the Nd-Fe-Al-B magnets as hard magnetic materials with nucleation dominated magnetisation reversal behaviour. The term "nucleation dominated behaviour" includes pinning at the surface of particles. By substituting Al for Fe in Nd-Fe-B magnets the character of the magnetisation reversal behaviour does not change. The demagnetisation curves and recoil loops for $Nd_{16}(Fe_{100-x}Al_x)_{78}B_6$ with x = 0, 6, and 8 are given in Figures 2a to 2c at temperatures 293 K and 100 K.

All samples with and without Al exhibit a dip in the second quadrant of the demagnetisation curve. The decrease of J at small demagnetising fields is small for x = 0, 2, and 4 and becomes more pronounced for x ≥ 6. The appearence of a dip in the demagnetisation curve as well as the shape of the major hysteresis loop point to the existence of a mixture of soft and hard magnetic phases. The enlargement of the dip with increasing Al-content is attributed to an increase of the volume portion of the soft magnetic phase.

Comparing the demagnetisation curves for different temperatures (see Figures 2a to 2c) one finds an enlargement of the dip at lower temperatures for a given Al-content. This behaviour may be connected with the spin reorientation and the appearence of an easy cone of magnetisation (see e.g. /9/).

One may perform a simple kind of magnetic phase analysis assuming the major hysteresis loops are given by a simple superposition of the hysteresis loops of the present soft and hard magnetic phases (see also /10/). This type of magnetic phase analysis enables us to estimate the increase of the volume portion α of the soft magnetic phase with increasing Al-content. The following values of α ($\alpha = J_s^{soft} \cdot V^{soft} / J_s^{total} \cdot V^{total}$; $V^{total} = V^{soft} + V^{hard}$, V - volume) are obtained: $\alpha \approx$ 0.08 for x = 0, 2, and 4, $\alpha \approx$ 0.13 for x = 6, and $\alpha \approx$ 0.74 for x = 8.

In this way also the values of the coercive field $_JH_c^*$ of the hard magnetic phase in the present phase mixture may be deduced. The values of $_JH_c^*$ versus x for $Nd_{16}(Fe_{100-x}Al_x)_{78}B_6$ at RT (see Table I) follow the observed behaviour of $_JH_c$ in $Nd_{16}(Fe_{100-x}Al_x)_{76}B_8$ /6/. The values of $_JH_c^*$ for $Nd_{16}(Fe_{100-x}Al_x)_{78}B_6$ differ remarkable from those of $_JH_c$ (coercive force of the alloy) for x > 6 (see Figure 3). The different dependence of $_JH_c$ on Al-concentration for these two series of permanent magnets and the appearence of a large dip in the demagnetization curves for $Nd_{16}(Fe_{100-x}Al_x)_{78}B_6$ with x ≥ 6 may indicate that the hard magnetic properties of this alloy system are already deteriorated at a lower Al-content by reducing the B-concentration.

The observed increase of $_JH_c^*$ in $Nd_{16}(Fe_{100-x}Al_x)_{78}B_6$ with increasing Al-content x does not correlate with the behaviour of the anisotropy field H_A as function of x. H_A decreases slightly with increasing x. The temperature and Al-concentration dependence

of H_A are given for a comparison in *Figure 4* and *Table I*, respectively.

The experimentally observed temperature dependence of $_JH_c$ for Nd-Fe-B permanent magnets may be well described over a large temperature range by a formula for nucleation of reversed domains in a soft magnetic region near the surface of the $Nd_2Fe_{14}B$ matrix grains (intergrain boundary region) /11/. However, the equation

$$_JH_c^{*} = H_n = 2\,(K_1 / J_s) \cdot (\delta_B / \pi\, r_o) - N_{eff} \cdot J_s$$

(N_{eff} - demagnetisation factor) fails for explaining the observed behaviour of $_JH_c^{*}$ versus Al-content in these Nd-Fe-Al-B permanent magnets assuming the value of ($\delta_B / \pi\, r_o$) remains unchanged (δ_B - domain wall width, r_o - half width of the inhomogeneous grain boundary). The influence of Al on the coercive force $_JH_c^{*}$ is probably caused by its metallurgical effects. The electron probe microanalysis indicates that beside a solubility of Al in the main phase $Nd_2Fe_{14}B$ already at x = 4 small regions rich in Al appear nearby the Nd-rich regions and within the matrix. At higher Al-content these Al-rich regions may give rise finally a division of the $Nd_2Fe_{14}B$ phase /8/.

A deeper understanding of the coercive mechanism demands further studies of the microstructure and of the micromagnetic parameters of the present phases in these permanent magnets.

Table I: Dependence of saturation magnetisation J_s, intrinsic coercive field $_JH_c$, coercive field $_JH_c^{*}$ of the hard magnetic phase, anisotropy field H_A, lattice parameter c at 293 K and Curie temperature T_c on the Al-content in $Nd_{16}(Fe_{100-x}Al_x)_{78}B_6$.

x		0	2	4	6	8	10
J_s	(T)	1.33	1.29	1.18	1.14	1.04	
$\mu_{o\,J}H_c$	(T)	0.91	1.33	1.52	1.70	0.48	0.37
$\mu_{o\,J}H_c^{*}$	(T)	0.9	1.3	1.5	1.65	1.8	
$\mu_o H_A$	(T)	7.5	7.3	6.9	6.7	6.4	6.2
c	(nm)	1.222	1.225	1.226	1.229	1.230	
T_c	(K)	590	583	575	568	556	546

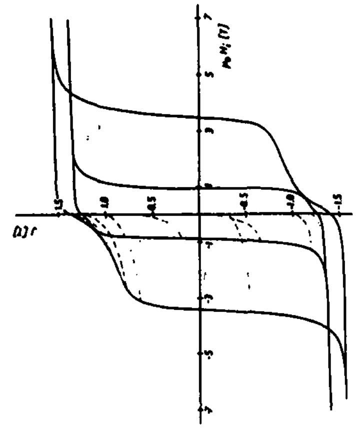


Figure 2: Hysteresis loops and recoil loops for $Nd_{16}(Fe_{100-x}Al_x)_{78}B_6$ at 293 K and 100 K.
a) x = 0

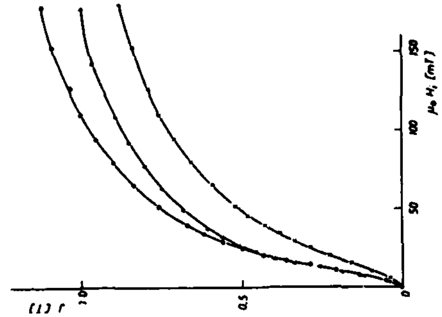


Figure 1: Virgin magnetization curves for $Nd_{16}(Fe_{100-x}Al_x)_{78}B_6$ at 293 K.

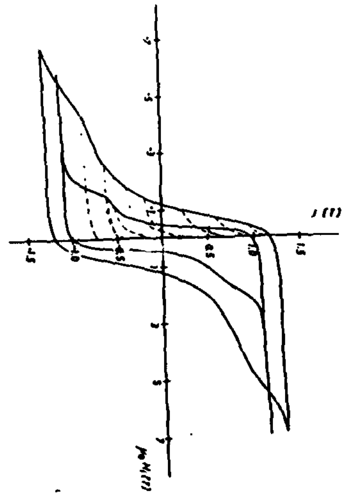


Figure 2a: x = 8

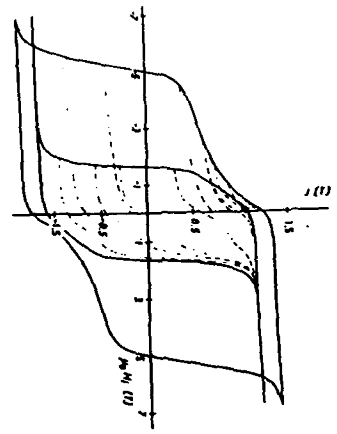
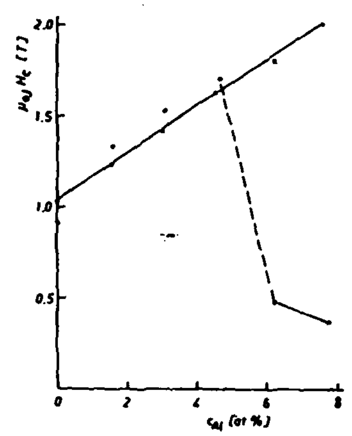


Figure 2b: x = 6



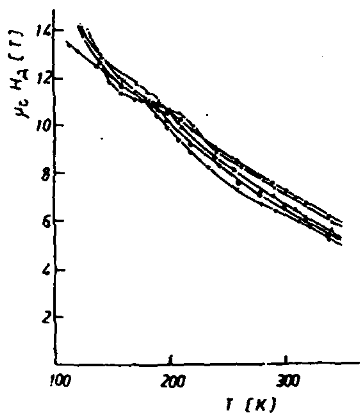


Figure 3: Dependence of the intrinsic coercive force $_JH_c$ on Al-concentration C_{Al}:
- • – $Nd_{16}(Fe_{100-x}Al_x)_{76}B_8$ /6/,
- o – $Nd_{16}(Fe_{100-x}Al_x)_{78}B_6$,
- x – $_JH_c^{\,M}$ (see Table 1).

Figure 4: Temperature dependence of the anisotropy field H_A for $Nd_{16}(Fe_{100-x}Al_x)_{78}B_6$:
• – x=0, x – x=2, Δ – x=4,
o – x=6, ▲ – x=8.

REFERENCES

/1/ M. Sagawa, S. Fujimura, H. Yamamoto, and K. Hiraga, IEEE Trans. Magn. MAG-20 (1985) p. 1584.

/2/ R. Grössinger, R. Krewenka, K.S.V.L. Narasimhan, and M. Sagawa, J. Magn. Magn. Mater. 51 (1985) p. 160.

/3/ Sun Guangfei, Xiao Yaofu, Zhou Shouseng, Liu Shiqiang, and Wang Run, Internat. Conf. on Magnetism, San Francisco, USA, 1985, paper 5Pd1.

/4/ Bao-Min Ma, K.S.V.L. Narasimhan, IEEE Trans. Magn. MAG-22 (1986) p. 916.

/5/ T. Mizoguchi, I. Sakai, H. Niu, and K. Inomata, IEEE Trans. Magn. MAG-22 (1986) p. 919.

/6/ Zhang Maocai, Ma Deqing, Jiang Xinling, and Liu Shiqiang, Proc. 8th Internat. Workshop on Rare-Earth Magnets (ed. K.J. Strnat), University of Dayton, Ohio, 1985, p. 541.

/7/ R. Grössinger, P. Obitsch, X.K. Sun, R. Eibler, H.R. Kirchmayr, F. Rothwarf, and H. Sassik, Mater. Letters 2 (1984) p. 539.

/8/ W. Fischer, N. Mattern, A. Handstein et al., to be published.

/9/ K.H. Müller, A. Handstein, D. Eckert, and J. Schneider, phys. stat. sol. (a) 99 (1987) p. K 61.

/10/ R. Grössinger, P. Haslinger, Zhang Shougong et al., to be published.

/11/ K.-D. Durst and H. Kronmüller, submitted to J. Magn. Magn. Mater. (1986).

MAGNETIC PROPERTIES OF SINTERED Nd-Fe-Al-B MAGNETS

W. Rodewald

VACUUMSCHMELZE GmbH, P.O. 2253, D-6450 Hanau, FRG

ABSTRACT

In sintered Nd-Fe-Al-B magnets a partial substitution of Fe by Al decreases the saturation polarization by ~ 0,04 T per at.% Al and the Curie temperature by ~ 8 K per at.% Al in the alloy. The magnetocrystalline anisotropy field strength is not changed up to Al concentrations of about 2 at.% Al. Higher Al concentrations up to 10 at.% cause a decrease of the anisotropy field strength by ~ 1,3 kA/cm per at.% Al. However there is an increased coercivity of sintered magnets which is probably due to an improved microstructure. The coefficient S_v of the thermal aftereffect increases from about 45 A/cm of ternary Nd-Fe-B magnets to about 90 A/cm for magnets containing 4 at.% Al.

1. INTRODUCTION

Sintered permanent magnets based on the $Nd_2Fe_{14}B$ compound have an excellent saturation polarization, but suffer from the low Curie temperature and the strong dependence of the intrinsic coercivity on the temperature. The Curie temperature can be increased by a partial substitution of Fe by Co /1, 5/, but the temperature dependence of the intrinsic coercive field strength is not improved.
The intrinsic coercivity can be increased by a partial substitution of Nd by Tb or Dy; that is due to the stronger anisotropy field strength of the $Tb_2Fe_{14}B$ or $Dy_2Fe_{14}B$ compounds /2/. From the investigations of Zhang Mocai /3/ it is known, that additions of Al increase the coercive field strength.
In this report we present the dependence of the saturation polarization J_s, the anisotropy field strength H_A, the intrinsic coercivity $_JH_c$ at temperatures of 20°C, 60°C, 100°C and 150°C, the Curie temperature T_c and the coefficient S_v of the thermal aftereffect on the Al-concentration.

****

Paper No.WP 8.14 at the 9th International Workshop on Rare-Earth Magnets and their Applications, Bad Soden, FRG, August 31 - September 2, 1987 (Proceedings Book by. Deutsche Physikalische Gesellschaft e.V., D-5340 Bad Honnef 1, FRG.

Adress inquiries to: W. Rodewald, VACUUMSCHMELZE GmbH, P.O. 2253, D-6450 Hanau 1, FRG

This work was partly supported by the Commission of the European Communities within the Stimulation Programme.

5̄3

12

DOES A Co SUBSTITUTION REALLY IMPROVE THE TEMPERATURE DEPENDENCE OF Nd-Fe-B BASED PERMANENT MAGNETS?

R. Grössinger

Institut für Expermentalphysik; Techn. Univ. Vienna, Austria

ABSTRACT

The anisotropy behaviour of $R_2Fe_{14-x}Co_xB$ (R=La,Nd,Pr) is surveyed. The system with the nonmagnetic La allows the study of the influence of the pure Fe-Co substitution on the magnetic anisotropy. The mixed crystal series with Nd show on the Co rich side two spinreorientations; one at a temperature T_1 below room temperature which is attributed to the Nd ion and a second at an elevated temperature T_2 which is caused by the competition between the uniaxial Nd and the planar (Fe,Co) sublattice. $Pr_2Fe_{14-x}Co_xB$ shows also such a high temperature spinreorientation. Generally the Co increases the temperature dependence of H_A; consequently the thus substituted magnets cannot solve the temperature problems of Nd-Fe-B based permanent magnets.

****

Paper no. S1.2 at the 5th International Symposium on Magnetic Anisotropy and Coercivity in Rare Earth-Transition Metal Alloys, Bad Soden, FRG, September 3, 1987 (Proceedings Book by: Deutsche Physikalische Gesellschaft e.V., D-5340 Bad Honef 1, FRG).

Address inquiries to: R. Grössinger; Inst. f. Experimentalphysik A-1040 Wien Karlsplatz 13; Austria.

Acknowledgement: This work was partly supported by the European Office of the U.S. Army (Contract no. DAJA-45-86-C-0010).

1 INTRODUCTION

The main problem in Nd-Fe-B based permanent magnets is the rather low Curie temperature of this material. Consequently the coercivity decreases with increasing temperature too fast. From a technical point of view a magnet material is desired which exhibits at 150°C an energy product of 160 kJ/m^3. At this temperature the demagnetizing curve should be linear (this means $B_r = {}_sH_c$) but also the irreversibel losses due to the elevated temperature should be negligible. Many efforts of the last years were therefore performed in order to overcome this restriction. The common step for increasing the Curie temperature is a partial Co substitution, e.g. 20% Co increases T_C from 580K to approximately 800K, which should be sufficient /1/. In order to develope a reasonable coercivity a high uniaxial magnetocrystalline anisotropy is necessary. Therefore the influence of the Fe by Co substitution on the magnetic anisotropy is of great importance for technical applications. For this purpose the anisotropy fields H_A of the following mixed crystal series were measured: $La_2Fe_{14-x}Co_xB$, $Nd_2Fe_{14-x}Co_xB$ and $Pr_2Fe_{14-x}Co_xB$. The effect of such a substitution on the 3d sublattice alone can be seen on the series $La_2Fe_{14-x}Co_xB$. A similar study exists on $Y_2Fe_{14-x}Co_xB$ /2/. The systems with Nd and Pr are first of all technical relevant. Additionally the interaction between the 4f-3d sublattice might cause some new interesting anisotropy effects. The details of these investigations were published in different other papers /3,4,5/. It is the aim of this paper to summerize all aspects and effects of a Fe-Co substitution and to discuss it with respect to the application in technical permanent magnets.

2 EXPERIMENTAL

All samples were prepared by arc melting under purified argon gas from starting materials of at least 99.9% purity. In order to get single phased specimen they were vacuum annealed for 3 weeks at about 900°C.

The temperature dependence of the anisotropy field was determined using the SPD (Singular Point Detection) method /6/. These measurements were performed in a pulsed field system (max. available field 28T; for details see /7/) between 4.2K and the Curie temperature. The lowest temperature were H_A was measured is determined by the magnitude of H_A which is only detectable up to a value of approximately 30% below the maximum of the available external field. In some cases magnetization measurements on aligned powder applying the external field parallel or perpendicular to the *preferential axis* using the high field facility of Amsterdam (max. achievable field 40T /8/) exists. The spinreorientation *was studied* by measuring the initial susceptibility between 4.2K and room temperature.

3 RESULTS AND DISCUSSION

3.1 $La_2Fe_{14-x}Co_xB$

La is nonmagnetic, therefore the system $La_2Fe_{14-x}Co_xB$ enables us to investigate the effect of a Fe-Co substitution. It should be noted that all $R_2Fe_{14}B$ compounds with a nonmagnetic R-ion as R= Y,La or Lu exhibit an easy c-axis /9/, whereas the corresponding Co compounds orientate preferential in the plane /10/. Additionally shows the temperature dependence of the anisotropy field of the $R_2Fe_{14}B$ compounds (R=nonmagnetic ions) *an anomaly*, i.e. it increases with temperature in the range 4-350 K and decreases at higher temperatures /9/. The tendency exists in Co substituted compounds also as visible regarding Fig.1 which shows $H_A(T)$ of $La_2Fe_{14-x}Co_xB$. *For a further discussion* the concentration dependence is also of interest as shown in Fig.2 /5/.

Both curves-the temperature and also the concentration *dependence*-reflects a complex anisotropy behaviour, which cannot be explained using a simple One Ion model. A possible explanation is either based on the assumption of a preferential substitution, as was recently found by /11/, or a consequence of a considerable spontaneous volume magnetostriction as was indeed

detected in these compounds /12,13/. Decisive experiments which explanation is valid are outstanding. The fact that $H_A(T)$ vanishes approximately at the ordering temperature supports the idea that the 3d magnetism and consequently its anisotropy behaviour is a band effect in this materials. Therefore the (Fe,Co) act together as a unit which develops as a whole a certain anisotropy with a preferential axis.

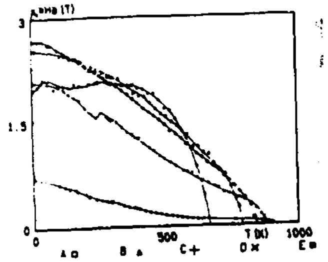


Fig.1 Temperature dependence of H_A of the mixed crystal series $La_2Fe_{14-x}Co_xB$.

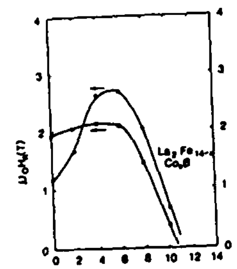
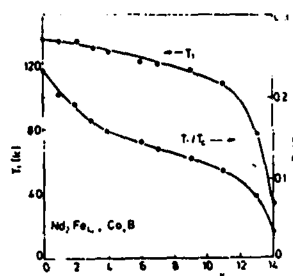


Fig.2 Concentration dependence of H_A at T=4.2K (●) and at room temperature (■) of $La_2Fe_{14-x}Co_xB$.

3.2 $Nd_2Fe_{14-x}Co_xB$

$Nd_2Fe_{14}B$ is the basic compound which causes the excellent hard magnetic properties of this new magnet family. It is uniaxial at room temperature but below 135K a spinreorientation to an easy cone occurs /14/. This spinreorientation is a crystal field effect of the Nd-ions. Substituting Fe by Co causes a decrease of this low temperatur spinreorientation temperature T_1 (see Fig.3) /3/. This spinreorientation causes a change of the sign of the first anisotropy constant K_1. Consequently a jump in M(H) below approximately 220K was detected which is generally called a FOMP (First Order Magnetization Process) transition /15/. It was recently shown that higher order anisotropy constants (especially the planar anisotropy energy constants) account for



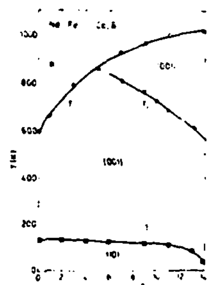


Fig.3 Concentration dependence of the spinreorientation temperature T_1 and its normalised value T_1/T_c of $Nd_2Fe_{14-x}Co_xB$ (left picture).

Fig.4 Magnetic phase diagram of $Nd_2Fe_{14-x}Co_xB$ (right picture).

this magnetization behaviour /16/. There is only a minor influence of the Co substitution on the transition temperature where such a FOMP can be detected (between $0 \leq x \leq 10$). The competition between the uniaxial Nd-sublattice and the planar (Fe,Co) sublattice causes a second spin reorientation at

elevated temperatures (called temperature T_s) on the Co rich side. The resulting magnetic phase diagram is shown in Fig.4. In order to get some information about the effect of the Co substitution on $H_A(T)$ a normalised plot $(H_A(T)/H_A(T=4.2K))$ vs T/T_c was used (see Fig.5 and Fig.6). The fact that the slope of this curve increases with increasing amount of Co (even on the Fe rich side where no second spinreorientation occurs) points to a systematic change of the temperature dependence of the anisotropy field. This explanation is very rough, however the situation in these systems is so complicated (six different 3d sites with different anisotropy contributions with different temperature dependencies which might additionally depend on the Fe-Co surrounding) that a clearer discussion is not yet possible. On the Co rich side the situation is dictated by the high temperature spinreorientation, which causes a vanishing of the uniaxial anisotropy field which is far below the ordering temperature.



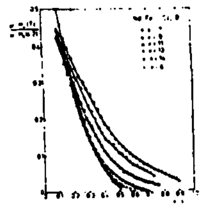


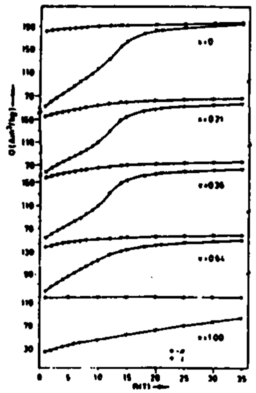
Fig.5 Reduced anisotropy field vs. reduced temperature in iron-rich $Nd_2Fe_{14-x}Co_xB$ compounds (left picture).

Fig.6 Reduced anisotropy Field vs. reduced temperature in cobalt rich $Nd_2Fe_{14-x}Co_xB$ compounds (right picture).

3.3 $Pr_2Fe_{14-x}Co_xB$

$Pr_2Fe_{14}B$ is uniaxial from 4.2K up to the Curie temperature /9,17/. However the M(H) curve (T=4.2K) of aligned powder, applying the external field perpendicular to the preferential axis, shows jumps at higher fields /4/. (see Fig.7). These jumps indicate also the importance of higher order anisotropy constants at low temperatures. Such FOMP transitions were first observed on the Fe rich side only, later we found it over the whole concentration range using a differentiating technique in a transient field. It is quiet shure that the Nd ion as well as the Pr ion is responsible for this anisotropy anomaly in such compounds. There exist several other compounds with these elements like e.g. $PrCo_5$ $Pr_2(Fe,Co)_{17}$ or $NdCo_5$ and $NdCo_2$ which show also spinreorientations or FOMP transitions (see e.g. /18-21/) indicating an energy level system which favours temperature or field induced reorientations.

Comparing the anisotropy behaviour of the boundary compounds of



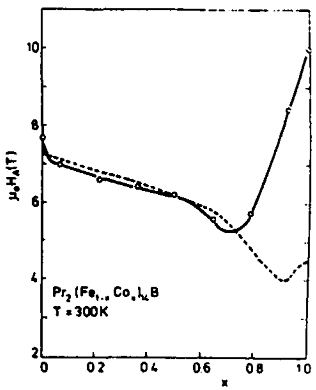


Fig.7 Magnetization curves at 4.2K of magnetically aligned $Pr_2(Fe_{1-x}Co_x)_{14}B$ compounds with the magnetic field applied parallel or perpendicular to the alignement direction (left picture).

Fig.8 Comparison of the room temperature anisotropy fields $\mu_0 H_A$ in $Pr_2(Fe_{1-x}Co_x)_{14}B$ (full line) and $Nd_2(Fe_{1-x}Co_x)_{14}B$ (broken line) (right picture).

the two mixed crystal series $R_2(Fe,Co)_{14}B$ (R=Nd,Pr) another curious fact becomes visible.

The anisotropy data of the there interesting compounds are shown in table I.

Table I: Anisotropy data of the compounds $R_2Fe_{14}B$ and $R_2Co_{14}B$ (R=Nd and Pr) /10,17/.

Compound	$\mu_0 H_A(T)$ at 4.2K
$Nd_2Fe_{14}B$	32
$Nd_2Co_{14}B$	30
$Pr_2Fe_{14}B$	29
$Pr_2Co_{14}B$	75

The remarkable high anisotropy of the $Pr_2Co_{14}B$ compound was reported by two different groups /10,22/. Inspite of the fact that H_A was determined by an extrapolation procedure the order of magnitude is believed. Additionally shows the concentration dependence of H_A (at room temperature) in both cases (R=Nd,Pr) an upturn on the Co rich side (see Fig.8). This increase is more pronounced in the Pr system. At lower temperatures this effect becomes stronger /22/. The concentration dependence of H_A points to a nonstatistical Fe-Co substitution. There exists up to now no reasonable explanation for the huge anisotropy of $Pr_2Co_{14}B$. The lattice constants and consequently the c/a ratios are very similar /4/. The corresponding RCo_5 and R_2Co_{17} (R=Pr or Nd) compounds are also not uniaxial at low temperatures /23,24/. In the case of the 1/5 materials it should be mentiomed that the rare earth contribution is negativ at 4.2K (easy plane case) and the competition with the uniaxial Co sublattice causes a cone structure at low temperatures /23/. The 2/17 compounds show for both sublattices and consequently for the material as a whole a preferential easy plane. This means that this comparison shows similarities between the easy axis behaviour of the 1/5 and the 2/14/1 compounds but it does not help to explain the unusual high anisotropy of $Pr_2Co_{14}B$. All data existing up to now leads

57

only to the assumption that the high anisotropy of $Pr_2Co_{14}B$ is a consequence of the Pr-Co interaction; possibly a polarisation effect of the Co on the Pr. Due to the uncertainty which exist by determining the anisotropy of $Pr_2Co_{14}B$ a reduced plot similar as that of Fig.5 and 6 for the corresponding Nd series was not possible. Inspite of this Fig.9 and Fig.10 shows the temperature dependence of H_A of the mixed crystal series $Pr_2Fe_{14-x}Co_xB$. It should be noted that the temperature dependence is rather similar for the Fe rich samples whereas the Co rich compounds show a with increasing Co content increasing slope of the curves. This might be a consequence of the high temperature spinreorientation which occurs on the Co rich side.

By measuring the temperature dependence of the anisotropy field of these samples, using the SPD method, below a certain temperature more than only one singularity became visible. Generally this means the existence of several uniaxial phases with different well distingiushable anisotropy fields. Two singularities could be observed in some 2/17 samples which exist in a hexagonal and in a rhomboedric modification- but the two phases could be detected by X-rays also. Fig. 11 demonstrates this for the sample $Pr_2Co_9Fe_5B$. In this case no remarkable other phases were observed by X-rays or by a thermomagnetic analysis.

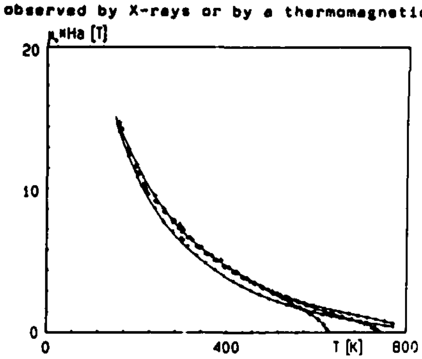


Fig.9 Temperature dependence of H_A of the system $Pr_2Fe_{14-x}Co_xB$ for x=1 (+), x=3 (▲), x=5 (●) and x=7 (x).

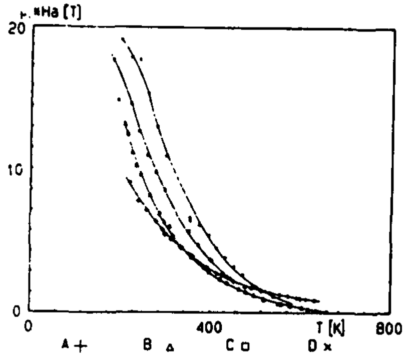


Fig.10 Temperature dependence of H_A of the system $Pr_2Fe_{14-x}Co_xB$ for x=9 (+), x=11 (△), x=13 (□) and x=14 (x).

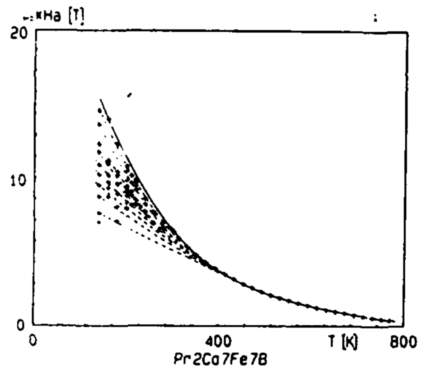


Fig.11 Temperature dependence of the sample $Pr_2Fe_7Co_7B$.

Nevertheless several peaks were observed there and additionally in other substituted samples also. We have no real explanation for this behaviour but there exists the following hypothesis: The substitution of Fe by Co increases the temperature

dependence of H_A: Pr has a similar effect. This means that $Pr_2(Fe,Co)_{14}B$ is a system with an unusual high temperature coefficient of H_A. It is well known that six different Fe sites exists in the 2/14/1 structure. The unusual temperature dependence of H_A of the $R_2Fe_{14}B$ compounds with nonmagnetic R ions initiates the suggestion that different 3d sites give different anisotropy contributions with different temperature dependencies. This effect is *enhanced* by the Co substitution and might cause now distinguishable anisotropy contributions which becomes especially visible at low temperatures where the strong temperaure dependence of the Pr ion helps additionally. It should be mentioned that this is a model which is in contradiction to the "3d-band picture" given in chapt. 3.1.
At higher temperatures a second spinreorientation occurs on the Co rich side- similar as was found for the Nd(Fe,Co)B mixed crystal series. The reason is there also the competition between the easy axis anisotropy of the Pr sublattice and the basal plane orientation of the (Fe,Co) sublattice.

3.4 Co substituted Nd-Fe-B based magnets

There exists various attempts to produce Co substituted Nd-Fe-B based permanent magnets /25,26/. Studies of the temperature and concentration dependence of the coercivity $_IH_C$ showed: i) the temperature coefficient of $_IH_c$ is proportional to that of H_A /25/; ii) the coercivity decreases fast by increasing the amount of Co /27/. The former behaviour can be expected assuming a correlation between $_IH_c$ and H_A as was proposed for nucleation controlled magnets by Herzer et al. /28/ and indeed found /29/. The later behaviour is not yet really understood. For instance a substitution of 10% Co causes a decrease of H_A of 2% but a decrease in $_IH_c$ of more than 17% /26/! The microstructure must strongly differ from that of a pure Nd-Fe-B magnet. It should be mentioned that the above given procentual decrease was determined on real sintered permanent magnets. The reduction of H_A in a stochiometric mixed crystal system like $Nd_2Fe_{14-x}Co_xB$ due to a 10% Co substitution is more then 5%. The smooth

concentration dependence of the lattice constants of this system /3/ shows that the major part of the Co enters indeed into the 2/14/1 lattice in the case of the stochiometric samples. Consequently in technical sintered magnets a remarkable part of the Co does not enter into the hard magnetic 2/14/1 grains. In this case the real off-stochiometric composition combined with the heat treatment determines indeed the ratio of substituted 2/14/1 grains and Co containing boundary phases. The amount of this boundary phases, its thickness and its magnetic properties influences strongly the coercivity. Carefull and conclusive analysis of the microstructure of Co substituted magnets which can explain the "bad Co effect" are still missing.

REFERENCES

/1/ S. Fujimura, M. Sagawa, Y. Matsuura, Y. Hitoshi, N. Togawa
European Patent 0134304 A1 (1983)

/2/ F. Bolzoni, J.M.D. Coey, J. Gavigan, D. Givord, O. Moze, L. Pareti, T. Viadieu
J. Magnetism a. Magn. Mat. 65 (1987) 123

/3/ R. Grössinger, R. Krewenka, X.K. Sun, R. Eibler, H.R. Kirchmayr, K.H.J. Buschow
J. Less-Common Metals 124 (1986) 165

/4/ R. Grössinger, R. Krewenka, H.R. Kirchmayr, S. Sinnema, Yang -Fu-Ming, Huang Ying-kai, F.R. de Boer, K.H.J. Buschow
J. Less-Common Metals (1987) in print

/5/ R. Grössinger, H.R. Kirchmayr, K.H.J. Buschow
J. Less Common Metals (1987) submitted

/6/ G. Asti, S. Rinaldi
J. Applied Phys. 45 (1974) 3600

/7/ R. Grössinger
J. Phys. D 15 (1982) 1545

/8/ R. Gersdorf, F.R. de Boer, J.C. Wolfrat, F.A. Muller, L.W. Roland in "High Field Magnetism" North Holland, Amsterdam 1983, M. Date Ed., p. 277

/9/ R. Grössinger, X.K. Sun, R. Eibler, K.H.J. Buschow, H.R. Kirchmayr
J. de Physique C6, Tome 46 (1983) C6-221

/10/K.H.J.. Buschow, D.B. de Mooij, S. Sinnema, R.J. Radwanski, J.J.M. Franse
J. Magnetism a. Magn. Mat. 51 (1985) 211

/11/H.M. van Noort, K.H.J. Buschow
J. Less-Common Metals 113 (1985) L9

/12/R. Grössinger, K.H.J. Buschow
J. Less-Common Metals (1987) in print

/13/M.R. Ibarra, P.A. Algarabel, A. Alberdi, J. Bartolome, A. del Moral
J. Applied Phys. 61 (8) (1987) 3451

/14/D. Givord, H.S. Li, J.M. Moreau, R. Perrier de la Bathie, E. du Tremolet de Lacheisserie
Physica B, 130 (1985) 323

/15/G. Asti, F. Bolzoni
J. Magnetism a. Magn. Mat. 15-18 (1980) 29

/16/F. Bolzoni, O. Moze, L. Pareti
J. Applied Phys. (1987) in print

/17/S. Sinnema, R.J. Radwanski, J.J.M. Franse, D.B. de Mooij, K. K.H.J. Buschow
J. Magnetism a. Magn. Mat. 44 (1984) 333

/18/G. Asti, F. Bolzoni, F. Leccabue, R. Panizzieri, L. Pareti, S. Rinaldi
J. Magnetism a. Magn. Mat. 15-18 (1980) 561

/19/D. Melville, W.I. Khan, S. Rinaldi
IEEE Trans. on Magn. MAG-12 (1976) 1012

/20/I. Mertense
J. canadien de physique 51 (1973) 2407

/21/U. Atzmony, M.P. Dariel, G. Dublon
Phys. Rev. B 14(9) (1976) 3713

/22/A.T. Pedziwiatr, S.Y. Jiang W.E. Wallace
J. Magnetism a. Magn. Mat. 62 (1986) 29

/23/A.S. Ermolenko
Proc. of 6th Int. workshop on rare earth-cobalt magnets (Ed. J. Fidler) (1982) p. 771

/24/E.Callen
Physica 114B (1982) 71

/25/R. Grössinger, R. Krewenka, F. Haslinger, M. Sagawa, H.R. Kirchmayr
Proc. of Intermag (1987) Tokyo; in print

/26/R. Grössinger, H. Harada, A. Keresztes, H.R. Kirchmayr, M. Tokunaga
Proc. of Intermag (1987) Tokyo; in print

/27/M. Sagawa, S. Fujimura, H. Yamamoto, Y. Matsuura, K. Hiraga
IEEE Trans. on Magn. MAG-20 (1984) 1584

/28/G. Herzer, W. Fernengel, E. Adler
J. Magnetism a. Magn. Mat. 58 (1986) 48

/29/R. Grössinger, A. Keresztes, H. Harada, Z. Shougong
this conference

14.207

13

Journal of the Less-Common Metals, *136* (1988) 367 - 373

MAGNETIC ANISOTROPY IN THE SYSTEM $La_2Fe_{14-x}Co_xB$ AND ITS RELATION TO THE SYSTEM $Nd_2Fe_{14-x}Co_xB$

R. GRÖSSINGER and H. KIRCHMAYR

Institute for Experimental Physics, University of Technology, Vienna (Austria)

K. H. J. BUSCHOW

Philips Research Laboratories, 5600 JA Eindhoven (The Netherlands)

(Received June 22, 1987)

Summary

We have studied the system $La_2Fe_{14-x}Co_xB$ by means of X-ray diffraction, magnetic measurements and singular point detection (SPD) measurements. We present experimental data on the concentration dependence of the lattice constants, Curie temperatures, saturation magnetization and anisotropy fields. Attention is mainly given to the determination of anisotropy fields, which were also studied as a function of temperature in the range from 4.2 K to the corresponding Curie temperatures. The experimental information obtained for the system $La_2Fe_{14-x}Co_xB$ was used to distinguish the relative anisotropy contributions of the neodymium sublattice and 3d sublattice in $Nd_2Fe_{14-x}Co_xB$.

1. Introduction

In a previous investigation [1] we studied the magnetic properties of the system $Nd_2Fe_{14-x}Co_xB$ and showed that compounds with low cobalt concentration give rise to only one spin reorientation below T_c, whereas compounds with high cobalt concentration exhibit two spin reorientations below T_c. The additional spin reorientation in the latter compounds occurs at fairly high temperatures and originates from the difference in sign and the difference in temperature dependence between the contributions of the neodymium sublattice anisotropy and the 3d sublattice anisotropy. In this investigation we also addressed the question of how far substitution of cobalt for iron in $Nd_2Fe_{14}B$ influences the anisotropy field and its temperature dependence in concentration ranges and temperature ranges of interest for permanent magnet applications of these materials. We showed that cobalt substitution generally lowers the room temperature anisotropy field, without offering a satisfactory explanation for this effect.

In the present investigation we have focused our attention on the magnetic properties of the system $La_2Fe_{14-x}Co_xB$. Since lanthanum is non-

0022-5088/88/$3.50

61

Best available

magnetic the study of this system enables us to obtain conclusive experimental information on the 3d sublattice anisotropy as a function of temperature and concentration. The results obtained from this investigation will be used to distinguish the relative contributions of the neodymium and 3d sublattice anisotropies in $Nd_2Fe_{14-x}Co_xB$. It will be shown that the reduction of the room temperature anisotropy with increasing x in $Nd_2Fe_{14-x}Co_xB$ is not caused by a reduction in crystal field interaction, but is mainly due to the strong decrease of the exchange field experienced by the neodymium moments when cobalt substitutes for iron in $Nd_2Fe_{14}B$.

2. Experimental details

Samples of $La_2Fe_{14-x}Co_xB$ compounds were prepared by arc melting under purified argon gas from starting materials of at least 99.9% purity. They were vacuum annealed for 3 weeks at about 850 °C. After this treatment the samples were examined by X-ray diffraction and found to be approximately single phase, the content of impurity phases being of the order of a few per cent.

The Curie temperatures of the various compounds were derived from measurements of the temperature dependence of the magnetization σ by means of the Faraday method. The values of T_c were obtained by plotting σ^2 *vs.* T and extrapolating to $\sigma^2 \to 0$.

The anisotropy field H_A was measured in a pulsed field system from 4.2 K up to the Curie temperature using the singular point detection (SPD) technique. This method leads to a singularity at $H = H_A$ in experimental curves of d^2M/dt^2 *vs.* H (M is the magnetization) if the c axis is the easy magnetization direction.

3. Results and discussion

X-ray diffraction showed that all $La_2Fe_{14-x}Co_xB$ compounds investigated have the tetragonal $Nd_2Fe_{14}B$-type structure [2]. The lattice constants are plotted as a function of concentration in Fig. 1. Both the a and the c axis decrease with increasing cobalt concentration in such a way that c/a varies only slightly for small x and decreases somewhat more strongly for large x.

The concentration dependence of the Curie temperature is shown in Fig. 2. At low cobalt concentrations, in particular, the values of T_c vary strongly with x, which may be associated with a preferred site occupation, as discussed in ref. 3. Included in this figure is the concentration dependence of the room temperature saturation magnetization, measured on magnetically aligned powder samples.

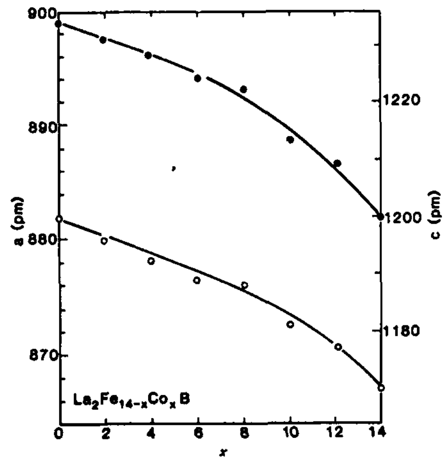
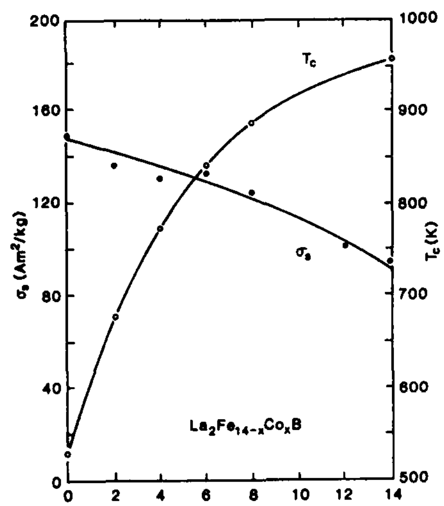


Fig. 1. Concentration dependence of the lattice constants in $La_2Fe_{14-x}Co_xB$.



Best available

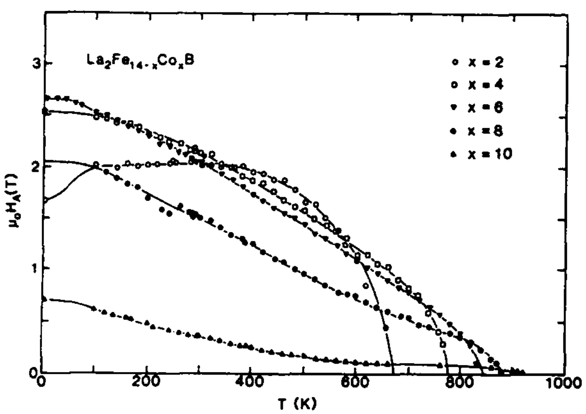


Fig. 3. Temperature dependence of the anisotropy field in various compounds of the series $La_2Fe_{14-x}Co_xB$.

decreases at higher temperatures [4]. This tendency of H_A to increase with temperature is also shown by $La_2Fe_{10}Co_2B$, albeit the corresponding temperature range is far more limited here than in $La_2Fe_{14}B$. The temperatures at which H_A goes to zero for the different compounds in Fig. 3 correspond to the Curie temperatures of these compounds (see also Fig. 2).

The concentration dependences of the anisotropy fields measured at 4.2 K and at 300 K can be compared in Fig. 4. It may be seen that at both temperatures $H_A(x)$ gives rise to a maximum. In general, it may be said that the development of a maximum becomes more pronounced when the temperature corresponding to these curves decreases. The occurrence of maxima in the $H_A(x)$ curves is intimately connected with the fact the H_A in the iron-rich compounds shows an anomalous temperature dependence in the low temperature regime. It is possible that this anomalous temperature dependence of H_A is closely connected with the development of a considerable spontaneous volume magnetostriction [5]. This may lead to a decrease in H_A with temperature and may counteract the normal tendency of H_A to increase with the magnetization, *i.e.* with decreasing temperature.

The anisotropy field H_A is related to the anisotropy constants $K_1, K_2 \ldots, K_n$ by means of the expression

$$\tfrac{1}{2} J_s H_A = K_1 + 2K_2 \qquad (1)$$

where J_s is the magnetic polarization. This latter quantity can be obtained from σ_s and the density. Using the X-ray density derived from the data given in Fig. 1 together with the σ_s data of Fig. 2 we have calculated room temperature values of $\frac{1}{2} J_s H_A$ and plotted this quantity as a function of concen-

63

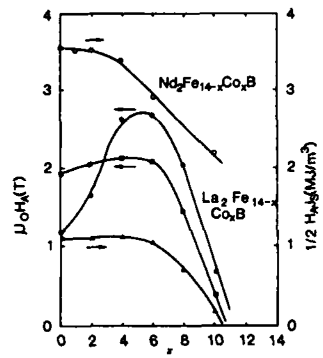


Fig. 4. Concentration dependence of the anisotropy fields H_A at 4.2 K (full circles) and 300 K (full squares) in $La_2Fe_{14-x}Co_xB$. The curve shown in the bottom part of the figure represents the concentration dependence of $K_1 = \frac{1}{2} H_A J_s$ at 300 K in $La_2Fe_{14-x}Co_x$ (full triangles). The curve in the top part of the figure (open circles) represents the concentration dependence of the neodymium sublattice contribution to the anisotropy energy $\frac{1}{2} H_A J_s$ (for more details see text).

tion dependence of K_1 for $La_2Fe_{14-x}Co_xB$. From published data of the concentration dependence of H_A [1] and σ_s [2] in $Nd_2Fe_{14-x}Co_xB$ we have calculated the concentration dependence of $\frac{1}{2} J_s H_A$ for this series of compounds. In this case, too, $\frac{1}{2} H_A J_s$ represents mainly K_1 since K_2 can practically be neglected at room temperature ($K_2 = \frac{1}{10} K_1$) [3,6]. The neodymium sublattice contribution may now be obtained after subtraction of the $\frac{1}{2} H_A J$ values found for $La_2Fe_{14-x}Co_xB$, the latter being regarded as representative of the 3d sublattice contribution. The curve of $\frac{1}{2} H_A J_s$ obtained in this way is shown in the top part of Fig. 4 (open circles). It may be seen that the anisotropy energy associated with the single-ion contribution of neodymium in $Nd_2Fe_{14-x}Co_xB$ remains almost constant at the lowest cobalt concentrations but decreases strongly at higher cobalt concentrations. Extrapolation to $Nd_2Co_{14}B$ would lead to a value more than a factor of 2 lower than in $Nd_2Fe_{14}B$.

It is well known that the single-ion contribution to the anisotropy in $Nd_2Fe_{14}B$ is crystal field induced and originates from the electrostatic interaction of the asymmetric 4f electron charge cloud with effective charge surrounding it [3,6]. The leading term in materials of uniaxial symmetry i of second order. This holds *a fortiori* when room temperature values of the anisotropy energy are considered. To a good approximation one may therefore take the anisotropy energy as proportional to the second-order crystal field parameter A_2^0. It has been shown on several occasions that the sign and magnitude of A_2^0 on a given rare earth site in a given crystal structure can be

Best available

follows from these measurements that the A_2° values in $R_2Co_{14}B$ are the same (within 20%) as the values of the corresponding compounds $R_2Fe_{14}B$. This means that on the basis of the effect of A_2° alone one would not expect such a strong concentration dependence of the rare earth anisotropy as follows from the results shown in the top part of Fig. 4. Honma *et al.* [9] have analysed the magnetocrystalline anisotropy in $Nd_2Fe_{14}B$ in terms of crystal field interaction and exchange interactions and showed that the anisotropy arises through a combined action of both types of interaction. Experimentally it is found that the 3d–4f coupling constant J_{R-3d} in $R_2Co_{14}B$ is roughly twice that in $R_2Fe_{14}B$, but owing to a smaller 3d moment in the former compound the exchange field $H_{ex} \propto J_{R-3d}\mu_{3d}$ acting on the 4f moment remains approximately the same in both series of compounds [10]. For completeness we note that the concentration dependence of T_c is not a measure of the variation in the 3d–4f exchange energy in $Nd_2Fe_{14-x}Co_xB$, since T_c reflects mainly the change in the 3d–3d exchange energy in these materials. One may state therefore that the concentration dependence of the rare earth anisotropy in $Nd_2Fe_{14-x}Co_xB$ cannot be explained by corresponding changes in A_2° and H_{ex}.

64

4. Concluding remarks

We have studied the magnetocrystalline anisotropy in the pseudoternary series $La_2Fe_{14-x}Co_xB$ and found that the room temperature anisotropy constant K_1 changes its sign at approximately $x = 11.5$. This sign change occurs at a slightly higher concentration than found in the series $Y_2Fe_{14-x}Co_xB$ ($x \approx 9.5$) [11]. By combining the results obtained in the course of the present investigation with those obtained previously for $Nd_2Fe_{14-x}Co_xB$ we were able to separate the contributions to the room temperature anisotropy in $Nd_2Fe_{14-x}Co_xB$. In the concentration range of technological interest (*i.e.* for relatively small cobalt concentrations) both contributions vary only little with concentration. In this concentration range and at room temperature the relative 3d sublattice contribution to the anisotropy is still a substantial proportion of the total anisotropy. It is roughly three times smaller than the neodymium sublattice contribution. The strong decrease in the latter anisotropy at higher cobalt concentrations cannot satisfactorily be explained in terms of the exchange field and the second-order crystal field parameter A_2° alone. This means that it is necessary to include higher order crystal field terms for describing the rare earth anisotropy in $Nd_2Fe_{14-x}Co_xB$, even at room temperature. Our results suggest that it is mainly the concentration dependence of these higher order terms which is responsible for the change in the rare earth anisotropy in this series.

2 J. F. Herbst, J. J. Croat, F. E. Pinkerton and W. B. Yelon, *Phys. Rev. B, 29* (198 4176.
3 K. H. J. Buschow, *Materials Science Reps., 1* (1986) 3.
4 R. Grössinger, X. K. Sun, R. Eibler, K. H. J. Buschow and H. R. Kirchmayr, *J. Mag Magn. Mater., 58* (1986) 55.
5 R. Grössinger and K. H. J. Buschow, *J. Less-Common Met., 135* (1987) 39.
6 J. M. D. Coey, *J. Less-Common Met., 126* (1986) 21.
7 M. Bogé, G. Czjzek, D. Givord, C. Jeandey, H. S. Li and J. L. Oddon, *J. Phys. F,* (1986) L67.
8 H. H. A. Smit, R. C. Thiel and K. H. J. Buschow, *Physica*, to be published.
9 H. Honma, M. Shimotomai and M. Doyama, *Proc. 5th Int. Conf. on Crystalline Fie and Anomalous Mixing Effects in f-Electron Systems, Sendai, April 1985.*
10 K. H. J. Buschow, D. B. de Mooij, S. Sinnema, R. J. Radwanski and J. J. H. Frans *J. Magn. Magn. Mater., 51* (1985) 221.
11 F. Bolzoni, J. M. D. Coey, J. Gavigan, D. Givord, O. Moze, L. Pareti and T. Viadie *J. Magn. Magn. Mater., 65* (1987) 123.

THE EFFECT OF SUBSTITUTION OF Al ON THE MAGNETIC PROPERTIES OF $Nd_{15}Fe_{77}B_8$ PERMANENT MAGNETS

R.Grössinger, F.Haslinger, Zhang Shougong [1]), R.Eibler, Liu Yinglie[1]), J.Schneider [*]), A. Handstein[*]), H.R.Kirchmayr

Inst. f. Experimentalphysik, T.U. Vienna, Austria
[1]) Inst. of Physics, Chinese Academy of Science; Bejing, China
[*]) Zentr. Inst. f. Festkörperf., Akad. d. Wissensch, Dresden, DDR

ABSTRACT

The temperature dependence of the anisotropy field H_A and of the coercivity of the mixed crystal series $Nd_{15}(Fe_{1-x}Al_x)_{77}B_8$ was measured between 100K and the Curie temperature T_C. The intrinsic properties (like $T_C(x)$, $H_A(x)$ but also the lattice constants and the concentration dependence of the spinreorientation temperature) indicate that a part of the Al enters indeed into the 2/14/1 lattice. The coercivity increases with increasing Al content. The analysis of a correlation between $_IH_C$ and H_A gives hints of a decoupling between the grains due to the Al but it shows also the limits of such attempts.

INTRODUCTION

Nd-Fe-B based permanent magnets exhibit excellent magnet properties at room temperature (e.g.1,2), but due to the rather low Curie temperature T_C the coercivity decreases too fast with increasing temperature (3). There exists various attempts to solve this problem: i) Increase of T_C by substituting Co (4). Unfortunately the coercivity $_IH_C$ breaks down due to the Co substitution (5). ii) Increase of $_IH_C$ by a heavy rare earth substitution. This causes a reduction of the saturation magnetization and consequently a reduction of the energy product (5). With a simultaneous Co and Dy substitution the best results were obtained up to now (6).

Another possibility to enhance the magnet properties are substitutions using small amounts of nonmagnetic elements such as Al, Si, Ga etc. (7). All these elements increase the coercivity at room temperature however the responsible mechanism is not yet clear. A first attempt to understand the magnetization process of Al substituted magnets was recently given (8). It is the aim of the present study to add anisotropy investigations and additional magnetic studies in order to get a better understanding of the role of the Al in Nd-Fe-B based magnets.

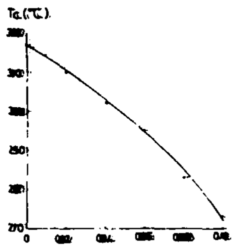
EXPERIMENTAL

The alloys of the nominal composition $Nd_{15}(Fe_{1-x}Al_x)_{77}B_8$ with X=0, 0.02, 0.04, 0.06, 0.08 and 0.1 were prepared by arc melting under purified argon atmosphere. The ingots were first crushed and then ball-milled to about 3-6µm in a protective liquid of petroleum ether. The powders were aligned in a magnetic field of about 1T and pressed in a direction perpendicular to the alignement direction. The green compacts were sintered at about 1060°C for 1 hour and then annealed at 550-600 °C for 1-2 hours. The Curie temperature was determined using a PAR vibrating sample magnetometer in a weak field. The spinreorientation temperature was determined from initial susceptibility measurements between 4.2K and room temperature. The anisotropy field and hysteresis loop measurements were performed in a pulsed field system between 100K and T_C. The anisotropy field was determined using the SPD (Singular Point Detection) technique (9).

RESULTS AND DISCUSSION

INTRINSIC PROPERTIES

In order to understand the effect of Al substitution our interest was focused on the concentration dependence of the intrinsic properties. Fig.1 shows that the Curie temperature T_C decreases with increasing Al amount indicating a weakening of the exchange due to the Al.
Fig.2 shows the with the Al concentration decreasing spinreorientation temperature T_S. It is well known that this spinreorientation is a crystal field effect of the Nd sublattice.



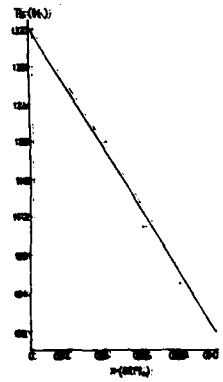


Fig.1: Concentration dependence of T_C of $Nd_{15}(Fe_{1-x}Al_x)_{77}B_8$ (left picture).
Fig.2: Concentration dependence of the spin reorientation temperature T_S of $Nd_{15}(Fe_{1-x}Al_x)_{77}B_8$ (right picture).

0018-9464/88/0300-1629$01.00©1988 IEEE

Best available

The crystal field is in a rough approximation influenced by the surrounding charges as well as by the interatomic distancies. It is worth to note that the lattice constant, espcially c, changes in a systematic manner with the Al content (8).
For the coercivity the magnetic anisotropy is one of the most important intrinsic properties. Fig.3 shows the temperature dependence of H_A of all samples. It should be mentioned that by applying the SPD technique only the uniaxial hard magnetic grains deliver a singularity at $H=H_A$. If additional phases, which are soft magnetic or not uniaxial, exist in the material they do not contribute to the singularity.

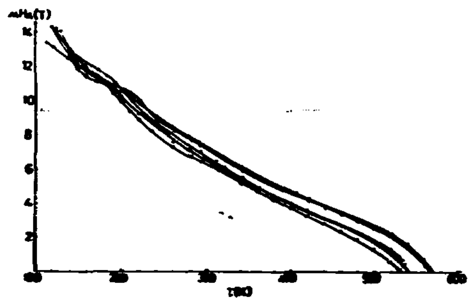


Fig.3: Temperature depnedence of H_A of the system $Nd_{15}(Fe_{1-x}Al_x)_{77}B_8$.

The upper curve is $H_A(T)$ for $x=0$. $H_A(T)$ decreases with the concentration x indicating also that a part of the Al enters indeed into the 2/14/1 lattice. At low temperatures (T<200K) the well known FOMP (First Order Magnetic Phase) transition, visibel as a jump at a critical field H_{cr} which is below H_A in M(H) was observed (for details see 10,11).
The change with the Al concentration of all these intrinsic properties can be taken as a proof that even a part of the Al substitutes positions in the 2/14/1 lattice. Comparing with the substitution behaviour of other rare earth-3d intermetallic compounds it is believed that the Al goes on Fe sites and not on boron sites (see e.g. $T_c(x)$).

PERMANENT MAGNETS

The coercivity field of technical permanent magnets is not only determined by the anisotropy but also by metallurgical parameters. Such parameters are the grain size, the grain surface, the existence of additional phases etc. The creation of walls as well as their mobility through all these imperfections determine the coercivity mechanism. First hints may come from the temperature dependence of the coercivity as shown in Fig.4. It should be mentioned here that the samples with x=0.08 and x=0.1 were according to the hysteresis loop no longer single phased. The hysteresis originates from a hard and a soft magnetic phase. The with increasing Al increasing $_IH_C(T)$ is obvious. Such a behaviour is in agreement with (4). It is a strong proof that the anisotropy alone does not determine the coercivity; this gives evidence that a metallurgical effect must be responsible for the $_IH_C$ enhancement.

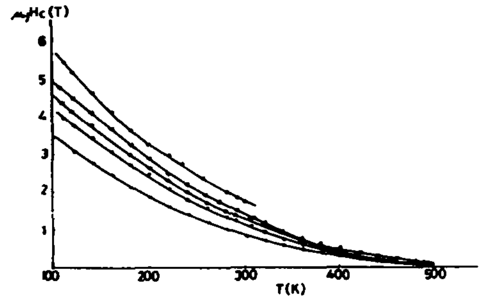


Fig.4: Temperature dependence of $_IH_C$ of the system $Nd_{15}(Fe_{1-x}Al_x)_{77}B_8$ (x=0 (o), x=0.02 (X), x=0.04 (□), x=0.06 (△), x=0.08 (o).

Searching for the coercivity mechanism of Nd-Fe-B based magnets different attempts finding a correlation between $_IH_C(T)$ and $H_A(T)$ were performed (12,13). In principle the following formulas can be taken:

$$_IH_C \text{ prop. } H_n^k$$

H_n...nucleation field; $H_n=2K_1/M_s-H_A$ can be taken if $K_2=0$ is assumed (14,15).
The power factor "k" can be between 1 and 5/2 depending on the different coercivity mechanism.

$$_IH_C=cH_n-nM_s$$

c...coupling factor;"$-nM_s$"...demagnetizing field acting between neighbouring grains.
The above given formula assumes a nucleation mechanism (15).

$$_IH_C=c(H_A(T))^k-nM_s$$

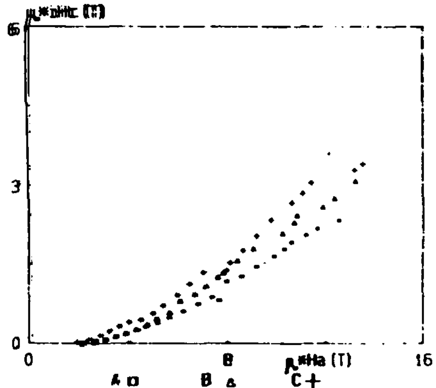


Fig.5: $_IH_C$ vs H_A of the samples $Nd_{15}(Fe_{1-x}Al_x)_{77}B_8$ for x=0 (□), x=0.02 (△) and x=0.04 (+).

In this case H_n is replaced by H_A and different coercivity mechanisms are described by the power factor "k". Measuring $_IH_C(T)$ and $H_A(T)$ and determining the parameters c, k and

$-nM_s$ using a least square procedure may deliver information about the coercivity mechanism.
For a first attempt $_{I}H_c$ was plotted versus H_A (see Fig.5). A nonlinear relation between these two parameters is obvious.
In an intermediate temperature range a linear relation between $_{I}H_c$ and H_A can be assumed. This leads to the in table I given parameters obtained using a formula of the type: $_{I}H_c(T)=c(H_A(T))-nM_s$

Table I Coefficients c and "$-nM_s$" in the series $Nd_{16}(Fe_{1-x}Al_x)_{76}B_8$.

x	c	$-nM_s$ (T)	T_v (K)
0.0	0.259	0.929	320
0.02	0.310	1.02	380
0.04	0.33	0.993	380
0.06	0.37	1.00	420
0.08h	0.35	0.38	300
0.08s	0.1	0.16	500
0.10h	0.359	0.424	300
0.10s	0.08	0.13	500

The values indicated with "h" are due to the hard magnetic phase that indicated with "s" are due to the soft magnetic one.
T_v...temperature up to which the linear fit seems to be possible.

As mentioned before another fit was also applied describing the coercivity mechanism with the power factor "k". The results of this fit procedure are summarised in table II.

Table II Coefficients c,k and $-nM_s$ in the system $Nd_{16}(Fe_{1-x}Al_x)_{76}B_8$.

x	c	k	$-nM_s$(T)
0.00	0.2	1.2	0.64
0.02	0.19	1.38	0.39
0.04	0.18	1.65	0.2
0.06	0.26	1.24	0.56
0.08h	0.28	1.11	0.00
0.08s	0.11	0.89	0.25
0.10h	0.27	1.15	0.00
0.10s	0.07	1.38	0.00

The linear relation fits below the temperature T_v quiet well but the more complex analysis as shown in table II gives a smaller error. There are now the following explanations possible: The linear but also the fit using the power factor "k" gives a with increasing x increasing c indicating decoupling between the grains. The trend between T_v and x is similar to that between c and x. These trends can be taken as a hint that the nucleation mechanism becomes valid over a larger temperature range by substituting Fe by Al. The demagnetizing field "$-nM_s$" increase also with x applying the linear fit; the reverse would be expected. According to table II "$-nM_s$" decreases but the trend is not so clear. The last x values are out of the series because these samples are not single phased. If $_{I}H_c$ of the soft magnetic phase is used for the anlysis it is clear that the correlation does no longer hold.
Nevertheless regarding Fig.5 it is evident that a nonlinear relation exists between $_{I}H_c$ and H_A over the whole temperature range. The description of this nonlinearity, from a simple mathematical point of view, can be performed in different ways. One is a power factor k≠1. Another possibility would be to use a temperature dependent demagnetizing field term "$-nM_s(T)$". Both fits can give a good description of the measured points however it is difficult to decide which desription is physically correct. Including the temperature dependence of the magnetization $M_s(T)$ looks not reasonable for these samples because not all of them are single phased. It should be mentioned that electron probe micro analysis studies showed that with increasing amount of Al an enrichment of Al in the Nd rich boundary phase was found. Consequently the volume of the main phase decreases a little bit with increasing Al.
Another much more important point is that in all attempts to analyse $_{I}H_c$ the nucleation field H_N was replaced by the anisotropy field H_A. If K_2 cannot be neglected-as is the case in Nd-Fe-B based magnets below room temperature- the use of H_A instead of H_N causes a with K_2 increasing error. A better analysis is only possible if $K_1(T)$ and $K_2(T)$ for the real composition of the hard magnetic grains is known. In the present case the amount of Al which enters indeed into the 2/14/1 lattice is unknown. Consequently the $_{I}H_c$-H_N correlation cannot be solved exactly.

REFERENCES

1) J.J.Croat, J.F.Herbst, R.W.Lee, F.E. Pinkerton
J. Appl. Phys. 55 (1984) 2078
2) M.Sagawa, S.Fujimura, M.Togawa, H. Yamamoto, Y.Matsuura
J. Appl. Phys. 55 (1984) 2083
3) R.Grössinger, H.R.Kirchmayr, R.Krewenka, K.S.V.L.Narasimhan, M.Sagawa
Proc. of 8th Int. workshop on rare- earth magnets (Dayton; USA) (1985) p.565
4) Zheng Maocai, Ma Deqing, Jiang Xiuling, Liu Shiqiang
Proc. of 8th Int. workshop on rare- earth magnets (Dayton; USA) (1985) p.541
5) M.Sagawa, S.Fujimura, H.Yamamoto, Y. Matsuura, K.Hiraga
IEEE Trans on Magn. MAG-20 (1984) 1584
6) R.Grössinger, H.Harada, A.Keresztes, H.R. Kirchmayr, M.Tokunaga
Proc. of Intermag; Tokyo (1987)
7) M. Endoh, M.Tokunaga, H.Harada
Proc. of Intermag; Tokyo (1987)
8) A.Handstein, J.Schneider, U.Heinecke, R. Grössinger, Zheng Shougong
Proc. of 9th Int. workshop on rare -earth magnets (Bad Soden; Fr l. Rep. Ger.)(1987)
9) G.Asti, S.Rinaldi
J. Appl. Phys. 45 (1974) 3600
10) G.Asti, F.Bolzoni JMMM 15-18 (1980) 29
11) F.Bolzoni, O.Moze, L.Pareti
J. Appl. Phys. (1987) in print
12) R.Grössinger, R.Krewenka, K.S.V.L. Narasimhan, H.R.Kirchmayr
IEEE Trans. on Magn. MAG-22 (1986) 760
13) R.Grössinger, R.Krewenka, F.Haslinger, M. Sagawa, H.R.Kirchmayr
Proc. of Intermag; Tokyo (1987)
14) R.Kütterer, H.R.Hilzinger, H.Kronmüller
JMMM 4 (1977) 1
15) G.Herzer, M.Fernengel, E.Adler
JMMM 58 (1986) 48

JOURNAL DE PHYSIQUE
Colloque C8, Supplément au n° 12, Tome 49, décembre 1988

THE EFFECT OF SUBSTITUTION IN $Nd_2Fe_{14-x}Z_xB$ (Z = Al, Si, Ga, Co, Ni) COMPOUNDS

R. Grössinger [1], X. C. Chou [2], R. Krewenka [1], G. Wiesinger [1], R. Eibler [1], X. K. Sun [2] and Y. C. Chuang [2]

[1] Inst. F. Experimentalphysik, Techn. Univ. Vienna, Austria
[2] Inst. of Metal Research, Academia Sinica, Shenyang, China

Abstract. – Almost every element substituting Fe in $Nd_2Fe_{14}B$ lowers the magnetocrystallined anisotropy. The effect on the ordering temperature T_c is different: in particular Al and Ni reduce T_c, whereas Si, Ga and Co increase T_c. Mössbauer experiments show that the Fe atoms are substituted in a non random manner. This is supported by the different magnetic properties due to the various substituents.

Introduction

Since the discovery of $Nd_2Fe_{14}B$ in 1983 by Sagawa *et al.* [1], great efforts have been undertaken in order to understand the physical origin of its high coercivity [2], but also to further improve the properties of magnets based on this compound [3]. The main disadvantage of $Nd_2Fe_{14}B$ is its rather low Curie temperature of 580 K which results in an upper limit of 100 °C for efficient operation of Nd-Fe-B magnets. Therefore attempts to improve the temperature behaviour have been made by substituting various elements. Co and Si were found to increase T_c, but to decrease the saturation magnetization [4, 5]; Mn, Ru and Al lower the ordering temperature [6-8]. Nevertheless, magnets with small amounts of Al exhibit a remarkable higher coercivity field $_IH_C$ [9] compared to the pure ternary compound. A similar effect was found by substituting small amounts of Ga [10]. In order to clarify the role of the different substituents, we systematically investigated samples of the composition $Nd_2Fe_{14-x}Z_xB$ (Z = Al, Si, Ga, Co, Ni) in the present work.

Experimental procedure

The samples were prepared from 99.9 % pure starting materials under purified argon gas in an arc furnace. Subsequently they were annealed for three weeks at 900 °C under vacuum. The spin reorientation temperature T_{sr} was deduced from the temperature dependence of the initial susceptibility $\chi_i(T)$. The anisotropy field was determined by applying the SPD-method (Singular Point Detection) in a pulsed field system [11]. The ^{57}Fe Mössbauer spectra were recorded at room temperature.

Results and discussion

In the systems $R_2Fe_{14-x}Ga_xB$ (R = Nd, Pr, Gd, Y) the magnetic ordering temperature T_c increases along with x ($x < 1$) up to about 30 K. A similar behaviour is found for Si substitution which is remarkable, since Ga and Si are nonmagnetic substituents. In the case of Si this finding was explained by a preferential substitution of Fe by Si [12].

$Nd_2Fe_{14}B$ exhibits a spin reorientation at about 135 K [13]. This fact is generally explained by competing terms of the Nd-sublattice crystal field. The substitution of Fe commonly causes a reduction of T_{sr} up to 30 K as shown in table I.

Table I. – *Spin reorientation temperature* T_{sr} *and anisotropy field* $\mu_0 H_A$ *at room temperature* (22 ± 0.5 °C) *of* $Nd_2Fe_{13}ZB$.

elements Z :	Fe	Co	Ni	Si	Al	Ga
T_{sr} (K)	135	133.5	115.5	112.5	105.5	110.5
$\mu_0 H_A$ (T)	6.99	6.88	7.04	7.33	6.32	7.2

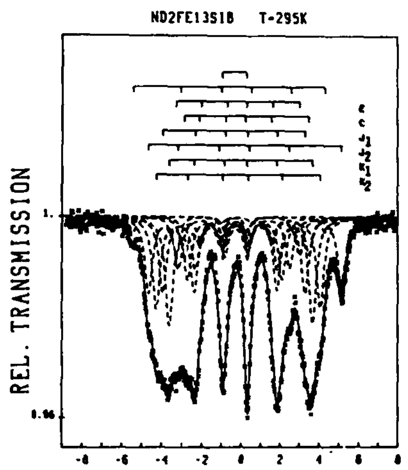


Fig. 1. – Mössbauer spectrum of $Nd_2Fe_{13}SiB$ recorded at room temperature; (× × × × ××) – experimental points, (——) computer fit.

15

68

The effect of different substitutions on the anisotropy field is also summarised in table I. Due to uncertainties in the demagnetizing field the error in H_A is ±0.1 T. Consequently H_A for the samples with Z = Fe, Co, Ni is equal within the experimental error. Al causes a drop in H_A, whereas Si and Ga lead to an increase. The rise in $_IH_C$ which for Al and Ga substituted magnets is more than 50 % compared to pure Nd-Fe-B cannot be explained by such small changes of the anisotropy. It is therefore supposed to be of metallurgical origin (pinning effects).

In order to clarify the role of the different substituents, systematic ^{57}Fe Mössbauer studies were carried out. In figure 1 $Nd_2Fe_{13}SiB$ is shown as a typical spectrum. The bars on the top of the spectrum indicate the line positions. The two uppermost represent an impurity ferromagnetic phase (presumably binary Fe-Si) and a nonmagnetic one ($Nd_{1.1}Fe_4B_4$). The binary precipitations are larger for Z = Ga (6 %) and Ni (8 %), for the remainder they occur to an amount less than 4 % . The Nd-rich phase remains below 3 %. In table II the results of a least square analysis of the spectra are summarised.

Table II. – *Relative intensities at the* k– *and the* j-*lattice sites and average hyperfine field of the compounds.*

Compound	k_1	k_2	j_1	j_2	B_{eff}(T)
$Nd_2Fe_{14}B$	1	1	0.5	0.5	30
$Nd_2Fe_{13}CoB$	1.05	0.95	0.5	0.55	29.4
$Nd_2Fe_{13}NiB$	0.85	0.85	0.55	0.55	27.9
$Nd_2Fe_{13}SiB$	0.9	0.8	0.65	0.65	24.3
$Nd_2Fe_{13}AlB$	1.1	0.9	0.55	0.45	24.8
$Nd_2Fe_{13}GaB$	1.1	0.6	0.75	0.55	26.4

Considering the analysis of the Mössbauer pattern with respect to a deviation from a random Fe substitution, attention is focused to those subspectra arising from the lattice sites with the largest occupation numbers, i.e. k_1, k_2, k_1, j_1, j_2. As can be seen from table II for the k and j sites a strong preference in either direction can be found; in any case the k_1 site is preferently occupied by Fe, the k_2 site by the substituent. As a whole the k sites are prefered by the substituent; in the case of Z = Ni, Si a preference of Fe for the j-sites is found. A distinct difference between the j-sites is obtained for Z = Al and Ga (Fe prefers the j_1 site, Z the j_2 site).

In the case of Co substitution a deviation from random occupation has already been found by neutron diffraction experiments of Herbst and Yelon [14], their results agreeing sufficiently well with the present one. Further evidence in this direction has been given by van Noort and Buschow [15].

The above discussion shows that just a preferential occupation cannot cause the different effects of the substitution of Fe on T_c and H_A. Other physical properties, such as the electronic structure or the local interatomic distancies might be the reason for the specific role of substituents.

Comparing tables I and II a hint may be obtained for the enhancement of the anisotropy field: a preference of the substituent for the k sites and a preference of Fe for the j sites favours larger H_A values.

Carefull lattice parameter determination and further theoretical calculations [16] would be most helpful in improving the understanding of this complex substitution process.

[1] Sagawa, M., Fujimura, S., Togawa, M., Yamamoto, H., Matsuura, Y., *J. Appl. Phys.* **55** (1984) 2083.

[2] Grössinger, R., Harada, H., Keresztes, A., Kirchmayr, H. R., Tokunaga, M., *IEEE Trans. Magn.* **MAG-23** (1987) 2117.

[3] Furst, C. D., Herbst, J. F., Alson, E. A., *J. Magn. Magn. Mater.* **54-57** (1986) 567.

[4] Huang, M. Q., Boltich, E. B., Wallace, W. E., *J. Magn. Magn. Mater.* **60** (1986) 270.

[5] Jurczyk, M., Kowalczyk, A., Wrzeciono, A., Proc. 9th Int. workshop on rare earth magnets. (Bad Soden) F.R.G. (1987) I, p. 701.

[6] Huang, M. Q., Boltich, E. B., Wallace, W. E., Oswald, E., *J. Less Common. Met.* **124** (1986) 55.

[7] Pedziwiatr, A. T., Wallace, W. E., *J. Magn. Magn. Mater.* **61** (1986) 173.

[8] Yang Ying Chang, Xu Li-Gang, *Acta Phys. Sin.* **35** (1986) 1001.

[9] Zhang Maocai, Ma Deqing, Jiang Xiuling, Liu Shiqiangn Proc. 8th Int. workshop on rare earth magnets. (Dayton) U.S.A. (1985) p. 541.

[10] Tokunaga, M., Koruge, H., Endoh, M., Harada, H., *IEEE Trans. Magn.* **MAG-23** (1987).

[11] Asti, G., Rinaldi, S., *J. Appl. Phys.* **45** (1974) 3600.

[12] Xing Feng, Ho Wen Wang, Proc. 9th Int. workshop on rare earth magnets. (Bad Soden) F.R.G. (1987) II, p. 47.

[13] Grössinger, R., Obitsch, P., Sun, X. K., Eibler, R., Kirchmayr, H., Rothwarf, F., Sassik, H., *Mater. Lett.* **2** 6 A& B (1984) 539.

[14] Herbst, J. F., Yelon, W. B., *J. Appl. Phys.* **60** (1986) 4224.

[15] Van Noort, H. M., Buschow, K. H. J., *J. Less Common. Met.* **113** (1985) L9.

[16] Szpunar, B., *J. Less Common. Met.* **127** (1987) 55.

69

JOURNAL DE PHYSIQUE
Colloque C8, Supplément au n° 12, Tome 49, décembre 1988

A NEW ANALYSIS OF Nd-Fe-B BASED PERMANENT MAGNETS

R. Grössinger [1], R. Krewenka [1], H. Buchner [1] and H. Harada [2]

[1] *Inst. f. Experimentalphysik, Techn. Univ. Vienna, A-1040 Wiedner Hauptst. 8 Vienna, Austria*

[2] *Hitachi Metals Ltd., Japan*

Abstract. – A large number of sintered Nd-Fe-B based magnets with three different heat treatments and also substituted samples (Nd by Dy, Fe by Co or both) were investigated by measuring the temperature dependence of both coercivity and anisotropy field. Additionally the ratio between Nd and (Fe, B) was varied systematically. These data were analysed using a nucleation model description. The reliability of this model was proved by comparing the analysis with that performed on a Sm_2Co_{17} based magnet.

Introduction

The main problem in the field of permanent magnets is the development of a generally applicable coercivity model. Up to now exist two important models [1]:

i) nucleation. Walls whenever present move easily;

ii) pinning at distortions (which can be impurities in the grains or the grain boundaries or precipitates).

The coercivity mechanism determine its temperature dependence. A comparison between the experimental and a theoretical temperature dependence can show the validity of a certain model.

For Nd-Fe-B based sintered magnets a nucleation dominated coercivity mechanism was found, which could be described by the following simple formula [2]:

$$_IH_C = c.H_n - n.M_s$$

H_n is the nucleation field (If the second order anisotropy constant is negligible H_n can be replaced by the anisotropy field H_A). $-nM_s$ is the demagnetizing field due to the neighbouring grains. In the present work the validity as well as the limitations of this model should be tested.

Experimental

In two previous papers the influence of heat treatment but also the effect of a Dy and a Co substitution on the temperature dependence of both coercivity and anisotropy field of highly substituted, sintered Nd-Fe-B magnets, was described [3, 4]. The samples used for this study had the following composition:

$$Nd\,(Fe_{0.92}B_{0.08})_{5.5}$$

$$(Nd_{1-x}Dy_x)\,(Fe_{0.92}B_{0.08})_{5.5} \quad x = 0.1,\ 0.2,\ 0.3$$

$$Nd\,(Fe_{0.92-x}Co_xB_{0.08})_{5.5} \quad x = 0.046,\ 0.092,\ 0.184$$

$$(Nd_{0.8}Dy_{0.2})\,(Fe_{0.92-x}Co_xB_{0.08}) \quad x = 0.092,\ 0.184.$$

Each sample existed in the sintered state, but also in two stages of heat treatment [3].

Additionally a set of sintered magnets of the composition:

$$Nd\,(Fe_{0.92}B_{0.08})_z \quad z = 4.4,\ 4.5,\ 5.0,\ 5.5,\ 6.2$$

was studied. The parameter "z" causes an increase of the distance between the grains as was shown by electron microscopy [5]. From all samples the temperature dependence of the hysteresis loop (from which $M_r(T)$ and $_IH_C(T)$ can be deduced) and also $H_A(T)$ (using the SPD-technique [6]) was measured between 100 K and the Curie temperature. The anisotropy field was measured in order to get an estimate for the nucleation field H_n.

Analysis

The temperature dependence of the coercivity field was explained using a model based on the assumption that $_IH_C(T)$ can be fitted using a general formula of the type:

$$_IH_C(T) = (c.H_A(T))^{k(1+aT)} - N.M_s(T).$$

The idea here was to get information about the different coercivity mechanism by fitting especially the power factor "k". The coupling constant "c" is approximately 0.25. In the Dy and Dy, Co substituted samples k is close to one. The only Co substituted sample gave a k value of 1.25. The temperature dependence of k was found to be negligible. The demagnetizing factor is between 0.7 and 0.9. The heat treatment influences the demagnetizing factor N but not k.

The demagnetizing field acting between the grains should be sensitive to a variation of the distance between the grains. In order to varify this we investigated the second set of sintered magnets with a continuous variation of "z".

Figure 1 shows $H_A(T)$ and figure 2 shows $_IH_C(T)$ of these samples.

The temperature dependence of H_A was found to be nearly independent from "z", which is a consequence of the small homogeneity range of the $Nd_2Fe_{14}B$ compound. The temperature dependence of the coercivity field was again analysed using the above developed model. The formula contains four free variables: c, k, a (a is the temperature coefficient of k) and N. k determines the coercivity mechanism. Holding one of these parameters constant and fitting the others showed that they depend strongly on each other. The most reliable results using this procedure were obtained with the following set of parameters:

$$c = 0.209 - 0.26; \quad k \simeq 1 - 1.2;$$

$$N = 0.5 - 0.74; \quad a \simeq 1 \times 10^{-4}.$$

Up to now no correlation between the fitted parameters and the variabel "z" could be found. A Sm_2Co_{17} based magnet was analysed with the same model in

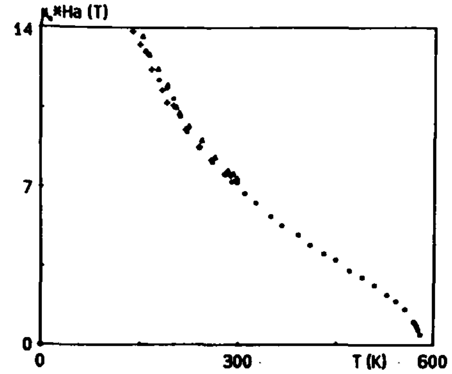


Fig. 1. – $H_A(T)$ of $Nd(Fe_{0.92}B_{0.08})_x$; $x = 4$ (□), 4.5 (△), 6.2 (+).

order to test it. It is well known, that the coercivity in these type of magnets is caused by pinning at precipitates [7]. The analysis is performed in the following manner: i) the measured values of the coercivity field are plotted as a function of the coercivity calculated in the framework of the present model; ii) then they are fitted assuming a linear relation between them. Finally plotting the corresponding standard deviation σ as a function of the coercivity a remarkable behaviour becomes visible comparing the different magnets:

a) the fit works good for a pure Nd-Fe-B based magnet (especially at higher temperatures). The $\sigma(H)$ curve shows a statistical spread (see Fig. 3);

b) in the case of a precipitation hardened 2/17 magnet as well as in a Dy substituted Nd-Fe-B magnet the $\sigma(H)$ curve has a monotonic functional character (see Fig. 4).

This indicates that in the latter case the fit becomes less reliable.

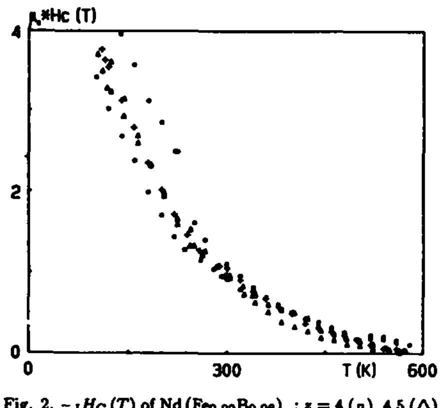


Fig. 2. – $_IH_C(T)$ of $Nd(Fe_{0.92}B_{0.08})_x$; $x = 4$ (□), 4.5 (△), 5 (+), $x = 5.5$ (▪), 6.2 (▲).

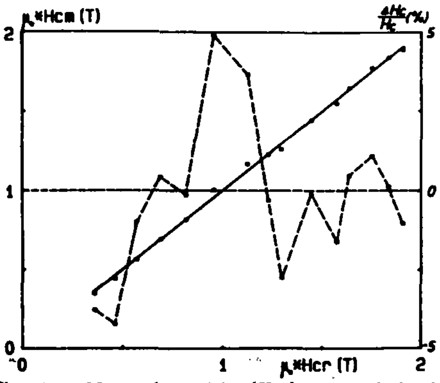


Fig. 3. – Measured coercivity (H_{cm}) *versus* calculated coercivity (H_{cr}) of a pure Nd-Fe-B sintered magnet. The standard deviation σ (dotted line) shows a statistical character.

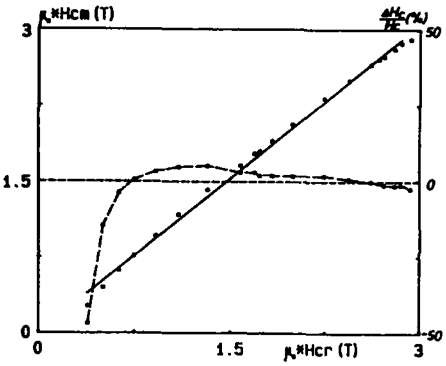


Fig. 4. – Measured coercivity (H_{cm}) *versus* calculated coercivity (H_{cr}) of a Dy substituted Nd-Fe-B based sintered magnet. The standard deviation σ (dotted line) shows a determined character.

[1] Becker, J. J., *IEEE Trans. Magn.* MAG-18 (1982) 1451.

[2] Herzer, G., Fernengel, W., Adler, E., *J. Magn. Magn. Mater.* **58** (1986) 48.

[3] Grössinger, R., Harada, H., Keresztes, A., Kirchmayr, H. R., Tokunaga, M., *IEEE Trans. Magn.* MAG-23 (1987) 2117.

[4] Grössinger, R., Keresztes, A., Harada, H., Shougong, Z., Proc. of 9-th Int. workshop on rare earth magnets (Bad Soden, F.R.G.) (1987) I/p. 593.

[5] Tokunaga, M. (private communication).

[6] Asti, G., Rinaldi, S., *J. Appl. Phys.* **45** (1974) 3600.

[7] Fidler, J., *J. Magn. Magn. Mater.* **30** (1982) 58.

ERA- Technol. Conf., London, June 1989. 17

Improvement of Nd-Fe-B Magnets

R.Grössinger
Inst. f. Experimentalphysik; Techn. Univ. Vienna; Austria

1) Introduction

The quality of modern permanent magnet materials are characterised by:

a) High energy products $(BH)_{max}$. This is a value which determines the achievable miniaturisation of magnetic components.

b) Coercivity field ${}_IH_C$. ${}_IH_C$ is important for the stability of the magnetized state; especially in dynamic applications.

c) Curie temperature T_C. T_C determines the temperature range where the magnet can be used.

Nearly all these requirements were achieved by the development of magnets based on rare-earth - 3d compounds. All these compounds have a uniaxial crystal structure (hexagonal, tetragonal). The 3d-elements (Co or Fe) ensure a high ordering temperature; the rare earth elements cause a high (uniaxial) anisotropy (of Single Ion type). A uniaxial anisotropy is necessary for the formation of a reasonable coercivity. It is clear that additionally the "right" microstructure is important for a high coercivity also. This is the general concept of rare-earth-3d permanent magnets. Table I summarises the magnet parameters (typical values at room temperature) of the three magnet families in use.

Material	T_C(K)	M_s(kG)	H_A(kOe)	${}_IH_C$(kOe)	$(BH)_{max}$(MGOe)
$SmCo_5$	1020	11.2	300	20	25
Sm_2Co_{17}	1195	12.8	65	12	30
$Nd_2Fe_{14}B$	580	16	75	10	40

M_s...saturation magnetization; H_A...anisotropy field.

It is evident that the Sm-Co magnets have according to its high ordering temperature an excellent thermal stability. However the high costs of the raw materials are prohibitive against industrial large scale applications of these magnets.

With the invention of the new Nd-Fe-B magnets it was possible to produce a Co-free, cheaper, high quality permanent magnet (1,2). The room temperature data are excellent but the rather low Curie temperature causes a with increasing temperature fast decreasing ${}_IH_C$ (3). For many

technical applications (e.g. motors) a working temperature of up to 150°C is necessary. It should be mentioned that for a high temperature application the with temperature changing optimal working point has to be taken into account. The $_{I}H_{C}$(T) behaviour is only a rough approximation. Additional the irreversibel losses which can occure in such a magnet are of importance if the magnet should be operated for longer time at elevated temperatures.
Therefore the work was focused on the search for improvements of the high temperature properties of high quality permanent magnets.

2) Concepts of improvements.

Nd-Fe-B magnets are based on $Nd_2Fe_{14}B$. This is a tetragonal compound (space group $P_{4_2}mnm$) with an ordering temperature of T_C = 580K and an easy c-axis between 135K and T_C (for deteails see e.g.4,5). At low temperatures an easy cone is formed. There exist the following possibilities to improve the high temperature properties:

2.1) Substitutions increasing T_C.

When Fe is partly substituted by other metallic elements the ordering temperature T_C can in- or decrease as is according to (6) shown in Fig. 1. Ni and Si and also Ga increase T_C slightly, but not Al. Mn and Cr might introduce an antiferromagnetic component. The most effective element is here Co. Therefore the mixed crystal system $Nd_2(Fe,Co)_{14}B$ was studied intensively (7,8). The magnetic phase diagram of this system is given in Fig.2. The Co sublattice preferes an easy plane. This causes on the Co-rich side a second spin reorientation above room temperature from the c-axis to the plane. From the phase diagram it can be seen that e.g. a compound $Nd_2(Fe_{0.8}Co_{0.2})_{14}B$ has a reasonable high T_C of more than 700 K. However producing a sintered Co substituted magnet $_{I}H_{C}$ decreases due to the Co substitution (see e.g. (9)). The reason is not a reduction of the anisotropy field which is nearly constant on the Fe-rich side (7). A comparison with the behaviour of rapidly quenched Nd-(Fe,Co)-B, where $_{I}H_{C}$ stays constant with small amounts of Co substitutions (10), shows, that the Co changes the microstructure (intermediate phase) in the sintered magnets unfavourable, thus reducing $_{I}H_{C}$.
Additionally becomes the temperature dependence of $_{I}H_{C}$

($d_I H_C/dT$) worse with the Co substitution (9). A similar behaviour was observed in the temperature characteristic of the anisotropy field (dH_A/dT) (7).

As mentioned above small amounts of elements like Si or Ga cause a slight increase of T_C (11). It is believed that this is a consequence of a preferential substitutions of some Fe sites (12). However Si substituted sintered magnets showed a strong decrease of $_I H_C$ (13). Ga substituted sintered magnets gave a large increase of $_I H_C$ (11). This behaviuor cannot be explained by the magnetic anisotropy; it must be an effect of the microstructure.

2.2 Substitutions increasing $_I H_C$

These substitutions can be subdivided in elements causing an intrinsic increase of the magnetic anisotropy and that which enhances $_I H_C$ due to a metallurgical effect. To the first group belong mainly Tb or Dy. the latter group is formed by elements like Al or Ga.

2.2.1 Substitutions increasing H_A

The substitution of Dy cause a remarkable increase of H_A (9), which is followed by a with the Dy concentration enhanced $_I H_C$ as is shown in Fig. 3a. In pure Nd-Fe-B as well as in Co substituted magnets the coercivity is formed after a heat treatment only (9). The idea that the improvement of $_I H_C$ is due to the larger H_A values is supported by the fact that for highly Dy containing magnets a coercivity is formed where the influence of the heat treatment becomes negligible.

Because of the antiparallel coupling between Dy and Fe the remanence M_r decrease with increasing amount of Dy as is seen in Fig. 3b. Dy substituted magnets have a high coercivity at room temperature (approximately 20 kOe) and can therefore be used also at 150°C but the price for this improvement is a reduced energy product ($(B.H)_{max}$ is prop. to $B_r^2/4$).

Some investigators tried now to combine the advantage of the Co sunbstitution (increase of T_C) with that of the Dy substitution (increase of $_I H_C$). In Fig. 4a the temperature dependence of H_A of a set of samples of the composition $Nd_{14.5}Dy_{1.5}(Fe_{77.5-x}Co_x)B_7$ is shown. Between 200 and 400K $H_A(T)$ is quiet similar. Only at higher temperatures (T >

400K) the effect of the increasing amount of Co becomes visible. Unfortunately this is not the case for the temperature dependence of $_{I}H_{C}$ as shown in Fig 4b. The higher Co content is of now influence on $_{I}H_{C}(T)$! This means that at elevated temperatures the coercivity reducing effect of Co overweights the coercivity enhancing role of the Dy. The temperature dependence of the remanence can be roughly described to be proportional to a Brillouin function. This means that the increase of T_C due to the Co substitution causes an improved temperature character of $M_r(T)$. Therefore in summary a Dy and Co substituted material (which is more expensive) show a better temperature behaviour up to 150°C, but the magnet parameters at room temperature are nearly the same than that of a pure Nd-Fe-B magnet (especially with respect to $(B.H)_{max}$). This way is therefore also not very convincing.

2.2.2 Nonmagnetic substitutions

Nonmagnetic substitutions such as Al or Ga cause also a remarkable increase of $_{I}H_{C}$. Values of 16 kOe are reached with Al (14) and 20 kOe with Ga (11). According to a simple picture the coercivity $_{I}H_{C}$ can be described in the following manner (15):

$$_{I}H_{C}(T) = c.H_{n}(T) - n.M_{S}(T)$$

c...coupling parameter ($0<c<1$); H_n...nucleation field (if only the first order anisotropy constant K_1 is imoportant H_n is equal to the anisotropy field H_A); $-n.M_S$...demagnetizing field caused by the neighbouring grains.
The addition of nonmagnetic elements might increase the thickness of an intermediate, nonmagnetic phase between the grains, thus decoupling the grains, consequently reducing the demagnetizing field causing an increase of $_{I}H_{C}$.

2.2.3 New compounds

There are two new copmounds to mention:

a) $R_2Fe_{14}C$. (R...rare earth elements). These compounds are isostructural with that which are formed with B (16). The anisotropy field is remarkyble higher than that of the B compounds. Unfortunately T_C is slightly lower ($\Delta T_C \simeq 30K$) than in the case of the B compounds. Therefore a magnet based on this compound will not solve the temperature problem.
b) Magnets based on the Th Mn_{12} compounds (17). There only the Sm containing material is of interest (uniaxial

anisotropy); however the highest Curie temperature found in this group of materials is 200°C which is again too low for a high quality permanent magnet.

3 Summary

Nd-Fe-B based magnets have good magnet values at room temperature. Substitutions increasing $_{I}H_{C}$ at room temperature (like Dy,Al,Ga) make a magnet possible which can be handled in temperatures up to 120°C. A Co substitution which cause a remarkable increase in T_c cause an improvement of the magnet parameters in rapidly quenched material only. Up to now no new compounds were found which have magnetic properties which can solve the problems at elevated temperatures really. Therefore further research on this field is still necessary in order to achieve a high quality permanent magnet with a reasonable low price which can be handled at 15)°C also.

Acknowledgement: This work was partly supported by the European Office of the U.S.Army (Contract number DAJA-45-86-C-0010)

References:

1. J.J.Croat, J.F.Herbst, R.W.Lee, F.E.Pinkerton
   J. Appl. Phys. 55 (1984) 2078
2. M.Sagawa, S.Fujimura, N.Togawa, H.Yamamoto, Y.Matsuura
   J. Appl. Phys. 55 (1984) 2083
3. R.Grössinger, R.Krewenka, K.S.V.L.Narasimhan, M.Sagawa
   JMMM 51 (1985) 160
4. J.F.Herbst, J.J.Croat, F.E.Pinkerton, W.P.Yelon
   Phys. Rev. B29 (1984) 4176
5. D.Givord, H.S.Li, J.M.Moreau, R.Perrier de la Bathie, E.du
   E. du Tremolet de Lachaisserie
   Physica 130B (1985) 323
6. M.Sagawa, S.Hirosawa, H.Yamamoto, S.Fujimura, Y.Matsuura
   Jap. J. of Applied Phys. 26 (1987) 785
7. R.Grössinger, R.Krewenka, X.K.Sun, R.Eibler,
   H.R.Kirchmayr, K.H.J.Buschow
   J. Less Common Met. 124 (1986) 165
8. M.Sagawa, S.Fujimura, H.Yamamoto, Y.Matsuura, K.Hiraga
   IEEE Trans on Magn. MAG-20 (1984) 1584
9. R.Grössinger, H.Harada, A.Keresztes, H.R.Kirchmayr,
   M.Tokunaga
   IEEE Trans. on Magn. MAG-23 (1987) 2117

10 J.Wecker, L.Schultz
   Proc. of 9th Int. Workshop on rare earth magnets;
   Bad Soden (FRG) (1987) 485

11 M.Tokunaga, H.Koruge, M.Endoh, H.Harada
   IEEE Trans on Magn. MAG-23 (1987)

12 R.Grössinger, X.C.Kou, R.Krewenka, G.Wiesinger, R.Eibler,
   X.K.Sun, Y.C.Chuang
   J. de Physique 49 (1988) 599

13 W.Fernengel (VAC)
   private coomunication

14 R.Grössinger, A.Keresztes, H.Harada, Z.Shougong
   Proc. of 9th Int. Workshop on rare earth magnets;
   Bad Soden (FRG) (1987) I/593

15 G.Herzer, W.Fernengel, E.Adler
   J. Magn. Magn. Mat. 58 (1986) 48

16 F.R.de Boer, Huang Ying-Kai, Zhang Zhi-Donq,
   D.B.de Moij, K.H.J.Buschow
   JMMM 72 (1988) 167

17 L.Schultz, J.Wecker
   J. Apllied Phys. 64 (1988) 5711

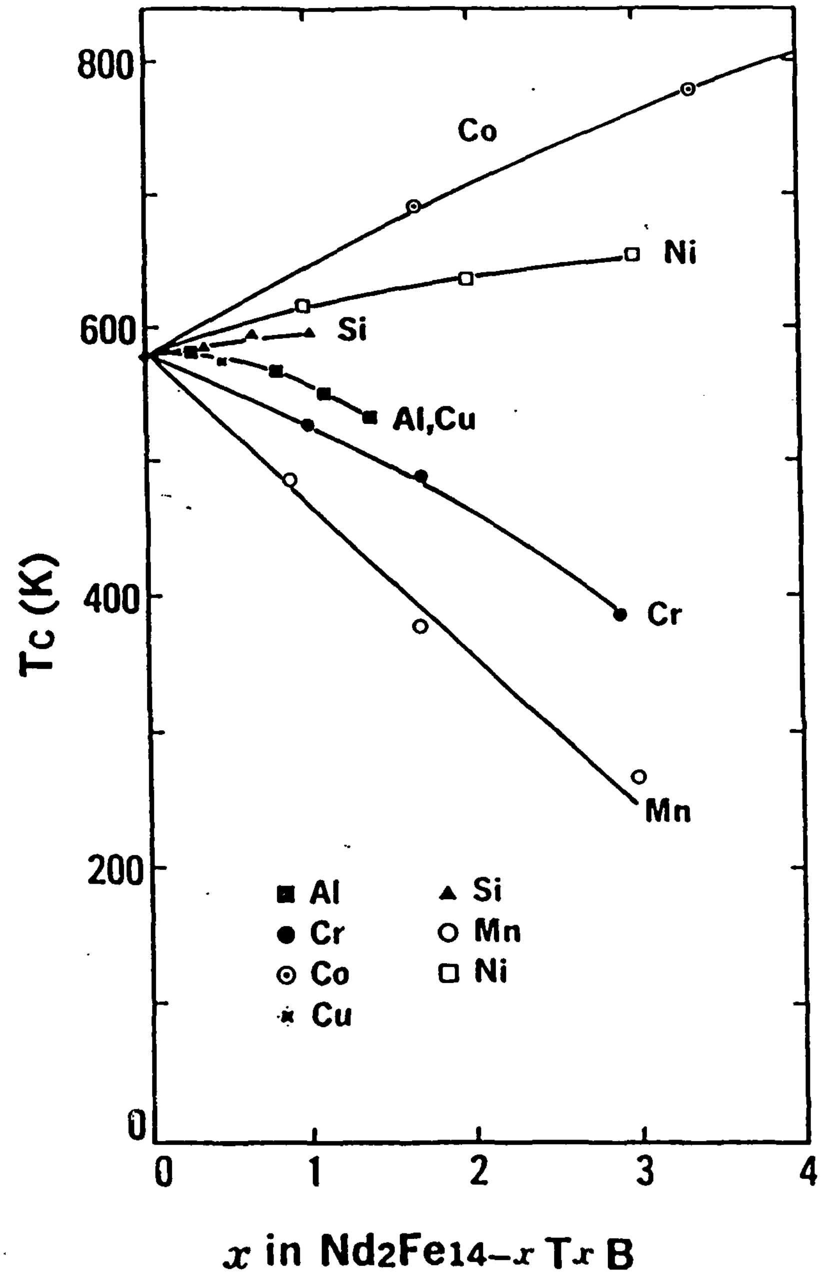


Fig.1 Magnetic ordering temperature (T_c) of $Nd_2(Fe_{1-x}T_x)_{14}B$ (6).

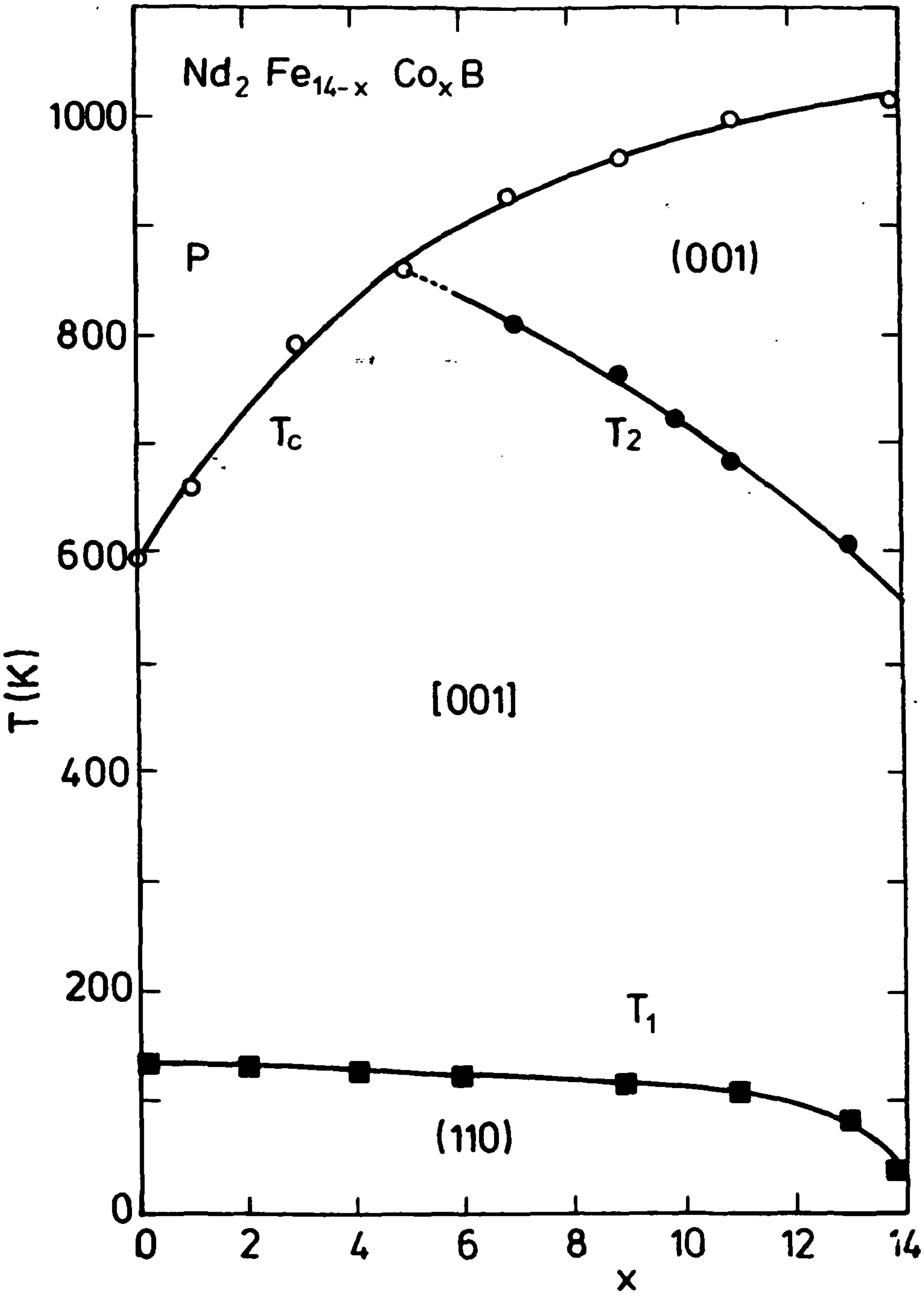


Fig.2 Magnetic phase diagram of $Nd_2Fe_{14-x}Co_xB$ (7).

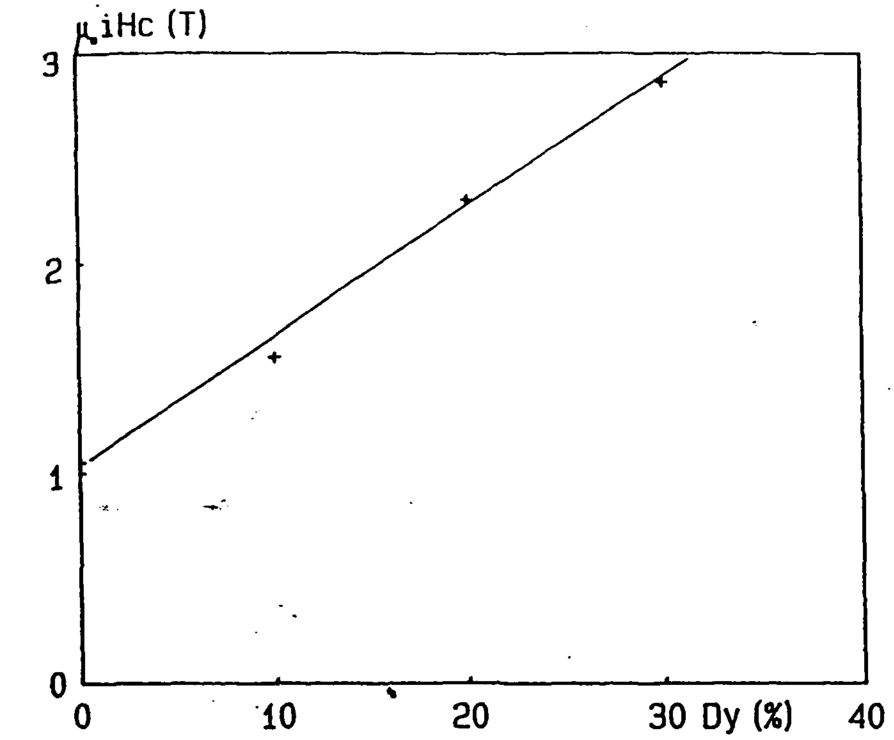


Fig.3a Concentration dependence of $_{I}H_{c}$ in $(Nd_{1-x}Dy_{x})(Fe_{0.92}B_{0.08})_{5.5}$

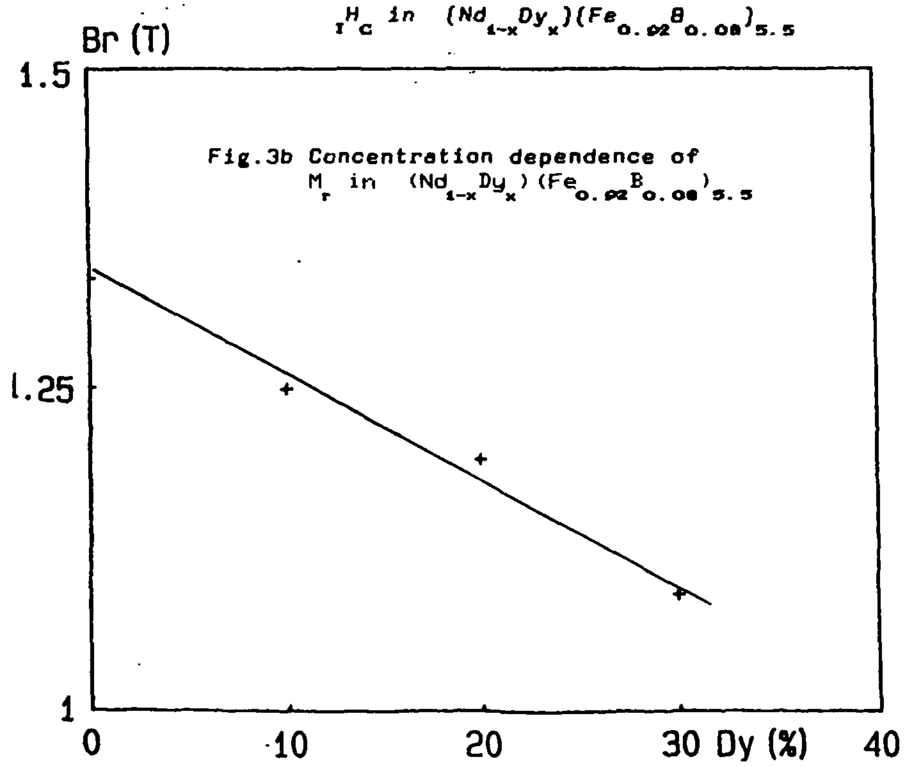


Fig.3b Concentration dependence of M_{r} in $(Nd_{1-x}Dy_{x})(Fe_{0.92}B_{0.08})_{5.5}$

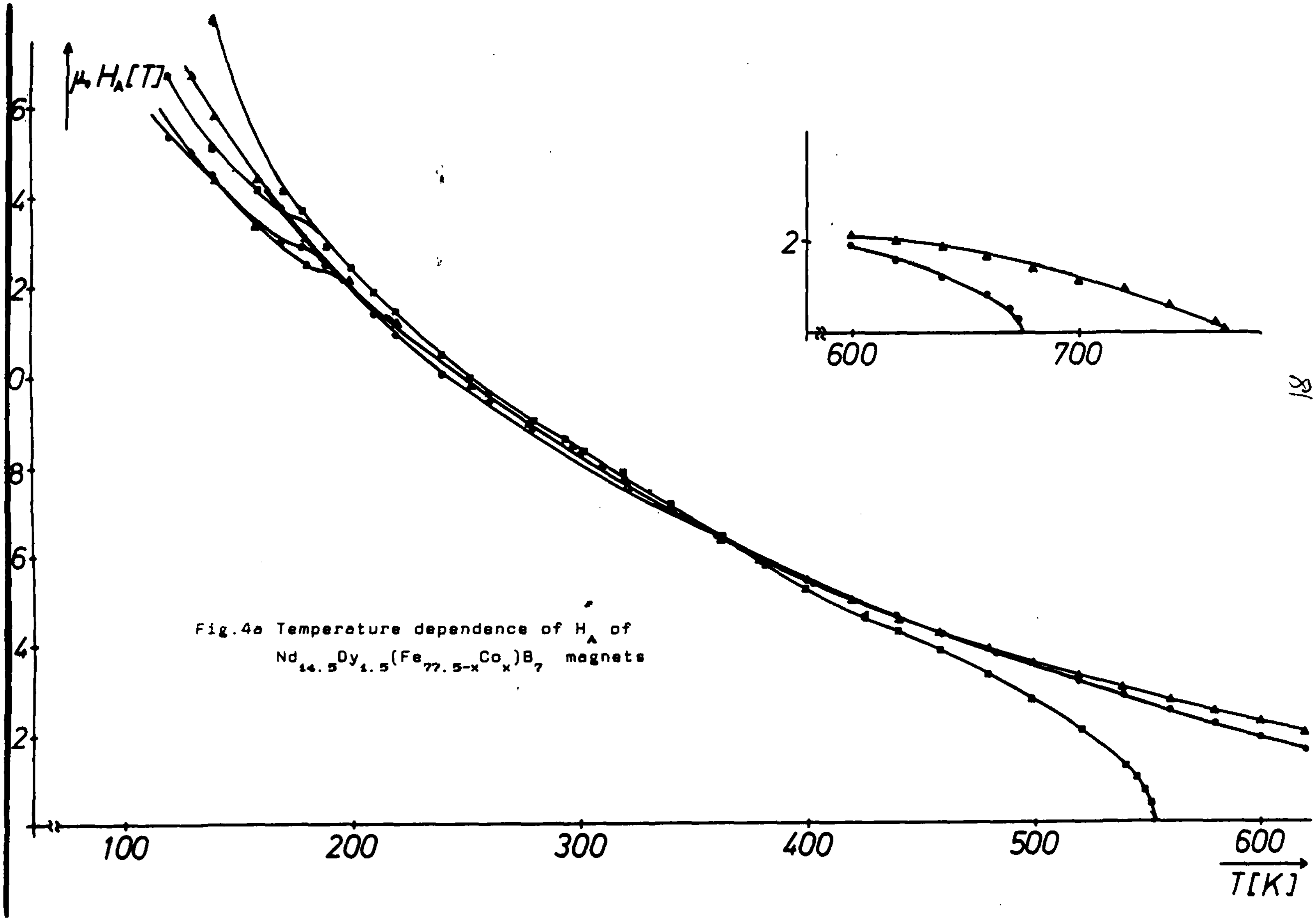


Fig.4a Temperature dependence of H_A of $Nd_{14.5}Dy_{1.5}(Fe_{77.5-x}Co_x)B_7$ magnets

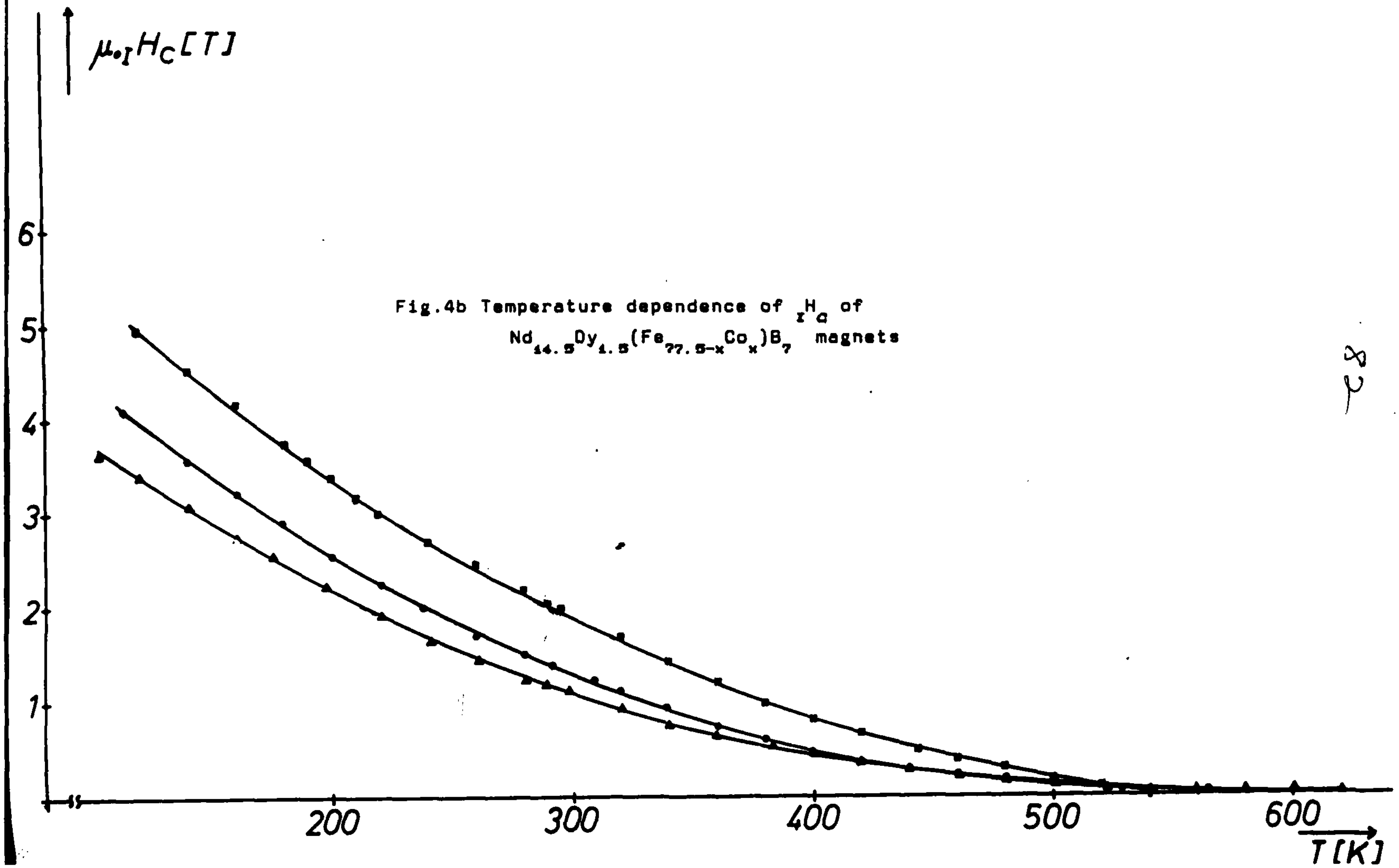


Fig.4b Temperature dependence of $_IH_c$ of $Nd_{14.5}Dy_{1.5}(Fe_{77.5-x}Co_x)B_7$ magnets

18

New Developments in the Field of Permanent Magnetic Materials

Josef Fidler and Peter Skalicky, Wien*)

Dedicated to the 80th birthday of Prof. Dr. Franz Lihl

The increasing importance of newly developed permanent magnetic materials in many electro-, magnetomechanical and electronic applications can be attributed to the drastic improvement of the magnetic energy density product and coercivity of the new materials. The influence of the microstructure of the magnets on their magnetic properties will be discussed in this review paper.

Neue Entwicklungen auf dem Gebiet dauermagnetischer Werkstoffe

Die zunehmende Bedeutung von neu entwickelten dauermagnetischen Werkstoffen in zahlreichen elektro-, magnetomechanischen und elektronischen Anwendungen ist auf eine Verbesserung des Energiedichteproduktes und der Koerzitivfeldstärke zurückzuführen. Der Einfluß der Mikrostruktur der Magnete auf ihre magnetischen Eigenschaften wird in diesem Übersichtsartikel diskutiert.

Produits nouveaux dans le domaine des aimants permanents

L'importance croissante des aimants permanents nouvellement développés, dans de nombreuses applications électro- et magnétomécaniques et électroniques, doit être attribuée à l'amélioration du produit de densité d'énergie et de l'intensité du champ coercitif. On résume et on discute dans cet article l'influence de la microstructure des aimants sur leurs propriétés magnétiques.

Introduction

The history of permanent magnetism reaches to the ancient Greece, where the ability of the loadstone to attract iron having been discovered. With the development of special alloy steels the modern history of permanent magnetic materials starts with the end of the last century. The intrinsic coercivity and the energy density product of such magnetic steel materials were rather low compared to recently developed hard magnetic materials. Table 1 shows the historical development of the intrinsic coercivity and the magnetic energy density product of hard magnetic materials. In the year 1931 Mishima discovered in Japan an alloy of 58 wt% Fe, 30 wt% Ni and 12 wt% Al with a coercivity of about double that of the best magnet steel material (30–40 wt% Co plus W and Cr) which was available at that time. Soon it was discovered that the addition of cobalt and copper improved the properties of the Mishima alloy leading to various types of AlNiCo magnetic materials. After second world war hard magnetic materials based on ceramic hexaferrites were developed particulary in Holland.

Since the 1960s most of the developments of permanent magnetic materials have been done on the improvment of the magnetic properties. The search for new materials has been shifted from shape anisotropy to crystal anisotropy. The new hard magnetic materials based on rare earth intermetallic compounds exhibit a considerably higher

Table 1

Historical development of coercivity and energy density product of hardmagnetic materials

magnet	coercivity	energy density product	year
magnetic carbon-steel	1 kA/m	2 kJ/m³	1890
AlNiCo	10 kA/m	15 kJ/m³	1940
AlNiCo	100 kA/m	90 kJ/m³	1955
hardferrites	200 kA/m	20 kJ/m³	1960
SmCo 1:5	1000 kA/m	200 kJ/m³	1975
SmCo 2:17	2000 kA/m	260 kJ/m³	1982
NdFeB	2000 kA/m	400 kJ/m³	1985

*) Univ.-Doz. Dr. Josef Fidler, o. Prof. Dr. Peter Skalicky, Institut für Angewandte und Technische Physik, Technische Universität Wien, Karlsplatz 13, A-1040 Wien, Austria

83

coercive force and energy density product than the traditional AlNiCo-alloys and hardferrites. In the late 1960s the high magnetocrystalline anisotropy, the basis for a good permanent magnet material, was discovered in the USA under the leadership of K. Strnat (1) in several rare earth – cobalt intermetallic compounds. Soon it was discovered that the combination of the high magnetic moments of iron and/or cobalt with the high magnetic moment of heavy rare earths leads to high magnetocrystalline anisotropy and retains the high magnetic ordering temperature particularly in the system samarium – cobalt. The rare earth permanent magnets were discovered in the USA, but recent developments in this field have come from Japan, especially by the invention of rare earth – iron based permanent magnets (2) having the best magnetic properties so far achieved, in the year 1983.

The magnetic hardness of permanent magnet materials depends critically on the microstructure of the individual magnets. In the light of the historical development of the coercivity and the energy density product of hard magnetic materials the improvement of the energy density product is closely connected with a better understanding of the mechanisms leading to higher coercive forces of the magnets. The coercive force of hard magnetic materials is determined either by the nucleation of reversed magnetic domains at magnetic fields which are lower than the theoretical maximum

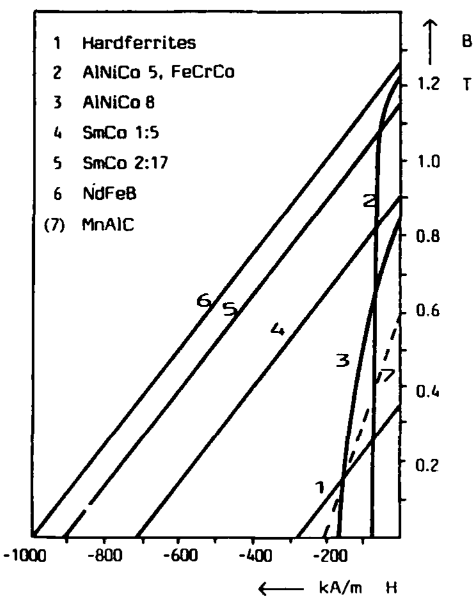


Fig. 1

Room temperature demagnetization curves of commercial *hardmagnetic materials*

Table 2

Magnetic properties of commercial hardmagnetic materials (at room temperature)

magnet	$(B \cdot H)_{max}$ kJ/m³	B_r T	$_BH_c$ kA/m	$_JH_c$ kA/m	T_C °C
hardferrites	25	0.35	280	320	450
$AlNiCo_5$	60	1.30	60	62	850
FeCrCo	60	1.30	60	62	850
$AlNiCo_8$	55	0.85	140	145	850
SmCo 1:5	200	0.90	720	2500	720
SmCo 2:17	260	1.15	920	3000	820
NdFeB	400	1.25	1000	2000	310

value of the anisotropy-field, or by the strong pinning of domain walls at crystal lattice defects and precipitates during the magnetization reversal (3). Analytical investigations for the characterization of the microstructural parameters, such as grain *size distribution, phase determination, chemical* homogeneity of the grains, crystal lattice defects and precipitates, are necessary for a better knowledge of the limiting factors of the coercivity.

As it has been the tradition for many years, special emphasis of our institute has been laid on the measurement of the hard magnetic properties and on the investigation of the microstructure of newly developed hard magnetic materials. Using high resolution and analytical electron microscopy together with X-ray microanalysis and metallography the microstructure of various magnetic materials were characterized.

1. New hard magnetic materials

Commercially available permanent magnet materials may be divided into seven groups. Fig. 1 shows the demagnetization curves of hardferrites, AlNiCo, rare earth permanent magnet materials and MnAlC magnets. The corresponding magnetic properties, such as energy density product, remanence, coercive forces and Curie temperature are summarized in Table 2. Magnets based on samarium-cobalt intermetallic compounds have gained an increased importance for the last 10 years and are strictly speaking not only limited to samarium. Depending on the producer a mixture of one or more rare earth elements with cobalt is used for the preparation of the magnets. In the following we distinguish two types of rare earth – cobalt magnets: the SmCo 1:5 and the SmCo 2:17 magnets, according as the main phase of the magnet exhibits the $SmCo_5$- or the Sm_2Co_{17}-structure.

Nevertheless, from the point of view of mass production the hardferrites and AlNiCo-magnets are the most important ones. Fig. 2 shows the estimated amount of Hardferrite, AlNiCo, REPM (rare earth permanent magnets) and other magnet materials to the western world production (Japan,

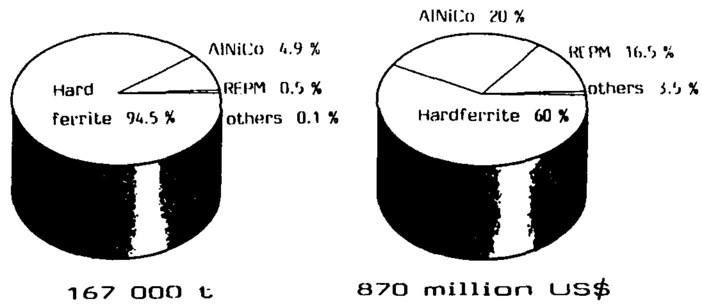


Fig. 2
Western world production of permanent magnet materials in the year 1984

USA and Europe) in the year 1984. Because of high raw material and production costs the cobalt based rare earth permanent magnets share only less than 20% of the annual total turnover, whereas the annual growth of this group has been in the order of more than 30% for the last few years. Through the invention of rare earth – iron based magnets which are less expensive from the raw material point of view, the annual growth of rare earth permanent magnets is expected to be increased worldwide. The production of the inexpensive ceramic Hardferrites increases annually in the order of 20%, whereas the one of AlNiCo magnets is slightly decreasing.

The drastic increase of the energy density product of newly developed hard magnetic materials (Table 2) enabled the invention of many new applications of permanent magnets. Permanent magnets are primarily used in magneto- and electromechanical applications and increasingly in beam guiding systems. Generally the magnetic field strength in the air gap of a magnetic circuit, containing a permanent magnet, is proportional to the energy density product and to the volume of the magnet, according to:

$$H_{air\ gap} \sim \sqrt{\frac{(B \cdot H)_m \cdot V_m}{V_{air\ gap}}} \qquad [1]$$

It is evident that the increase of the energy density product reduces besides the volume also the weight of the permanent magnet containing device and new designs of dynamic devices (motors, generators, etc.) and static devices (charged beam guiding systems) are possible.

2. Microstructure and properties of permanent magnets

2.1 Conventional magnets (Hardferrite and AlNiCo magnets)

Besides the *barium- and strontium-hardferrites* the group of AlNiCo magnets have been the most dominant commercial permanent magnet materials for many years (fig. 2). The hexagonal crystal structure of the hardferrites imparts a strong magnetocrystalline anisotropy. Magnets are made by sintering of aligned particles of about 10–100 μm in diameter. Metallographic investigations show that the shape of the demagnetization curve and therefore also the coercivity strongly depends on the grain size of the final magnet (4). The coercivity is controlled by the nucleation of reversed domains at low anisotropy regions. After the abrupt reversal of the magnetization in the individual grains after applying of an opposite external magnetic field, the further expansion of the reversed magnetic domains might be hindered by the pinning of domain walls at the grain boundary region. Finally, the coercivity of the individual magnet depends on the processing parameters (milling and annealing) and is directly correlated to the microstructure of the material.

The *AlNiCo magnets* are hard and brittle and are manufactured by casting of a liquid alloy, leading to the large grain size up to the order of millimeters, or by pressing and sintering metal powders leading to small grain sizes. Fig. 3a is an optical micrograph showing a large grain size of a cast AlNiCo 5 magnet. The transmission electron micrograph of this magnet (fig. 3b) shows a duplex microstructure of Fe-Co rich α_1-phase and a Ni-Al rich α_2-matrix phase. Depending on the type of the AlNiCo magnet different multi-stage heat treatments, including magnetic field anneals, are necessary to produce optimum properties. The effect of adding small amounts of Ti, Nb or Ta is to increase the coercivity but to decrease the remanence (AlNiCo 8). Depending on the cooling condition rodlike, coherent precipitates of the bcc-crystal structure type are formed parallel to the external magnetic field direction during cooling. The cause of the magnetic hardness of AlNiCo magnets is primarily the shape anisotropy of the rod-shaped and strongly magnetic Fe-Co rich α_1-phase and the difference of the magnetization between the two phases. The rods of the α_1-phase of the AlNiCo 5 magnet of fig. 3b are of the order

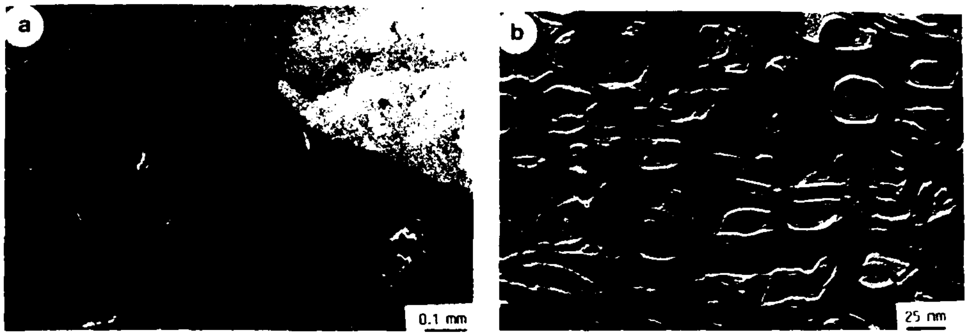


Fig. 3
Optical (a) and electron (b) micrographs showing the grainsize distribution and the duplex microstructure of a cast AlNiCo 5 magnet

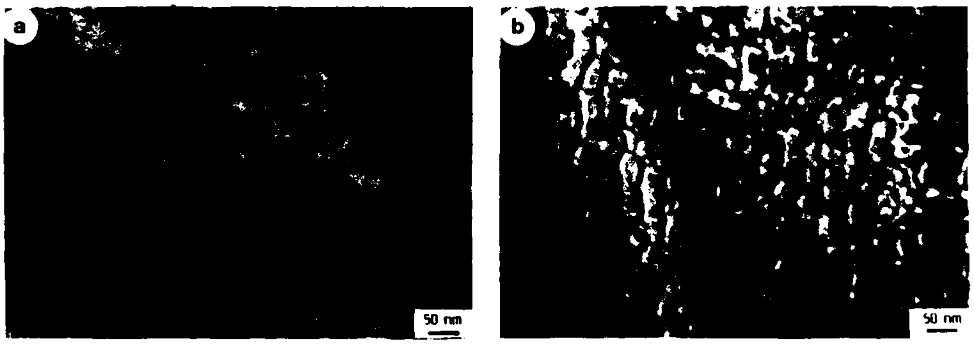


Fig. 4
Transmission electron micrograph of a cast AlNiCo 5 magnet. Magnetic domain walls are visible within the weak magnetic Al-Ni rich matrix phase in the defocused Fresnel image (b)

of 30x30x120 nm^3. From the Lorentz electron micrograph of fig. 4b showing magnetic domain walls within the weakly magnetic α_2-matrix phase, it is evident that the influence of the Ni-Al phase on the moving domain walls during the magnetization reversal must be taken into account. Electron microscopic investigations (fig. 5) show that titanium additions change the shape of the α_1-rods and decrease the volume fraction of the strongly magnetic Fe-Co rich α_1-phase and therefore change the coercivity and remanence. The interpretation of the coercivity of AlNiCo magnets is based on the combination of magnetization reversal models of single domain particles with domain wall motion models of interacting domains (5), (6), (7).

Ductile permanent magnet alloys based on the *Fe-Cr-Co* system have received considerable attention to be hot or cold worked into wire, sheet



Fig. 5
Transmission electron micrograph of a cast Ti-containing AlNiCo 8 magnet

or other forms. The magnetic properties and the microstructure are quite similar to AlNiCo 5 magnets. During cooling the alloy decomposes spinodally into the Fe rich α_1-phase and the Cr rich α_2-phase. Similar to the AlNiCo magnets the particle morphology (shape anisotropy) of the strongly magnetic α_1-phase predominatly determines the coercivity. The magnetic characteristics have been gradually improved by adding various minority elements such as Mo-Si, Nb, Al, V, T, and Cu ,8), (9).

2.2 Rare earth permanent magnets (REPM)

According to the phase diagrams of rare earth intermetallic compounds five compounds ($RECo_2$, $RECo_3$, RE_2Co_7, $RE_5 19_{19}$ and $RECo_5$) appear in the composition range 66.7–83.3 at% Co (10). The crystal structures of these phases are closely related with each other and are based on a regular stacking of two kinds of layers, one is a layer of $SmCo_2$-laves phase structure and the other is that of $SmCo_5$-structure. There exist two groups of REPM, the *RE-cobalt magnets* and the recently developed *RE-iron magnets*. The RE-cobalt magnets can be divided into five types depending on wether the magnet has a single-phase or a two-phase microstructure. The ideal microstructure of the single phase magnets consists of aligned single-domain particles with a $SmCo_5$- or Sm_2Co_{17}-crystal structure. Two types of precipitation hardened magnets can be distinguished: the one type contains 2:17-precipitates in a 1:5-matrix, the other type has 1:5-precipitates in a 2:17-matrix. Besides these magnets there are the bonded magnets, in which the single domain particles are embedded in a non magnetic phase. Rare earth-cobalt magnets are produced by a powder metallurgical process, whereas rare earth-iron magnets can be produced either by a powder metallurgical process (11) or derived from rapidly solidified melt-spun ribbons (12). The main process steps for the production of sintered rare earth permanent magnets are shown in fig. 6. The general production steps include alloy preparation, milling, composition control and adjustment, particle alignment and pressing, sintering and aging, machining and final magnetizing. Besides the parameters which determine the composition of the phases within the magnets there are also processing parameters, particularly during sintering and annealing steps such as sintering temperature, cooling rate, aging temperature and time (fig. 7), which must carefully be controlled in order

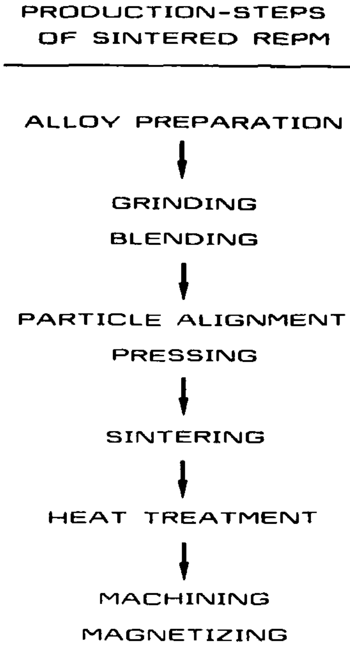


Fig. 6
Main process steps for the production of sintered rare earth permanent magnets

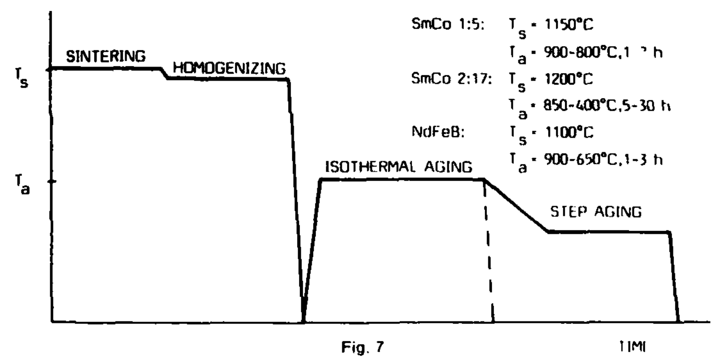


Fig. 7
Schematic sintering and post-sintering heat treatment curves of rare earth permanent magnets

to achieve maximum magnetic properties. Fig. 7 shows a typical schematic heat treatment curve of SmCo 1:5 SmCo 2:17 and NdFeB magnets. The heat treatment sequence to sinter multi-phase SmCo 2:17 magnets is more complicated and time consuming than the ones for sintering SmCo 1:5 or NdFeB magnets. The reason for different heat treatment sequencies for the different materials is due to the formation of different microstructures (13). The different types of initial magnetizing behaviour of demagnetized single phase SmCo 1:5, multi phase SmCo 2:17 and NdFeB magnets and the dependence of the coercivity on the magnetizing fields is shown in fig. 8. The different behaviour of the SmCo 1:5, SmCo 2:17 and NdFeB magnets is caused by different microstructures.

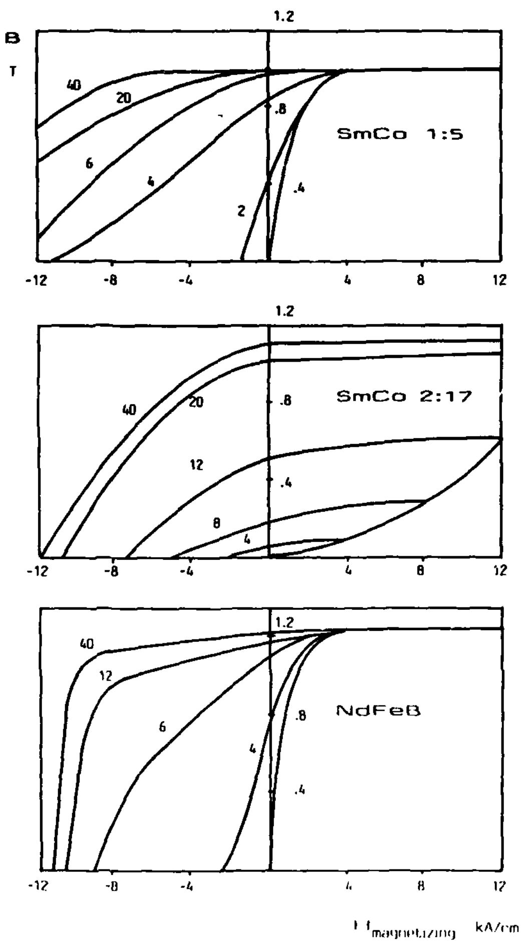


Fig. 8
Initial magnetization curves and dependence of the coercive force on the magnetizing external fields of different types of rare earth permanent magnet materials

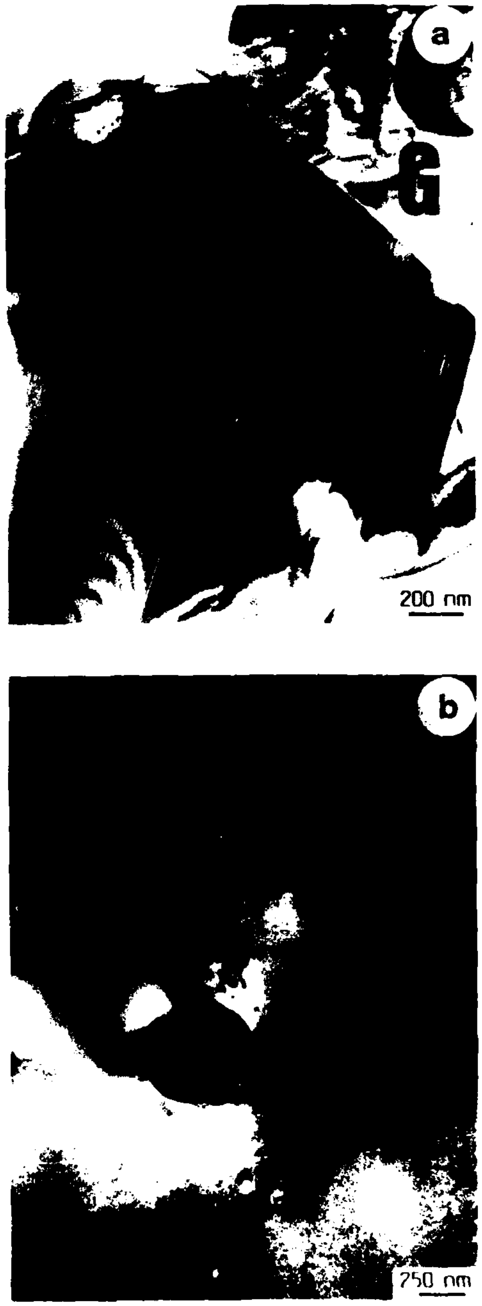


Fig. 9
Electron micrographs showing a grain with densly packed planar faults (a) and small precipitates (b) of a sintered SmCo 1:5 magnet

46

For the understanding of the different magnetization behaviour of demagnetized SmCo 1:5, SmCo 2:17 and NdFeB magnets we have used transmission electron microscopy and X-ray microanalysis together with optical metallography to characterize *crystal defects, precipitates and different* phases and to study the magnetic domain structure and their interaction with crystal lattice defects and precipitates. The microstructure of *single phase SmCo 1:5 magnets* consists of grains oriented parallel to the alignment direction, of precipitates with diameters comparable to the grain size and of precipitates with diameters up to 500 nm (14). Most of the $SmCo_5$ grain interiors *show a low defect density and their grain diameter* exceeds the theoretical single domain size (1:2 μm) and is in the order of 5–10 μm. Except isolated grain boundary inclusions, partly identified as a CaO-phase, our electron microscope investigation does not show a preferential segregation of a second phase at grain boundaries. Besides 1:5-grains also grains with densly packed, parallel stacking faults perpendicular to the hexagonal c-axis are observed (fig. 9a). Such basal stacking faults correspond to a transformation of the 1:5-crystal structure into the Sm-rich Sm_2Co_7 and Sm_5Co_{19} structure types. Using high resolution electron microscopy together with X-ray STEM microanalysis the different polytypes and structural modifications of these Sm-rich phases can be distinguished (15), (16). In all of the single phase SmCo 1:5 sintered magnets incoherent precipitates with diameters up to 0.5 μm were found (fig. 9b). Some of these precipitates show only intense Sm-peaks in their X-ray spectra (fig. 10). These precipitates were identified as Sm_2O_3-particles. Occasionally some of the X-ray spectra of grains and especially of grain boundaries and precipitates an additional Si-peak was found. In some of the CaO- and Sm_2O_3-particles sulphur could be detected. In single phase SmCo 1:5 sintered magnets the coercivity is determined by the nucleation field of reversed domains which is lower than the coercive force of a magnetically saturated particle with a single domain structure. The nucleation of reversed domains takes place in regions with low magneto-crystalline anisotropy. Rare earth-rich precipitates mainly deteriorate the coercivity of the final magnet. The reason for the formation of these phases is due to the

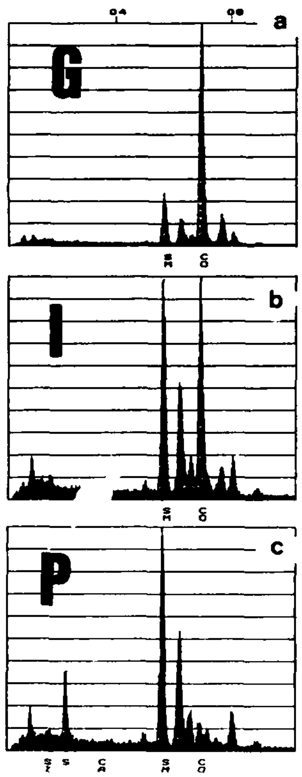


Fig. 10
Energy dispersive X-ray spectra of a hard magnetic grain G, of a rare earth-rich phase I and of a rare earth-oxide phase P of a sintered SmCo 1:5 magnet



Fig. 11
Electron micrograph showing the cellular precipitation structure of a sintered SmCo 2:17 magnet. Rhombic cells – phase A – are separated by a cell boundary phase B. In high coercivty magnets a platelet phase C is found

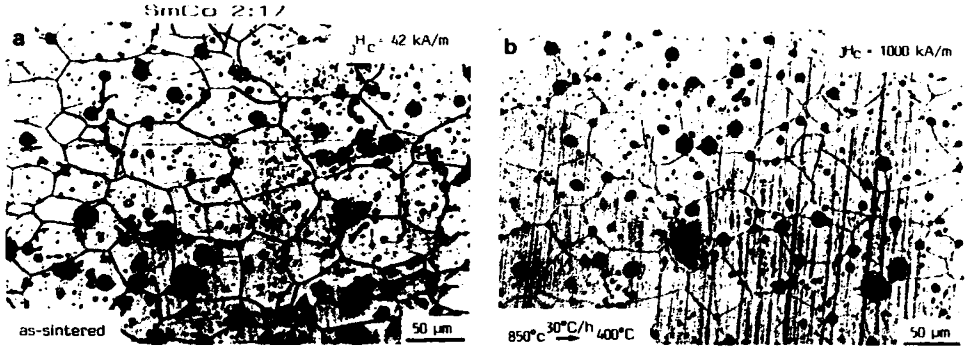


Fig. 12
Optical micrographs show no difference in the grain size distribution in the as-sintered and after an optimum post-sintering heat treatment of a SmCo 2:17 magnet

addition of a rare earth-rich sintering aid phase before the sintering process. The coercivity can be improved by adding small amounts of transition metal powders or transition metal oxides. Microstructural investigations on $(CeMM,Sm)Co_5$ and $(Pr,Sm)Co_5$ sintered magnets showed similar results as in the case of single phase $SmCo_5$ sintered magnets (16), (17). The corresponding X-ray spectra of the different phases showed a mixture of rare earth elements due to their ratio of the nominal composition of the magnet. Our analytical electron microscope study shows that the chemical composition, the size distribution and the impurity content of the starting powder material are important factors for the magnetic properties of SmCo 1:5 sintered magnets.

Copper containing cobalt rare earths with a composition of $Sm(Co,Fe,Cu,TM)_{6-8}$ TM = Zr,Ti,Hf show a tine scale, cellular microstructure (18), (19). Rhombic cells of the type $Sm_2(Co,Fe,TM)_{17}$ – phase A – are separated by a $Sm(Co,Cu,TM)_5$ cell boundary phase – phase B (fig. 11). In magnets with high coercivities (> 1000 kA/m) thin platelets are found perpendicular to the hexagonal c-axis. Our high resolution electron microscope investigations (18) show that the crystal structure of the platelet phase C is close to the hexagonal Sm_2Co_{17} structure with a c-crystal parameter of 0.8 nm, which is in agreement with metallurgical considerations (20). The development of the cellular precipitation structure of highest coercivity magnets is controlled by the growth process and the chemical redistribution process and is determined by the direction of zero deformation strains due to the crystal lattice misfit between the different phases (21). Growth occurs primarily during the isothermal aging procedure and involves the diffusion of samarium. The cellular precipitation structure is formed during the isothermal aging procedure, whereas the chemical redistribution of the transition metals during the step aging procedure increases the coercivity of the final magnet (fig. 7). The optical micrographs of fig. 12 show no difference in the grain size distribution after sintering and after the postsintering heat treatment, whereas in the corresponding electron micrographs of fig. 13 the formation of the cellular precipitation structure after the heat treatment is shown. Contrary to high coercivity magnets which contain large crystallographic twins (fig. 14a) in low coercivity magnets (<500 kA/m) a microtwinning within the cell interior phase A is observed by high resolution electron microscopy (fig. 14b). By means of Lorentz electron microscopy (fig. 15) we have shown that the cellular precipitation structure acts as attractive pinning centre for magnetic domain walls (21). We found that maximum coercivities (~2000 kA/m) occurred in magnets with cell diameters of about 200 nm. The compositional difference between the cell boundary phase B and the cell interior phase A determines the coercivity. The platelet phase C predominately acts as diffusion path for the transition metals and leads to a better chemical redistribution after the isothermal aging treatment and therefore to a higher coercivity of the magnet. Impurities, primarily such as oxygen and carbon, lead to the formation of macroscopic precipitates of the Sm_2O_3, ZrC, TiC etc.

Table 3

Phases in sintered $Nd_{15}Fe_{77}B_8$ magnets

				MH
A	$Nd_2Fe_{14}B$	tetr.	a = 0.88 nm, c = 1.22 nm	950
B	$Nd_{1.1}Fe_4B_4$	tetr.	a = 0.71 nm, c = 14.5 nm	1430
C	Nd-rich	f.c.c.	a = 0.52 nm	360
D	Nd-oxides	hex.	a = 0.38 nm, c = 0.60 nm	
E	α – Fe	b.c.c.	a = 0.29 nm	190

Not detected: Nd_2Fe_{17}, $NdFe_2$ / MH . . . microhardness

90

and therefore impede the formation of the platelet phase C and finally impede the chemical redistribution process.

Sintered *NdFeB magnets* with a nominal composition $Nd_{15}Fe_{77}B_8$ exhibit the highest energy density products so far (3). These magnets show magnetization curves according to the nucleation of reversed domains (fig. 8). As result of our microstructural investigations an identical microstructure in various magnets, supplied by different producers, was observed. The following phases were detected by analytical electron microscopic techniques and are summarized in table 3. The optical (fig. 16a) and the electron (fig. 16b) micrographs show three different types of phases, each with a different chemical composition, occurring in sin-

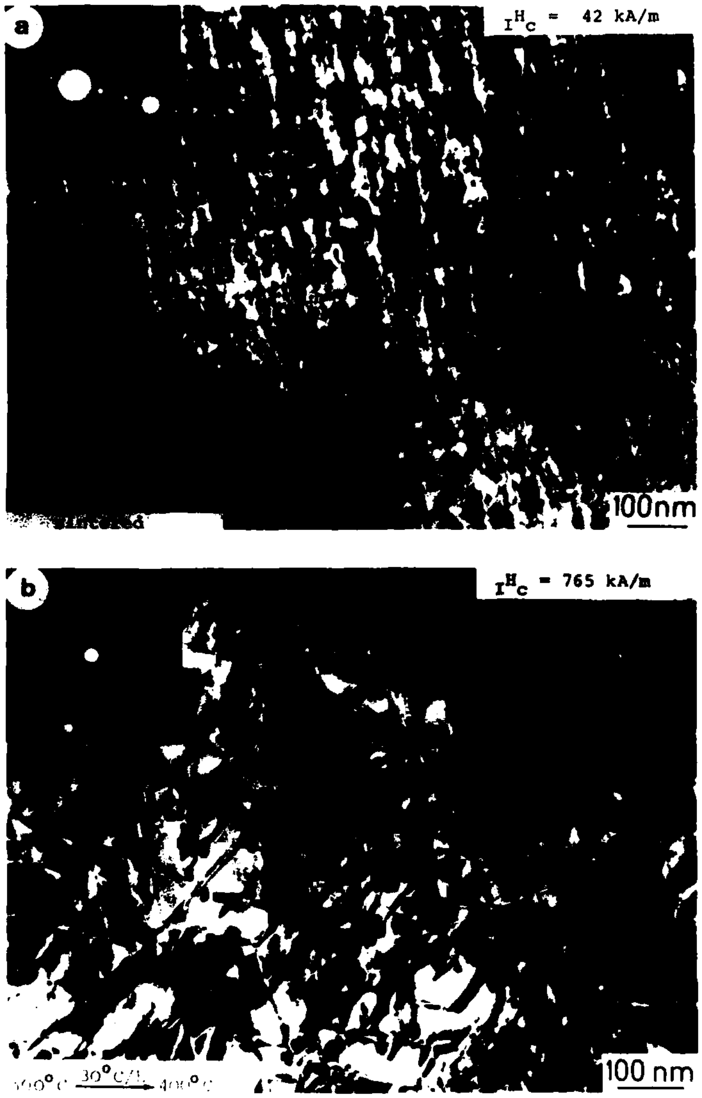


Fig. 13
Electron micrographs showing the influence of the heat treatment on the cellular microstructure and therefore on the coercivity of the magnets of fig. 12

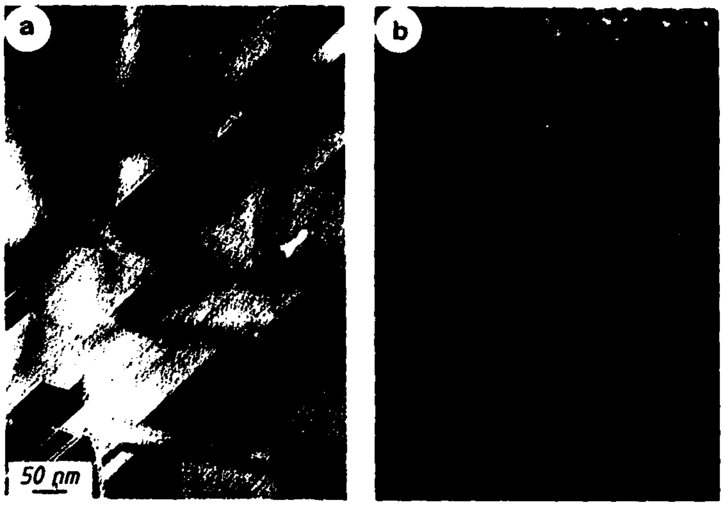


Fig. 14
Bright field (a) and high resolution (b) electron micrographs showing the twinning in high coercivity (1000 kA/m) and low coercivity (400 kA/m) SmCo 2:17 magnets

tered NdFeB magnets. Phase A is always found to be free of crystal lattice defects and corresponds to the hard magnetic boride $Nd_2Fe_{14}B$. In the energy dispersive X-ray spectrum of phase A (fig. 17a) the FeKB-peak lies between the NdLA- and NdLB1-peaks. Phase B is Nd-richer than phase A. In the corresponding X-ray spectrum the FeKB-peak is smaller than the NdLB1-peak (fig. 17b). The ratio of the Fe- to the Nd-concentration (in at%) was found to be in the range 3.6 to 3.9. Our high resolution electron studies revealed a crystal lattice periodicity of 0.4 nm, 4.8 nm and 14.5 nm (22). Both results, obtained by X-ray STEM microanalysis and high resolution electron microscopy, are in agreement with structural and compositional data of the phase $Nd_{1.109}Fe_4B_4$ (23). The grain interior of phase B shows a high crystal defect density, which explains the large value of the microhardness (see table 3). Phase C is found to be a Nd-rich sintering aid phase. The ratio of the Nd- to Fe-concentration (in at%) determined by X-ray microanalysis is about 6 corresponding to about 85 at% Nd. This phase may also occur with some content of oxygen and/or boron. Phase C is mainly found as isolated inclusions near grain boundaries or as layer phase along grain boundaries. It should be mentioned that depending on the raw material used by the producer various impurities such as silicon, chlorine, phosphorus, niobium, platinum, tin etc. are found in all of the phases listed above. As result of our investigations of sintered NdFeB magnets, produced by a powder metallurgical process, the coercivity is primarily determined by the magnetization reversal within the hard magnetic $Nd_2Fe_{14}B$ grains and is limited by the nucleation and expansion field for reversed domains. The layer phase, separating the hard magnetic grains, contributes also to the coercivity. Replacing neodymium by dysprosium (Nd:Dy = 10:1) increases the coercivity, but does not show any drastic effect on the composition of the different phases, whereas generally the grain size of such magnets is considerably smaller than in magnets without dysprosium.



Fig. 15
Foucault electron micrograph showing the pinning of a magnetic domain wall at the continuos cellular precipitation structure

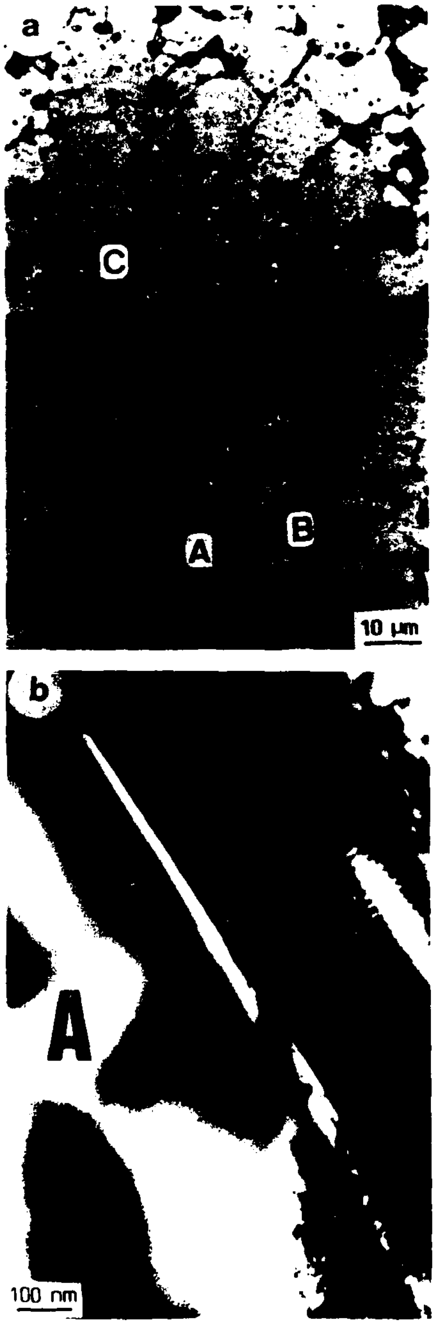


Fig. 16
Optical (a) and transmission electron (b) micrographs showing various phases in a sintered $Nd_{15}Fe_{77}B_8$ magnet

3. Conclusions

Newly developed magnetic materials such as rare earth permanent magnets are increasingly used in many magneto- and electromechanical and electronic applications. One of the reasons is a better understanding of the microstructure of the materials which determines besides the processing parameters the magnetic properties of the magnets (fig. 18). Effectively the magnetic energy density product and the coercivity could be improved drasticly during the last ten years. As result of analytical investigations it is evident that the coercivity is closely related to the individual microstructure of the magnets. In the case of shape anisotropy materials (AlNiCo, FeCrCo) the magnetocrystalline anisotropy is relatively small and the coercivity is controlled by shape anisotropy, the volume fraction of the strongly magnetic phase and the difference of the magnetization of the different phases. In hardferrites, SmCo 1:5 and NdFeB magnets the high coercive forces are primarily obtained by the high magnetocrystalline

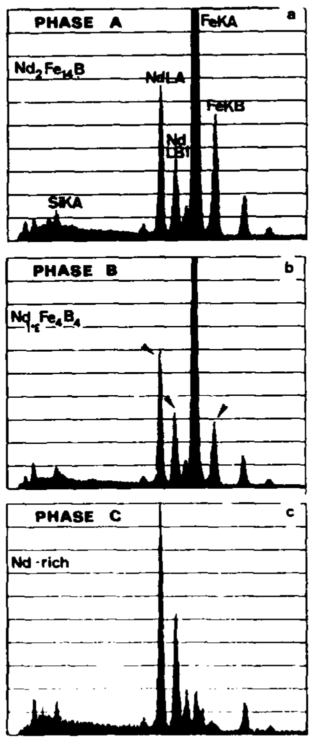


Fig. 17
Energy dispersive X-ray spectra taken by STEM-microanalysis of the various phases of a sintered $Nd_{15}Fe_{77}B_8$ magnet

anisotropies and are limited by the nucleation and expansion of reversed domains. In precipitation hardened SmCo 2:17 magnets the coercivity is determined by the domain wall pinning at a continuous precipitation structure during the magnetization reversal process. The newly developed NdFeB permanent magnet materials exhibit high remanences, energy density products and coercive forces at room temperature (table 2), but due to the low Curie temperature the maximum operation temperature is limited at present to about 120°C. It can be expected that this upper limit of the operation temperature can be increased by a further magnetic hardening in the next few years.

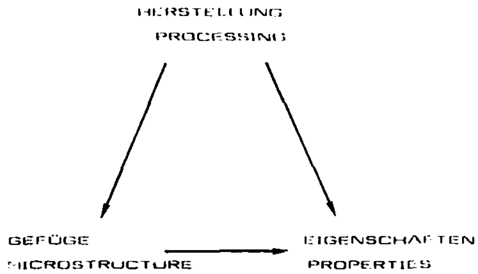


Fig. 18
The magnetic properties of permanent magnet materials are primarily determined by processing parameters and by the microstructure

Acknowledgement

The authors are grateful for the financial support of this work by the Austrian Forschungsförderungsfonds (Project No. P4640), by the Austrian Nationalbank (Projekt No. 2088) and by the U.S. Army European Research Office, London (Contract No. DAJA 45-84-C-0010).

References

1. Strnat, K. J., G. Hoffer, J. Oson and W. Ostertag: "A family of new cobalt-base permanent magnet materials", J. Appl. Phys. 38, p. 1001 (1967).
2. Sagawa, M., S. Fujimura, N. Togawa, H. Yamamoto and Y. Matsuura: "New material for permanent magnets on a base of Nd and Fe", J. Appl. Phys., 55, p. 2083 (1984).
3. Kronmüller, H.: "Theory of magnetic hardening mechanisms in RE-cobalt magnets", Proc. VII. Int. Workshop RE-Co Perm. Magn., p. 339, Beijing 1983.
4. Heimke, G.: "Keramische Magnete", Springer Verlag, Wien, New York, 1976.
5. McCurrie, R. A.: Ferromagnetic Mat., Vol. 3, ed. E. P. Wohlfarth, N. Holland, Amsterdam, p. 107 (1982).
6. Iwama, Y., and M. Takeuchi: "Spinodal decomposition in AlNiCo8 magnet alloy", Transactions of the Japan Institute of metals, Vol. 15, p. 371 (1974) and Vol. 17, p. 399 (1976).
7. Hetherington, M. G., A. Cerezo, J. P. Jakubovics and G. D. W. Smith: "Observations on the microstructure and magnetization of AlNiCo permanent magnets", Journal de Physique, Coll. C9, Cuppl. 12, Tome 45, p. 429 (1984).
8. Cremer, R., and I. Pfeiffer: "Untersuchungen zum Ausscheidungsverhalten von Cr–Co–Fe Dauermagnetlegierungen", Physica 80B, p. 164 (1975).
9. Kaneko, H., M. Homma and M. Okada: "Fe–Cr–Co ductile magnet with (B · H) = 8 HGOe", AIP Conf. Proc. 29, p. 620 (1975).
10. Stadelmaier, H. H.: „Structural classification of transition-metal/rare earth compounds between T and T_5R", Z. Metallkunde, 75, p. 227 (1984).
11. Sagawa, M., S. Fujimura, H. Yamamoto, Y. Matsuura and K. Hiraga: "Permanent magnet materials based on the rare earth-iron-boron tetragonal compounds", IEEE Trans. Magn. MAG-20, p. 1584 (1984).
12. Lee, R. W., E. G. Brewer and N. A. Schaffel: "Processing of neodymium-iron-boron melt-spun ribbons to fully dense magnets", IEEE-Trans. Magn. MAG-21, p. 1958 (1985).
13. Fidler, J., P. Skalicky and F. Rothwarf: "Analytical electron microscopy of rare-earth permanent magnet materials", Mikrochimica Acta (Wien), Suppl. 11, p. 371 (1985).
14. Fidler, J.: "Transmission electron microscopy of single-phase Co_5Sm permanent magnets", Phil. Mag., B 46, p. 565 (1982).
15. Fidler, J., and P. Skalicky: "Microanalysis and microstructure of cobalt-containing permanent magnets", Metallurgie, in press.
16. Ghandehari, M. H., and J. Fidler: "Microstructural studies of oxide doped $PrCo_5$ magnets", IEEE Trans. Magn., MAG-21, p. 1973 (1985).
17. Rodewald, W., and J. Fidler: "Improvement of coercivity of (CeMM, Sm)Co_5-magnets", Proc. 3rd Int. Symp. on Magn. Anisotropy and Coercivity of Rare Earth Transition Metal Alloys (J. Fidler, ed.), Baden/Austria, p. 339 (1982).
18. Fidler, J., P. Skalicky and F. Rothwarf: "High resolution electron microscope study of $Sm(Co, Fe, Cu, Zr)_{7.5}$ magnets", IEEE-Tran. Magn. MAG-19, p. 2041 (1983).
19. Mishra, R. K., G. Thomas, T. Yoneyama, A. Fukuno and T. Ojima: "Microstructure and properties of step aged rare earth alloy magnets", J. Appl. Phys. 52, p. 2517 (1981).
20. Ray, A. E.: "Metallurgical behavior of $Sm(Co, Fe, Cu, Zr)_z$ alloys", J. Appl. Phys., 55, p. 2094 (1984).
21. Fidler, J.: "Coercivity of precipitation hardened cobalt rare earth 17:2 permanent magnets", J. Magn. Magn. Mat. 30, p. 58 (1982).
22. Fidler, J.: "Analytical microscope studies of sintered Nd-Fe-B magnets", IEEE Trans. Magn. MAG-21, p. 1955 (1985).
23. Bezinge, A., H. F. Braun, J. Muller and K. Yvon: "Tetragonal rare earth-iron borides $R_{1+\varepsilon}Fe_4B_4$ ($\varepsilon \simeq 0.1$) with incommensurate rare earth and iron substructures", Solid State Commun., in press.

94

19

Journal of Magnetism and Magnetic Materials 66 (1987) 74–78
North-Holland, Amsterdam

ELECTRON MICROSCOPE STUDY OF PRECIPITATION IN A NIOBIUM-CONTAINING (Nd, Dy)–Fe–B SINTERED MAGNET

S.F.H. PARKER, P.J. GRUNDY and J. FIDLER *

Department of Pure and Applied Physics, University of Salford, Salford M5 4WT, UK
* *Inst. of Appl. Physics, Technical University of Vienna, Karlsplatz 13, A-1040 Vienna, Austria*

Received 29 September 1986

The microstructure of a niobium-containing (Nd, Dy)–Fe–B alloy has been investigated using transmission electron microscopy, STEM and SEM X-ray microanalysis and optical microscopy. Magnetic measurements showed an increase in coercivity when niobium was added to a (Nd, Dy)–Fe–B magnet. The microstructure was found to be similar to that of a ternary Nd–Fe–B magnet but with two additional phases, a Laves Fe_2Nb compound and a finely dispersed niobium containing coherent precipitate found in the magnetically hard phase. Lorentz microscopy indicated domain wall interactions with the fine precipitates which may be responsible for the enhanced coercivity of the niobium doped magnet.

1. Introduction

High energy product sintered magnets based on the composition $Fe_{77}Nd_{15}B_8$ [1] are well established as replacements for SmCo and ferrites. Magnets with energy products approaching 40 MGOe are commercially available and energy products of up to 50 MGOe have been achieved in the laboratory. The origin of the coercivity in this magnet has been the subject of many studies and is thought to result from the difficulty of nucleating reverse domains [2].

The application of these magnets has been limited by the low Curie temperature ($\approx 300°C$) of the hard magnetic $Fe_{14}Nd_2B$ phase. To extend the temperature range over which these magnets can be used, attempts have been made to increase the room temperature coercivity so that reasonable properties are still maintained at elevated temperatures. The addition of Dy to the ternary alloy [3] is known to increase the anisotropy field of the $Fe_{14}Nd_2B$ phase and hence the coercivity of the magnet. An alternative approach is to introduce small precipitates or interfaces into the hard magnetic phase to produce domain wall pinning. Our measurements have shown that an increase in coercivity is produced when Nb is added to a Nd, Dy–Fe–B magnet. We have used electron microscopy and X-ray microanalysis to identify the different phases present and to gain an understanding of the coercivity mechanism.

2. Experimental

The magnets investigated were fabricated by Mullard Magnetic Components and were prepared from 99.5% pure cast material supplied by Rare Earth Products. The compositions of the alloys were $Nd_{14.5}Dy_{1.5}Fe_{76.0}B_{7.0}Nb_{1.0}$ and $Nd_{16.0}Dy_{1.1}Fe_{75.1}B_{7.8}$. The powdered alloy was pressed parallel to the alignment direction prior to sintering at 1080°C and then heat treated for 1 h at 630°C. Due to the purity level of the cast material and the parallel pressing the magnets did not have optimum properties. Specimens for electron microscopy were prepared by electropolishing using a 10% perchloric/90% glacial acetic acid electrolyte followed by ion thinning using 5keV argon ions. They were examined with a JEOL 200CX or a Philips EM430 electron microscope both equipped with X-ray microanalysis fascilities. Scanning electron microscopy was performed on

95

polished samples using a Cambridge Stereoscan 604 equipped with an X-ray microanalyser.

3. Results and discussion

Hysteresis properties were measured using a pulse magnetometer to saturate the specimen which was then transfered to a permeameter to trace the demagnetising curve. The values obtained for the Nb containing magnet are as follows: $B_r = 10.5$ kG, $H_{ic} = 16.0$ kOe, $(BH)_{max} = 24.8$ MGOe. The values obtained for a Nd, Dy–Fe–B magnet fabricated under identical conditions were: $B_r = 10.5$ kG, $H_{ic} = 12.8$ kOe, $(BH)_{max} = 19.8$ MGOe. These are obviously not optimum magnetic properties but they do show that the addition of Nb to the Nd, Dy–Fe–B magnet produces a significant increase in coercivity.

In our study of the Nb containing magnet we observed four other phases in addition to the main $Fe_{14}Nd_2B$ phase. There distribution is shown in an optical micrograph, fig. 1. Phase A is the hard magnetic phase, most grains of this phase contained small precipitates of 200–500 Å diameter and a density of 10^{21} nuclei/m^3, fig. 2. X-ray microanalysis of these particles, fig. 3, showed them to be richer in Nb than the surrounding matrix, fig. 4, but the ratio (Fe + Nb)/Nd was the same indicating that Nb was replacing iron in the $Fe_{14}Nd_2B$ phase. However, because of the small size of these particles it was impossible to avoid a contribution to the X-ray spectrum from the surrounding matrix. Convergent beam diffraction showed a small rotation of the zone pattern as the beam was moved through the particles but the lattice constants of the particles and matrix were very close. The substitution of Nb for Fe at over 15% of the Fe sites will presumably result in a fall in magnetisation. A Lorentz micrograph, fig. 5, taken from the hard magnetic phase shows the domain walls changing direction as they pass through and near the precipitates. These precipitates are therefore acting as domain wall pinning sites although it is not possible to say whether they contribute significantly to the coercivity of the magnet.

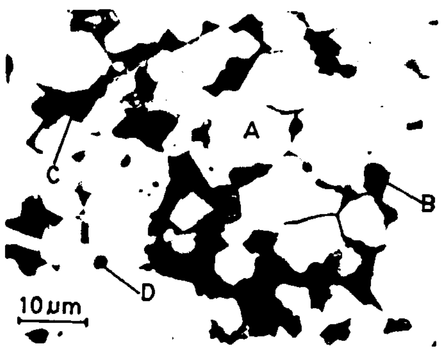


Fig. 1. Optical micrograph showing four phases A, B, C, D in the sintered magnet.



Fig. 2. Transmission electron micrograph showing small Nb containing precipitates in phase A.

Phase B is the tetragonal Fe_4B_4Nd phase which is thought to be non-ferromagnetic and is usually present, at least in the ternary FeNdB magnet [4], at a volume fraction of 5%. STEM X-ray microanalysis of this phase revealed a variation in iron content between different grains. It was found that the grains with the highest iron content (5–6 at% Fe/Nd) had a larger lattice constant $c_0 = 48$ Å and were more heavily faulted. Fig. 6a is a TEM micrograph showing a lattice fringe image with a 48 Å spacing corresponding to the (001) lattice planes in the B-phase and fig. 6b is its associated X-ray spectrum.

96

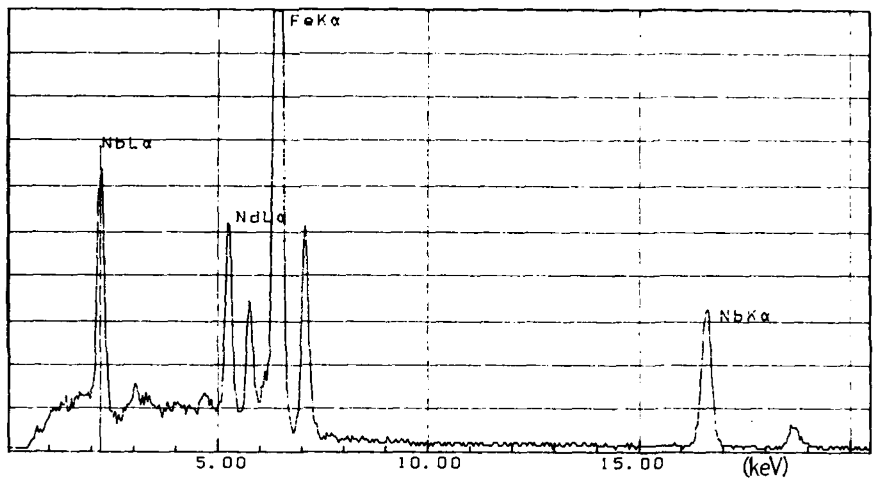


Fig. 3. STEM X-ray microanalysis of a Nb containing precipitate in phase A.

Phase C is the Nd rich sintering aid phase. TEM specimens showed little of this phase, possibly as a result of preferential etching during sample preparation. SEM specimens showed this phase to be located mainly around the grain boundaries of the A-phase at a volume fraction of around 10%. The presence of this phase made the preparation of optical and SEM specimens difficult as it tended to oxidise rapidly and break out of the surface to leave pores.

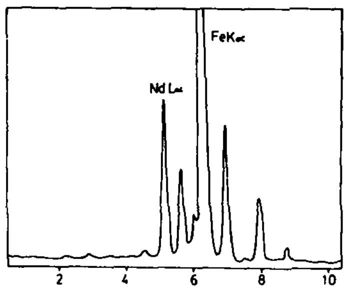


Fig. 4. STEM X-ray microanalysis of phase A.

Phase D was identified as a Laves phase Fe_2Nb having a $MgZn_2$ structure [5] and lattice parameters ($a_0 = 4.82$ Å, $c_0 = 7.87$ Å). Fig. 7a shows a TEM micrograph of this phase with its associated

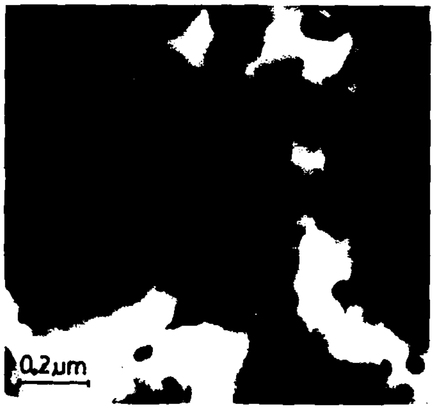


Fig. 5. Lorentz micrograph showing Nb containing precipitates in phase A.

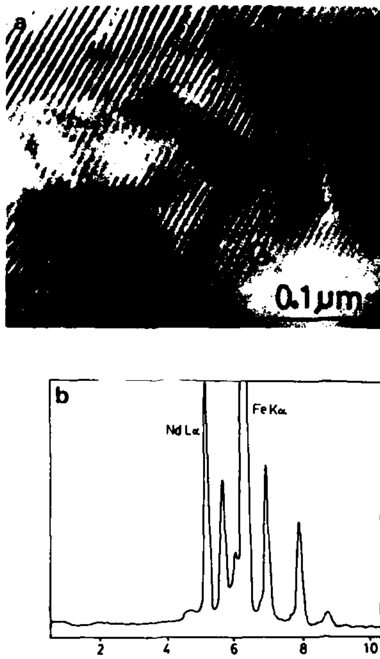


Fig. 6. (a) Transmission electron micrograph showing lattice fringe image of B phase; (b) associated X-ray spectrum.

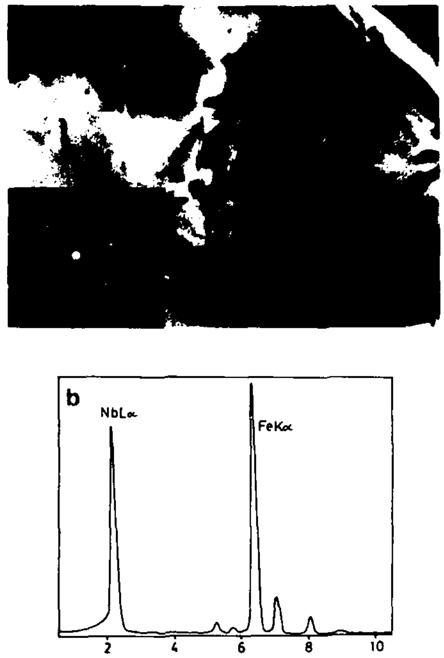


Fig. 7. (a) Transmission electron micrograph; (b) associated X-ray microanalysis of phase D.

diffraction pattern ([011] zone axis). Fig. 7b shows X-ray microanalysis of the Fe_2Nb phase. The Nb content of this phase can vary from 22–44 at% and above 33% Nb this phase is found to be non-ferromagnetic [5]. The Fe_2Nb phase was present as small inclusions of 2 µm diameter in the hard magnetic phase. It was found to contain small amounts of Nd probably occupying the same atom sites as the Nb since there exists a Laves phase of the type Fe_2Nd. Domains have not been observed in this phase indicating that it is probably non-magnetic unlike the smaller Nb containing precipitates also found in the hard magnetic phase.

4. Conclusion

The microstructure of the Nb containing magnet was found to be similar to that of a ternary FeNdB magnet [2] but with the addition of two Nb containing phases which were found inside grains of the hard magnetic phase. The larger inclusions were identified by electron diffraction and X-ray microanalysis as the Laves phase Fe_2Nb. The absence of domain walls within this phase suggest that it is probably non-ferromagnetic but the relatively large size of these inclusions, of the order 2 µm, means they would not form sites for domain wall pinning. However, the smaller Nb containing precipitates are of a size (200–500 Å) which could produce domain wall

94

pinning. If these precipitates do produce strong pinning then their presence would explain the enhanced coercivity of the Nb containing magnet.

Acknowledgements

The authors would like to thank Dr.C.A. Faunce and R.J. Pollard for their assistance with SEM and optical microscopy and Dr. J. Ormerod and E. Rozendaal for preparing the samples and magnetic measurements. We would also like to thank G. Cliffe of the Department of Metallurgy, University of Manchester for his help with X-ray microanalysis. This work was supported by the UK Science and Engineering Research Council and the Concerted European Action on Magnets programme (CEAM) of the European Community Stimulation Action.

References

[1] J. Ormerod, J. Less-Common Metals 111 (1985) 49.
[2] J. Fidler, IEEE Trans. Magn. MAG-21 (1985) 1955.
[3] M. Sagawa, S. Fujimura, H. Yamamoto, Y. Matsuura and K. Higara, IEEE Trans. Magn. MAG-20 (1984) 1584.
[4] K.D. Durst and H. Kronmüller, J. Magn. Magn. Mat. 59 (1986) 86.
[5] H.J. Goldschmidt, J. Iron Steel Inst. 194 (1960) 168.

99

20

MICROSTRUCTURAL EVIDENCE FOR THE MAGNETIC SURFACE HARDENING OF Dy_2O_3-DOPED $Nd_{15}Fe_{77}B_8$ MAGNETS

M.H. GHANDEHARI
Unocal Science and Technology Division, Unocal Corporation, Brea, CA 92621, USA

and

J. FIDLER
Institute of Applied and Technical Physics, Technical University of Vienna, Vienna, Austria

Received 18 March 1987

Microstructures of $(NdDy)_{15}Fe_{77}B_8$ prepared by alloying with Dy, and using Dy_2O_3 as a sintering additive, have been determined using electron microprobe and transmission electron microscopy. A two-step, post-sintering heat treatment has been applied to both systems in order to improve the coercivity. The results show that the second-step heat-treatment temperature is lower for the oxide-doped magnets for an optimum intrinsic coercivity. In a typical Dy_2O_3-doped sample, a high concentration of Dy was found close to the grain boundary of the hard 2–14–1 phase. In contrast, Dy was found uniformly substituted in a magnet to which Dy was added in the alloying step. It is proposed that a high concentration of Dy at the surface of the $(NdDy)_2Fe_{14}B$ improves the coercivity by increasing the required field for domain reversal nucleation at or near the grain boundaries.

1. Introduction

Magnetic hardness of a permanent magnet results from the inherent magnetic crystalline anisotropy of the material and the structural changes, in particular, those occurring at the grain boundaries. The coercivity enhancement of $Nd_{15}Fe_{77}B_8$ by Dy substitution has been attributed to the higher magnetic crystalline anisotropy of the magnetic phase $(NdDy)_2Fe_{14}B$ [1]. It has also been shown that Dy can be introduced by the reaction of Dy_2O_3 with $Nd_{15}Fe_{77}B_8$ powder during the sintering [2]. In addition, the Dy intensity profile from X-ray spectrometer has shown an uneven distribution of Dy across several grains in the Dy_2O_3-doped magnets. In this study, we have prepared magnets by Dy substitution in the alloying step, and by Dy_2O_3 doping prior to sintering. The resultant microstructures have been compared by scanning transmission electron microscopy (STEM) and electron microprobe. Finally, a two-step post-sintering heat treatment was employed to develop the coercivity which is also compared for the two systems.

Table 1
Intrinsic coercivity of $Nd_{13.5}Dy_{1.5}Fe_{77}B_8$ as a function of post-sintering heat treatment (all samples were sintered at 1070°C for 1 h)

Sample	Post-sintering heat treatment		${}^iH_c$ (Oe)
	T (°C)	t (h)	
1	900	2	13500
1	900 630	2 1	13800
1	900 630 680	2 1 2	15100
2	900	2	13600
2	900 680	2 1	15000

100

Table 2
Intrinsic coercivity of Dy_2O_3-doped $Nd_{15}Fe_{77}B_8$ as a function of post-sintering heat treatment (all samples were doped with 4 wt% Dy_2O_3 and sintered at 1070°C for 1 h)

Sample	Post-sintering heat treatment		^iH_c (Oe)
	T (°C)	t (h)	
1	900	2	
	610	1	17000
2	900	2	
	590	1	17500
3	900	2	
	570	1	15400
4	900	2	
	630	1	16300
5	900	2	
	570	1	17000
6	900	2	
	550	1	14800
7	900	2	
	600	1	16200
8	900	2	
	610	1	16900
9	900	2	
	590	1	15200
10	900	2	
	620	1	15600

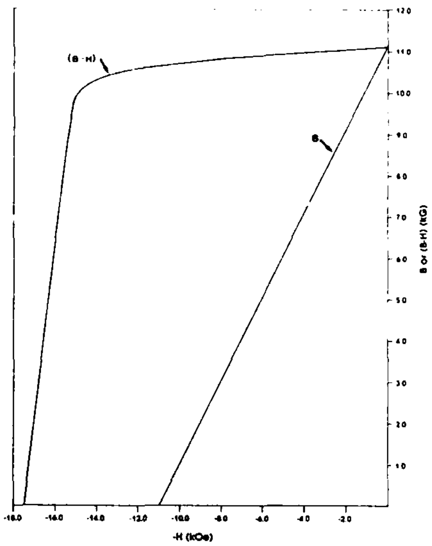


Fig. 1. Demagnetization curves of a Dy_2O_3-doped $Nd_{15}Fe_{77}B_8$ (sample 2 from table 1).

2. Experimental

Powder samples were prepared from a nominal $Nd_{15}Fe_{77}B_8$, and an alloy in which 3.5 wt% (approximately 10 atomic %) of Nd was replaced by Dy in the alloying step. Both of these powder samples were prepared under identical conditions and contained typically 0.5 to 0.6 wt% oxygen prior to pressing and sintering. 4.0 wt% Dy_2O_3 (3.5 wt% Dy equivalent) was hand mixed with the former, and both types of magnets were sintered at 1070°C for 1 h and annealed in two steps [3]. The first step of the annealing process consisted of 900°C for 2 h and the second step varied between 550 and 680°C for 1 h. Samples were rapidly quenched in a cooler part of the furnace in between the two steps. After the magnetic measurements, the sintered samples were analyzed for O_2 by a vacuum fusion technique. Boron,

Table 3
Chemical analysis of a Dy-alloyed and a Dy_2O_3-doped $Nd_{15}Fe_{77}B_8$ sintered magnet

Sample	^iH_c (Oe)	Elements (wt%)				
		Nd	Dy	Fe	B	O_2
Dy-alloyed [a]	15000	27.7	3.13	70.0	1.36	0.5
Dy_2O_3-doped [b]	17500	29.8	3.51	65.2	1.22	1.2

[a] Sample 2 from table 1. [b] Sample 1 from table 2.

Nd, Dy and Fe were analyzed chemically by inductively coupled plasma (ICP) spectroscopy. Wavelength dispersive spectrometer was employed with the electron microprobe to scan for Dy.

Samples for TEM analyses were mechanically thinned to 200 μm and electropolished using a solution of perchloric acid and methanol. The surfaces of the thin foils were cleaned by ion milling and were examined in a JEOL 200 CX microscope at 200 keV equipped with a high-take-off-angle X-ray detector. The quantitative X-ray analysis was carried out using the *k*-factors and standards from the software system.

3. Results and discussion

Tables 1 and 2 show the intrinsic coercivity of the magnets prepared by Dy-alloying and by Dy_2O_3-

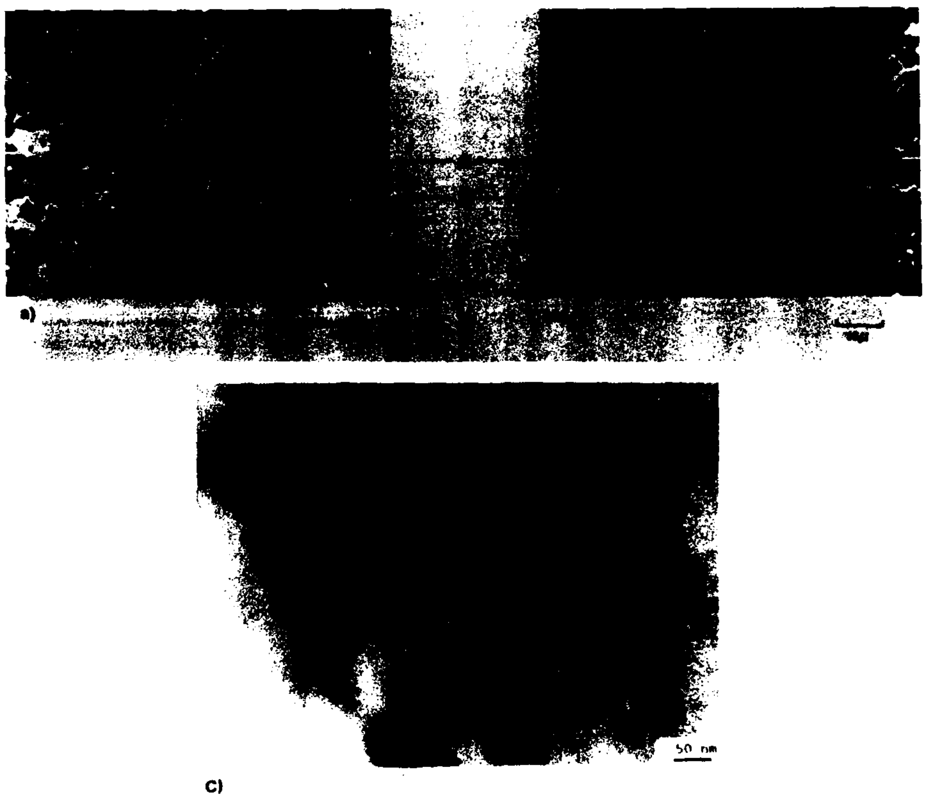


Fig. 2. Dy line scan of (a) Dy_2O_3-doped $Nd_{15}Fe_{77}B_8$ magnet and (b) $Nd_{13.5}Dy_{1.5}Fe_{77}B_8$ magnet: (A) Scan line; (B) Dy intensity profile from X-ray spectrometer. (c) Transmission electron micrograph of a Dy_2O_3-doped $Nd_{15}Fe_{77}B_8$. Region A_5 near the grain boundary shows a higher concentration of Dy than region A_4 in the middle of the grain.

doping, respectively, as a function of the second-step post-sintering heat treatment described above. Table 3 compares a chemical analysis for two samples selected from tables 1 and 2. The optimum second-step post-sintering heat treatment for the Dy_2O_3-doped magnets is lower by about 50 to 90°C while affording a higher intrinsic coercivity (see tables 1 and 2). As expected, the Dy_2O_3-doped sample (table 3) has a higher oxygen concentration than the Dy-alloyed magnet. About 0.5 wt% oxygen is introduced in the sample as a result of adding 4 wt% Dy_2O_3 to the magnet powder in these experiments. It is also noted that the Dy_2O_3-doped sample of table 3 has a slightly higher Dy content. This, however, does not fully account for the observed difference in the ${}^iH_c$ values between the two systems. The control samples in the absence of Dy_2O_3 showed an ${}^iH_c$ increase of about 2000 Oe for 1 wt% Dy. The chemical analyses of table 3 are accurate within a relative error of ± 3%.

Remanence, B_r, and the energy product, BH_{max}, were not affected significantly by the added oxide concentration. A typical demagnetization curve for the heat-treated Dy_2O_3-doped $Nd_{15}Fe_{77}B_8$ magnets is shown in fig. 1. This indicates a good curve squareness and a characteristic energy product, for the magnets of this type.

Dy line scans of the samples shown in figs. 2a and 2b indicate that Dy is distributed unevenly in the Dy_2O_3-doped magnet. Consistent with this result, fig. 2c shows a TEM of a Dy_2O_3-doped magnet indicating a higher Dy concentration near the grain boundaries.

The sintered Nd–Fe–B magnets display a multiphase microstructure which consists of the hard magnetic 2:14:1 grains, a B-rich and a Nd-rich phase [4]. Because of its lower melting point, the latter phase is preferentially formed along the grain boundaries. Compared to the alloyed NdDyFeB magnets, a higher Dy concentration is found in the Nd-rich phase of the Dy_2O_3-doped magnets (see fig. 2). This leads to a higher concentration of Dy close to the grain boundary region of the hard magnetic 2:14:1 phase. The domain reversal at the substituted 2:14:1 sites near the grain boundaries is expected to be more difficult to nucleate. The added oxide concentration at the grain boundaries, as by-product Nd_2O_3 [2], can account for the lowering of the second-step post-sintering heat treatment of the Dy_2O_3-doped magnets (see tables 1 and 2). During this heat treatment the Nd, Dy-rich phase around the grain boundary is homogenized. A uniform NdDy-rich phase along the boundaries of the 2:14:1 grains leads to a better separation of these grains. This can delay the expansion field of the reversed nuclei, across the non-magnetic grain boundaries, which in turn can account for a higher intrinsic coercivity.

Acknowledgement

The authors would like to thank K.L. McNutt for assistance in magnet preparation and Unocal's management for permission to publish this work. Useful discussion with Dr. R. Ramesh of the Department of Materials Science, University of California, Berkeley, is also acknowledged.

References

[1] M. Sagawa, S. Fujimura, H. Yamamoto, H. Matsuura and K. Hiraga, IEEE Trans. Mag. MAG-20 (1984) 1584.
[2] M.H. Ghandehari, Appl. Phys. Letters 48 (1986) 548.
[3] M. Tokunaga, M. Meguro, M. Endoh, S. Tanigawa and H Harada, IEEE Trans. Mag. MAG-21 (1985) 1964.
[4] J. Fidler, IEEE Trans. Mag. MAG-21 (1985) 1955.

103

I-MAG 23 5 19536

21

On the Role of the Nd-Rich Phases in Sintered Nd-Fe-B Magnets

Joef Fidler

104

Reprinted from
IEEE TRANSACTIONS ON MAGNETICS
Vol. MAG-23, No. 5, September 1987

ON THE ROLE OF THE ND-RICH PHASES IN SINTERED ND-FE-B MAGNETS

Joef Fidler, IEEE Member

Institute of Applied and Technical Physics
TU Vienna, Karlsplatz 13, A-1040 Vienna, Austria

Abstract: Sintered Nd15-Fe77-B8 magnets contain a multiphase microstructure. Our analytical transmission electron microscope study reveals that the Nd-rich phase, which is an essential part of the liquid phase sintering process can be divided into at least 4 subtypes with different Nd:Fe-ratios. Impurities of the raw material such as Nd-oxides and Nd-chlorides are randomly found in magnets, partly in the form of small inclusions up to 500 nm diameter within 2:14:1-hard-magnetic grains and partly in the form of large grains up to several microns diameter. As consequence of this analytical study a high concentration of boron vacancies as well as iron vacancies, especially in grain boundary regions is proposed. We have found that the degree of continuity of the intergranular Nd-rich phase is proportional to the intrinsic coercivity of the magnet. The intrinsic coercivity of sintered Nd-Fe-B magnets is determined by the nucleation of reversed domains and by the expansion of the reversed muclei, which is hindered by the non-magnetic Nd-rich oxide grain boundary layer phase.

Introduction

The magnetic hardness of recently developed rare earth-iron-boron based permanent magnets is primarily determined by the magnetocrystalline anisotropy of the hard-magnetic phase, but is limited by metallurgical parameters. In sintered and "magnetquench" Nd-Fe-B magnets a multiphase microstructure is found [1-9]. Measurements of magnetic parameters, such as crystal anisotropy, magnetization etc. do not explain quantitatively the dependence of the intrinsic coercivity on the grain size and heat treatment parameters. In fact, metallurgical parameters, such as distribution of phases, chemical composition and crystal structures of phases determine the value of the coercive force of the sintered magnets. The purpose of our work is todetermine the significant phases which occur in a series of magnets prepared by various producers. Special emphasis of this paper is laid on the characterization of the Nd-rich phase, which is an essential part in the liquid phase sintering process of Nd-Fe-B magnets.

Experimental

Optical metallograpy, microprobe analysis and transmission electron microscopy together with STEM X-ray microanalysis have been used to identify the multiphase microstructure of a series of more than 20 sintered magnets with a nominal composition close to Nd15-Fe77-B8, but prepared under different conditions and partly containing small amounts of dysprosium, aluminium and niobium. The intrinsic coercivities of these magnets ranged from 300 kA/m till 2000 kA/m. The magnets were produced by standard powdermetallurgical processing techniques by various producers under different post-sintering heat treatments. Sintered Nd-Fe-B magnets are very sensitive to electron and ion bombardments [10]. To avoid radiation damage especially of some of the metastable Nd-rich phases special care was taken to the specimen preparation for transmission electron microscopy. All specimens were electropolished using a perchloric acid-methanol solution. Ion milling was used only for cleaning the surfaces from contamination. Scanning transmission electron microscope (STEM) X-ray microanalysis was performed on a JEOL 200 CX analytical microscope fitted with a LaB_6 filament and an EDAX high take off-angle energy dispersive X-ray analyzer. A beryllium double tilt specimen stage was used to reduce background intensities. All X-ray spectra were taken under [0001]-orientation of the specim ens and were analyzed using the EDAX 9100 quantitative software program for thin samples.

Results and Discussion

In sintered Nd15-Fe77-B8 magnets three categories of phases occur [1]. Besides the hardmagnetic $Nd_2Fe_{14}B$-boride phase (A) grains with a composition $Nd_{1.1}Fe_4B_4$ (B) and Nd-rich phases (C) preferentially at grain boundary junctions and extending to grain boundaries are detected by optical metallography and microprobe analysis. Due to the multiphase microstructure only the hardmagnetic 2:14:1-phase (A) contributes to the magnetic properties of the magnet. The volume fraction of this phase vA determines the remanence and therefore the maximum energy density product of the magnet. The composition of phase (C) and the volume fractions of the boride phase (B) vB and of the Nd-rich phase (C) vC are given by the following formulae, taking into account a nominal starting composition of Nd15Fe77B8 and that phase (C) is deficient in boron:

$$aC = (12.78 - 10.16 \cdot vA) / (0.818 - 0.866 \cdot vA)$$
$$bC = (69 - 76.4 \cdot vA) / (0.818 - 0.866 \cdot vA)$$

$$vB = 0.182 - 0.134 \cdot vA$$
$$vC = 0.818 - 0.866 \cdot vA$$

aC and bC are the Nd- and Fe-concentrations of phase (C), respectively.

If phases (B) and (C) are nonferromagnetic at room temperature the volume fraction vA of phase (A) can be determined from the ratio of the saturation magnetization of the magnet ($\simeq$1.35 T) and the value of the single 2:14:1-phase (1.63 T) as vA = 0.83. From the equations above the volume fractions of phases (B) and (C) are calculated as vB = 0.07 and vC = 0.10. Further, the composition of phase (C) is dertermined as to be $Nd_{43.7}Fe_{56.3}$ with the ratio Fe:Nd = 1.3:1. This, in fact, is not in accordance with analytical electron microscopic investigations. Energydispersive X-ray spectra especially taken from particles, which appear as dark to black in electron micrographs, show a ratio in at% of Fe:Nd<1. From the characterization of more than 100 Nd-rich (C)-phases, the following various Nd-rich subtypes of (C) with different Fe:Nd-ratios were found:

(a) 1 : 1.2-1.4
(b) 1 : 2.0-2.3
(c) 1 : 3.5-4.4
(d) > 1 : 7

According to the ternary phase diagram after Matsuura et al. [11] the phases which we detected, can be attributed: (b) to Nd_2FeB_3, which coexists with phases (A) and (B) within the ternary Nd-Fe-B phasediagram; (c) to the ternary eutectic point E2 [11] and (d) to the Nd-rich phase U12 [11]. Three different forms of Nd-rich phases are found by transmission electron microscopy. First in the shape of particles with diameters up to

0018-9464/87/0900-2106$01.00©1987 IEEE

several microns embedded between hardmagnetic 2:14:1-grains. Second as intergranular phases at grain junctions and extending to grain boundaries. Figures 1 and 2 show typical examples of the Nd_2FeB_3 and the ternary eutectic phases, respectively. Note that the interiors of many of such particles show individual dislocations, which were probably formed under high pressure and high temperature conditions. In fig.2 the sintering neck between the hardmagnetic grain and the Nd-rich particle is shown. Third, in the form of randomly distributed precipitates with diameters up to 500 nm within the 2:14:1-grains. Figure 3 show two different precipitates within a hardmagnetic grain. The composition of the larger one is found to be close to the (B)-phase and the smaller one is found to be Nd-rich.

Besides the Nd_2FeB_3 phase the exact composition and crystal structure of the other phases could not yet



Fig.1: Transmission electron micrograph and X-ray spectrum of a Nd_2FeB_3-grain containing a high density of dislocations. A is a hardmagnetic 2:14:1 grain.



Fig.2: An individual Nd-rich grain C is linked by a sintering neck to the hardmagnetic grain A. The composition of C (Nd:Fe=4.4:1) is close to the ternary eutectic E2 [11].

exactly be identified, since ligth elements such as boron and oxygen are difficult to be quantitatively analyzed by an energydispersive detector with high spatial resolution using STEM. X-raymicroprobe analysis of large Nd-rich particles show a high oxygen content and electron diffraction patterns can partly be indexed by the hexagonal Nd_2O_3 crystal structure. Therefore it is assumed that most of the Nd-rich phases including the "fcc Nd-rich" phases also found by other authors [3,5,6,7] contain oxygen.

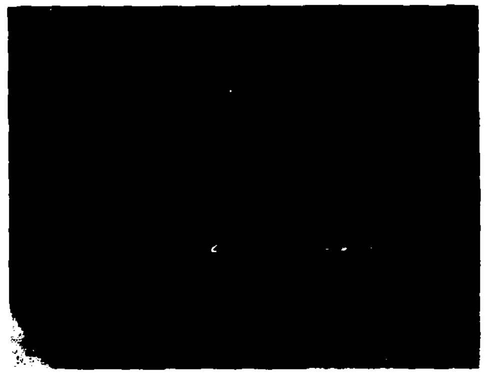


Fig.3: Electron micrographs of two hardmagnetic grains showing a spherical $(1+\varepsilon)$:4:4-precipitate B and small Nd_2O_3-inclusions (marked by arrows) within the hardmagnetic grain A.

Especially the randomly distributed Nd-rich precipitates within the 2:14:1-grains were identified as hex. Nd_2O_3-inclusions, which were already formed before the sintering process. The melting point of Nd_2O_3 is about 2270°C, whereby the sintering temperature is below 1100°C. Oxide impurities and other inclusions may origine from impurities of the starting material. Actually, we frequently detected besides the oxides in different magnets also Nd-chlorides (fig.4) such as $NdCl_2$, Nd-chlorate and $Nd(OH)_2Cl$ and iron-phosphate-sulfate phases up to several microns in diameter.
It should be mentioned that most of the Nd-rich phases occur in the form of metastable phases with unknown chemical composition and crystal structure. The experimental observation of Nd-rich phases cannot be explained by the previous estimate of the volume fractions of different phases. So far, Fe-rich phases of the type $(Nb,Mo)Fe_2$ [12] and close to NbFeB4 we only detected in niobium-containing magnets. Optical metallographic investigations show large grains of phase (B) [13]. As shown in fig.3 spherical precipitates with a composition close to $(1+\varepsilon)$:4:4 are detected within the 2:14:1-grains. It is difficult to determine the volume fraction of phase (B) experimentally, but the calculated value of $v_B = 0.07$ seems to be too small.

During sintering a liquid Nd-rich phase is formed in Nd-Fe-B compacts. The densification is probably due to the heavy alloy liquid phase sintering mechanism and is accelerated by the presence of vacant iron and boron lattice sites. Interdiffusion between phases and the capillary pressure is responsible for the movement and distribution of the liquid phase. Our investigations show that each individual magnet contains a variety of grain boundary structures with different thickness and completeness. A high amount of grain boundaries does not show any intergranular phase at all. Besides the presence of boron vacancies also a high concentration of iron vacancies in 2:14:1-grains especially near

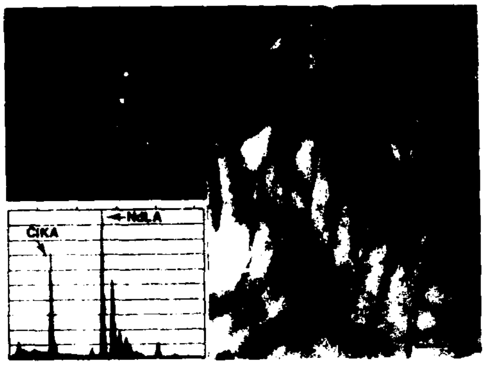


Fig.4: Electron micrographs and X-ray spectrum of a large Nd-chlorine phase containing a high density of dislocations.

grain boundaries has to be assumed. Actually our analytical investigations revealed a distribution of different Fe:Nd-ratios in 2:14:1-grains even in the same magnet material. Table 1 summarizes the range of Fe:Nd-ratios of different magnets of various producers.

Table 1: Range of Fe:Nd-ratios in at% of the hard-magnetic 2:14:1-grains found in a series of sintered Nd-Fe-B magnets by means of X-ray STEM microanalysis.

Producer	Fe:Nd	Fe:Si	Dopants
I	6.7-6.9	27-80	
II	7.7-7.9	22->200	Dy
III	6.2-6.7	92->200	
IV	5.9-6.2	44->200	
V	6.7-7.2	34->200	
	6.1-6.8	50-90	Al
	7.2-8.8	40-66	Dy
	7.0-8.4	15->200	Al, Dy
VI	6.4-7.0	23->200	
	6.8-7.8	14->200	Dy
	6.0-6.5	40->200	Al
	6.3-7.3		Dy, Nb

The ratio of Fe:Nd in dysprosium-containing magnets is >7. In magnets prepared under production conditions a high amount of silicon is found. Comparing the ratios (Fe+Si):Nd, it is evident that silicon atoms replace iron atoms within the 2:14:1-grains. The amount of silicon is found to be higher in regions close to grain boundaries.

Summary

As result of our analytical electron microscopic investigations of a series of more than 20 sintered Nd-Fe-B magnets several, probably metastable, Nd-rich phases are formed during the sintering and post-sintering treatments. Interdiffusion takes place by lattice and surface diffusion processes especially near grain boundaries, whereby a high concentration of iron and boron vacancies is demanded. From metallurgical reasons the liquid phase between the 2:14:1 grains has to be a Nd-rich phase with probably a high amount of oxygen. The nucleation of reversed domains primary determines the coercivity mechanism of sintered Nd-Fe-B magnets. The expansion of reversed domain-nuclei is hindered by the existence of a continuous non-magnetic Nd-O rich intergranular phase. The coercive force is proportional to the uniformity and completeness of the intergranular phase in the magnet.

Acknowledgements

The author wishes to extend his appreciation to Prof. W. E. Wallace for stimulating discussions during his stay at the Carnegie Mellon University and the partial support from the Magnetic Materials Research Group, through the Division of Materials Reserach National Science Foundation, under Grant No. DMR-8613386. I am also grateful to Hitachi Met., Shin-Etsu Chem.Comp., Sumitomo Spec.Met., Japan, CISRI Beijing, China, Crucible Materials and Unocal, USA for providing the magnets used in this study. This work was partly sponsored by the US Army European Research Office, London, UK under contract No.DAJA-86-C-0010.

References

[1] J.Fidler, IEEE Trans.Magn., Vol. MAG-21, p.1955, 1985.
[2] K.D.Durst and H.Kronmueller, in press.
[3] R.K.Mishra, J.K.Chen and G.Thomas, J.Appl.Phys., Vol.59, p.2244, 1986.
[4] G.C.Hadjipanayis, Y.F.Tao and K.R. Lawless, IEEE Trans.Magn., Vol.MAG-22, p.1845, 1986.
[5] R.Ramesh, K.M.Krishnan, E.Goo, G.Thomas, M.Okada and M.Homma, J.Magn.Magn.Mat., Vol.54-57, p.563, 1986.
[6] N.A.El-Masry and H.H.Stadelmaier, Materials Letters, Vol.3, p.405, 1985.
[7] P.Schrey, IEEE Trans.Magn., Vol. MAG-22, p.913, 1986.
[8] R.K.Mishra and R.W.Lee, Appl.Phys.Lett, Vol.48, p.733, 1986.
[9] R.K.Mishra, J.Magn.Magn.Mat., Vol.54-57, p.450, 1986.
[10] W.E.Wallace, private communication.
[11] Y.Matsuura, S.Hirosawa, H.Yamamoto, S.Fujimura, M.Sagawa and K.Osamura, Jap.J.Appl.Phys., Vol.24, p.L635, 1985.
[12] S.F.H.Parker, P.J.Grundy and J.Fidler, J.Magn. Magn.Mat., in press.
[13] J.Fidler and L.Yang, Proc. 8th Int.Workshop on Rare Earth Magnets and their Applications ed. by K.Strnat (University of Dayton, Dayton), p.647, 1985.

ANALYTICAL ELECTRON MICROSCOPE STUDY OF HIGH- AND LOW-COERCIVITY SmCo 2:17 MAGNETS

JOSEF FIDLER , J. BERNARDI AND P. SKALICKY
Institute of Applied and Technical Physics, University of Technology, Karlsplatz 13, A-1040 Vienna, Austria.

ABSTRACT

Sintered, precipitation hardened SmCo 2:17 magnets contain a multiphase microstructure. Our electron microscopic investigations reveal that the size of the rhombic, cellular precipitation structure and the formation of cell interior and cell boundary phases is determined by the nominal composition of the alloy and the postsintering heat treatment conditions and primarily control the intrinsic coercivity of the magnet. Selected area electron diffraction together with high resolution electron microscopy showed a high density of basal stacking faults (microtwinning) of the cell interior phase of low coercivity ($_iH_c$ < 700 kA/m) magnets with a (c/a)*- ratio of the basic structural unit of > 0.843. High coercivity magnets ($_iH_c$ > 1000 kA/m), containing a high density of the platelet phase perpendicular to the c-axis, exhibit cell diameters up to 200 nm with a (c/a)*-ratio of the basic structural unit of the cell interior phase of < 0.843.

INTRODUCTION

Commercially available permanent magnet materials may be divided into hardferrites, AlNICo-magnets and rare earth (RE)-permanent magnets (PM). There exist two groups of REPM, the RE-cobalt magnets and the recently developed RE-iron magnets. The RE-cobalt magnets can be divided into five types depending on whether the magnet has a single-phase or a two-phase microstructure. The ideal microstructure of the single phase magnets consists of aligned single-domain grains with a $SmCo_5$- or Sm_2Co_{17}-crystal structure. Two types of precipitation hardened magnets can be distinguished: the one type contains 2:17-precipitates in a 1:5-matrix, the other type forms 1:5-precipitates in a 2:17-matrix. Besides these magnets there are the bonded magnets, in which the single domain particles are embedded in a non magnetic phase. Rare earth-cobalt magnets are produced by a powder metallurgical process with complicated post-sintering heat treatment procedures in the case of precipitation hardened SmCo 2:17-magnets. In fact, the nominal composition, the sintering and annealing parameters determine the intrinsic coercivity of SmCo 2:17 magnets. To understand the microstructure and the reasons for high coercivity of sintered SmCo 2:17 magnets transmission electron microscopy has widely been used [1-5]. The purpose of this work is to compare the microstructure of low coercivity ($_iH_c$<700 kA/m) and high coercivity ($_iH_c$>1000 kA/m) precipitation hardened SmCo 2:17-magnets, containing a cellular microstructure.

EXPERIMENTAL

Besides optical metallography and microprobe analysis we have used transmission electron microscopy together with STEM X-ray microanalysis to

22

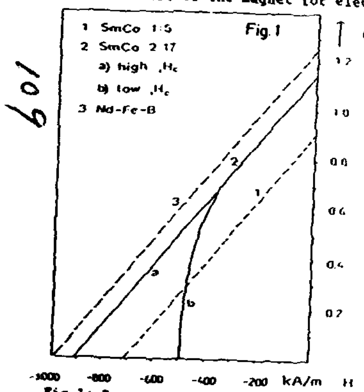
108

identify the precipitation and to study the magnetic domain structure and their interaction with the precipitation structure. The investigations have been carried out on a JEOL 200CX microscope equipped with a high take-off angle energy dispersive detector for X-ray microanalysis. The specimens for transmission electron microscopic investigations were prepared by a combination of electropolishing and ionbeam thinning procedure.

The investigated samples were sintered magnets with a nominal composition close to $Sm(Co_{.68}Fe_{.22}Cu_{.08}Zr_{.02})_{7.5}$.

They were prepared and given a systematically varying heat treatment after sintering to achieve maximum magnetic hardness by different producers, such as *KRUPP WIDIA GmbH., FRG*, *TDK Corp.* and *SHIN-ETSU Chem.Corp., Japan*. For some unknown reason different coercivities were obtained under the same preparation conditions. Magnets with low coercivities (< 700 kA/m) and magnets with high coercivities (> 1000 kA/m) were choosen for transmission electron microscopy. Commercial sintered SmCo 2:17 magnets can also be divided into high $_iH_c$ and low $_iH_c$ magnets (fig.1).

In order to study the influence of the effect of the nominal Samarium content on the microstructure and coercivity a set of samples was prepared and given a systematically varying heat treatment by THYSSEN Edelstahlwerke, FRG with a Sm-content of 23.9 wt% ($_iH_c$=250 kA/m), 24.8 wt% ($_iH_c$ > 1700 kA/m) and 25.7 wt% ($_iH_c$=800 kA/m). Thin slices of these magnets were cut parallel to the alignment direction and different discs were prepared near the edge and the centre of the magnet for electron microscopy as shown in fig.2.



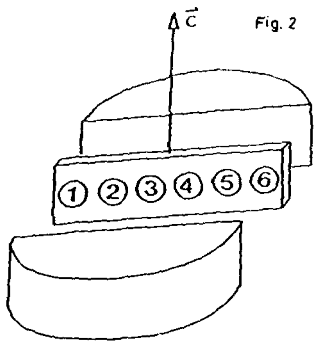


Fig.1: Room temperature demagnetization curves of rare earth permanent magnets.

Fig.2: Schematic diagram showing the preparation of discs for transmission electron microscopy of a cylindrical magnet.

CRYSTALLOGRAPHY OF Sm_2Co_{17}

The compounds $SmCo_5$ and Sm_2Co_{17} may be regarded as layered structures with different stacking sequences of a basic structural layer, consisting of a Co-layer and a mixed Sm- and Co-layer. The stacking sequence of the hexagonal Sm_2Co_{17} structure is

.....ABABABABA..... (1)

and the one of the rhombohedral Sm_2Co_{17} structure is

.....ABCABCABCA..... (2)

Besides these perfect layer structures structures containing stacking faults in the basal plane also occur in real magnets. In rhombohedral SmCo 2:17 crystals the close packed planes are the (0001)-basal planes, which are also the glide planes and coherent twin planes. The twin orientation corresponds to a mirror plane reflection about (0001). The stacking sequence for a coherent twin with the dashed line and asterisk as the centre of the fault is

.....ABCABCBACBA..... (3)

A coherent twin is formed by a <u>multiple</u> shearing operation on the (0001)-plane, if the displacement is 1/3·[1010]. On the other hand an intrinsic stacking fault is formed when <u>one</u> layer of the basic structural unit is removed from the normal sequence, leaving

....ABCABC¦BCABCA.... (4)

It should be mentioned that this fault can also be regarded as being formed by two twinning operations (marked by asteriks) separated by <u>one</u> basic layer (microtwinning).

An extrinsic stacking fault is formed by the addition of <u>one</u> layer of the structural unit to the normal sequence, giving

....ABCABCBABCABCA.... (5)

Again this can also be regarded as being formed by two twinning operations seperated by <u>two</u> basic layers (microtwinning).

A combination of an intrinsic stacking fault with the formation of a coherent twin gives the stacking sequence

...ABCABCABACBACBA.... (6)

All the above faults preserve close packing and exhibit low surface energies compared with other higher order planar faults which are summarized for the case of perfect and imperfect modifications of Sm_2Co_{17} compounds by C.W. Allen et al. [6].

From the stacking sequence of the planar faults (4) and (6) within the rhombohedral Sm_2Co_{17}-crystal it can be seen that due to the crystallographic shear a platelet with one unit cell thickness of the hexagonal Sm_2Co_{17}-phase with the stacking sequence BC and AB are formed.

$RECo_5$ compounds crystallize in the ordered $CaCu_5$ structure type. Substitution of rare earth atoms by Co-atoms lead to the formation of the disordered $TbCu_7$-structure type in which rare earth atoms are replaced by

pairs of Co-atoms [6]. When nearly 22% of the RE atoms have been substituted by pairs of Co atoms, the disordered $TbCu_7$-structure is no longer stable and a two-phase microstructure is formed. Substituting 33% of the RE atoms by Co-atom pairs leads to RE Co [10]. In the case of Sm-(Co,Fe) alloys the rhombohedral Sm_2Co_{17} modification is more stable than the hexagonal modification [7]. The (c/a)* - ratio of the reduced basic structural unit of the rhomb. Sm_2Co_{17}-structure is found to be close to 0.843 (± 0.006) [8]. Only in hyperstöichiometric Sm_2Co_{17}-alloys, such as $Sm(Co,Fe)_{9-12}$, the hexagonal modification with a ratio (c/a)* > 0.85 is found as stable room temperature phase [9]. Table I summarizes the crystal structure - relationships, the range of stability and (c/a)*-ratios of phases occurring in $Sm(Co,Fe)_{5+x}$ alloys (0 ≤ x ≤ 7).

TABLE I: CRYSTAL STRUCTURE RELATIONSHIPS OF $Sm(Co,Fe)_{5+x}$ - ALLOYS

x = 0	$CaCu_5$	P6/mmm	(c/a)* = 0.795	ordered
0<x<2	$TbCu_7$	P6/mcm	0.795 < (c/a)* < 0.837	disordered
x=3.5	Th_2Zn_{17}	$R\bar{3}m$	0.837 ≤ (c/a)* ≤ 0.849	ordered
3.5≤x≤7	Th_2Ni_{17}	$P6_3/mmc$	(c/a)* > 0.85	ordered
	"Th_2Ni_{17}"hyperst.	$P6_3/mmc$	P6/mmm	partly disordered

(c/a)* is the ratio of the basic structural unit; data taken from [9,10]



Fig.3: Rhombic cellular microstructure of a sintered precipiation hardened SmCo 2:17 magnet. A is the cell interior phase, B the cell boundary phase and C the platelet phase perpendicular to the alignement direction.

110

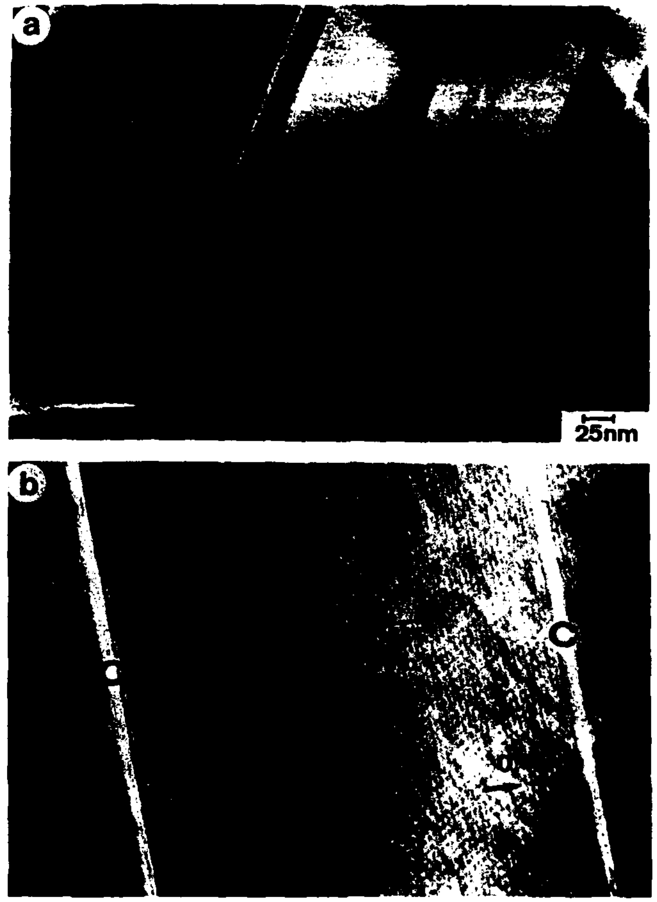


Fig.4: Electron micrographs showing coherent twinning in high coercivity ($_iH_c$>1000 kA/m) magnets. C is the platelet phase and B the cell boundary phase.

RESULTS

Microstructure of high coercivity SmCo 2:17-magnets

Copper containing RE-cobalt magnets with a nominal composition of $Sm(Co,Fe,Cu,TM)_{6-8}$ with TM=Zr,Ti or Hf show a fine scale, cellular microstructure [5]. Rhombic cells of the type $Sm_2(Co,Fe)_{17}$ rhomb. - phase A - are separated by a $Sm(Co,Cu,TM)_{5-7}$ cell boundary phase - phase B. In magnets with high coercivities thin platelets - phase C - are found perpendicular to the hexagonal c-axis (fig.3). Our high resolution electron microscope investigations [5] show that the crystal structure of the platelet phase C is close to the hexagonal Sm_2Co_{17} structure with a c-crystal parameter of 0.8 nm. This is in agreement with metallurgical considerations on the formation of various phases in sintered SmCo 2:17 magnets by A.E. Ray [9,12,13]. Remarkable for high coercivity SmCo 2:17 magnets is also the observed twinning within the rhombohedral 2:17-cell interior phase. The electron micrographs of fig.4a and b, taken under different reflection conditions, show the cellular microstructure and the twinning with the basal plane as twin boundary. Twin boundaries may coincide with the platelet phase but also occur within the rhomb. 2:17-phase (fig.4b), corresponding to planar faults of the type (6) and (3), respectively.

Microstructure of low coercivity SmCo 2:17 magnets

From our investigations it is obvious that there are different reasons for low coercivities. Since in precipitation hardened SmCo 2:17 magnets the the *cellular precipitation structure acts as attractive pinning centre* for magnetic domain walls during the magnetization reversal (fig.5) [14,15], the

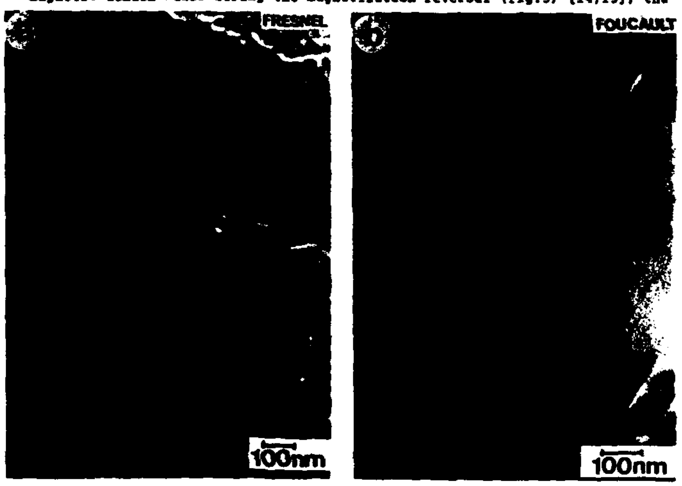


Fig.5: Lorentz electron micrographs showing the attractive domain wall pinning at the continuous cell boundary phase in the demagnetized state.

size, the composition and the completeness of the continuus cellular precipitation structure controll the coercivity. The platelet phase (C) predominately acts as diffusion path for the chemical redistribution process during the post-sintering heat treatments and is favourable for the formation of the cell boundary phase of the 1:5-ordered type or 1:7-disordered type. Figure 6 shows two electron micrographs of the magnet with 23.9 wt% nominal Sm-content. A high density of the platelet phase is shown, but due to the lack of samarium the formation of the cell boundary phase is

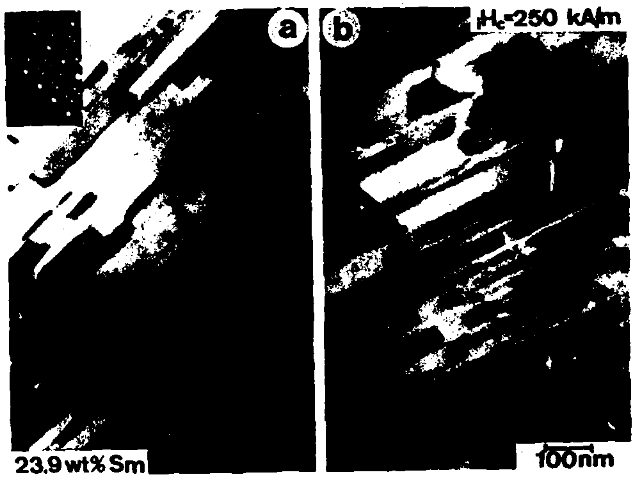


Fig.6: Bright field electron micrographs of a low coercivity magnet. Due to the lack of samarium the cell boundary phase is only incompletely formed. A high density of the platelet phase is observed.

poor leading to an intrinsic coercivity of 250 kA/m. Impurities, primarily such as oxygen and carbon, lead to the formation of macroscopic precipitates of Sm_2O_3, ZrC, TiC etc. A high amount of these phases in the magnet impedes the formation of the platelet phase and the cellular precipitation structure. It has been shown [16] that small amounts of Zr, Ti or Hf are necessary for the formation of the platelet phase (C).

The high resolution electron micrograph of fig.7 shows the cell interior of a magnet with an intrinsic coercivity of $_iH_c$ = 600 kA/m. No platelet phase (C) is found and X-ray microanalysis shows that this region of the magnet is depleted from zirconium [11]. The contrast of this image correspond to the atomic positions along the [11$\bar{2}$0]-zone axis. A high density of stacking faults, and therefore also microtwinning is observed. It should be noted that the distance between atomic layers in the basal plane varies, especially near stacking faults. The development and growth of the cellular precipitation structure occurs during the isothermal aging procedure and involves diffusion of samarium, whereas the chemical redistribution of the transition metals during the step aging procedure following the isothermal aging increases the coercivity [16]. Possible

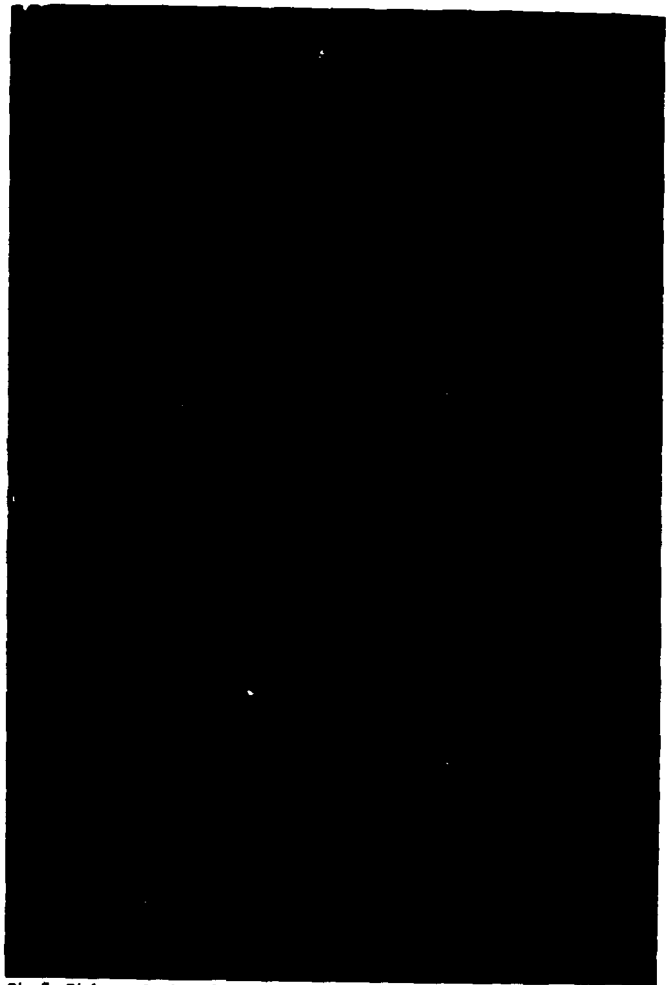


Fig.7: High resolution electron micrograph of the cell interior phase of a low coercivity (${}_iH_c$=600 kA/m) magnet showing a high density of stacking faults in the basal plane (microtwinning).

diffusion paths for this diffusion process are the platelets of phase (C) and the disordered regions near planar stacking faults and twin boundaries in the basal plane as observed in fig.7.

Our electron microscopic investigations of magnets with low coercivity revealed also a strong dependence of the size of the cellular microstructure on the position of the magnet where the samples were taken. The Kerr-optical micrograph of fig.8 shows the magnetic domain structure perpendicular to the



Fig.8: Kerr-optical micrograph of a polished surface perpendicular to the alignment direction showing the magnetic domain structure and chemical inhomogeneities from the edge to the centre of the sintered SmCo 2:17 magnet.

alignment direction of a cylindrical magnet near the edge of the magnet with about 20 mm in diameter. From differences in the domain structure chemical inhomogeneities within the material are concluded. Especially regions with large domain widths in the demagnetized state as in fig.8 are (Co,Fe)-enriched regions with low magnetocrystalline anisotropy.

DISCUSSION AND SUMMARY

Selected area electron diffraction, high resolution and analytical transmission electron microscopy of low (< 700 kA/m) and high (>1000 kA/m) coercivity magnets revealed different microstructures. The electron diffraction patterns are different for magnets containing the platelet phase (C) -high coercivity- (fig.9.a) and magnets containing a high density of stacking faults and microtwins, respectively -low coercivity- (fig.9.b and c). Due to the narrowness of the rhombohedral Sm_2Co_{17} regions the rhombohedral <n0$\bar{n}$n> with (n=1,2)- diffraction spots are streaked. As shown earlier, due to microtwinning under certain contitions thin layers of a hexagonal Sm_2Co_{17} phases are formed. Fig.9c was taken from such a region and shows also the hexagonal <10$\bar{1}$1> reflections. The c/a-ratio which is sensitive to the chemical composition (see Table I) of the cell interior phase can directly be determined from fig.9. Table II summarizes the reduced (c/a)* - ratios of the basic structural unit determined from magnets with different intrinsic coercivities. It is obvious that a ratio larger than the ideal value of the rhombohedral 2:17-type (0.843) is due to a hyperstoichiometric concentration of the cell interior phase and leads to the formation of a high density of stacking faults which is linked with the transformation to the hexagonal Sm_2Co_{17} structure type. On the other hand a ratio less than the ideal value is an indication for the formation of the platelet phase (C) and leading to high intrinsic coercive forces.

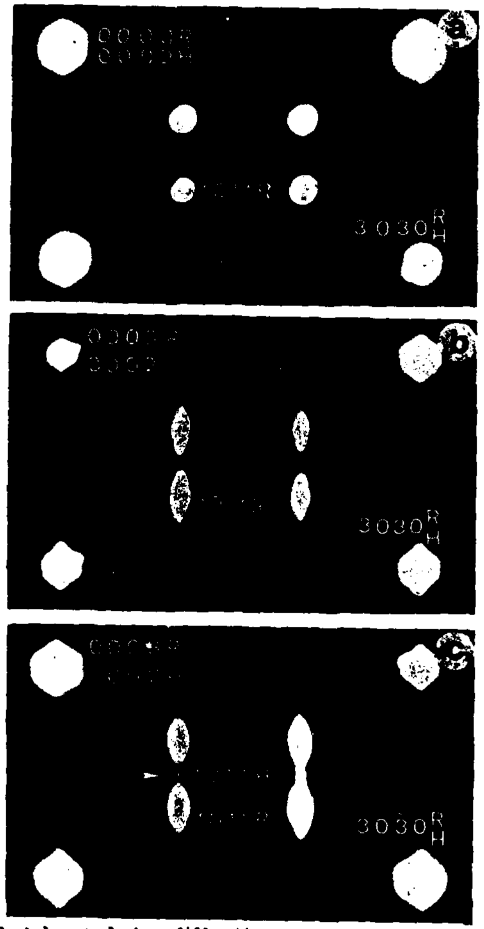


Fig.9: Selected area electron diffraction patterns taken parallel to [1$\bar{2}$10] of a high coercivity magnet (a) and low coercivity magnets (b) and (c). The streaking of the rhombohedral 2:17 reflections in (b) and (c) is due to microtwinning of the cell interior phase.

113

TABLE II: (c/a)* - RATIOS OF THE BASIC STRUCTURAL UNIT OF THE CELL INTERIOR PHASE OF MAGNETS WITH DIFFERENT INTRINSIC COERCIVITIES

magnet	(c/a)*	$_iH_c$ [kA/m]	remarks
# 1	.842	400	microtwinning
# 2	.853	600	microtwinning, hex.<10$\bar{1}$1>
# 3	.814	> 2000	platelets
# 4	.824	1200	platelets
# 5	.820	1000	platelets, overaged
# 6	.846	42	as sintered
# 7	.835	250	nominal 23.9 wt% Sm, platelets
# 8	.829	800	nominal 25.7 wt% Sm, platelets
# 9	.838	> 1700	nominal 24.8 wt% Sm, platelets

In sintered precipitation hardened SmCo 2:17 magnets the coercivity *primarily depends on the multiphase microstructure. The degree* of completeness of the rhombic cellular precipitation structure determines the effectiveness of the domain wall pinning and therefore the intrinsic coercivity. The shape of the rhombic, cellular structure is determined by the direction of zero deformation strains due to the crystal lattice misfit between the different cell boundary and cell interior phases and the acute angle of the of the rhombic cells is an indication for the compositional difference between these phases [17]. We also found earlier that the postsintering heat treatment is very sensitive to the observed cell size and coercivity of the magnet [5,17].

In contrast to sintered SmCo 1:5 and Nd-Fe-B based permanent magnets in the case of SmCo 2:17 magnets the grain size is not changed during the post sintering heat treatment and does not influence the coercivity [18]. We found that maximum coercivities (> 2000 kA/m) occur in magnets with cell diameters of about 200 nm and containing a high density of the platelet phase (C). As result of our investigations we revealed several factors limiting the intrinsic coercivity. Chemical inhomogeneities especially near the edges of a magnet influence the Sm-rich precipitation structure with whether an ordered $CaCu_5$ or *disordered* $TbCu_7$ *structure type. A high content* of oxygen and carbon impurities locally deplete the magnet from samarium. An optimum postsintering heat treatment is necessary for the nucleation and growth of the continuus cellular precipitation structure.

Acknowledgements

One of the authors (J. Fidler) would like to thank *Profs. D.E. Laughlin* and W.E. Wallace for stimulating discussions during his stay at the Carnegie Mellon University and the partial support from the Magnetic Materials Research Group, through the Division of Materials Research, National Science Foundation, under Grant No. DMR-86133386. The authors are grateful to Drs. K. Kuntze and H. Nagel from Thyssen Edelstahlwerke AG,FRG for providing samples with different nominal composition.

References

1. J.D. Livingston and D.L. Martin, J. Appl. Phys. 48, 1350 (1977).
2. R.K. Mishra, G. Thomas, T. Yoneyama, A. Fukuno and T. Ojima, J.Appl.Phys. 52, 2517 (1981).
3. G.C. Hadjipanayis, E.J. Yadlowsky and S.H. Wollins, J. Appl. Pys. 53, 2386 (1982).
4. J. Fidler and P. Skalicky, J. Magn. Magn. Mat. 27, 127 (1982).
5. J. Fidler, P. Skalicky and F. Rothwarf, IEEE Trans. Magn. MAG-19, 2041 (1983).
6. C.W. Allen, D.L. Kuruzar and A.E. Miller, IEEE Trans. Mag. MAG-10, 716 (1974).
7. Y. Khan, Acta Cryst. B29, 2502 (1973).
8. Q. Johnson, G.S. Smith and D.H. Wood, Acta Cryst. B25, 464 (1969).
9. A.E. Ray, Proc. of Soft and Hard Magnetic Materials with Applications, Lake Buena Vista, Florida, Oct.1986, to be published by ASM.
10. Y. Khan, Pys. Stat. Sol.(a) 21, 69 (1974).
11. J. Fidler, P. Skalicky and F. Rothwarf, Mikrochimica Acta [Wien] Suppl. 11, 371, (1985).
12. A.E. Ray, J. Appl. Phys. 55, 2094 (1984).
13. A.E. Ray, IEEE Trans. Magn. MAG-20, 1614 (1984).
14. J. Fidler, J. Mag. Magn. Mat. 30, 58 (1982).
15. H. Kronmüller, K.D. Durst, W. Ervens and W. Fernengel, IEEE Trans. Magn. MAG-20, 1569 (1984).
16. L. Rabenberg, R.K. Mishra and G. Thomas, J. Appl.Phys. 53, 2389 (1982).
17. J.Fidler, R. Grössinger, H. Kirchmayr and P. Skalicky, ERO - Report of U.S. Army, Pr.No. DAJA (1983) 37-82-C-0050.
18. J. Fidler and P. Skalicky, Radex-Rundschau 2/3, 63 (1986).

114

MICROSTRUCTURAL STUDIES OF HIGH COERCIVITY $Nd_{15}Fe_{77}B_8$ SINTERED MAGNETS

M. H. GHANDEHARI* AND J. FIDLER**
* Unocal Corporation, Science and Technology Division, P.O. Box 76, Brea, CA 92621 USA
**Institute of Applied and Technical Physics, Technical University of Vienna, Vienna, Austria

ABSTRACT

Microstructures of $Nd_{15-x}Dy_xFe_{77}B_8$ prepared by alloying with Dy, and by using Dy_2O_3 as a sintering additive, have been determined using electron microprobe and transmission electron microscopy. The results have shown a higher Dy concentration near the grain boundaries of the 2-14-1 phase for magnets doped with Dy_2O_3, as compared to the Dy-alloyed magnets. A two-step post sintering heat treatment was also studied for the two systems. The resultant concentration gradient of Dy in the 2-14-1 phase of the oxide-doped magnets is explained by the reaction of Dy_2O_3 with the Nd-rich grain boundary phase and its slow diffusion into the 2-14-1 phase. Increased Dy concentration near the grain boundary is more effective in improving the coercivity, as domain reversal nucleation originates at or near this region.

INTRODUCTION

$Dy_2Fe_{14}B$ displays a much higher single crystal anisotropy than the corresponding Nd compound [1,2]. Therefore, a Dy-substituted sintered $Nd_{15}Fe_{77}B_8$, which embodies the 2-14-1 phase displays a higher practical coercivity, as first reported by Sagawa and coworkers [2]. As a low-cost approach in introducing Dy, the reaction of Dy_2O_3 as a sintering additive with $Nd_{15}Fe_{77}B_8$ powder was investigated by one of the authors [3]. This resulted in Dy_2O_3-doped magnets with coercivities similar to those prepared by substitution of Dy for Nd in the alloying step [3]. In this study, we compare the resultant microstructures by scanning transmission electron microscopy (STEM) and by electron microprobe. A two-step post-sintering heat treatment, employed to optimize the coercivity, is also compared for the two systems.

EXPERIMENTAL

Powder samples were prepared from a nominal $Nd_{15}Fe_{77}B_8$, and an alloy in which 3.5 wt% (approximately 10 atomic %) of Nd was replaced by Dy in the alloying step. Both of these powder samples were prepared under identical conditions and contained typically 0.5 to 0.6 wt% oxygen prior to pressing and sintering. 4.0 wt% Dy_2O_3 (3.5 wt% Dy equivalent) was hand-mixed with the former, and both types of magnets were sintered at 1070°C for an hour and annealed in two steps [4]. The first step of the annealing process consisted of 900°C for 2 hours and the second step varied between 550 and 680°C for an hour. Samples were rapidly quenched in a cooler part of the furnace in between the two steps. After the magnetic measurements, the sintered samples were analyzed for O_2 by a vacuum fusion technique. Boron, Nd, Dy and Fe were analyzed chemically by inductively coupled plasma (ICP) spectroscopy. A wavelength dispersive spectrometer was employed with the electron microprobe to scan for Dy.

23

115

Samples for TEM analyses were mechanically thinned to 200 micron and electropolished using a solution of perchloric acid in methanol. The surface of the thin foils were cleaned by ion milling and were examined in a JEOL 200 CX microscope at 200 keV equipped with a high-take off angle X-ray detector. The quantitative X-ray analysis was carried out using the k-factors and standards from the software system.

RESULTS

Magnetic Properties & Chemical Composition

Tables I and II show the intrinsic coercivity of the magnets prepared by Dy-alloying and by Dy_2O_3-doping, respectively, as a function of the second step post-sintering heat treatment described above. Table III compares a chemical analysis for two samples selected from Tables I and II. The optimum second step post-sintering heat treatment for the Dy_2O_3-doped magnets is lower by about 50 to 90°C while affording a higher intrinsic coercivity (*see Tables I and II*). As expected, the Dy_2O_3-doped sample (Table III) has a higher oxygen concenctration than the Dy-alloyed magnet. About 0.5 wt% oxygen is introduced in the sample as a result of adding 4 wt% Dy_2O_3 to the magnet powder in these experiments. It is also noted that the Dy_2O_3-doped sample of Table III has a slightly higher Dy content. This, however, does not fully account for the observed difference in the ^iHc values between the two systems. The control samples in the absence of Dy_2O_3 showed an ^iHc increase of about 2,000 Oe for 1 wt% Dy. The chemical analysis of Table III are accurate within a relative error of ±3%.

Remanence, Br, and the energy product, BHmax, were not affected significantly by the added oxide concentration. A typical demagnetization curve for the heat-treated Dy_2O_3-doped $Nd_{15}Fe_{77}B_8$ magnets is shown in Figure 1. This indicates a good curve squareness and a characteristic energy product, for the magnets of this type.

Microstructural Determinations

Dy line scans of the samples shown in Figures 2a and b indicate that Dy is distributed unevenly in the Dy_2O_3 doped magnet. Consistent with this result, Figure 2c shows a TEM of a Dy_2O_3-doped magnet indicating a higher Dy concentration near the grain boundaries. An X-ray spectrum (not shown) near the region A_4 showed a remarkably low ratio of Fe:Nd, indicating lack of Dy, whereas region A_5 near the grain boundary showed a high Fe:Nd ratio. These results are consistent with uneven distribution of Dy in the electron microprobe line scans. X-ray analyses of Dy-alloyed magnets, under transmission electron microscope showed a much more homogeneous distribution of Dy in the 2-14-1 grains.

DISCUSSION

The sintered Nd-Fe-B magnets display a multiphase microstructure which consists of hard magnetic 2:14:1 grains, a B-rich and a Nd-rich phase [5]. Because of its lower melting point, the latter phase is preferentially formed along the grain boundaries. Compared to the alloyed NdDyFeB magnets, a higher Dy concentration is found near the grain boundary of the 2-14-1 phase in the Dy_2O_3-doped magnets (see Figure 2c). This may be explained by considering the reaction of Dy_2O_3 with the liquid, Nd-rich layer, and its subsequent displacement of Nd in the $Nd_2Fe_{14}B$ phase, as depicted in Figure 3. Such a diffusion process is apparently slow enough to create a Dy gradient, with a higher Dy near the reaction zone at the grain boundary.

TABLE I

INTRINSIC COERCIVITY OF $Nd_{13.5}Dy_{1.5}Fe_{77}B_8$ AS A FUNCTION OF POST-SINTERING HEAT TREATMENT

(ALL SAMPLES WERE SINTERED AT 1070°C FOR 1 HOUR)

SAMPLE	POST-SINTERING HEAT TREATMENT T (°C)	POST-SINTERING HEAT TREATMENT t (HOURS)	^iH_c(Oe)
1	900	2	13,500
1	900	2	
	630	1	13,800
1	900	2	
	630	1	15,100
	680	2	
2	900	2	13,600
2	900	2	
	680	1	15,000

TABLE II

INTRINSIC COERCIVITY OF Dy_2O_3-DOPED $Nd_{15}Fe_{77}B_8$ AS A FUNCTION OF POST-SINTERING HEAT TREATMENT

ALL SAMPLES WERE DOPED WITH 4 WT% Dy_2O_3 AND SINTERED AT 1070°C FOR 1 HOUR)

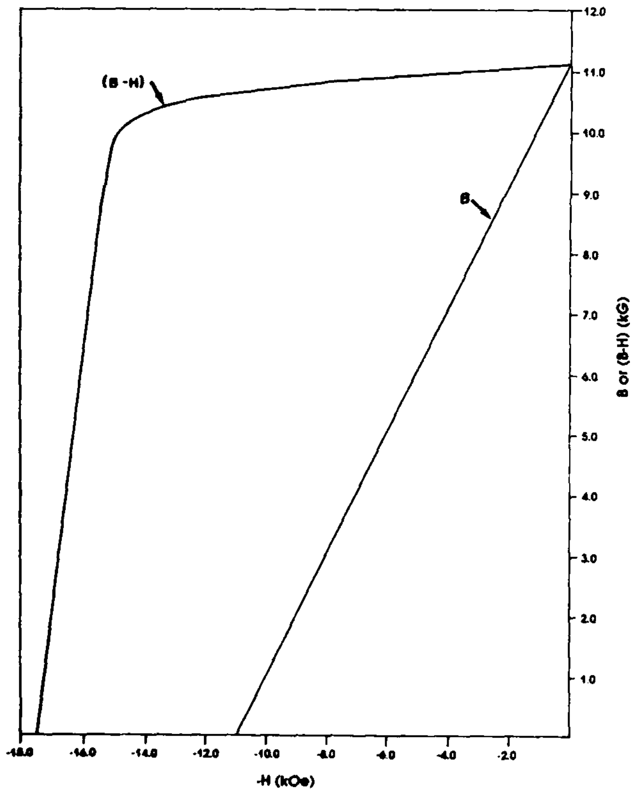
SAMPLE	POST-SINTERING HEAT TREATMENT T (°C)	POST-SINTERING HEAT TREATMENT t (HOURS)	$_iH_c$(Oe)
1	900	2	
	610	1	17,000
2	900	2	
	590	1	17,500
3	900	2	
	570	1	15,400
4	900	2	
	630	1	16,300
5	900	2	
	570	1	17,000
6	900	2	
	550	1	14,800
7	900	2	
	600	1	16,200
8	900	2	
	610	1	16,900
9	900	2	
	590	1	15,200
10	900	2	
	620	1	15,600

TABLE III

CHEMICAL ANALYSES OF A Dy-ALLOYED AND A DY_2O_3-DOPED $Nd_{15}Fe_{77}B_8$ SINTERED MAGNETS

		ELEMENTS (wt%)				
Sample	$_iH_c$ (Oe)	Nd	Dy	Fe	B	O_2
Dy-ALLOYED	15,000	27.7	3.13	70.0	1.36	0.5
Dy_2O_3-DOPED	17,500	29.8	3.51	65.2	1.22	1.2

FIG. 1 - DEMAGNETIZATION CURVES OF A Dy_2O_3- DOPED $Nd_{15}Fe_{77}B_8$ (SAMPLE 2 FROM TABLE I)



118

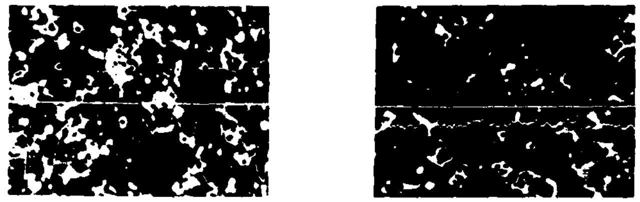


FIG. 2 a, b - Dy LINE SCAN OF: a) Dy_2O_3 DOPED $Nd_{15}Fe_{77}B_8$ MAGNET & b) $Nd_{13.5}Dy_{1.5}Fe_{77}B_8$ MAGNET

A) SCAN LINE
B) Dy INTENSITY PROFILE FROM X-RAY SPECTROMETER



FIG. 2c - TRANSMISSION ELECTRON MICROGRAPH OF A Dy_2O_3 DOPED $Nd_{15}Fe_{77}B_8$. REGION A_5 NEAR THE GRAIN BOUNDARY SHOWS A HIGHER CONCENTRATION OF Dy THAN REGION A_4 IN THE MIDDLE OF THE GRAIN

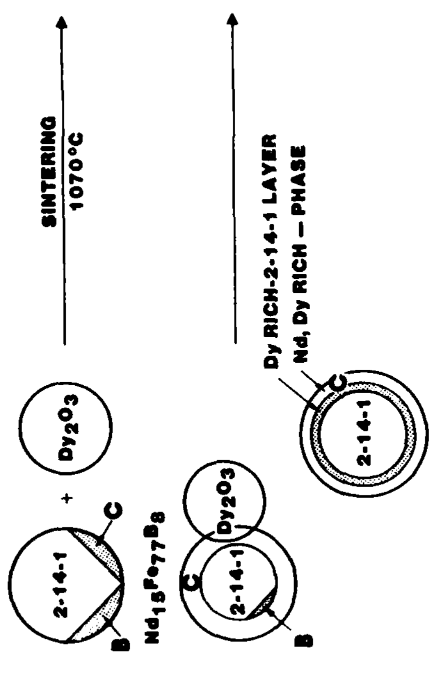


FIG. 3 — SCHEMATIC DIAGRAM SHOWING THE REACTION OF Dy_2O_3 WITH $Nd_{15}Fe_{77}B_8$ DURING THE SINTERING. REGIONS B AND C DESIGNATE THE B-RICH AND Nd-RICH PHASES.

The nucleation of reversed domains takes place at regions with high local demagnetization fields and low magnetocrystalline anisotropies, such as soft magnetic precipitates and disturbed regions near the grain boundaries. As the grain boundary is concentrated with the Dy-substituted *2-14-1 phase, the region's anisotropy* increases, translating to a higher intrinsic coercivity as indicated in Tables I & II for the Dy_2O_3-doped magnet. The expected high coercivity may be partially offset by undissolved, and large size Nd_2O_3 particles by-product, or unreacted Dy_2O_3. At the same time, dissolved oxide at the grain boundary could lower the melting point of the Nd-rich phase, thus accounting for the lower second-step post sintering heat treatment for optimum coercivity (see Tables I and II). A uniform NdDy-rich phase along the boundaries of the 2:14:1 grains leads to a better separation of these grains. This can delay the expansion field of the reversed nuclei across the non-magnetic grain boundaries which in turn can account for a higher intrinsic coercivity.

ACKNOWLEDGMENT

The authors would like to thank K. L. McNutt for assistance in magnet preparation and Unocal's management for permission to publish this work. Useful discussion with Dr. R. Ramesh of the Department of Materials Science, University of California, Berkeley, is also acknowledged.

REFERENCES

[1] S. Hirosawa, Y. Matsuura, H. Yamamoto, S. Fujimura and M. Sagawa, J. Appl. Phys. 59 (3), 873 (1986).

[2] M. Sagawa, S. Fujimura, H. Yamamoto, H. Matsuura, and K. Hiraga, IEEE Trans. Mag. MAG-20, 1584 (1984).

[3] M. H. Ghandehari, Appl. Phys. Lett. 48 (8), 548 (1986).

[4] M. Tokunaga, M. Meguro, M. Endoh, S. Tanigawa, and H. Harada, IEEE Trans. Mag. MAG-21, 1964 (1985).

[5] J. Fidler, IEEE Trans. Magn., MAG-21, 1955 (1985).

24

Mikrochim. Acta [Wien] 1987, I, 115—124

Mikrochimica Acta

Metallurgical Factors Determining the Coercivity of Nd-Fe-B Magnets

Josef Fidler* and Peter Skalicky

Institut für Angewandte und Technische Physik, Technische Universität Wien, Karlsplatz 13, A-1040 Wien, Austria

Abstract. In Nd-Fe-B based permanent magnets a high magnetocrystalline anisotropy of the hardmagnetic phase is necessary for a high intrinsic coercivity. In fact, metallurgical parameters (distribution of phases, chemical composition and crystal structures of phases) and processing parameters (alloy preparation, size and shape of particles, sintering and annealing treatments) determine the value of the coercive force of each sintered Nd-Fe-B magnet. Our analytical electron microscope study shows that "melt-spun" and sintered Nd-Fe-B based magnets contain more or less a distribution of nucleation centres for reversed domains, such as iron-rich phases and α-iron precipitates within the hardmagnetic 2 : 14 : 1-grains. A continuous non-magnetic layer phase between the hardmagnetic 2 : 14 : 1-grains increases the expansion field of reversed domains and increase the coercivity. In "melt-spun" magnets the contribution of the pinning of magnetic domain walls becomes effective during the magnetization reversal process.

Key words: permanent magnets, electron microscopy, coercivity.

The hardmagnetic properties of permanent magnets based on Nd-Fe-B are controlled by the magnetocrystalline anisotropy of the hardmagnetic phase and by metallurgical factors, such as the nominal composition of the starting alloy, purity, particle size distribution, grain size and precipitates. The nature of the raw material and processing parameters, such as quenching rates, sintering and annealing conditions, have a major effect on the final hardmagnetic properties. Nd-Fe-B based permanent magnets exhibit outstanding magnetic energy density products at room temperature but due to the low coercivity at elevated temperatures and, therefore, the low operating temperature this potential permanent magnetic material has

* To whom correspondence should be addressed

/20

not yet become a replacement for the SmCo 1 : 5 and SmCo 2 : 17 permanent magnets [1, 2]. In principle there are two different types of magnets based on a nominal composition of the starting alloy close to Nd15-Fe77-B8: The "magnequench" magnets, prepared by rapidly quenching and new compacting techniques [3], and the sintered magnets, prepared by conventional powdermetallurgical techniques [4]. Much progress in our understanding of the reasons for coercivity has been achieved since 1983, when Nd-Fe-B magnets were discovered, by studying the magnetic properties and by the examination of the microstructure. In sintered and "magnequench" Nd-Fe-B magnets a multiphase microstructure is found [5, 6]. Optical metallography, microprobe analysis and transmission electron microscopy together with STEM X-ray microanalysis have so far widely been used to identify the multiphase structure of Nd-Fe-B based magnets [5—29]. The purpose of this paper is to show the progress in understanding the microstructure and coercivity mechanism of Nd-Fe-B based magnets during the last two years.

Experimental

The magnets investigated were commercial grade magnets in peak aged condition of the general nominal composition Nd15-Fe77-B8, but prepared under different conditions and partly containing small amounts (< 1 wt.%) of dysprosium, aluminium, niobium, zirconium and magnesium, respectively. The intrinsic coercivities of these magnets ranged from 300 kA/m to 4000 kA/m. The magnets were produced by various producers under different processing and post-sintering heat treatment conditions. A series of more than 20 sintered magnets, supplied by Hitachi Met., Shin-Etsu Chem. Comp. and Sumitomo Spec. Met., Japan, CISRI Beijing, China, Crucible Materials and Unocal, USA, was studied by means of optical metallography, microprobe analysis and transmission electron microscopy together with STEM X-ray microanalysis in order to identify the multiphase microstructure. Thin slices perpendicular to the magnetic alignment direction were cut from each of the demagnetized magnets. The specimens were thinned for TEM by electropolishing using a perchloric acid-methanol solution. Ion milling was used only for cleaning the surfaces from contamination in order to avoid ion beam damage. Scanning transmission electron microscope (STEM) X-ray microanalysis was performed on a JEOL 200 CX analytical microscope fitted with a LaB6 filament and an EDAX high take off angle energy dispersive X-ray analyzer. A beryllium double tilt specimen stage was used to reduce the background intensities. All X-ray spectra were taken under [0001]-orientation of the specimens and were analyzed using the EDAX 9100 quantitative software program for these samples.

Results and Discussion

The analytical electron microscope investigation of Nd-Fe-B based magnets revealed in all of the peak aged magnets the same multiphase micro-

121



Fig. 1. Transmission electron micrograph of a slightly underquenched "melt-spun" Nd-Fe-B magnet

structure with three categories of phases [5]. Besides the hardmagnetic $Nd_2Fe_{14}B$ boride phase (*A*) also grains with a composition $Nd_{(1+\varepsilon)}Fe_4B_4$-phase (*B*) and Nd-rich phases (*C*) preferentially at grain-boundary junctions and extending to grain boundaries are detected by optical metallography and microprobe analysis. Grain size and grain size distribution are important criteria for the intrinsic coercivity of the final magnet.

"Melt-Spun" Magnets

The average grain size of magnets derived from rapidly solidified ribbons (about 50 nm) is approximately 100—300 times smaller than the one of sintered magnets (5—15 μm). Fig. 1 shows a transmission electron micrograph of a slightly underquenched "melt-spun" magnet. The uniform microstructure consists only of hardmagnetic grains, partly separated by a thin layer of a Nd-rich phase [6]. Melt-spun materials with maximum properties do not contain grains of phase (*B*), individual Nd-rich precipitates [30] or Nd_2O_3-inclusions. The nominal composition of the starting material and the quenching rate are important criteria for the precipitation of α-iron and Nd-rich phases within $Nd_2Fe_{14}B$-grains. The electron micrographs of Fig. 2 a and b show small α-iron precipitates with diameters of < 5 nm (black dotty background) and Nd-rich precipitates, respectively, of an underquenched melt-spun material. In the darkfield image of Fig. 2 a taken in the reflection of the α-iron phase the precipitates clearly show up as bright dots.

Sintered Magnets

We extensively studied the microstructure of sintered Nd-Fe-B magnets by means of analytical electron microscopy [2, 27—29]. The presence of Fe-rich precipitates was first found in sintered magnets showing a slight kink in the demagnetization curve. α-iron precipitates were also found in many other sintered magnets with a nominal composition close to Nd15-Fe77-B8. The dark filed micrograph of Fig. 2 c shows α-Fe precipitates within a hardmagnetic 2 : 14 : 1-grain.

The sintering of Nd-Fe-B magnets is primarily determined by the liquid phase type of the sintering mechanism which involves the presence of a low melting, viscous Nd-rich eutectoid [17], and secondly by the solid state type of sintering. During sintering the driving force for the densification of Nd-Fe-B magnets is the capillary pressure and the surface tension. Both surface diffusion along grain boundaries and volume diffusion also play an important role during densification. Liquid phase sintering occurs most readily when the liquid thoroughly wets the solid particles at the sintering temperature. The liquid in the narrow channels between the particles results in substantial capillary pressure. The particle size, sintering temperature and time, the uniformity of particle packing, the particle shape and the particle size distribution are extremely important parameters. Fine particle size powder can be sintered more rapidly and at lower temperature than

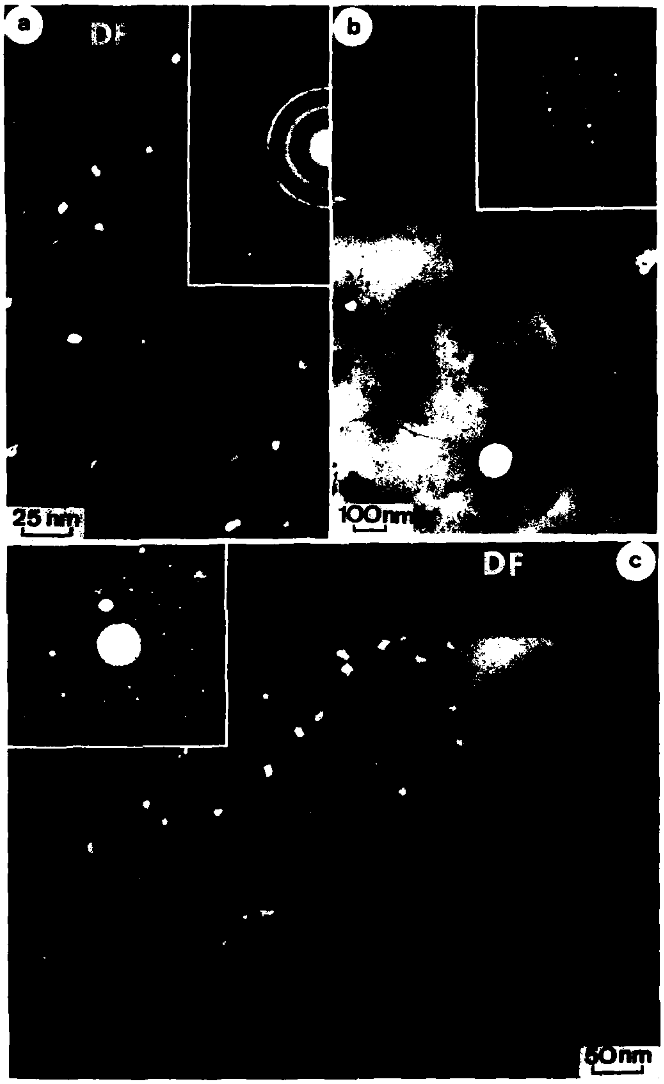


Fig. 2. Electron micrographs showing α-iron precipitates in **a** "melt-spun" and **c** sintered magnets and **b** dislocations and inclusions in an underquenched "melt-spun" material

124

coarser powder. If particle packing is not uniform in the pressed „green" compact, it will be difficult to avoid porosity during sintering. The scanning electron micrograph of Fig. 3 a shows the formation of agglomerates of irregular shaped particles with different size, which is a common source of nonuniformity of the powder. The schematic drawing of Fig. 3 c shows the difference between particles, individual grains and agglomerates of the "green" powder. Smaller particles exhibit a higher driving force for densification (higher capillary pressure and higher surface energy) than coarser particles. The rate of liquid phase sintering is strongly affected by the sintering temperature. A small increase in temperature results in a substantial increase in the amount of liquid present, but on the other hand, this increase causes an excessive grain growth, which deteriorates the magnetic hardness. The transmission electron micrograph of Fig. 3 b shows various grains of a sintered magnet. Grains appearing dark in electron micrographs and marked by arrows in Fig. 3 b, were characterized as Nd-rich phases [29]. It is obvious that the pores in the "green" compact are filled by Nd-rich grains after sintering. Depending on the cooling rate and post-sintering heat treatments various Nd-rich phases (*C*) occur in the final magnet. This is in good agreement with our analytical electron microscopic investigations which show that the Nd-rich phase (*C*) can be divided into at least four subtypes with different chemical compositions [29]. According to the ternary Nd-Fe-B phase diagram [17, 31, 32] we detected the Nd_2FeB_3 phase, ternary eutectic phases and other Nd-rich phases in sintered magnets [29]. Three different forms of Nd-rich phases including Nd_2O_3-inclusions are found by means of transmission electron microscopy. Firstly in the shape of grains with diameters up to several microns embedded between hardmagnetic 2 : 14 : 1-grains. Secondly, as intergranular phases at grain junctions and extending to grain boundaries. Thirdly, in the form of randomly distributed precipitates with diameters up to 500 nm within the 2 : 14 : 1-grains.

Since an agglomeration of several particles is always observed (Fig. 3 a), it can be shown that some of the larger particles also contain individual grains. In this case two types of grain boundaries will be formed after sintering (Fig. 3 d). In the first case, grain boundaries (GB1), separating particles will exhibit a Nd-rich layer phase between the grains, whereas in the second case the grain boundaries (GB2), originally separating grains within particles will be high-angle grain boundaries with virtually no Nd-rich layer phase. The composition and particle size of the alloyed and blended powder mainly determines the shape and distribution of the grains in the sintered magnet. Our investigations show that each sintered magnet contains a variety of grain boundary structures with different thickness and degree of completeness. A high amount of grain boundaries does not show any intergranular phase at all [33].

The individual microstructure of each magnet is already influenced during the alloy preparation, grinding, blending and pressing process before sintering. For instance, the oxygen content of the sintered magnet is proportional to the milling time and indirectly porportional to the particle size of the powder. The microstructure of the final magnet also strongly

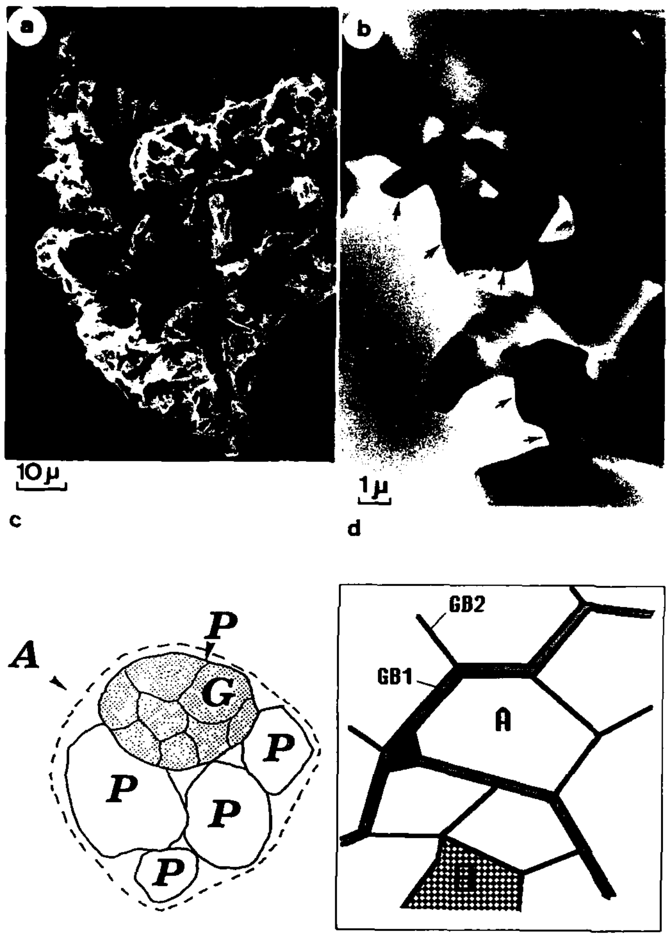


Fig. 3. **a** Scanning and **b** transmission electron micrographs showing agglomerates (*A*), particles (*P*) and grains (*G*) before sintering and Nd-rich (*C*) grains (marked by arrows) after sintering, respectively. Two different types of grain boundaries occur in sintered Nd-Fe-B magnets

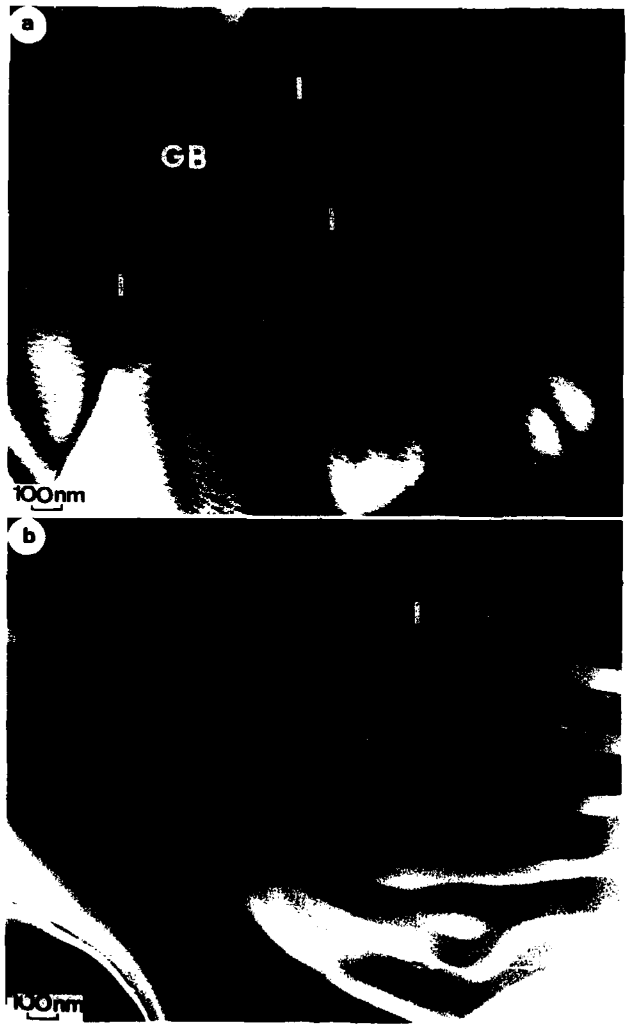


Fig. 4. Transmission electron micrographs showing Nd_2O_3 inclusions (*I*), in sintered magnets with a small grain size (< 5 μm). In the Lorentz micrograph **b** the magnetic domain structure surrounding an inclusion is shown

127.

depends on the purity of the raw material which was used for the preparation of the starting alloy.

Reasons for Coercivity of Nd-Fe-B Magnets

Metallurgical factors primarily control, besides the magnetocrystalline anisotropy of the 2 : 14 : 1-phase, the intrinsic coercive field of the individual magnet. Generally speaking, the coercive field is indirect porportional to the grain size, and the hor ogeneity of the distribution of the Nd-rich phases along grain boundaries can be correlated to the coercivity of the final magnet. Nd-Fe-B sintered magnets belong to the group of "nucleation controlled" permanent magnets [34, 35]. A non-magnetic layer phase between the hardmagnetic 2 : 14 : 1-grains increases the expansion field of reversed domains and increases the coercivity.

It seems that in melt-spun magnets, besides nucleation, the pinning of magnetic domain walls also controls the magnetization reversal process. Individual softmagnetic precipitates, such as α-iron, extremely deteriorate the intrinsic coercive field of magnets.

Studying sintered magnets with an extremely small g-ain size of 3—5 μm, but with a high coercivity of $iHc > 2000$ kA/m we found a high amount of hex. Nd_2O_3 inclusions within the 2 : 14 : 1-grains (Fig. 4 a). Finely dispersed inclusions act as an obstacle for the migration of grain boundaries and grain growth during sintering. The Lorentz electron micrograph of Fig. 4 b shows the magnetic domain structure surrounding a non-magnetic Nd_2O_3-inclusion in the demagnetized state.

During the last two years attempts were made to increase the coercivity by adding small amounts of elements, such as Al, Nb, Zr, Mo, Si, Mg, Ga, etc. Since the magnetocrystalline anisotropy is not affected by these additions there must be an influence on the microstructure of the magnet. If the addition is less than appoximately 1 wt%, the elements are mostly homogeneously distributed in all phases and possibly influence the magnetic properties of softmagnetic precipitates. Under certain conditions (i.e. heat treatment) the Nd-rich phase (*C*) and therefore the grain boundary layer phase gets enriched by the dopant. This depends also on the type of dotation, whether during the alloying or during blending [36]. The effect of various alloying elements on coercivity strongly depends on the processing conditions of the individual magnet. Recently Tokunga et al. [37] reported on a magnet with nominally containing seven (!) elements (Nd-Dy-Fe-Co-B-Nb-Ga) showing a reasonably high coercivity and remanence. From our electron microscope investigation we assume that each individual, sintered Nd-Fe-B based magnet contains a distribution of nucleation centres for reversed domains. For a better understanding of the coercivity mechanism of Nd-Fe-B magnets further microstructural investigations have to be made.

Acknowledgements. The authors are grateful to Hitachi Met., Shin-Etsu Chem. Comp., Sumitomo Spec. Met., Japan, CISRI Beijing, China, Crucible Materials and Unocal, USA, for providing the magnets used in this study. This work was partly sponsored by the US Army European Research Office, London, UK, under contract No. DAJA-86-C-0010 and by the Austrian Nationalbank under contract No. 3065.

References

[1] K. J. Strnat, *Proceedings of ASM Symposium on Soft and Hard Magnetic Materials with Applications*, Amer. Soc. for Metals, Orlando, Florida, USA, Oct. 4—9, 1986.
[2] D. Li, H. F. Mildrum, K. J. Strnat, *J. Appl. Phys.* **1985**, *57*, 4140.
[3] R. W. Lee, N. Schaffel, L. Brewer, *IEEE Trans. Magn.* **1985**, *21*, 1958.
[4] M. Sagawa, S. Fujimura, N. Togawa, H. Yamamoto, Y. Matsuura, *J. Appl. Phys.* **1984**, *55*, 2083.
[5] J. Fidler, *IEEE Trans. Magn.* **1985**, *21*, 1955.
[6] R. K. Mishra, *J. Magn. Mat.* **1986**, *54—57*, 450.
[7] Y. L. Chen, *IEEE Trans. Magn.* **1985**, *21*, 1967.
[8] T. S. Chin, Y. Hara, E. J. Lavernia, R. C. O'Handley, N. J. Grant, *J. Appl. Phys* **1986**, *59*, 1297.
[9] K. D. Durst, H. Kronmüller, in press.
[10] N. A. El-Masry, H. H. Stadelmaier, *Mat. Letters* **1985**, *3*, 405.
[11] G. C. Hadjipanayis, K. R. Lawless, R. C. Dickerson, *J. Appl. Phys.* **1985**, *57*, 4097.
[12] G. C. Hadjipanayis, Y. F. Tao, K. R. Lawless, *IEEE Trans. Magn.* **1986**, *22*, 1845.
[13] K. Hiraga, M. Hirabayashi, M. Sagawa, Y. Matsuura, *Jap. J. Appl. Phys.* **1985**, *24*, L30.
[14] K. Hiraga, M. Hirabayashi, M. Sagawa, Y. Matsuura, *Jap. J. Appl. Phys.* **1985**, *24*, 699.
[15] J. D. Livingston, *J. Appl. Phys.* **1985**, *57*, 4137.
[16] Y. Luo, N. Zhang, G. D. Graham, in press.
[17] Y. Matsuura, S. Hirosawa, H. Yamamoto, S. Fujimura, M. Sagawa, K. Osamura, *Jap. J. Appl. Phys.* **1985**, *24*, L635.
[18] R. K. Mishra, J. K. Chen, G. Thomas, *J. Appl. Phys.* **1986**, *59*, 2244.
[19] R. K. Mishra, R. W. Lee, *Appl. Phys. Lett.* **1986**, *48*, 733.
[20] T. Mizoguchi, I. Sakai, H. Niu, K. Inomata, *IEEE Trans. Magn.* **1986**, *22*, 919.
[21] R. Ramesh, K. M. Krishnan, E. Goo, G. Thomas, M. Okada, M. Homma, *J. Magn. Magn. Mat.* **1986**, *54—57*, 363.
[22] M. Sagawa, S. Fujimura, H. Yamamoto, Y. Matsuura, K. Higara, *IEEE Trans. Magn.* **1984**, *20*, 1584.
[23] T. Suzuki, K. Hiraga, M. Sagawa, *Jap. J. Appl. Phys.* **1984**, *23*, L421.
[24] T. Suzuki, K. Hiraga, *J. Magn. Magn. Mat.* **1986**, *54—57*, 527.
[25] P. Schrey, *IEEE Trans. Magn.* **1986**, *22*, 913.
[26] M. Tokunaga, M. Tobise, N. Meguro, H. Harada, *IEEE Trans. Magn.* **1986**, *22*, 904.
[27] J. Fidler, P. Skalicky, F. Rothwarf, *Mikrochim. Acta [Wien]* **1985**, *Suppl. 11*, 371.
[28] S. H. F. Parker, P. Grundy, J. Fidler, *J. Magn. Magn. Mat.* **1987**, *66*, 74.
[29] J. Fidler, *IEEE Trans. Magn.* **1987**, in press.
[30] R. K. Mishra, personal communication.
[31] G. Schneider, E. Th. Henig, H. H. Stadelmaier, G. Petzow, *Proc. 1986th Int. Powder Metallurgy Conf. PM 86, Düsseldorf*, Verlag Schmid GmbH, Freiburg, 1986, p 1197.
[32] D. S. Tsai, T. S. Chin, S. E. Hsu, M. P. Hung, *IEEE Trans. Magn.* **1987**, in press.
[33] J. Fidler, *Proc. Vth Int. Symp. on Magnetic Anisotropy and Coercivity in Rare Earth-Transition Metal Alloys, Bad Soden, Sept 1987*, Vol. 2, DPG e.V., Bad Honef, 1987, p. 363.
[34] H. Kronmüller, K. D. Durst, G. Martinek, in press.
[35] J. D. Livingston, *IEEE Trans. Magn.* **1987**, in press.
[36] M. H. Ghandehari, J. Fidler, *Materials Letters* **1987**, *5*, 285.
[37] M. Tokunaga, M. Endoh, H. Harada, *IEEE Trans. Magn.* **1987**, in press.

Received July 16, 1987.

129

25

THE ROLE OF THE MICROSTRUCTURE ON THE COERCIVITY OF ND-FE-B SINTERED MAGNETS

Josef Fidler

Institut für Angewandte Physik, TU Wien, Vienna, Austria

ABSTRACT

Besides the magnetocrystalline anisotropy also the microstructural parameters determine the coercive force of the sintered magnets. Measurements of magnetic parameters, such as crystal anisotropy, magnetization etc. do not explain quantitatively the dependence of the intrinsic coercivity on the grain size and heat treatment parameters. In fact, metallurgical parameters, such as distribution of phases, chemical composition and crystal structures of phases determine the value of the coercive force of the individual sintered magnet. Our analytical electron microscope study revealed at least five different categories of phases in addition to the hardmagnetic 2:14:1-phase in sintered Nd15-Fe77-B8 magnets. Iron-rich phases and α-iron precipitates within the 2:14:1-grains were found in several magnets. Also other possible nucleation sites for reversed domains were also detected inside the grains, such as precipitates close to the composition of the $(1+\varepsilon)$:4:4-phase. Magnets with an increased coercivity due to the dotation by small amouts of Al, Nb, Mg, Zr, Ga and other refractory elements showed a homogeneous distribution of these elements in all phases, resulting in a change of the magnetic properties of possible nucleation centres. In several cases, the Nd-rich phase and single precipitates are found to be enriched by these elements. In magnets with extreme small grain sizes of 3-5 µm and threfore with coercivities up to iHc= 2000 kA/m we found a large number of inclusions with a high melting temperature within the 2:14:1-grains. A large volume fraction of such inclusions and a small inclusion size (< 1µm) is very effective in retarding grain growth during the sintering process. In conclusion the more homogeneous the composition and the distribution of the hardmagnetic and the Nd-rich phases are, the higher will be the coercivity.

****

Paper No. S3.2 at the 5th International Symposium on Magnetic Anisotropy and Coercivity in Rare Earth-Transition Metal Alloys, Bad Soden, FRG, September 3, 1987 (Proceedings Book by: Deutsche Physikalische Gesellschaft e.V., D-5340 Bad Honnef 1, FRG).

Address inquiries to: J.Fidler, Institut für Angewandte Physik, Technische Universität, Karlsplatz 13, A-1040 Vienna, Austria.

This work was partly sponsored by the US Army European Research Office, London, UK under contract No.DAJA-86-C-0010 and by the Austrian Nationalbank under contract No.3065.

1. Introduction

The intrinsic magnetic coercivity of recently developed rare earth-iron based permanent magnets is primary determined by the magnetocrystalline anisotropy of the hardmagnetic phase. But in fact, the microstructure and metallurgical parameters, respectively, limit the magnetic coercivity of this class of permanent magnets. Nd-Fe-B based permanent magnets exhibit outstanding magnetic energy density products at room temperature, but due to the low coercivity at elevated temperatures and therefore the low operating temperature this potential permanent magnetic material has not yet become a replacement for the SmCo 1:5 and SmCo 2:17 permanent magnets. Originally the coercivity of Nd-Fe-B magnets was increased by replacing Nd with small amounts of Dy or Tb [1,2] resulting in a higher magnetocrystalline anisotropy but at the expense of a lower saturation magnetization. Sintered magnets with a composition close to Nd7Dy8Fe77B8 exhibit intrinsic coercivities iHc ≥ 4000 kA/m but show only (B.H)max = 160 kJ/m3 at room temperature [3]. Since the last RCO-Meeting in Dayton 1985 numerous suggestions have been reported to increase the intrinsic coercivity, especially of <u>sintered</u> Nd-Fe-B based magnets. In most of these cases the coercivity could be increased by the addition of small amounts of

* aluminium
* niobium
* magnesium
* zirconium
* gallium
* dysprosium-oxide

to magnets close to the nominal composition Nd15-Fe77-B8. In many cases the addition of small amounts of refractory elements did not affect drasticly the magnetocrystalline anisotropy. The reason for the increase of the coercivity is the influence of the changed microstructure on the magnetic domain structure and magnetization reversal process, respectively.

Besides the addition of small amounts of various elements, also the post-sintering heat treatment procedure has been modified in order to maximize the coercivity, which is very sensitive to aging temperatures, annealing times, quenching- and cooling rates [2].

Rare earth-iron based magnets can be divided into two groups, the sintered magnets, prepared by conventional powdermetallurgical techniques, and the "magnequench" magnets, prepared by rapidly quenching and new compacting techniques. In sintered and "magnequench" Nd-Fe-B magnets a multiphase microstructure is found [4]. Optical metallography, microprobe analysis and transmission electron microscopy together with STEM X-ray microanalysis have widely been used to identify the multiphase structure of Nd-Fe-B based magnets so far [4-13]. Special emphasis of this tutorial lecture has been laid on the influence of alloying parameters on the microstructure and therefore on the coercivity of sintered Nd-Fe-B based magnets.

2. Experimental

The material used for the microstructural investigation was commercial grade sintered magnets with a nominal composition close to Nd15-Fe77-B8, but prepared under different conditions and partly containing small amounts of dysprosium, aluminium, niobium, zirconium and magnesium, respectively. The intrinsic coercivities of these magnets ranged from 300 kA/m till 4000 kA/m. The magnets were produced by standard powdermetallurgical processing techniques by various producers under different post-sintering heat treatments. A series of more than 20 sintered magnets, supplied by Hitachi Met., Shin-Etsu Chem.Comp. and Sumitomo Spec.Met., Japan, CISRI Beijing, China, Crucible Materials and Unocal, USA was studied by means of optical metallograpy, microprobe analysis and transmission electron microscopy together with STEM X-ray microanalysis in order to identify the multiphase microstructure. Thin slices perpendicular to the magnetic alignment direction were cut from each of the demagnetized magnets. The specimens were thinned for TEM by electropolishing using a perchloric acid-methanol solution. Ion milling was used only for cleaning the surfaces from contamination. Scanning transmission electron microscope (STEM) X-ray microanalysis was performed on a JEOL 200 CX analytical microscope fitted with a LaB6 filament and an EDAX high take off angle energy dispersive X-ray analyzer. A beryllium double tilt

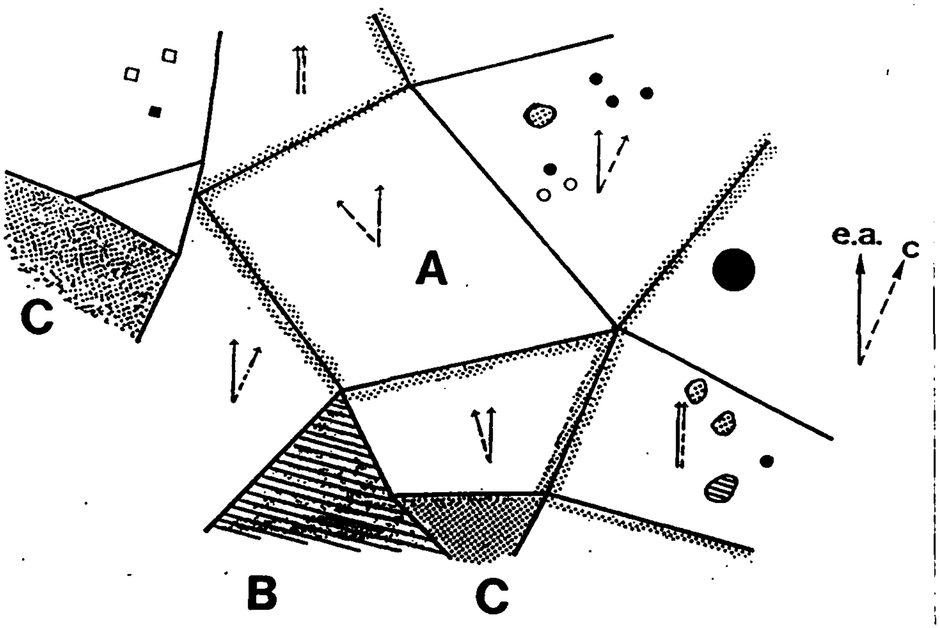


Fig.1: Schematic drawing of the multiphase microstructure found in sintered Nd-Fe-B magnets.

132

specimen stage was used to reduce background intensities. All X-ray spectra were taken under [0001]-orientation of the specimmens and were analyzed using the EDAX 9100 quantitative software program for this samples.

3. Results

In sintered Nd_{15}-Fe_{77}-B_8 magnets three categories of phases occur [4,5,13]. Besides the hardmagnetic $Nd_2Fe_{14}B$ boride phase (A) also grains with a composition $Nd_{(1+\varepsilon)}Fe_4B_4$ - phase (B) and Nd-rich phases (C) preferentially at grain boundary junctions and extending to grain boundaries are detected by optical metallography and microprobe analysis. Figure 1 shows a schematic drawing of the microstructure obtained in most of the sintered magnets. Irregular shaped grains with different grain sizes are separated by grain boundaries which only partly contain a Nd-rich phase (C). Within the hardmagnetic grains there is always a special amount of randomly distributed precipitates and inclusions, respectively, with diameters up to 0.5 µm. In some of the magnets, especially in the ones which show a kink in the demagnetization curve a high amount of Fe-rich phases (D) and α- Fe precipitates (E) are found. Actually , we frequently detected mostly in a large number of production grade magnets large inclusions up to several microns in size of "exotic phases" (F) such as Nd-chlorides, $NdCl_2$, Nd-chlorate and $Nd(OH)_2Cl$ and iron -phosphate-sulfate phases [13]. Table 1 summarizes the phases detected in Nd-Fe-B based sintered magnets by means of analytical transmission electron microscopy.

Table 1: PHASES IN SINTERED ND-FE-B MAGNETS DETECTED BY ANALYTICAL STEM

(A)	HARDMAGNETIC BORIDE [2:14:1]	different grain size different orientation
(B)	BORON-rich [(1+):4:4]	big grains, precipitates
(C)	NEODYMIUM-rich	grains, precipitates, grain boundary layer (C1) Nd:Fe (at%) = 1 : 1.2-1.4 (C2) 1 : 2.0-2.3 (C3) 1 : 3.5-4.4 (C4) > 1 : 7
	NEODYMIUM-OXID	grains, inclusions
(D)	IRON-rich	precipitates
(E)	α - IRON	
(F)	"EXOTIC PHASES"	grains, inclusions (F1) Nd - Cl (F2) Nd - P - S

Hardmagnetic 2:14:1 phase (A)
Due to the multiphase microstructure only the hardmagnetic 2:14:1-phase (A) contributes to the magnetic properties of the magnet. The volume fraction of this phase determines the remanence and therefore the maximum energy density product of the magnet. Using transmission electron microscopy together with X-ray microanalysis precipitates with diameters up to a few hundreds nm of phases (B), (C), (D) and (E) within the hardmagnetic 2:14:1 grains have been identified. Our microscopic investigations did not reveal any significant evidence of other crytal lattice defects besides the precipitates and inclusions within the hardmagnetic grains (fig.2). Determining the Fe/Nd - ratios revealed that most of the additions (Al, Nb, Zr, etc.) are partly replacing the Fe-sites in the 2:14:1-grains. In production grade magnets this was also found for silicon. It should also be mentioned that the misorientation between alignment direction and c-axis of the individual grains is found by electron diffraction in the order of 10°, which is in good agreement with values measured by x-ray diffraction [5]. Moreover our analytical investigations revealed a distribution of different Fe:Nd-ratios in 2:14:1-grains even in the same magnet material [13].

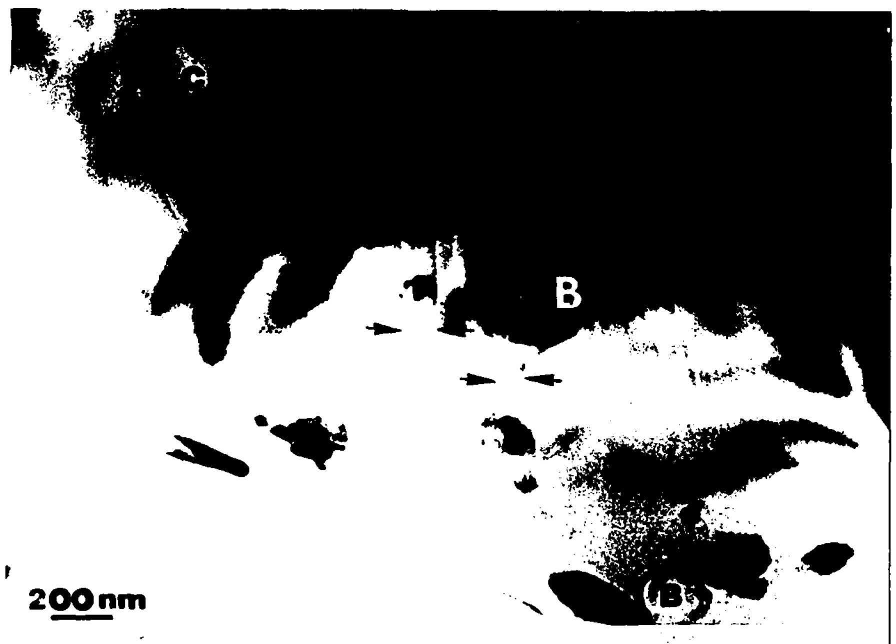


Fig.2: Lorentz electron micrograph showing boron-rich (B) and neodymium-rich precipitates together with magnetic domain walls within a hardmagnetic grain.

134

(1+ε):4:4-phase (B)

Transmission electron micrographs of grains of phase(B) show a high defect density of dislocations and planar defects especially in larger grains up to 15 μm (fig.3). Phase (B) occurs in the form of individual grains as well as in the form of incoherent precipitates within 2:14:1-grains (fig.2) We have a strong evidence that phase (B) occurs in different metastable modifications in sintered magnets and is still under certain conditions ferromagnetic at room temperature which is in contrary to measurements of the Curie temperature of (1+ε):4:4- crystalline material [14,15]. The heavily faulted phase (B) mostly differs in the chemical composition especially in the content of other elements, such as silicon, aluminium, zirconium etc.The ratio of the Fe- to the Nd-concentration (in at%) was found to be in the range 3.6 to 3.9. By means of high resolution electron microscopy and elctron diffraction, crystal lattice periodicities of 0.4 nm, 4.8 nm and 14.5 nm were found [16].This is the reason why the density and the type of the modification of the (B) phase within the 2:14:1-grains could be a contribution in limiting the coercivity. The nucleation of reversed domains can easily take place at such ferromagnetic precipitates. The defocused Lorentz electron micrograph of fig.1 shows a magnetic domain structure. Domain walls are visible as bright and dark lines. In one of the (1+ε):4:4-phase domain walls also occur within the precipitate.

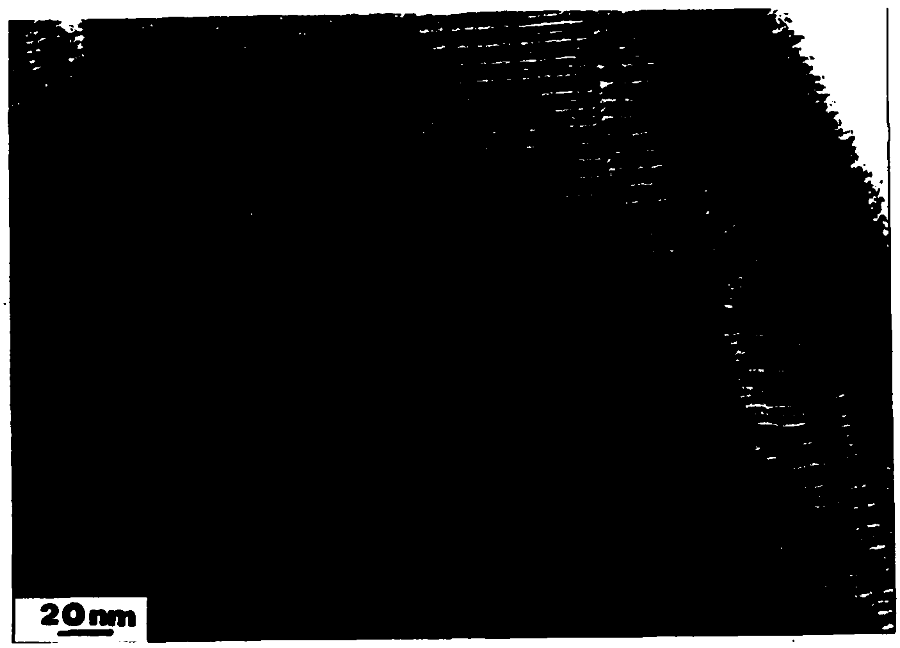


Fig.3: High resolution electron micrograph showing faulted regions within a (1+ε):4:4-grain.

Nd-rich phases (C)

Another result of our analytical electron microscopic investigations [13] is the fact that the Nd-rich phase (C) can be divided into at least four subtypes with different chemical composition. From the characterization of more than 100 Nd-rich (C)-phases, the following various Nd-rich subtypes with different Fe:Nd-ratios were found:

(a) 1 : 1.2-1.4
(b) 1 : 2.0-2.3
(c) 1 : 3.5-4.4
(d) > 1 : 7

According to the ternary phase diagrams by Y. Matsuura et al. [17], G. Schneider et al. [18] and D.S. Tsai et al. [19] we detected the Nd_2FeB_3 phase, ternary eutectic phases and other Nd-rich phases, whereby some of them could not yet be exactly identified. Three different forms of Nd-rich phases are found by transmission electron microscopy (fig.4). First in the shape of grains with diameters up to several microns embedded between hardmagnetic 2:14:1-grains. Second ,as intergranular phases at grain junctions and extending to grain boundaries. Third, in the form of randomly distributed precipitates with diameters up to 500 nm within the 2:14:1-grains.

X-ray microprobe analysis of large Nd-rich particles show a high oxygen content and electron diffraction patterns can partly be indexed by the hexagonal Nd_2O_3 crystal structure. Especially the randomly distributed Nd-rich precipitates within the 2:14:1-grains were identified as hex. Nd_2O_3-inclusions, which were already formed before the sintering process. The melting point of Nd_2O_3 is about 2270°C, whereby the sintering temperature is below 1100°C. Oxide impurities and other inclusions may origine from impurities of the starting material. It should be mentioned that most of the Nd-rich phases occur in the form of metastable phases with unknown chemical composition and crystal structure and it must be assumed that oxygen plays an important role in these Nd-rich phases.

Iron-rich phases (D) and (E)

The presence of Fe-rich precipitates was first found in Nb-containing Nd_{15}-Fe_{77}-B_8 magnets. The microstructure of such magnets was found to be similar to that of the ternary magnets, but with the addition of two Nb containing phases which we found inside grains of the hard magnetic phase [20]. The larger precipitates were identified by electron diffraction and X-ray microanalysis as Laves phase $NbFe_2$. The absence of domain walls within this phase suggest that it is probably non-ferromagnetic but the relatively large size of these inclusions, of the order of several microns, means they would not form sites for domain wall pinning. However we also found smaller Nb-containing precipitates of the size up to 50 nm which could produce domain wall pinning. If these precipitates do produce strong pinning then their presence would explain the enhanced coercivity of the Nb-containig magnet.

136



Fig.4: Electron micrographs showing a Nd-rich grain (a), separated by two grain boundaries GB from hardmagnetic grains with a high dislocation density inside, and hex. Nd_2O_3-inclusions in a high coercivty magnet with a small grain size.

137

Taking into account the nominal composition Nd15-Fe77-B8 and considering the values of the volume fractions of phases (A), (B) and (C) [5], it is evident that in sintered magnets Fe-rich phases or pure iron precipitates have to be formed, which is also in agreement with Mössbauer measurements of sintered Nd-Fe-B magnets [21]. The electron micrographs of fig.5 show α-Fe precipitates within a hardmagnetic grain. Special care has to be taken in order to study the iron precipitation. Sample preparation, especially long ion-milling and extended electron bombardment under observation in the microscope, may origine the formation of hex. Nd2O3 and iron-rich regions within the 2:14:1-grains [10].



Fig.5: Bright field electron micrograph and electron diffraction pattern showing a high density of α-Fe precipitation within a 2:14:1-grain of a magnet showing a slight kink in the demagnetization curve.

Exotic phases (F)

In most of the Nd-chlorine phases a high density of dislocations was found (fig.6). The role of these phases on the coercivity has not yet been fully clarified, since the magnetic properties and crystallographic properties of these partly metastable phases are unknown. These inclusions may origine from impurities of the starting material.

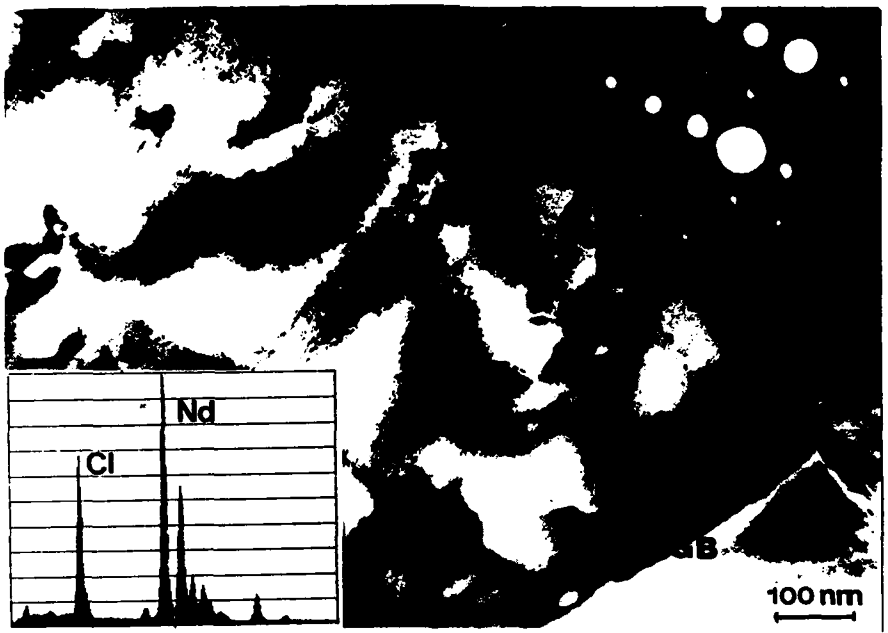


Fig.6: Electron micrograph and X-ray spectrum of a large Nd-Cl phase containing dislocations

Grain boundary regions

Our investigations do not agree with other electron microscopic investigations showing a new, so called "bcc" phase" near grain boundary regions and we do not agree with their conclusions upon the coercivity mechanism [22,23]. Scanning electron microscope micrographs of pressed powders show irregular shaped particles with different particle sizes (fig.7). The agglomeration of several particles is always observed. It can be shown that larger particles contain individual grains. In this case two types of grain boundaries will be formed after sintering. In the first case, grain boundaries, separating particles will exhibit a Nd-rich layer phase between the grains, whereas in the second case the grain boundaries, originally separating grains within particles will be high-angle grain boundaries with more or less no Nd-rich layer phase. The composition and particle size of the alloyed and blended powder mainly determines the shape and distribution of the grains in the sintered magnet.

Our investigations show that each individual magnet contains a variety of grain boundary structures with different thickness and degree of completeness. A high amount of grain boundaries does not show any intergranular phase at all. The high resolution electron micrograph of fig.8 shows a 37°-high angle grain boundary of a magnet with iHc=1500 kA/m without a grain boundary layer phase.

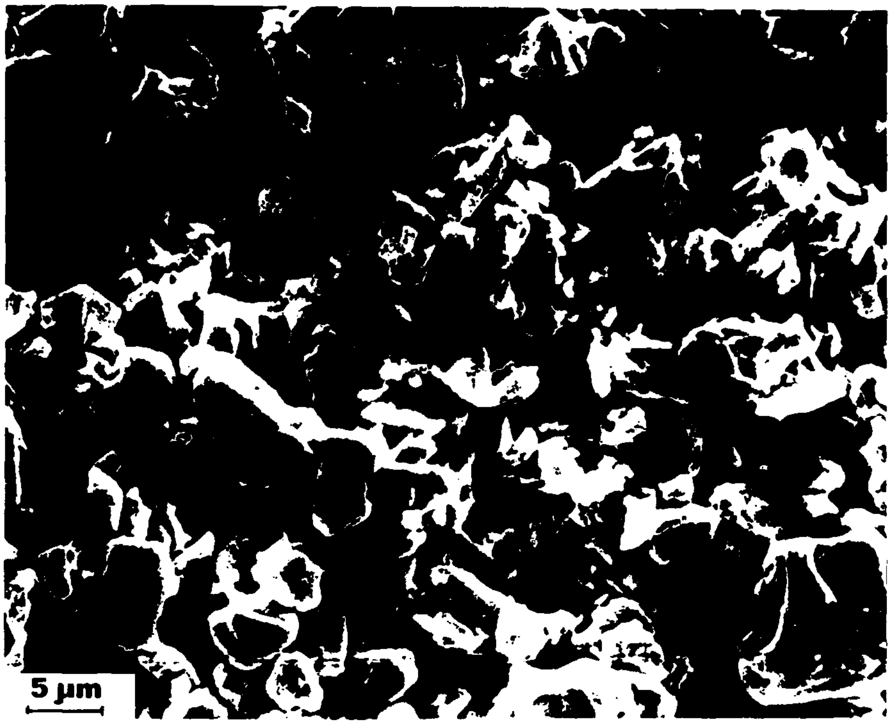


Fig.7: Scanning electron micrograph showing the irregular shaped particles of a green compact, before sintering.

As result of X-ray microanalysis we found a gradient of the concentration from the centre of a hardmagnetic grain in direction to the grain boundary. The ratio of the doped elements (Dy, Al, Nb) and silicon to iron is higher in regions near grain boundaries than in the middle of grains. Chen et al. found by nanoprobe x-ray microanalysis an enrichment of Al within the Nd-rich grain boundary layer [24]. Dysprosium additions increase the coercivity, because of the higher magnetocrystalline anisotropy of the hardmagnetic phase (A). The type of the Dy-dotation (as Dy-metal or Dy-oxide) [25] and the post-sintering heat treatment strongly influence the final coercive force. This effect can be explained by the change of the composition of the (NdDy)-rich grain boundary phase leading to a magnetocrystalline "surface hardening" of the hardmagnetic grains in oxide doped magnets [26].

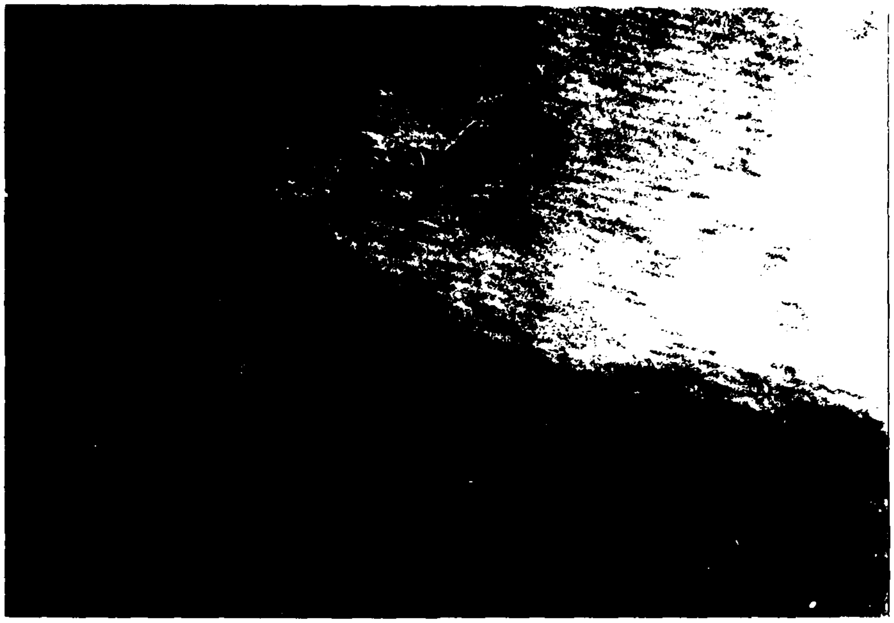


Fig.8: Lattice fring image showing a 37° high-angle grain boundary with no Nd-rich layer phase between the 2:14:1-grains

4. Discussion

Our microstructural investigations have shown that the microstructure of sintered Nd-Fe-B magnets is more complicated than the one of single phase SmCo1:5 magnets, which is also a typical example for a "nucleation controlled" magnet. The individual microstructure of each magnet is already influenced during the alloy preparation, grinding, blending and pressing process before sintering. For instance the oxygen content of the sintered magnet also depends on the milling time and therefore on the particle size of the powder. The microstructure of the final magnet also strongly depends on the purity of the raw material which was used for the preparation. Thus, the microstructure of "laboratory" grade magnets differs from "commercial" grade magnets. In fact metallurgical and processing factors,such as

* *AVERAGE PARTICLE SIZE*
* *PARTICLE SIZE DISTRIBUTION*
* *PARTICLE SHAPE*
* *PARTICLE SURFACE (OXIDATION)*
* *PARTICLE CHEMISTRY AND STRUCTURE*

---

* *GRAIN SIZE, MISORIENTATION & TEXTURE*
* *DISTRIBUTION AND COMPOSITION OF PHASES*
* *GRAIN-BOUNDARY LAYERPHASE*

---

* *ANNEALING PARAMETERS (temp., time, cooling rate)*

primary control , besides the magnetocrystalline anisotropy of the 2:14:1-phase, the intrinsic coercive field of the individual magnet. Generally speaking, the coercive field is indirect proportional to the grain size, and the homogeneity of the distribution of the Nd-rich phases along grain boundaries can be correlated to the coercivity of the final magnet. This is also the reason of the fact why different post-sintering heat treatments have an influence on the coercivity. The more homogeneous the composition and the distribution of the Nd-rich phases (C) in the magnet are, the higher will be the coercivity of the sintered magnet. A non-magnetic layer phase between the hard magnetic 2:14:1-grains increases the expansion field of reversed domains and increases the coercivity.

As result of the study of the microstructure of a magnet with an extreme small grain size of 3-5 µm and a coercivity of iHc= 2000 kA/m we found a high amount of hex. Nd2O3 inclusions within 2:14:1-grains (fig.4.b). The problem of migration of grain boundaries and grain growth during sintering of rare earth permanent magnets is well known and the presence of finely dispersed inclusions can act as obstacle for such processes. A given volume fraction of inclusions is much more effective in retarding grain growth when the particles are very small (< 1 µm).

There is a twofold influence of the addition of small amounts of elements, such as Al, Nb, Zr, Mo, Si, Mg, Ga etc. on the microstructure. First, if the amount of addition is less than approximately 1 wt%, the elements are mostly homogeneously distributed in all phases (A), (B) and (C), but might influence the magnetic properties of the softmagnetic precipitates, especially of phase (B) within the hardmagnetic grain interior. Under certain conditions (i.e. heat treatment) phase (C) and therefore the grain boundary layer phase gets enriched by the dopant. This depends also on the type of dotation, whether during alloying or during blending. On the other hand, if the amount of addition exceeds a critical value, individual grains of new phases are formed, such as Al13Nd23Fe64 [10] or NbFe2 [20]. Between these extreme cases there is also the possibility for the formation of precipitates. The influence of such precipitates on the magnetization reversal and therfore on the coercive force is not yet clear. Attempts to find a textured precipitation structure within the hardmagnetic phase are made, thus the pinning force for magnetic domain walls could overcome the nucleation fields for reversed domains within the 2:14:1-grains. In zirconium-containing magnets needle shaped precipitates are found by transmission electron microscopy [27].

The porosity in the "green" compacts is non-interconnected. During sintering a liquid Nd-rich phase is formed in Nd-Fe-B compacts. The densification is probably due to the heavy alloy liquid phase sintering mechanism and is accelerated by the presence of vacant iron and boron lattice sites. Interdiffusion between phases and the capillary pressure is responsible for the movement and distribution of the liquid phase.

Interdiffusion takes place by lattice and surface diffusion processes especially near grain boundaries, whereby a high concentration of iron and boron vacancies is demanded. From metallurgical reasons the liquid phase between the 2:14:1 grains has to be a Nd-rich phase with a high amount of oxygen.

The nucleation of reversed domains primary determines the coercivity mechanism of sintered Nd-Fe-B magnets. From our electron microscope investigation we assume that sintered Nd-Fe-B based magnets contain a distribution of nucleation centres, such as precipitates of type (B), (D) or (E), for reversed domains within the hardmagnetic 2:14:1-grains. The expansion of reversed domain-nuclei is hindered by the existence of a continuous non-magnetic Nd-O rich intergranular phase, separating the hardmagnetic grains. For a better understanding of the coercivity mechanism of Nd-Fe-B magnets further microstructural investigations have to be made.

References

[1] M.Sagawa, S.Fujimura, H.Yamamoto, Y.Matsuura and K.Hiraga, IEEE Trans.Magn. Vol.Mag.-20, 1584 (1984).

[2] M.Tokunaga, N.Meguro, M.Endoh, S.Tanigawa and H.Harada, IEEE Trans.Magn. Vol.Mag.-21, 1964 (1985).

[3] M.Sagawa, S.Hirosawa, K.Tokuhara, H.Yamamoto and S.Fujimura, J.Appl.Phys., (1987), in print.

[4] J.Fidler, IEEE Trans.Magn., Vol. Mag.-21, 1955, (1985).

[5] K.D.Durst and H.Kronmueller, in press.

[6] R.K.Mishra, J.K.Chen and G.Thomas, J.Appl.Phys., Vol.59, 2244,(1986).

[7] G.C.Hadjipanayis, Y.F.Tao and K.R. Lawless, IEEE Trans. Magn., Vol.Mag.-22, (1845), (1986).

[8] R.Ramesh, K.M.Krishnan, E.Goo, G.Thomas, M.Okada and M.Homma, J.Magn.Magn.Mat., Vol.54-57, 563, (1986).

[9] N.A.El-Masry and H.H.Stadelmaier, Materials Letters, Vol.3, 405, (1985).

[10] P.Schrey, IEEE Trans.Magn., Vol. Mag.-22, 913, (1986).

[11] R.K.Mishra and R.W.Lee, Appl.Phys.Lett, Vol.48, 733, (1986).

[12] R.K.Mishra, J.Magn.Magn.Mat., Vol.54-57, 450, (1986).

[13] J.Fidler, IEEE Trans.Magn., Sept. 1987, in print.

[14] D.Givord, J.M.Moreau and P.Tenaud, Solid State Comm. Vol.55, 303, (1985).

[15] K.H.J. Buschow, D.B.de Mooij, J.L.C.Daams and H.M.van Noort, J.Less Comm.Metals Vol.115, 357, (1986).

[16] J.Fidler, P.Skalicky and F.Rothwarf, Mikrochimica Acta [Wien], Suppl.11, Vol.11, 371, (1985).

[17] Y.Matsuura, S. Hirosawa, H.Yamamoto, S. Fujimura, M. Sagawa and K.Osamura, Jap.J.Applied Physics Vol.24, L635,(1985).

[18] G.Schneider, E.Th.Henig, H.H.Stadelmaier,and G.Petzow, Proc. 1986th Int. Powder Metallurgy Conf. P/M 86, (ed. Verlag Schmid GmbH, Freiburg), Düsseldorf, FRG, 1986,p.1197.

[19] D.S.Tsai, T.S.Chin, S.E.Hsu and M.P.Hung, IEEE Trans.Magn., Sept.1987, in print.

[20] S.H.F.Parker, P.J.Grundy and J.Fidler, J.Magn.Magn.Mat., Vol.66, 74, (1987).

[21] G.Wiesinger, private communication.
[22] M.Sagawa, S.Hirosawa, H.Yamamoto, Y.Matsuura, S.Fujimura, H.Tokuhara and K.Hiraga, IEEE-Trans.Magn., Vol.MAG-22, 910, (1986).
[23] M.Tokunaga, M.Tobise, N.Meguro and H.Harada, IEEE Trans. Magn. Vol.Mag.22, 904, (1986).
[24] J.K.Chen and G.Thomas, Int. MRS Spring Meeting, April 1987, Anaheim, CA,USA.
[25] M.H.Ghandehari, Appl.Phys.Lett. Vol.48, 548, (1986).
[26] M.H.Ghandehari and J.Fidler, Materials Letters, in print.
[27] S.H.F.Parker, private communication.

IEEE TRANSACTIONS ON MAGNETICS, VOL. 24, NO. 2, MARCH 1988

TEM-STUDY OF THE PRECIPITATION OF IRON IN ND-FE-B SINTERED MAGNETS

Josef Fidler and Yoshio Tawara°

Institute of Applied Physics, T.U. Vienna,
Karlsplatz 13, A-1040 Vienna, Austria.
°Shin-Etsu Chemical Co. Ltd., Takefu, Japan.

Abstract:
We have extensively studied the microstructure of sintered *Nd-Fe-B magnets by means of* analytical electron microscopy. The presence of Fe-rich precipitates was first found in magnets showing a small kink in the demagnetization curve, which is an evidence for soft magnetic nucleation centres for reversed magnetic domains within the magnet. α-iron precipitates ocurred outside as well as within the hard magnetic 2:14:1 grains and were also found in other commercial grade magnets with a nominal composition close to Nd15-Fe77-B8.

Introduction

The coercivity of rare-earth iron based permanent magnet materials is determined by the high magnetocrystalline anisotropy of the hard magnetic boride phase $RE_2Fe_{14}B$ [1]. The nucleation of reversed domains at regions with low magnetocrystalline anisotropy is the reason why the theoretical coercive forces are not obtained in practice in Nd-Fe-B sintered magnets. This type of magnet usually contains a multiphase microstructure. The intrinsic nucleation of reversed magnetic domains in Nd-Fe-B magnets has already been treated theoretically including the effect of second order anisotropy constant and oblique applied magnetic fields on the nucleation field of uniaxial single domain particles [2]. Besides the theoretical models and magnetic measurements [3], microstructural studies are also necessary for the understanding of the coercivity mechanisms and magnetization reversal in sintered Nd-Fe-B magnets. Although optical metallography, microprobe analysis and transmission electron microscopy together with STEM X-ray microanalysis have widely been used to identify the multiphase structure of Nd-Fe-B based magnets so far [4-28], no electron microscopic characterization of softmagnetic precipitates or inclusions in Nd-Fe-B magnets has been reported so far. The purpose of this study is to identify soft-magnetic centres for reversed domains within Nd-Fe-B based sintered permanent magnets.

Experimental

The magnet which was primarily investigated in this study was fabricated by conventional powder metallurgical processing technique, using a powder which was prepared by the calciothermic Co-reduction process [29]. The composition of the alloy was close to $Nd_{15}Fe_{76}B_8Al_1$. After pulverization using jet milling the pressed compact was sintered at 1070°C and then heated at 620°C. The studied magnet was in peak aged condition and the magnetic properties are as follows: *Br*=12.1 kG, *iHc*=13.6 kOe, $(B.H)_{max}$=34.8 MGOe and squareness=95.1.
The hysteresis curve (fig.1) clearly shows a slight kink in the demagnetising curves. In addition to this magnet material we also studied commercial grade Nd-Fe-B sintered magnets with intrinsic coercivities in the range between 8 and 12 kOe for the presence of iron precipitation.

The specimens were thinned for TEM by electropolishing using a 17% perchloric acid / 83% methanol electrolyte. Ion milling was used only for cleaning the surfaces from contamination. Scanning transmission electron microscope (STEM) X-ray microanalysis was performed on a JEOL 200 CX analytical microscope equipped with a LaB_6 filament and an EDAX high take off angle energy dispersive X-ray analyzer. A beryllium double tilt specimen stage was used to reduce background intensities.

Results and Discussion

The analytical electron microscope investigation of Nd-Fe-B based magnets revealed in all of the peak aged sintered magnets the same multiphase microstructure with three categories of phases [4,5]. Beside the hard-magnetic $Nd_2Fe_{14}B$ boride phase (A) also grains with a composition $Nd_{(1+\epsilon)}Fe_4B_4$ - phase (B) and Nd-rich phases (C) preferentially at grain boundary junctions and extending to grain boundaries were detected. Grain size and grain size distribution are important criteria for the intrinsic coercivity of the final magnet.

The presence of Fe-rich precipitates was first detected in Nb-containing Nd15-Fe77-B8 magnets. The microstructure of such magnets was found to be similar to that of the ternary magnets, but with the addition of two Nb containing phases which we found inside grains of the hard magnetic phase [28]. The larger precipitates were identified by electron diffraction and X-ray microanalysis as Laves phase $NbFe_2$.

Taking into account the nominal composition Nd15-Fe77-B8 and considering the values of the volume fractions of phases (A), (B) and (C) [4], it is evident that in sintered magnets Fe-rich phases or pure iron precipitates have to be formed, which is also in agreement with Mössbauer measurements of sintered Nd-Fe-B magnets [30]. Special care has to be taken in order to study the iron precipitation. Sample preparation, especially long ion-milling and extended electron bombardment under observation in the microscope may cause the formation of hex. Nd_2O_3 and iron-rich regions within the 2:14:1-grains [25].

0018-9464/88/0300-1951$01.00©1988 IEEE

In order to detect iron precipitates we started with a magnet material showing a slight kink in the demagnetizing curve (fig.1). This is an evidence for a high

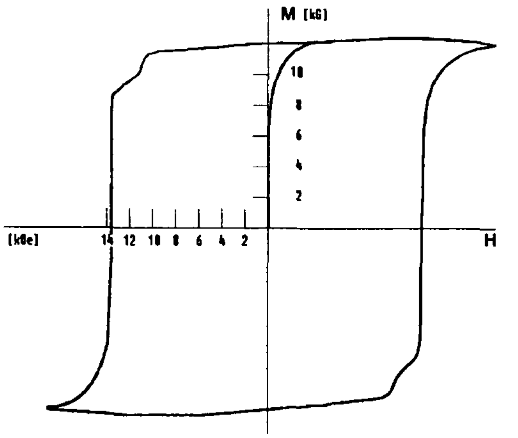


Fig.1: Hysteresis curve of a sintered Nd-Fe-B magnet containing softmagnetic iron precipitates .

density of softmagnetic nucleation sites for reversed domains occuring in the magnet. Meanwhile we also detect iron precipitation in commercial grade Nd-Fe-B sintered magnets. Three different forms of α-iron precipitation in sintered Nd-Fe-B magnets were observed. First, we detected separated α-iron regions outside of 2:14:1-grains with diameters less than 1 μm, as shown in fig.2. The electron

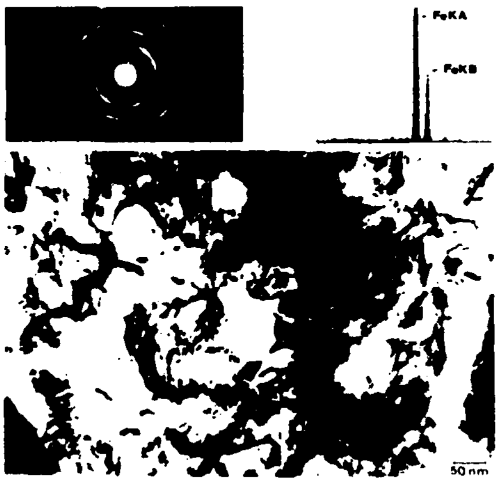


Fig.2: Transmission electron micrographs and associated X-ray spectrum showing a bright field image and diffraction pattern of an iron precipitate outside of hardmagnetic grains.

diffraction image shows a b.c.c. ring pattern with some degree of texture. In the corresponding X-ray spectrum only FeKA and FeKB peaks are visible. The interior of this iron phase is heavily faulted and contains a high density of dislocations. Second, iron precipitation is found within individual 2:14:1-grains. The bright field (fig.3a) and dark field (fig.3c) electron micrographs of such a grain show precipitates with diameters up to 10 nm. The electron diffraction pattern (fig.3b) shows overlapping diffraction spots of the hardmagnetic phase and the b.c.c. ring pattern of the precipitates. In the dark field image (fig.3c), taken with the [011]-reflexion of the iron phase, the precipitates are

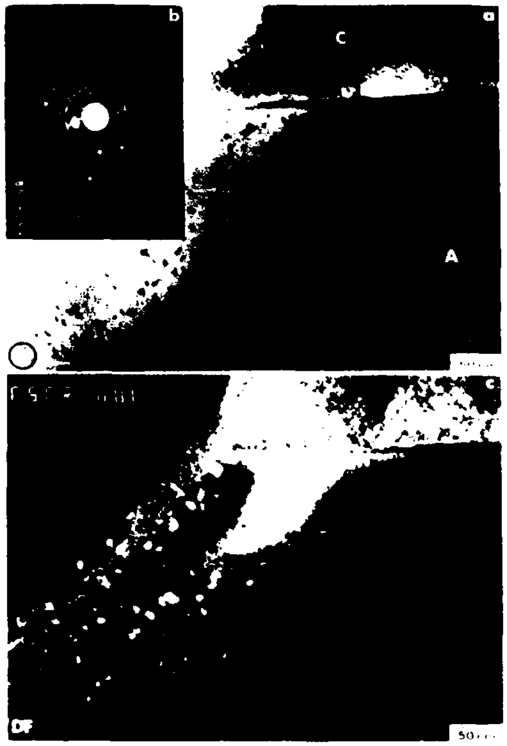


Fig.3: Bright (a) and dark (c) field electron micrographs showing α-iron precipitates within a hardmagnetic 2:14:1-grain.

bright. Besides the hardmagnetic grain A also a neighbouring Nd-rich grain C is visible in fig.3. Third, we found individual 2:14:1-grains with a high density of iron precipitation, as shown in fig.4. In the two-beam case at the exact Bragg condition a very strong contrast of these precipitates is observed. The reason for that are probably the homogeneous deformation strains of the misfitting precipitates. The exact nature of this type of precipitation is not yet clear and is still under investigation.

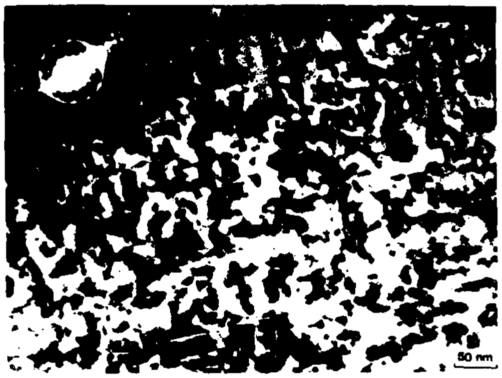


Fig.4: Transmission electron micrograph showing a high density of α-iron precipitation within a hardmagnetic 2:14:1-grain.

In order to achieve high intrinsic coercivities a *high magnetocrystalline anisotropy* is necessary but not sufficient. In fact, metallurgical parameters, such as distribution of phases, chemical composition and crystal structures of phases and processing parameters, such as alloy preparation, size and shape of particles, sintering and annealing treatments, determine the value of the corcive force of each individual sintered Nd-Fe-B magnet. In any case the formation of soft magnetic precipitates and inclusions should be avoided. Kinks in the demagnetization curve are the evidence for softmagnetic nucleation centres for reversed magnetic domains. We found by experiments that such kinks of the demagnetization curve can be avoided in a twofold way. Either by increasing the neodymium content of the starting alloy or by decreasing the temperature of the final post-sintering heat treatment. Without the detailed knowledge of the quaternary phase diagram Nd-Fe-B-O the quantitative explanation for our experimental results, i.e. the mechanism for the iron precipitation cannot be given.

Acknowledgements

This work was partly sponsored by the US Army European Research Office, London, UK under contract No.DAJA-86-C-0010 and by the Austrian Nationalbank under contract No.3065.

References

[1] M. Sagawa, S.Fujimura, H. Yamamoto, Y. Matsuura and K. Hiraga, IEEE Trans.Magn., Vol.MAG-20, p.1584, 1984.
[2] H. Kronmüller, K.D. Durst and G. Martinek, in press.
[3] K.D. Durst and H. Kronmüller, in press.
[4] J. Fidler, IEEE Trans.Magn., Vol.MAG-21, p.1955, 1985.
[5] J. Fidler, IEEE Trans.Magn., Sept. 1987, in press.
[6] R K. Mishra, J.Magn.Magn.Mat., Vol.54-57, p.450, 1986.
[7] Y.L. Chen, IEEE Trans.Magn., Vol.MAG-21, p.1967, 1985.
[8] T.S. Chin, Y.Hara, E.J. Lavernia, R.C. O'Handley and N.J. Grant, J.Appl.Phys., Vol.59, p.1297, 1986.
[9] J.Fidler and P. Skalicky, Mikrochimica Acta [Wien], Vol.Suppl.12, 1987, in press.
[10] N.A. El-Masry and H.H. Stadelmaier, Mat.Letters,Vol.3,p.405,1985.
[11] G.C. Hadjipanayis, K.R. Lawless and R.C. Dickerson, J.Appl.Phys., Vol.57, p.4097, 1985.
[12] G.C. Hadjipanayis, Y.F. Tao and K.R. Lawless, IEEE Trans. Magn., Vol. MAG-22, p.1845, 1986.
[13] K. Hiraga, M.Hirabayashi, M.Sagawa and Y. Matsuura, Jap. J.Appl.Phys., Vol.24, p.L30, 1985.
[14] K. Hiraga, M.Hirabayashi, M.Sagawa and Y. Matsuura, Jap. J.Appl.Phys., Vol.24, p.699, 1985.
[15] J.D. Livingston, J.Appl.Phys., Vol.57, p.4137, 1985.
[16] Y. Luo, N. Zhang and G.D. Graham, in press.
[17] Y. Matsuura, S. Hirosawa, H. Yamamoto, S. Fujimura, M. Sagawa, and K. Osamura, Jap.J.Appl.Phys., Vol.24, p.L635, 1985.
[18] R.K. Mishra, J.K. Chen and G. Thomas, J.Appl.Phys., Vol.59, p.2244, 1986.
[19] R.K. Mishra and R.W. Lee, Appl.Phys.Lett., Vol.48, p.733, 1986.
[20] T. Mizoguchi, I. Sakai, H. Niu and K. Inomata, IEEE Trans.Magn., Vol.22, p.919, 1986.
[21] R. Ramesh, K.M. Krishnan, E. Goo, G. Thomas, M. Okada and M. Homma, J.Magn.Magn.Mat., Vol.54-57, p.363, 1986.
[23] T. Suzuki, K. Hiraga and M. Sagawa, Jap.J.Appl.Phys., Vol.23, p.L421, 1984.
[24] T. Suzuki and K. Hiraga, J.Magn.Magn.Mat., Vol.54-57, p.527, 1986.
[25] P. Schrey, IEEE Trans.Magn., Vol.MAG-22, p.913, 1986.
[26] M.Tokunaga, M.Tobise, N.Meguro and H. Harada, IEEE Trans.Magn., Vol.MAG-22, p.904, 1986.
[27] J.Fidler, P. Skalicky and F. Rothwarf, Mikrochimica Acta [Wien], Vol.Suppl.11, p.371, 1985.
[28] S.H.F. Parker, P. Grundy and J. Fidler, J.Magn.Magn.Mat., Vol.66, p.74, 1987.
[29] C.Herget, Proc. 8th Int. Workshop on Rare Earth Magnets and their Applications, ed. by K.Strnat (University of Dayton, Dayton),1985, p.407.
[30] G. Wiesinger, private communication.

Proceedings IX. European Congress on Electron Microscopy (EUREM)
York, England, September. 1988, in print.

27

Electron microscopy in the development of new magnetic materials

Josef Fidler

Institute of Applied Physics, Technical University Vienna,
Wiedner Hauptstr. 8-10, A-1040 Vienna, Austria.

ABSTRACT: Electron microscopic techniques including the observation of magnetic domains have become more important for the characterization of soft and hard magnetic materials in both, university and manufacturer laboratories. For the development of new magnetic materials the knowledge of the interaction between the magnetic domain structure and the microstructure is important for a better understanding of the magnetic properties. In newly developed permanent magnets with outstanding hard magnetic properties microstructural parameters limit the coercivity of the magnet material.

1. INTRODUCTION

A ferro- or ferrimagnetic body consists of uniformly magnetized regions, i.e. the magnetic domains. The magnetic domains are separated from each other by magnetic domain walls. Micromagnetic models revealed different types of magnetic domain walls (Hubert 1974). New transmission electron microscopic techniques were developed in order to study the magnetization distribution and the domain wall character in detail and the existence of asymmetric domain walls was proved (Zepper and Hubert 1976). Using these techniques, the character and thickness of a domain wall can accurately be determined. The size and shape of the magnetic domains are determined by the total free energy (magnetic stray field energy plus domain wall energy) and depend on the magnetic properties (magnetization, magnetocrystalline anisotropy and magnetostriction) and on the geometry of the magnet. The mobility of domain walls in an external magnetic field determines the shape of the magnetic hysteresis curve. The intrinsic coercive force iHc, which is a characteristic parameter of the hysteresis curve, strongly depends on the interaction force between domain walls and the microstructure of the material. In order to improve the magnetic properties of soft magnetic materials with a low coercive force and of hard magnetic materials with a high coercive force investigations of the microstructure and the domain structure are necessary.

Electron microscopy is widely being used to study and characterize magnetic materials in both, university and manufacturer laboratories. This paper is intended to be a brief, general introduction in this field. Numerous articles on this topic have been published in international journals and conference proceedings within the last years. In summary, the typical applications of electron microscopy in the field of the development of new magnetic materials are divided into three categories:

(a) Soft magnetic materials:
    amorphous iron-rich materials
(b) Magnetic information-storage materials:
    magnetic particles (α-Fe_2O_3, CrO_2, metallic),
    recording disc - materials (Co-P, Co-Ni, Co-Cr, Rare Earth-Co/Fe),
    magnetooptic and bubble domain materials (amorphous Rare Earth-Co/Fe, garnets, ortho- and hexaferrites)
(c) "Supermagnets":
    Rare Earth (RE) - Co/Fe

The purpose of this paper is to briefly discuss the different electron microscopic techniques to study magnetic materials and to show, as an example, transmission electron microscopic results on new hard magnetic "supermagnets", since in the light of the historical development of hard magnetic materials the improvement of the coercivity is closely related with a better microstructural understanding of the mechanisms leading to higher coercive forces.

2. ELECTRON MICROSCOPIC METHODS TO STUDY MAGNETIC MATERIALS

The oldest and most commonly used techniques for magnetic domain observation are the light optical techniques. The lack of the poor spatial resolution leads to the application of electron optical techniques for domain and microstructural investigation. The different microscopic techniques for microstructural and magnetic domain observation are listed in Table 1. The electron optical methods (Lorentz electron microscopy) for domain observation are based on the fact that electrons are deflected because of the Lorentz-force of the magnetic strayfield outside the specimen or the magnetization inside the domains (Grundy and Tebble 1968, Jakubovics 1964). Two types of techniques are distinguished in the case of conventional scanning electron microscopy. The magnetic contrast is pro-

Table 1: Comparison of microscopic techniques used for microstructural and magnetic domain investigations of magnetic materials

METHODS	*MICROSTRUCTURE*	*MAGNETIC DOMAINS*
Light optical microscope (LOM)	Grain boundaries Large precipitates and inclusions	Bitter technique Kerr technique Faraday technique
Scanning electron microscope (SEM)	Grain boundaries Precipitates X-ray microanalysis	Strayfield technique (type 1) Tilted [illegible] Electron polarization techn.
Scanning transmission electron microscope (STEM)	Defect analysis Precipitates X-ray microanalysis	Double or quadrant detector technique
Convent. transmission electron microscope (CTEM)	Defect analysis Precipitates X-ray microanalysis	Fresnel technique Foucault technique Holographic interference techn.
Field ion microscope (FIM) Atom probe analysis (AP)	Phase analysis	

duced whether by external stray fields (Type 1) or by internal magnetic induction (Type 2). These techniques are widely used to study the surface domain structures of magnetic recording materials and soft magnetic materials (Jones 1987).

Differential phase contrast together with STEM is a new method for domain observation (Chapman et al 1978, Tsuno and Inoue 1984). The advantage of this method, where double or quadrant detectors are used, is the possibility to study the domain wall thickness very accurately. An advantage of conventional TEM is to identify crystal lattice defects or small precipitates and the magnetic domain structure simultaneously. The magnetic contrast is produced whether by defocussing (Fresnel technique) or by shifting the objective aperture diaphragm (Foucault technique) (Grundy and Tebble 1968). Examples for the interaction between crystal lattice defects and precipitates, respectively, and magnetic domain walls are shown in Figure 1a. The defocussed micrograph shows besides dislocations, stacking faults and grain boundaries the pinning of magnetic momain walls (marked by arrows) at microtwin-boundaries in a Mn-Al-C permanent magnet material, which was produced by an extrusion process. The interaction force and the density of such pinning centres for magnetic domain walls determine the coercive force. Maximum interaction between domain walls and precipitates occur, when domain wall thickness and diameter of precipitates are comparable Taylor 1980a). Crystallization centres in amorphous, soft magnetic alloys deteriorate the magnetic properties. Such an interaction in a partly crystallized Fe-Ni-B ribbon is shown in Figure 1b. The crystallization and the change of the magnetic domain structure was studied in-situ by heating the specimen within the electron microscope (Fidler and Skalicky 1981).

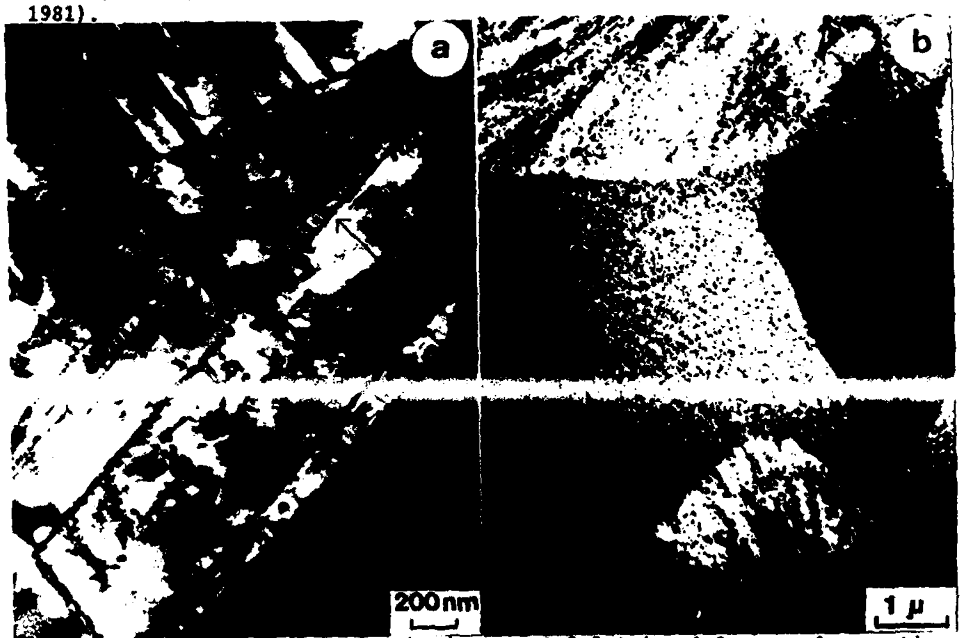


Fig. 1. Electron micrographs showing crystal lattice defects and magnetic domain walls (marked by arrows) in an Mn-Al-C magnet (a) and in a partly cryrtallized, amorphous Fe-Ni-B ribbon (b).

Special care has to be taken in order to study the magnetic domain struc-

ture under controlled conditions, and the specimen has to be shielded from the high magnetic field of the objectiv pole piece. In top-entry goniometer stages the specimen must be withdrawn to a position of a low magnetic field (Valdre 1964, Taylor 1980b), and in side-entry stages shielded objective pole pieces have to be used (Tsuno 1983). The electron optical techniques for domain investigation, described so far, can be performed on conventional electron microscopes after being adapted for domain observation. Such optional attachments are commercially available from electron microscope manufacturers. Other electron optical techniques need a more expensive and intricate instrumentation. Holographic interference electron microscopy, together with a field emmission gun, have been used for magnetic domain investigation (Tonomura et al 1980). Lines according to the direction of magnetization are directly observed as contour fringes which overlap individual bright field micrographs. The recent development of scanning electron microscopy with polarization analysis (SEMPA) has made the direct observation of magnetic structures with submicron spatial resolution possible (Koike and Hayakawa 1985, Unguris et al 1986). Other microanalytical techniques based on field ion microscopy and atom probe analysis have recently been used and were reported to analyze the different phases of permanent magnetic materials, such as AlNiCo-, FeCrCo- and RE-cobalt/iron - magnets (Hütten and Haasen 1986, Hetherington et al 1986, Zhu et al 1986).

3. ELECTRON MICROSCOPY OF NEW "SUPERMAGNETS"

The outstanding hardmagnetic properties of permanent magnets based on RE-Co/Fe are controlled by the magnetocrystalline anisotropy of the hard magnetic phase and by metallurgical factors, such as the chemical composition, crystal structure and distribution of phases. Besides other ana-

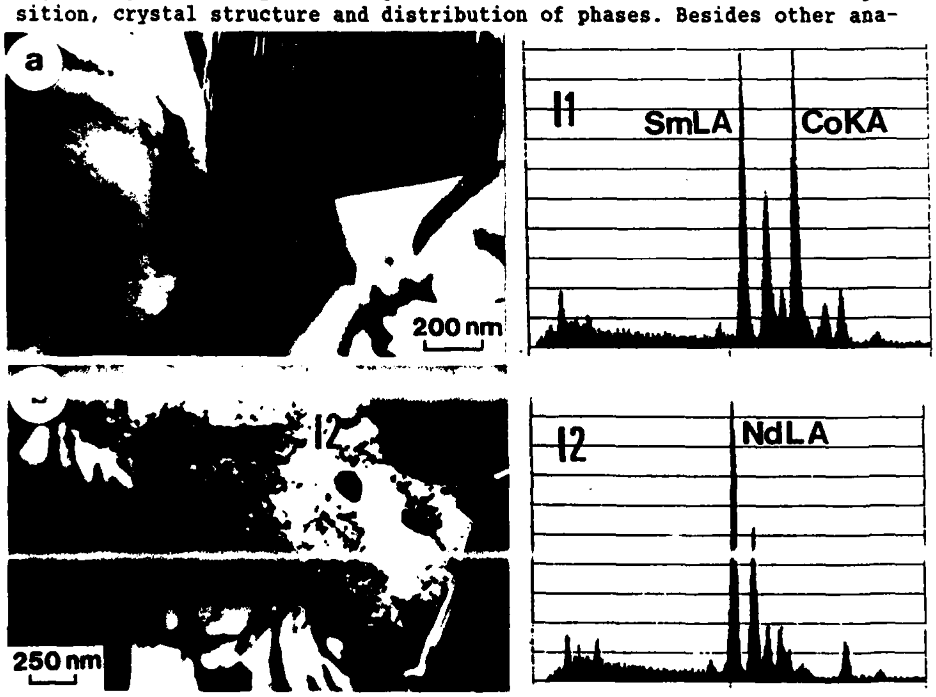


Fig. 2. In sintered SmCo 1:5 (a) and Nd-Fe-B (b) magnets rare earth rich inclusions are found which deteriorate the coercivty.

lytical techniques, such as chemical analysis, magnetic measurements, X-ray analysis and X-ray diffraction, electron microscopy is increasingly used to characterize such materials after different steps of processing (i.e sintering, annealing). Commercially available RE-Co/FE permanent magnet materials can be divided into three groups. SmCo 1:5, SmCo 2:17 and Nd-Fe-B magnets and are produced by a powder metallurgical process with complicated post-sintering heat tratment procedures. The ideal microstructure if SmCo 1:5 and Nd-Fe-B magnets, in which the coercivity is controlled by the nucleation field for reversed magnetic domains, consists of aligned single-domain $SmCo_5$- and $Nd_2Fe_{14}B$-grains , respectively. In fact, analytical electron microscopy shows inclusions and precipitates of other phases, which deteriorate the magnetic hardness (Figure 2)(Fidler 1982,1985). The distribution of these RE-rich phases, which are magnetic in the case of SmCo 1:5 and non magnetic in the case of Nd-Fe-B, determine the coercivity of the magnet material. The coercivity of SmCo 2:17 magnets is controlled by the pinning field of magnetic domain walls at a continuous, cellular precipitation structure (Figure 3a) (Fidler et al 1983, Hadjipanayis 1984, Livingston 1978, Mishra et al 1981, Rabenberg et al 1982). In high coercivity magnets (iHc > 1000 kA/m) the microstructure consists of three phases, the cell interior phase A, the cell boundary phase B and the platelet phase C, whereby the optimum cell size for highest coercivity is in the order of 100 to 200 nm. In contrast to this no platelet phase is found in low coercivity magnets (iHc < 800 kA/m) and high resolution electron microscopy and electron diffraction patterns show a high density of microtwins within the cell interior phase A and an increased value of the c/a-ratio, respectively (Figure 3b).

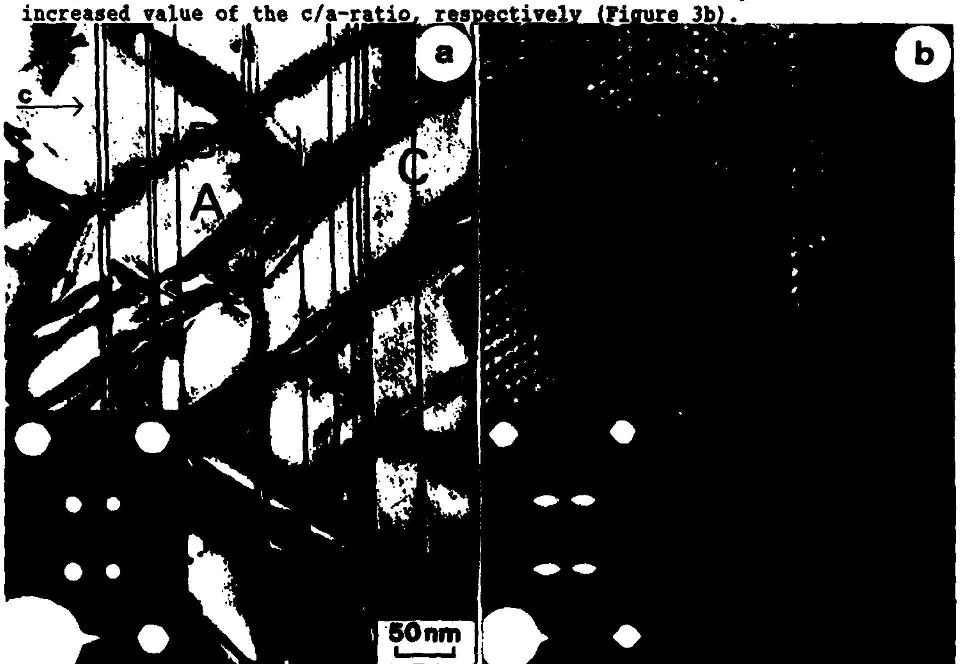


Fig. 3. Electron micrographs showing the cellular precipitation structure of precipitation hardened SmCo 2:17 magnets (a). In low coercivity magnets a high density of microtwins is found within the cell interior phase (b).

The Foucault micrograph of Figure 4 shows that the cellular precipitation structure acts as attractive pinning centre for the magnetic domain walls during the magnetization reversal.



Fig. 4. Magnetic domain wall pinning at the continuous precipitation structure in SmCo 2:17 sintered magnets.

Acknowledgements

I would like to thank Prof. Skalicky for advice and valuable discussion. This work was partly sponsored by the the Austrian Nationalbank (Pr.No. 3065), the Austrian Forschungsfonds FWF (Pr.No.P6935P) and the US Army European Research Office, London, UK, under contract No. DAJA-86-C-0010.

Chapman J N, Batson P E, Waddell E M and Ferrier R P 1978 Ultramicroscopy 3 203
Fidler J 1982 Phil.Mag. B46 565
Fidler J 1985 IEEE Trans.Magn. MAG-21 1955
Fidler J and Skalicky P 1981 Appl.Phys.Lett. 39 573
Fidler J, Skalicky P and Rothwarf F 1983 IEEE Trans.Magn. MAG-19 2725
Grundy P J and Tebble R S 1968 Advances in Physics 17 153
Hadjipanayis G C 1984 J.Applied Physics 55 2091
Hetherington M G, Smith G D W and Jakubovics J P 1986 Metallurgical Transactions A 17A 1629
Hubert A 1974 Theorie der Domänenwände in geordneten Medien (Berlin: Springer Verlag)
Hütten A and Haasen P 1986 J.de Physique 1986 C7 205
Jakubovics J P 1964 Phil. Mag. 10 277
Jones G A 1978 J.Magn.Magn.Mat. 8 263
Koike K and Hayakawa 1985 J.Appl.Phys. 57 4244
Livingston J D 1978 IEEE Trans.Magn. MAG-14 668
Mishra R K, Thomas G, Yoneyama T, Fukuno A and Ojima T, 1981 J.Appl. Phys. 52 2517
Rabenberg L, Mishra R K and Thomas G 1982 J.Appl.Physics 53 2389
Taylor R A 1980a J.Magn.Magn.Mat. 15-18 1173
Taylor R A 1980b Electron Microscopy 4 38
Tonomura A, Matsuda T, Endo J, Arii T and Mihama K 1980 Phys.Rev.Lett. 44 1430
Tsuno K and Taoka T 1983 Jap.J.Applied Physics 22 1041
Tsuno K and M Inoue 1984 Optik 4 363
Unguris J, Hembree G G, Celotta R J and Pierce D T 1986 J.Magn.Magn.Mat. 54 1629
Valdre U 1964 J.Sci.Instrum. 41 327
Zepper L and Hubert A 1976 J.Magn.Magn.Mat. 2 18
Zhu F, Haasen P and Wagner R 1986 Acta Metall. 34 457

28 57

Analytical TEM study of Al-doped, "two-phase" Nd–Fe–B sintered magnets

J. Fidler
Institut für Angewandte Physik, T. U. Wien, Wiedner Hauptstr. 8-10, A-1040 Wien, Austria

K. G. Knoch, H. Kronmüller, and G. Schneider
Max-Planck-Institut für Metallforschung, Heisenbergstr. 1, D-7000 Stuttgart 80, Federal Republic of Germany

(Received 21 December 1988; accepted 3 March 1989)

The microstructure and the coercivity of sintered $Nd_{20}Fe_{(73.5-x)}B_{6.5}Al_x$ ($x = 0, 2.5$) permanent magnets are influenced by the Al concentration. In Al-containing magnets we found a homogeneous distribution of Al in the hard magnetic phase and the occurrence of an intergranular $Nd(Fe, Al)_2$ phase between the hard magnetic grains. Our analytical TEM study revealed that in "Al_2O_3-doped" magnets the crystal structure of the Nd-rich intergranular phase partly changes from fcc ($a = 0.52$ nm) to hcp ($a = 0.39$ nm, $c = 0.61$ nm), whereas the content of iron simultaneously decreases from 5–10 at.% to 1.5–4 at.%. A platelet-shaped phase, embedded in the Nd-rich intergranular phase, was determined as a $Nd_5Fe_2(B, O)_x$ phase. The influence of the microstructure on the coercivity in Al-doped magnets is discussed.

I. INTRODUCTION

The high magnetocrystalline anisotropy of the $Nd_2Fe_{14}B$ phase primarily determines the intrinsic coercivity of this new class of permanent magnets. It is generally agreed that the nucleation hardening mechanism is effective in sintered magnets.[1,2] The formulae describing the coercivity of sintered magnets in general contain micromagnetic parameters, which, however, have not been related quantitatively to special microstructures so far. In fact, microstructural parameters (distribution of phases, chemical composition and crystal structures of phases, grain size distribution) and processing parameters (alloy preparation, size and shape of grains, alignment of grains, sintering and annealing treatments) determine the value of the coercive field of sintered magnets. $Nd_2Fe_{14}B$ based permanent magnets exhibit a complex, multiphase microstructure. Optical metallography, microprobe analysis, and transmission electron microscopy (TEM) together with x-ray microanalysis have been used widely to identify this multiphase microstructure.[3–23] In accordance with the ternary phase diagram of Nd–Fe–B,[24] three types of phase are found in $Nd_{15}Fe_{77}B_8$ sintered magnets, the hard magnetic $Nd_2Fe_{14}B$ phase (ϕ), the boride $Nd_{(1+\epsilon)}Fe_4B_4$ phase ($\cap$), and the intergranular Nd-rich phase (n). Analytical electron microscopic investigations have shown that several Nd-rich phases with different Nd/Fe ratios are found preferentially at grain boundary junctions and extending along grain boundaries in sintered magnets.[18,22] It is fairly well known that the coercivity of Nd–Fe–B magnets is increased by the addition of small amounts of Al, Nb, Mg, Zr, Ga, and other refractory elements either to the prealloy or before sintering. The reason for the significant increase of the coercivity (up to 30%) is attributed to microstructural effects, since the magnetocrystalline anisotropy decreases slightly.[25–27] In the so-called "two-phase" Nd–Fe–B sintered magnets the boride phase $\cap$ is suppressed by choosing a suitable nominal composition of the magnet[24] in order to decrease the high volume fraction of the nonmagnetic phases.

The present study was undertaken to determine the influence of the Al-doping on the microstructure and coercivity of "two-phase"-$Nd_{20}Fe_{73.5}B_{6.5}$ sintered magnets. Two types of doping have been used: doping of the prealloy with Al or adding Al_2O_3 powder to the Nd–Fe–B powder before sintering. Changes of the intergranular phases have been found to affect the intrinsic coercivity. The increase of the coercivity is discussed in terms of the nucleation hardening mechanism.

II. EXPERIMENTAL PROCEDURE

The samples investigated were optimally sintered magnets (in the peak aged condition) which were prepared by the conventional powder metallurgical processing technique as described in detail by Schneider.[28] The alloys were prepared from 99.8% pure iron, 99.9% pure neodymium, and a ferro-boron master alloy Fe–18.5B wt.%. The specimens were arc melted under argon and remelted five times to ensure homogeneity. The powder processing for the magnets was done in glove boxes under a purified argon atmosphere. The ingots were crushed to a coarse powder and then ground in a vibration ball mill. To avoid particles larger than 20 μm the powder was sieved. The powder was aligned in a field of 0.5 T perpendicular to the pressing direction and was compacted with 500 MPa. The compacts were sealed in tubes of fused silica, sintered at 1060 °C for 1 h and annealed at 600 °C for 1 h. The magnetic properties were measured in a vibrating sample magnetometer.

·JMR 88-261 Fidler Galley 72 of 79* MRS/JMR 88-261 Fidler Galley 73 of 79*
4-10-89 tr, hv mem (4-18-89 cb) (4-20-89 tly) 3271 4-10-89 tr, hv mem (4-18-89 cb)

154

Three different types of sintered magnets were investigated by optical metallography and analytical TEM in order to identify the multiphase microstructure. The composition and the intrinsic coercive field H_{ic} of the investigated magnets are listed in Table I. In magnet NFB–Al 0.99 wt.% aluminum was added to the prealloy and in magnet NFB–Al_2O_3 a small amount of Al_2O_3 (1.48 wt.%) was added to the powder *before compacting*.

Thin slices were cut from the magnets parallel and perpendicular to the alignment direction. The disks for electron microscopy were mechanically ground and polished to a thickness of 100 μm and finally thinned by ion-milling. The specimens were examined in a JEOL 200 CX scanning transmission electron microscope (STEM) fitted with a LaB_6 filament, a TRACOR NORTHERN energy dispersive x-ray analyzer (EDS) of high take-off angle, and a GATAN electron energy loss spectrometer (EELS). A beryllium double tilt specimen stage was used to reduce background intensities. All x-ray spectra were analyzed using the quantitative software program for thin samples.

III. RESULTS

The characteristic multiphase microstructure of the "two phase" Nd–Fe–B sintered magnet (sample NFB) is shown in Fig. 1. Optical metallography reveals a complex microstructure of the intergranular phase in grain boundary junctions and between the bright hard magnetic grains (ϕ), with grain diameters of the order of 10–20 μm. In Fig. 1(a) two different intergranular phases (with different brightness) occur in the NFB magnet and at least three different phases are found in the Al-containing magnets [Fig. 1(b)]. The black, spherical inclusions shown in Fig. 1 are Nd_2O_3 and are found in both the ternary NFB magnet and in the Al-doped magnets.

Energy dispersive x-ray microanalysis taken in the TEM shows a difference in the Al content of the hard magnetic phase. In both the NFB-Al [Fig. 2(b)] and NFB–Al_2O_3 magnets an additional AlKA-peak is found in the x-ray spectra of the ϕ phase compared with that of the ternary NFB magnet [Fig. 2(a)].

TABLE I. Nominal composition and intrinsic coercive field H_{ic} of the investigated magnets.

Magnet	Composition (at.%) Nd	Fe	B	Al	H_{ic} (kA/m)
NFB	20	73.5	6.5	0.0	776
NFB–Al	20	71.0	6.5	2.5	1384
NFB–Al_2O_3	20	71.2	6.5	2.3	1400

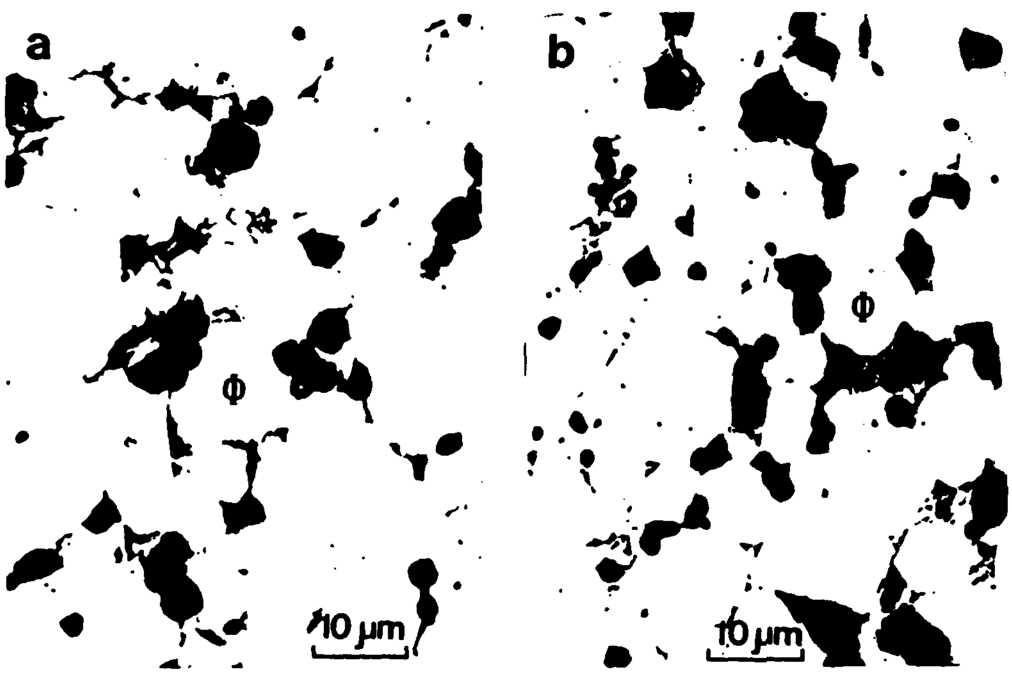


FIG. 1. Optical metallographic micrographs of (a) the NFB magnet and (b) the NFB–Al_2O_3 magnet. Differences in the intergranular phases between the hard magnetic grains ϕ are visible. In the Al_2O_3-doped magnet (b) additional phases occur.

157

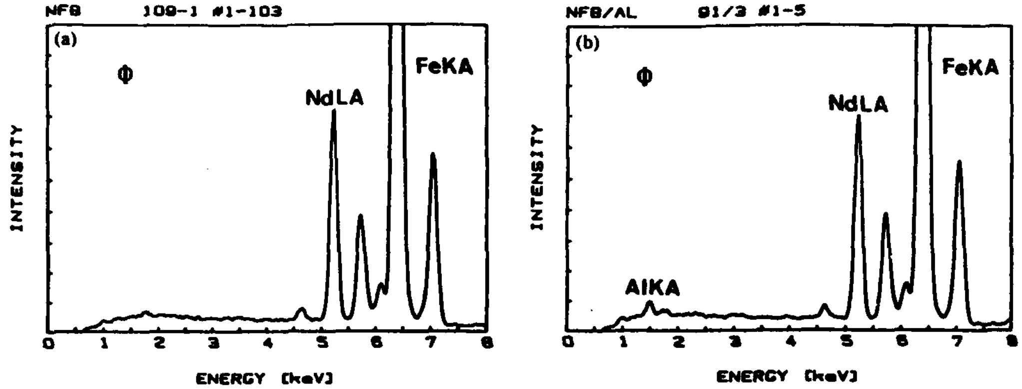


FIG. 2. Energy dispersive x-ray spectra from the hard magnetic grains ϕ of (a) the NFB magnet and (b) the NFB–Al magnet. Aluminum dissolves into the hard magnetic phase in the doped magnets NFB–Al and NFB–Al_2O_3.

Figure 3 shows a TEM micrograph of the NFB magnet. Besides the hard magnetic ϕ grain, two intergranular phases are visible. Both of them are Nd-rich. The phase (n1), with high dislocation density, exhibits the fcc crystal structure with a = 0.52 nm, whereas the crystal structure of the platelet-shaped phase (pl), with a thickness of about 0.1 μm and a length of about 1–5 μm, has not yet been unambiguously determined. In addition to these two phases, a Nd(Fe, Al)$_2$ phase (al) occurs in the Al-doped magnets, NFB–Al and NFB–Al_2O_3. A similar phase was found previously by Schrey[15] in Al-containing Nd–Fe–B sintered magnets. The Al-containing phase is mostly found embedded in the fcc Nd-rich (n1) phase, as shown in Fig 4. From the lattice fringe image of this phase a crystal lattice periodicity of about 1.2 nm was determined. The crystal structure and the crystal lattice parameters of this Al-containing phase are unknown at present. The composition of this phase is determined from the x-ray spectrum of Fig. 5 as Nd(Fe, Al)$_2$. Only in the NFB–Al_2O_3 magnet was another Nd-rich phase (n2), with the hcp crystal structure (a = 0.39 nm and c = 0.61 nm), detected by electron diffraction. The TEM micrographs of Fig. 6 and the corresponding x-ray spectra of Fig. 7 show the difference between the n1 phase (fcc) and the n2 phase (hcp). Besides



FIG. 3. Transmission electron micrograph showing a hard magnetic grain ϕ and two intergranular phases (n1 and pl) in the NFB magnet.

JMR 88-261 Fidler Galley 75 of 79*
4-10-89 tr, hv mem (4-18-89 cb)



FIG. 4. Transmission electron micrograph of the NFB–Al magnet showing the $Nd(Fe,Al)_2$ phase (a1), embedded in the Nd-rich intergranular phase n1. The lattice fringe contrast within this phase corresponds to an interplanar spacing of about 1.2 nm.

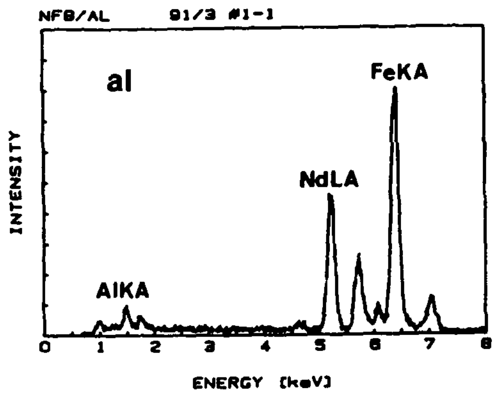


FIG. 5. Energy dispersive x-ray spectrum from the $Nd(Fe,Al)_2$ phase (al) of the NFB–Al magnet.

the highly faulted n1 phase the n2 phase, with only individual dislocations within its interior, is visible in Figs. 6(a) and (b), respectively. Figure 7 reveals a remarkable difference of the x-ray spectra. Phase n1 always shows a higher Fe content (>4.5 at.%) than phase n2 (<4.5 at.%). It should be noted that our investigations never revealed any Al enrichment of the Nd-rich phases n1 and n2. This result is in contrast with previously reported data, which showed a partial enrichment of Al in the Nd-rich intergranular phase.[15,20]

The platelet-shaped phase (pl) (Fig. 8) is detected in the ternary NFB magnet as well as in the NFB–Al and NFB–Al_2O_3 magnets. According to x-ray microanalysis (Fig. 9), no Al content was found in the platelets and the ratio between Nd:Fe (in at.%) was determined to be 2.5:1. In order to determine the light element content (B or O) of this phase EELS investigations were carried out. Preliminary results of this study show that the platelet phase has a composition of about $Nd_5Fe_2(B,O)_x$.[29] Binary Nd_2O_3 inclusions are randomly spread throughout the hard magnetic grains and intergranular grains (Fig. 1). Figure 10 shows a TEM micrograph of such a polycrystalline, hexagonal Nd_2O_3-inclusion (a = 0.38 nm, c = 0.60 nm) with a diameter of 350 nm within the hard magnetic phase ϕ. Nd_2O_3-inclusions are found with diameters between 20 and 500 nm.

IV. DISCUSSION AND CONCLUSIONS

In $Nd_2Fe_{14}B$ based sintered magnets the intrinsic coercivity is controlled by the nucleation of reversed magnetic domains during the magnetization reversal process. In general, in this case the coercive field is given[1] by:

$$H_c = \alpha \cdot \frac{2 \cdot K_1}{M_s} - N_{eff} \cdot M_s ,$$

with

$$\alpha = \alpha_K^{nuc} \cdot \alpha_\phi .$$

Here K_1 is the first anisotropy constant, M_s is the spontaneous magnetization, and N_{eff} denotes an effective demagnetization factor depending on the morphology and the microstructure of ϕ grains and intergranular phases. The





FIG. 6. Transmission electron micrographs of the NFB–Al_2O_3 magnet, showing two Nd-rich intergranular phases n1 and n2. The crystal structure of phase n1 is fcc and that of phase n2 is hcp. Different dislocation densities are observed in phases n1 and n2.

microstructural parameter α is divided into α_K^{nuc}, which describes the effect of the inhomogeneity of the magnetocrystalline anisotropy on the nucleation field and α_ϕ, which describes the magnetic decoupling and misalignment of ϕ grains.

Previous TEM studies[22] showed that two types of grain boundaries occur in Nd–Fe–B sintered magnets: grain boundaries composed of nonmagnetic Nd-rich phases and grain boundaries without any intergranular phases. The TEM results of this study have shown that new phases occur in Nd–Fe–B:(Al; Al_2O_3) sintered magnets in the intergranular region between hard magnetic ϕ grains. Within the $Nd_2Fe_{14}B$ grains Al is completely dissolved and no precipitation of Al-containing phases was found. Table II summarizes the composition (in at.%) of the various phases found in the NFB, NFB–Al, and NFB–Al_2O_3 magnets. Since light element analysis was not possible in our EDS analysis, boron and oxygen are not considered in

158

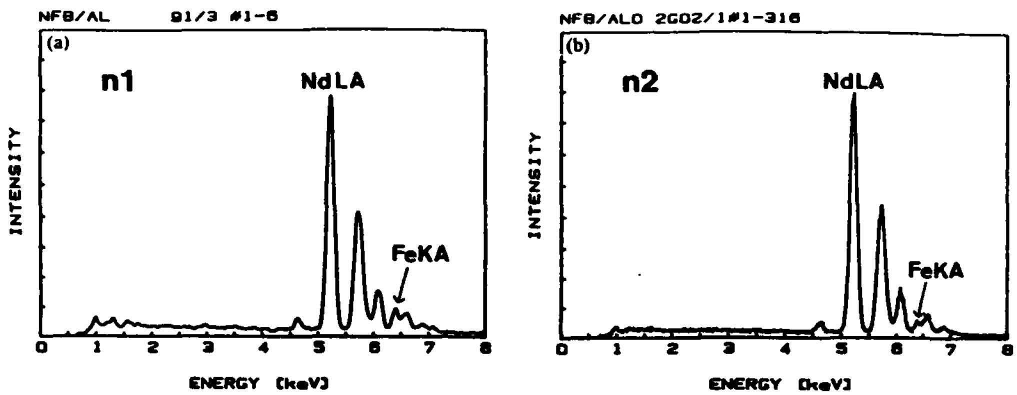


FIG. 7. Energy dispersive x-ray spectra from the Nd-rich intergranular phases n1 and n2 of (a) the NFB–Al magnet and (b) the NFB–Al_2O_3 magnet, respectively. Different Fe content is observed in the spectra of phases n1 (a) and n2 (b). No Al peak is observed in either phase.

TABLE II. Composition (in at.%) determined by EDS x-ray microanalysis of the hard magnetic phase (φ), the Nd-rich phases (n1) and (n2), the platelet phase (pl), the $Nd(Fe,Al)_2$ phase (al), and the Nd_2O_3 inclusions, found in the NFB, NFB–Al, and NFB–Al_2O_3 magnets. (Light elements such as boron and oxygen are not considered.)

Magnet	φ (at.%)	n1 (fcc) (at.%)	n2 (hcp) (at.%)	pl (at.%)	al (at.%)	Nd_2O_3 (at.%)
NFB						
Nd	13.6	94.5–95.9	···	73.7	···	93.5–94.0
Fe	86.4	4.1– 5.5	···	26.3	···	6.0– 6.5
NFB–Al						
Nd	12.8–13.9	90.4–93.2	···	64.9	29.5–39.5	92.7
Fe	83.7–84.0	6.8– 9.6	···	35.1	51.9–63.6	7.3
Al	1.6– 2.6	···	···	···	5.2– 7.9	···
NFB–Al_2O_3						
Nd	13.1–13.6	90.3–94.8	95.5–98.5	67.2–67.6	31.0–31.5	94.9–95.3
Fe	84.3–84.4	5.2– 9.7	1.5– 4.5	32.4–32.8	58.1–59.5	4.7– 5.1
Al	2.0– 2.6	···	···	···	5.9– 8.5	···

TABLE III. Comparison of the crystal structure, crystal lattice parameters, and the stability range of metallic lanthanum and neodymium. Values taken from K. A. Gschneidner.[32]

Crystal structure	La (nm)		Nd (nm)	
dhcp	α–La $a = 0.377$ $c = 1.216$	<310 °C	α–Nd $a = 0.366$ $c = 1.180$	<860 °C
hcp			α′–Nd $a = 0.39$ $c = 0.61$	(a)
fcc	β–La $a = 0.530$	310–860 °C	β′–Nd $a = 0.52$	(a)
bcc	γ–La $a = 0.426$	>860 °C	β–Nd $a = 0.413$	>860 °C

(a) found by electron diffraction in Nd–Fe–B magnets.

Table II. In the NFB–Al magnet the $Nd(Fe,Al)_2$-phase is observed besides the Nd-rich phase (n1) as additional intergranular phase. In accordance with our result, this phase was recently detected as a stable phase in the ternary system Fe–Al–Nd by Grieb *et al.*[30] In the NFB–Al_2O_3 magnet a Nd-rich phase without any Al and with the hcp crystal structure was identified in addition to the phases (n1), (al), and (pl). Table III compares the crystal structure, crystal lattice parameters, and the stability range of metallic La and Nd. In $Nd_2Fe_{14}B$ sintered magnets both Nd-rich phases, the one with fcc and the one with hcp crystal structure, have so far been identified.[6,11] The metastable (n1) phase is probably stabilized by additional elements. Auger electron spectroscopy of *in situ* fractured surfaces and EDS x-ray microanalysis taken with an ultrathin window detector[19] revealed an oxygen pick-up by this phase. Our systematic investigations show that besides

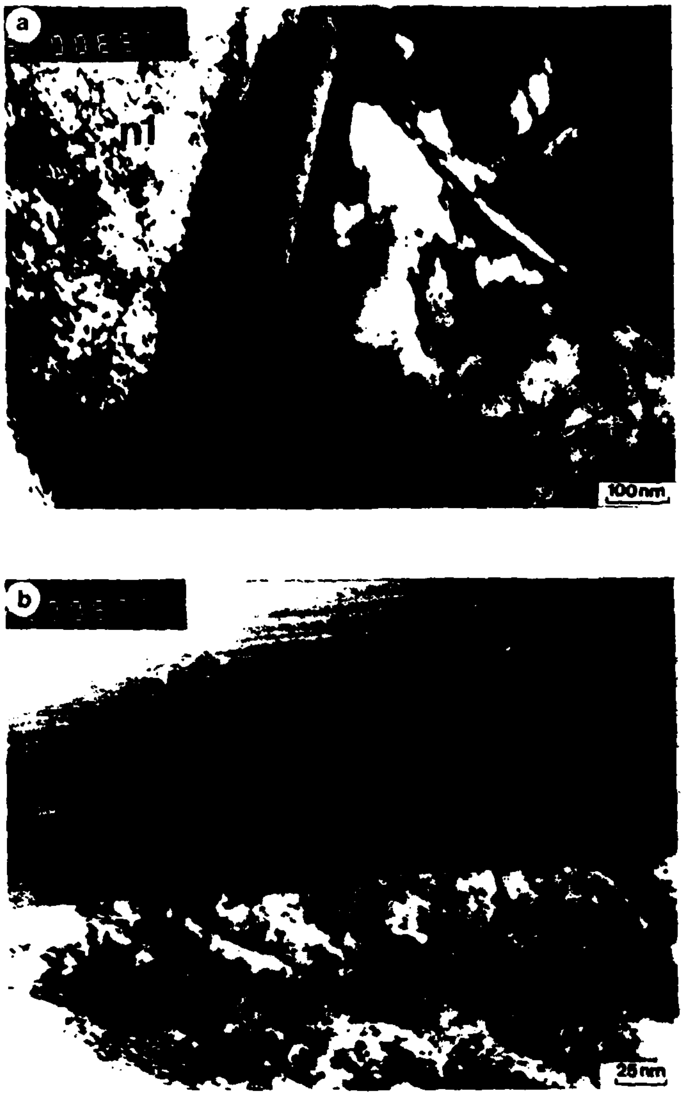
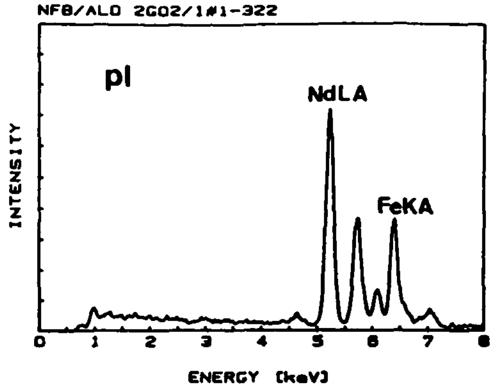


FIG. 8. Transmission electron micrographs of the platelet-shaped phase (pl) embedded in the intergranular phases n1 and n2 in the NFB–Al_2O_3 magnet (a). The platelets exhibit a high density of planar defects along their length (b).

oxygen, a small amount of Fe also must be considered as a stabilizing factor. With decreasing Fe content (<5 at.%) the Nd-rich phase changes from the fcc to the hcp crystal structure.

The increase of the coercive field of the doped magnets $Nd_2Fe_{14}B$:(Al, Al_2O_3) is attributed to the presence of $Nd(Fe, Al)_2$ and hcp Nd-rich phases, because no change of the morphology and microstructure of the fcc Nd-rich phase (n1) is observed (no Al content). For the explanation of the increased coercivity two effects are essential: First, there is a better *wettability* of these phases compared to the fcc Nd-rich phase[11]; thus the volume fraction of grain boundaries containing an intergranular phase is increased, which leads to a large magnetic decoupling factor α_ϕ. Second, the *smoothness* of the surface of the hard magnetic grains during the liquid phase sintering process is influ-



Al₂O₃ FIG. 9. Energy dispersive x-ray spectrum from the platelet phase (pl) in the ~~NFB–Al~~ magnet. The Nd/Fe ratio in at.% is approximately 2:1. No Al peak is observed in the platelet phase.

enced, leading to a higher value of α_K^{exc}. In Al_2O_3-doped sintered magnets the $Nd(Fe, Al)_2$ phase is formed and free oxygen is used to stabilize the hcp Nd-rich phase; thus the coercive field is further increased compared to the Al-doped magnet.

In conclusion, our TEM analysis indicates that the increase of the coercive field of Nd–Fe–B:(Al; Al_2O_3) sintered magnets has to be attributed to the change of the constitution and the wettability by the intergranular phases. In doped sintered magnets coercivity is increased by a higher contiguity of the intergranular region (decoupling of hard magnetic grains) and by suppression of nucleation sites for reversed domains (surface hardening of hard magnetic grains).

ACKNOWLEDGMENTS

The authors are grateful to Dr. E.-Th. Henig for many helpful discussions and Dr. E. Bischoff for EELS and EDS measurements. One of the authors (J. Fidler) acknowledges financial support from the Max-Planck-Gesellschaft and partial support of this work by the Austrian Nationalbank (No. 3065), the Austrian Forschungsfonds FWF (P6935P) and the United States Army European Research Office, London, U.K., under contract No. DAJA-86-C-0010.

REFERENCES

[1] H. Kronmüller, K. D. Durst, and M. Sagawa, J. Magn. Magn. Mat. 74, 291 (1988).
[2] D. Givord, E-MRS Fall Meeting, Nov. 1988, Strasbourg, France, J. Magn. Magn. Mat., to be published.
[3] M. Sagawa, S. Fujimura, H. Yamamoto, Y. Matsuura, and K. Hiraga, IEEE Trans. Magn. MAG-20, 1584 (1984).
[4] J. Fidler, IEEE Trans. Magn. MAG-21, 1955 (1985).
[5] N. A. El-Masry, and H. H. Stadelmaier, Mater. Lett. 3, 405 (1985).
[6] J. Fidler and L. Yang, *Proc. IV Int. Symp. on Magnetic Anisotropy and Coercivity in Rare Earth–Transition Metal Alloys*, edited by K. J. Strnat (University of Dayton, Dayton, OH, 1985), p. 647.
[7] K. Hiraga, M. Hirabayashi, M. Sagawa, and Y. Matsuura, Jap. J. Appl. Phys. 24, L30 (1985).
[8] K. Hiraga, M. Hirabayashi, M. Sagawa, and Y. Matsuura, in Ref. 7, p. 699.
[9] G. C. Hadjipanayis, K. R. Lawless, and R. C. Dickerson, J. Appl. Phys. 57, 4097 (1985).
[10] Y. Matsuura, S. Hirosawa, H. Yamamoto, S. Fujimura, M. Sagawa, and K. Osamura, in Ref. 8, p. L635.

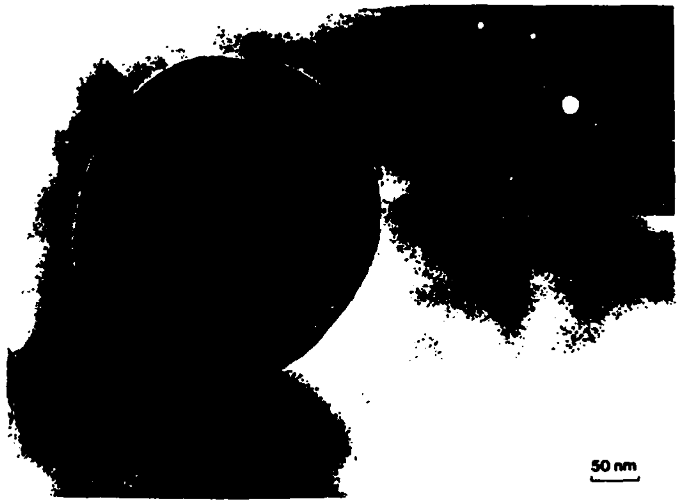


FIG. 10. Transmission electron micrograph of a spherical inclusion of Nd_2O_3 of hexagonal crystal structure embedded in the hard magnetic grain. Such Nd oxides are found with different diameters in the NFB magnet as well as in the Al-doped magnets.

[11]G. C. Hadjipanayis, Y. F. Tao, and K. R. Lawless, IEEE Trans. Magn. MAG-22, 1845 (1986).
[12]R. K. Mishra, J. K. Chen, and G. Thomas, J. Appl. Phys. 59, 2244 (1986).
[13]T. Mizoguchi, I. Sakai, H. Niu, and K. Inomata, IEEE Trans. Magn. 22, 919 (1986).
[14]R. Ramesh, K. M. Krishnan, E. Goo, G. Thomas, M. Okada, and M. Homma, J. Magn. Magn. Mat. 54–57, 363 (1986).
[15]P. Schrey, IEEE Trans. Magn. MAG-22, 913 (1986).
[16]M. Tokunaga, M. Tobise, N. Meguro, and H. Harada, IEEE Trans. Magn. MAG-22, 904 (1986).
[17]Yu-Jin Chang and Xiang-Rong Qian, Phys. Status Solidi A 93, 573 (1986).
[18]J. Fidler, IEEE Trans. Magn. MAG-23, 2106 (1987).
[19]R. Ramesh, J. K. Chen, and G. Thomas, J. Appl. Phys. 61, 2993 (1987).
[20]J. K. Chen and G. Thomas, Mat. Res. Soc. Symp. Proc. 96, 221 (1987).
[21]S. F. H. Parker, P. J. Grundy, and J. Fidler, J. Magn. Magn. Mat. 66, 74 (1987).
[22]J. Fidler, *Proc. V Int. Symp. on Magnetic Anisotropy and Coercivity in Rare Earth–Transition Metal Alloys*, edited by Deutsche Physikalische Gesellschaft e.V. (D-5340 Bad Honef 1, FRG, Bad Soden, FRG, 1987), Vol. 2, p. 363.
[23]R. J. Pollard, P. J. Grundy, S. F. H. Parker, and D. G. Lord, IEEE Trans. Magn. MAG-24, 1626 (1988).
[24]G. Schneider, E.-Th. Henig, H. H. Stadelmaier, and G. Petzow, in Ref. 22, p. 347.
[25]S. Hock and H. Kronmüller, in Ref. 22, p. 275.
[26]S. Hock, Thesis, Univ. Stuttgart, FRG, 1988.
[27]W. Rodewald and W. Fernengel, in Ref. 23, p. 1638.
[28]G. Schneider, Thesis, Univ. Stuttgart, FRG, 1988.
[29]K. G. Knoch, J. Fidler, and E. Bischoff, Mater. Lett. (submitted).
[30]B. Grieb, K. G. Knoch, E.-Th. Henig, and G. Petzow, E-MRS Fall Meeting, Nov. 1988, Strasbourg, France, J. Magn. Magn. Mat., (to be published).
[31]K. G. Knoch, G. Schneider, J. Fidler, E.-Th. Henig, and H. Kronmüller, IEEE Trans. Magn., ~~(to be submitted)~~. in press
[32]K. A. Gschneidner, *Rare Earth Alloys* (Van Nostrand Co., 1961), p. 19.

Elsevier Science Publishers B.V., P.O. Box 103, Amsterdam
Northprint MMM0104S
Page 9 1st proof: 19

IN ALL CORRESPONDENCE CONCERNING THIS PAPER REFER TO:
Magma 0104S

29 58

Journal of Magnetism and Magnetic Materials 80 (1989) MMM0104S
North-Holland, Amsterdam

11 MEI 1989

1

INVITED PAPER

ELECTRON MICROSCOPY OF Nd–Fe–B BASED MAGNETS

J. FIDLER

Institut für Angewandte Physik, T.U. Wien, Wiedner Hauptstr. 8–10, A-1040 Vienna, Austria

and

K.G. KNOCH

Max-Planck-Institut für Metallforschung, Heisenbergstr. 1, D-7000 Stuttgart 80, Fed. Rep. Germany

Transmission electron microscopy has been used widely to characterize the complex multiphase microstructure of $Nd_2Fe_{14}B$ based permanent magnets. The grain size of the magnets strongly depends on the processing technique. Our study of sintermagnets revealed two types of grain boundaries: one containing no intergranular phase between hard magnetic grains and one composed of nonmagnetic Nd-rich phases. In doped sintermagnets the dopant is dissolved in the hard magnetic ϕ-phase. In the case where the solubility of the dopant is low at the sintering temperature (Nb, Mo, Zr), precipitates are formed within the ϕ-phase. Dopants also form new intergranular phases and influence the wetting of the liquid phase and the smoothness of the surface of the ϕ-grains during sintering and therefore affect the coercivity.

1. Introduction

Microstructural investigations of rare earth (RE) permanent magnets with a high energy density product are necessary for a better understanding of the contribution of the microstructure to the hard magnetic properties. The application of RE–Fe–B based magnets has been limited by the low Curie temperature of the hard magnetic phase $RE_2Fe_{14}B$, which results in a high temperature dependence of the coercive field. The high irreversible thermal losses are reduced and the reversible temperature coefficient of the remanence B_r is increased by partial substituting Co for Fe and Dy for Nd and adding small amounts of additional elements [1–4]. The high magnetocrystalline anisotropy at room temperature of the $Nd_2Fe_{14}B$ phase primary determines the intrinsic coercivity and substituents such as Dy, which increase the anisotropy field, effectively increase the coercive field. Another possibility to enhance the coercivity is to add a small amount (< 1 wt%) of dopants, such as Al, Nb, Zr, Mo, Ga or other refractory elements. The influence of the dopants on the coercive field is not fully understood, but it is agreed that the increase of coercivity (up to 30%) is due to a microstructural effect, since the anisotropy field only changes slightly (mostly decreases) [5,6].

In fact, microstructural parameters (distribution of phases, chemical composition and crystal structures of phases, grain size distribution) and processing parameters (alloy preparation, size and shape of particles, processing and annealing treatments) determine the value of the coercive field of each individual magnet. Four different processing techniques for RE–Fe–B magnets are distinguished:

- Powdermetallurgical processing (sintering),
- Process derived from melt-spun materials,
- Mechanically alloying process,
- Cast and extrusion process. [, hot pressing]

RE–Fe–B based permanent magnets exhibit a complex, multiphase microstructure. Optical metallography, microprobe analysis, transmission electron microscopy (TEM) together with X-ray microanalysis and field ion microscopy have been used to identify the multiphase microstructure of "melt-spun" [7–11] and sintermagnets [12–33]. In

0304-8853/89/$03.50 © Elsevier Science Publishers B.V.
(North-Holland Physics Publishing Division)

REQUEST
Author, please indicate
- printer's errors in BLUE
- author's changes in RED

IMPORTANT
1. Please correct the proofs carefully; the responsibility for detecting errors rests with the author.
2. Restrict corrections to instances in which the proof is at variance with the manuscript
3. Recheck all reference data
4. A charge will be made for extensive alterations
5. Return proofs by airmail within **3 days** of receipt

Thank you.

163

the present paper the relationship between the microstructure of magnets prepared under different processing techniques is shown and the influence of dopants on the microstructure in sintermagnets is discussed.

2. Experimental

The magnets investigated were commercial grade magnets in peak aged condition of the general nominal composition $Nd_{15}Fe_{77}B_8$, but prepared under different conditions and partly containing small amounts of dysprosium and of dopants (< 1 wt%) such as Al, Al_2O_3 Nb, Zr, Mg and Dy_2O_3, respectively. The intrinsic coercivities of these magnets ranged from 300 to 2500 kA/m. The magnets were produced by various producers (Hitachi Met., Shin-Etsu Chem. Comp. and Sumitomo Spec. Met., Japan, CISRI Beijing, China, Crucible Materials and Unocal, USA) under different processing and post-sintering heat treatment conditions. Doped, "two-phase" $Nd_{20}Fe_{bal}B_{6.5}$: (Al; Al_2O_3) sintermagnets were prepared by the Max-Planck-Institut für Metallforschung, Stuttgart, Fed. Rep. Germany and a $Pr_{15}Fe_{62.5}Co_{16}B_{5.5}Al$ sintermagnet was prepared by the Carnegie Mellon University, Pittsburgh, USA. A mechanically alloyed Nd–Fe–B magnet sample was supplied by Siemens, Erlangen, Fed. Rep. Germany [34]. The magnets were studied by means of optical metallography, microprobe analysis and transmission electron microscopy (TEM) together with STEM X-ray microanalysis in order to identify the multiphase microstructure. The specimens were thinned for TEM by electropolishing using a perchloric acid–methanol solution and by ion milling. Scanning transmission electron microscope (STEM) X-ray microanalysis was performed on a JEOL 200 CX analytical microscope fitted with a LaB_6 filament and a high take off angle energy dispersive X-ray analyzer. A beryllium double tilt specimen stage was used to reduce background intensities. All X-ray spectra were analyzed using the quantitative software program for thin specimens.



Fig. 1. Transmission electron micrograph of a "melt-spun" Nd–Fe–B magnet.

3. Microstructure of Nd–Fe–B based magnets

The analytical electron microscope investigation of Nd–Fe–B based magnets revealed in all magnets the same multiphase microstructure. According to the ternary phase diagram Nd–Fe–B [35–37] at least three types of phases are found in $Nd_2Fe_{14}B$-based magnets [13,15]:

(A) the hard magnetic $Nd_2Fe_{14}B$ phase (ϕ),
(B) the boride $Nd_{1+\epsilon}Fe_4B_4$ phase (η),
(C) the intergranular Nd-rich phases (n).

3.1. Microstructure of fine-grained magnets

Grain size and grain size distribution are important criteria for the intrinsic coercivity of the final magnet. Depending on the type of the processing technique different grain sizes are found in the magnet. The average grain size of magnets derived from rapidly solidified ribbons (about 50 nm) is approximately 100–300 times smaller than the one of sintered magnets (5–15 μm). Fig. 1 shows a transmission electron micrograph of a slightly underquenched "melt-spun"-magnet. The uniform microstructure consists only of hard magnetic grains, partly separated by a thin layer of a Nd-rich phase. Melt-spun materials with maximum properties do not contain grains of phase (η), individual Nd-rich precipitates or Nd_2O_3-inclusions [9,10]. The nominal composition of the



Fig. 2. Transmission electron micrograph of a mechanically alloyed Nd–Fe–B magnet.

starting material and the quenching rate are important criteria for the precipitation of α-iron and Nd-rich phases. In comparison to the "melt-spun" and sintered magnets the microstructure of mechanically alloyed magnets is similar to the one of the "melt-spun" magnets with an average grain size between 100 and 500 nm (fig. 2). The microstructure of cast and extruded magnets is rather unknown, but first investigations show that the grain diameters are comparable with the one of sintered magnets [38].

3.2. Coercivity and microstructure of Nd–Fe–B based magnets

Besides the magnetocrystalline anisotropy of the $Nd_2Fe_{14}B$-phase, metallurgical factors control primarily the intrinsic coercive field of the individual magnet. The nature of the coercivity mechanism of the fine-grained magnets ("melt-spun" magnets) is not fully understood at present. It seems that domain wall pinning processes are involved during the magnetization reversal process [39]. In the case of coarse-grained magnets (sintermagnets) it is generally agreed that the nucleation hardening mechanism is effective [39–41]. The formulae describing the coercivity of sintermagnets in general contain micromagnetic parameters, which, however, were not related quantitatively to special microstructures so far. The aim of our electron microscopic investigations is to determine the microstructural parameters affecting the coercivity. The coercive field is indirectly proportional to the grain size, and the homogeneity of the distribution of the Nd-rich phases along grain boundaries can be correlated to the coercivity of the final magnet.

3.3. Microstructure of sintermagnets Nd sintered magnet

In Nd–Fe–B sintermagnets a nonmagnetic layer phase between the hard magnetic φ-grains is desirable in order to increase the expansion field of reversed domains and to decrease the coupling field between neighbouring grains. Individual large, soft magnetic phases in the form of precipitates or inclusions, such as α-Fe or Fe-rich phases, cause on extreme deterioration of the intrinsic coercive field and have to be avoided [31,33]. In principle, small soft magnetic precipitates within the φ-grains could act as domain wall pinning centres, if the density and size of precipitates were optimized. In fact, no sintermagnets with effective domain wall pinning were reported so far.

We have studied extensively the microstructure of sintered Nd–Fe–B magnets and our investigations revealed at least five different types of phases in addition to the hard magnetic φ-phase (see table 1) [31]. Several Nd-rich phases with different Nd/Fe ratios are found preferentially as intergranular phases at grain boundary junctions and extending to grain boundaries. Previous TEM studies showed [31,42] that two types of grain boundaries occur in Nd–Fe–B sintermagnets: grain boundaries (GB1) without any intergranular phases and grain boundaries (GB2) composed of nonmagnetic Nd-rich phases. The schematic drawing of the multiphase structure of fig. 3a shows a typical microstructure found in Nd–Fe–B sintermagnets by TEM.

Sintering of Nd–Fe–B magnets is determined primarily by the liquid phase type of sintering mechanism which involves the presence of a low melting, viscous Nd-rich eutectoid [35–37]. During sintering the driving force for densification of Nd–Fe–B magnets is the capillary pressure and the surface tension. Both surface diffusion along grain boundaries and volume diffusion also play an important role during densification. Liquid

Table 1
Phases found in doped Nd–Fe–B based magnets by analytical STEM

Type	Phase	Label	Composition/ structure
(A)	$Nd_2Fe_{14}B$ (grains)	ϕ	tetr.
(B)	$Nd_{1+\epsilon}Fe_4B_4$ (grains)	η	tetr.
(C)	Nd-rich (intergranular)	n1	$NdO_?$ – fcc
		n2	$NdO_?$ – hcp
	Nd-platelet (intergranular)	p1	$Nd_5Fe_2B_6O_?$
	Nd-oxide (precipitate)	no	Nd_2O_3 – hex
(D)	Fe-rich (Fe–Nd-oxide)	fo	Fe/Nd ≈ 4
	dopant-enriched (intergranular)	al	$Nd(Fe, Al)_2$
	dopant-enriched (precipitate)	nb1	$NbFe_2$
		nb2	NbFeB
		zr1–3	
		mo1	Mo_2FeB_2
(E)	α-Fe	f	bcc
(F)	"impurity" Nd–Cl phases	i1	
	"impurity" Nd–P–S phases	i2	

phase sintering occurs most readily when the liquid thoroughly wets the solid particles at the sintering temperature. The liquid in the narrow channels between the particles results in substantial capillary pressure. The particle size, sintering temperature and time, the uniformity of particle packing, the particle shape and the particle size distribution are extremely important parameters. Fine particle size powder can be sintered more rapidly and at lower temperature than coarser powder. If particle packing is not uniform in the pressed "green" compact, it will be difficult to avoid porosity during sintering. Smaller particles exhibit a higher driving force for densification (higher capillary pressure and higher surface energy) than coarser

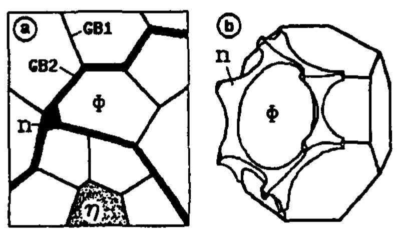


Fig. 3. Schematic drawing of the multiphase microstructure found in Nd–Fe–B based sintermagnets by TEM (a). A continuous network of Nd-rich phase along the three grain junctions occurs if the dihedral angle exceeds 60° (b) [43,44].

particles. The rate of liquid phase sintering is strongly affected by the sintering temperature. A small increase in temperature results in a substantial increase in the amount of liquid present, but on the other hand this causes excessive grain growth, which deteriorates the magnetic hardness. In order to get a high amount of intergranular Nd-rich phases, good wetting between (n)- and ϕ-phases is favourable. A high dihedral angle between the ϕ-grains during the liquid phase sintering process restrains the liquid phase from penetration into the grain boundaries. For a dihedral angle over 60° the liquid becomes isolated at the triple points between grains and forms a continuous network along the three grain junctions (fig. 3b) [43,44]. This is in good agreement with our analytical TEM investigations with two types of grain boundaries (GB1) and (GB2) in a two dimensional section (fig. 4). The high resolution electron micrograph of a fig. 4a shows two hardmagnetic ϕ-grains without any intergranular phase. Depending on the cooling rate and post-sintering heat treatments various Nd-rich phases (n) occur in the magnet. Two types of Nd-rich intergranular phases with minor Fe-content are found. The phase (n1) with a high dislocation density (fig. 4b) exhibits a fcc crystal structure with $a = 0.52$ nm [12], whereas phase (n2) exhibits a hcp crystal structure with $a = 0.39$ nm and $c = 0.61$ nm which was determined by electron diffraction. Within the interior of the (n2) phase only individual dislocations are visible (fig. 4c). Analytical TEM investigations reveal a remarkable difference of the X-ray spectra [45]. With decreasing Fe content (< 5 at%) the Nd-rich phase changes from the fcc (n1) to the hcp (n2) crystal structure. Doped magnets contain an increased amount of the (n2) phase.

Our TEM investigations occasionally revealed Nd-rich intergranular phases with a higher iron content than the (n1)-phase and an unknown crystal structure [26,31] and also a platelet shaped phase with an approximate composition of $Nd_5Fe_2B_6O_?$ embedded in the (n1)-phase [45]. Polycrystalline, spherical Nd_2O_3-inclusions are found with diameters up to 500 nm within the hard magnetic ϕ-grains as well as embedded in the intergranular phase [26,31,45].

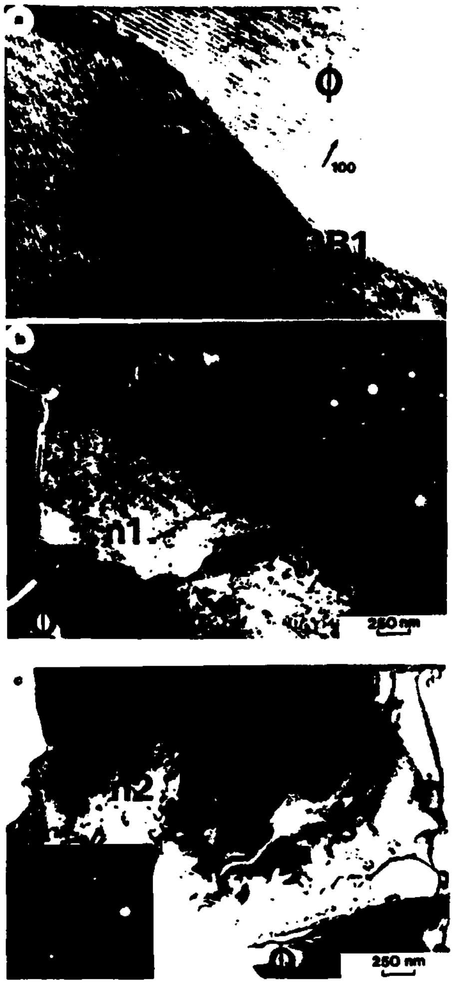


Fig. 4. Electron micrographs showing different cases where hardmagnetic ϕ-grains are separated by no intergranular phase (a), by the fcc Nd-rich (n1)-phase (b) and by the hcp Nd-rich (n2)-phase (c).

3.4. *Effect of dopants on the microstructure of sintermagnets*

If dopants are added to the prealloy or before sintering (in the form of oxides) the microstructure is affected in a twofold way:

1. Precipitation within the hard magnetic ϕ-phase,
2. Formation of new intergranular phases.

The dopant element is always found to replace the Fe-sites in the hard magnetic ϕ-grains. Energy dispersive X-ray microanalysis shows an additional AlKα-peak in the X-ray spectrum of the ϕ-phase (fig. 5a). A low solubility of the dopant element at sintering temperature leads to the formation of precipitates enriched by the dopant, such as in the case of Nb, Mo and Zr [30,32,46]. In Al-doped sintermagnets no such precipitation has been found. In order to decrease the dihedral angle and therefore to increase the amount of intergranular phases separating the hard magnetic

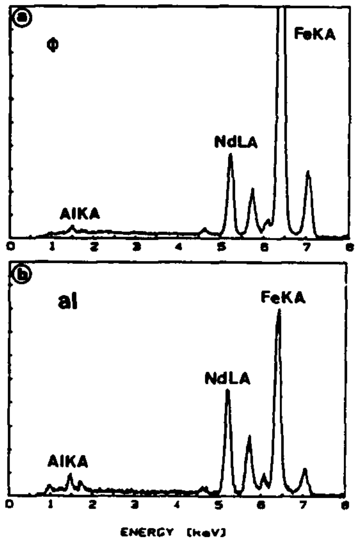


Fig. 5. Energy dispersive X-ray spectra taken from a ϕ-grain (a) and from the intergranular phase $Nd(Fe,Al)_2$ of an Al-doped Nd-Fe-B sintermagnet.

167



Fig. 6. Electron micrograph of an Al-doped Nd–Fe–B magnet showing a hard magnetic ϕ-grain and intergranular phases (n1) and (al). The lattice fringe contrast within the (al)-phase corresponds to an interplanar spacing of about 1.2–1.4 nm.

ϕ-grains, the formation of new intergranular phases positively influence the coercivity [47]. The coercivity of Nd–Fe–B sintermagnets is increased by adding small amounts of Al or Al_2O_3. Our study of such doped materials revealed a high amount of an Al-containing phase (al). From X-ray microanalysis (fig. 5b) we determined the composition of this phase as $Nd(Fe, Al)_2$, which is in accordance with Grieb et al., who detected this phase as a stable phase in the ternary system Fe–Al–Nd [48]. The high resolution electron micrograph of fig. 6 shows such an (al)-phase embedded between ϕ-grains and (n1)-phases. The crystal structure and the crystal lattice parameters of this Al-containing phase are unknown at present. From the lattice fringe image of this phase a crystal lattice periodicity of about 1.2–1.4 nm was determined. It should be mentioned that our investigations never revealed any Al-enrichment of the Nd-rich phases (n1) and (n2) [45]. Fig. 7 shows the X-ray spectrum of phase (n1) of a Nd–Fe–B : Al sintermagnet (fig. 7a) and the spectrum of the Pr-rich phase of a Pr–(Fe, Co)–B : Al magnet (fig. 7b). This result is in contrast with previously reported data, which showed a partial enrichment of Al in the Nd-rich intergranular phase [23,28].

Parker et al. reported on Nb-precipitation within the ϕ-grains in Nb-doped (Nd, Dy)–Fe–B

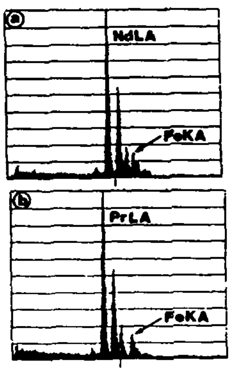


Fig. 7. Energy dispersive X-ray spectra of the intergranular phase (n1) of a Nd–Fe–B:Al sintermagnet (a) and of the Pr-rich phase of a Pr–(Fe, Co)–B:Al magnet (b). No AlKα-peak is observed.

168

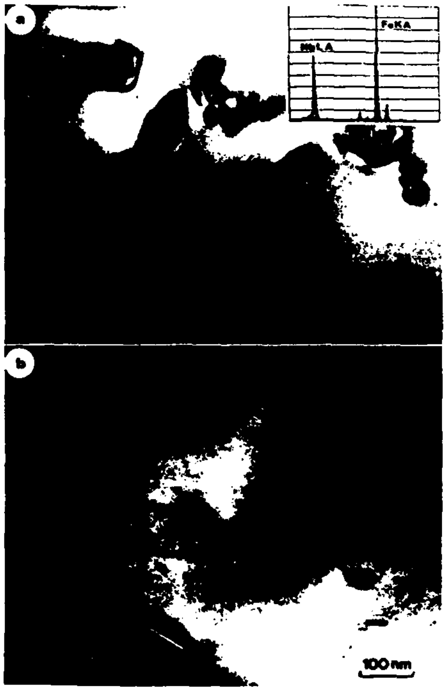


Fig. 8. Electron micrographs and X-ray spectrum of incoherent, spherical $NbFe_2$-precipitates within a ϕ-grain in a Nb-doped sintermagnet (a) and of spherical and needle-shaped precipitates in a Zr-doped sintermagnet.

magnets [30]. Two types of precipitates have been identified: the Laves phase type $NbFe_2$ having a $MgZn_2$ structure ($a = 4.82$ nm and $c = 7.87$ nm) and the FeNbB-phase. The electron micrograph and the inserted X-ray spectrum of fig. 8 show incoherent, spherical $NbFe_2$-precipitates with diameters in the order of 100 nm within a ϕ-grain. Zirconium additions result in three different, partly coherent Zr-rich or Zr-containing precipitates within the ϕ-grains [32]. Fig. 8b shows such needle-shaped and spherical precipitates. A similar precipitation behaviour was reported in Mo-doped Nd-(Fe, Co)-B magnets [46].

Other Fe-rich phases and α-Fe precipitates within the $Nd_2Fe_{14}B$-grains were found in several magnets with decreased coercivity [26,31]. Such phases are probably byproducts of an oxidation process [49,50].

4. Conclusions

Our TEM analysis performed indicates that in $Nd_2Fe_{14}B$ based sintermagnets the intrinsic coercivity is controlled by the nucleation of reversed magnetic domains during the magnetization reversal process and that the increase of the coercive field of doped sintermagnets has to be attributed to the change of the constitution and the wettability by the intergranular phases. The general formula describing the coercive field in the case of domain wall nucleation contains two microstructural parameters [40]: α_ψ, which describes the magnetic decoupling and misalignment of ϕ-grains and α_K^{nuc}, which describes the effect of the inhomogeneity of the magnetocrystalline anisotropy on the nucleation field. The increase of the coercive field of the doped magnets $Nd_2Fe_{14}B$: (Al; Al_2O_3) is attributed to the presence of $Nd(Fe, Al)_2$ and hcp Nd-rich phases, because no change of the morphology and microstructure of the fcc Nd-rich phase (n1) is observed (no Al content). An increased *wetting* due to these phases results in a higher volume fraction of grain boundaries containing an intergranular phase, which increases the magnetic decoupling factor α_ψ. The *smoothness* of the surface of the hard magnetic ϕ-grains during the liquid phase sintering process is influenced by the dopant, leading to a higher value of α_K^{nuc}. In Al_2O_3-doped sintermagnets the $Nd(Fe, Al)_2$ phase is formed and free oxygen is used to stabilize the hcp Nd-rich phase, thus the coercive field is further increased compared to the Al-doped magnet [47]. A similar effect was found in Dy_2O_3-doped sintermagnets [51].

It seems that the microstructure of doped ternary Nd-Fe-B magnets is fairly well understood, but in order to explain the contribution of the complex, multiphase microstructure of doped (Nd, Dy)-Fe-B and (Nd, Dy)-(Fe, Co)-B sintermagnets (with an increased number of new

phases [21,29]) to the coercivity, more systematic microstructural (TEM) investigations will have to be undertaken.

Acknowledgements

The partial financial support of this work by the Austrian Nationalbank (no. 3065), the Austrian Forschungsfonds FWF (P6935P) and the US Army European Research Office, London, UK, under contract no. DAJA-86-C-0010 is acknowledged.

References

[1] D. Li, H.F. Mildrum and K.J. Strnat, J. Appl. Phys. 57 (1985) 4140.
[2] Bao-Min Ma, K.S.V.L. Narasimhan and J.C. Hurt, IEEE Trans. Magn. MAG-22 (1986) 1081.
[3] M. Tokunaga, H. Kogure, M. Endoh and H. Harada, IEEE Trans. Magn. MAG-23 (1987) 2287.
[4] M. Endoh, M. Tokunaga and H. Harada, IEEE Trans. Magn. MAG-23 (1987) 2290.
[5] W. Rodewald and W. Fernengel, IEEE Trans. Magn. MAG-24 (1988) 1638.
[6] S. Hock and H. Kronmüller, Proc. 5th Intern. Symp. on Magn. Anisotropy and Coercivity in RE–Transition Metal Alloys, eds. C. Herget, H. Kronmüller and R. Poerschke, Bad Soden, Fed. Rep. Germany, vol. 2 (1987) p. 275.
[7] Y.L. Chen, IEEE Trans. Magn. MAG-21 (1985) 1967.
[8] G.C. Hadjipanayis, R.C. Dickenson and K.R. Lawless, J. Magn. Magn. Mat. 69 (1986) 557.
[9] R.K. Mishra and R.W. Lee, Appl. Phys. Lett. 48 (1986) 733.
[10] R.K. Mishra, J. Magn. Magn. Mat. 54 (1986) 450.
[11] A. Hütten and P. Haasen, J. Appl. Phys. 61 (1987) 3769.
[12] M. Sagawa, S. Fujimura, H. Yamamoto, Y. Matsuura and K. Hiraga, IEEE Trans. Magn. MAG-20 (1984) 1584.
[13] J. Fidler, IEEE Trans. Magn. MAG-21 (1985) 1955.
[14] N.A. El-Masry and H.H. Stadelmaier, Mater. Lett. 3 (1985) 405.
[15] J. Fidler and L. Yang, Proc. 4th Intern. Symp. on Magn. Anisotropy and Coercivity in RE–Transition Metal Alloys, ed. K.J. Strnat, Univ. of Dayton, USA (1985) p. 647.
[16] K. Hiraga, M. Hirabayashi, M. Sagawa and Y. Matsuura, Japan. J. Appl. Phys. 24 (1985) L30.
[17] K. Hiraga, M. Hirabayashi, M. Sagawa and Y. Matsuura, Japan. J. Appl. Phys. 24 (1985) 699.
[18] G.C. Hadjipanayis, K.R. Lawless and R.C. Dickerson, J. Appl. Phys. 57 (1985).
~~Samura, Japan. J. Appl. Phys. 24 (1985) L635.~~
[19] G.C. Hadjipanayis, Y.F. Tao and K.R. Lawless, IEEE Trans. Magn. MAG-22 (19860 1845.
[20] R.K. Mishra, J.K. Chen and G. Thomas, J. Appl. Phys. 59 (1985) 2244.
[21] T. Mizoguchi, I. Sakai, H. Niu and K. Inomata, IEEE Trans. Magn. MAG-22 (1986) 919.
[22] R. Ramesh, K.M. Krishnan, E. Goo, G. Thomas, M. Okada and M. Homma, J. Magn. Magn. Mat. 54–57 (1986) 363.
[23] P. Schrey, IEEE Trans. Magn. MAG-22 (1986) 913.
[24] M. Tokunaga, M. Tobise, N. Meguro and H. Harada, IEEE Trans. Magn. MAG-22 (1986) 904.
[25] Yu-Jin Chang and Xiang-Rong Qian, Phys. Stat. Sol. (a) 93 (1986) 573.
[26] J. Fidler, IEEE Trans. Magn. MAG-23 (1987) 2106.
[27] R. Ramesh, J.K. Chen and G. Thomas, J. Appl. Phys. 61 (1987) 2993.
[28] J.K. Chen and G. Thomas, Mater. Res. Soc. Symp. Proc. 96 (1987) 221.
[29] T. Mizoguchi, I. Sakai, H. Niu and K. Inomata, IEEE Trans. Magn. MAG-23 (1987) 2281.
[30] S.H.F. Parker, P. Grundy and J. Fidler, J. Magn. Magn. Mat. 66 (1987) 74.
[31] J. Fidler, Proc. 5th Intern. Symp. on Magn. Anisotropy and Coercivity in RE–Transition Metal Alloys, eds. C. Herget, H. Kronmüller and R. Poerschke, Bad Soden, Fed. Rep. Germany, vol. 2 (1987) p. 363.
[32] R.J. Pollard, P.J. Grundy, S.F.H. Parker and D.G. Lord, IEEE Trans. Magn. MAG-24 (1988) 1626.
[33] J. Fidler and Y. Tawara, IEEE Trans. Magn. MAG-24 (1988) 1951.
[34] L. Schultz, J. Wecker and E. Hellstern, J. Appl. Phys. 61 (1987) 3583.
[35] Y. Matsuura, S. Hirosawa, H. Yamamoto, S. Fujimura, M. Sagawa and K. Osamura, Japan. J. Appl. Phys. 24 (1985) L635.
[36] G. Schneider, E-Th. Henig, H.H. Stadelmaier and G. Petzow, Proc. 5th Intern. Symp. on Magn. Anisotropy and Coercivity in RE–Transition Metal Alloys, eds. C. Herget, H. Kronmüller and R. Poerschke, Bad Soden, Fed. Rep. Germany, vol. 2 (1987) p. 347.
[37] D.S. Tsai, T.S. Chin, S.E. Hsu and M.P. Hung, IEEE Trans. Magn. MAG-23 (1987) 3607.
[38] J.P. Nozières, R. Perrier de la Bâthie and D.W. Taylor, J. Magn. Magn. Mat. 80 (1989) S125 (this issue).
[39] D. Givord, presented at the E-MRS Fall Meeting, Strasbourg, France, 8–10 November 1988. (this issue)
[40] H. Kronmüller, K.D. Durst and M. Sagawa, J. Magn. Magn. Mat. 74 (1988) 291.
[41] J.D. Livingston, IEEE Trans. Magn. MAG-23 (1987) 2109.
[42] J. Fidler and P. Skalicky, Mikrochimica Acta (Vienna) I (1987) 115.
[43] R.M. German, Liquid Phase Sintering (Plenum Press, New York, 1985).
[44] W. Beere, Acta Met. 23 (1975) 131.
[45] J. Fidler, K.G. Knoch, H. Kronmüller and G. Schneider, J. Mater. Res. ~~submitted.~~ 4 (Vol. 4, No. Jul/Aug)
[46] W. Rodewald, DPG-Spring Meeting, Karlsruhe (March 1988).

170

[47] K.G. Knoch, G. Schneider, J. Fidler, E.-Th. Henig and H. Kronmüller, IEEE Trans. Magn. ~~submitted~~. in press.
[48] B. Grieb, K.G. Knoch, E.-Th. Henig and G. Petzow, J. Magn. Magn. Mat. 80 (198() 123S (this issue).
[49] D. Cochet-Muchy and S. Paidassi, Proc. ICM Conf., Paris, France (1988).
[50] J. Jacobson and K. Kim, J. Appl. Phys. 61 (1987) 3763.
[51] M.H. Ghandehari and J. Fidler, Mater. Lett. 5 (1987) 285.

30

ON THE ROLE OF MICROSTRUCTURE ON COERCIVITY OF RARE EARTH PERMANENT MAGNETS

Josef Fidler
Institut für Angewandte und Technische Physik, T.U. Wien,
Wiedner Hauptstr. 8-10, A-1040 Wien, Austria.

Abstract:
Rare earth permanent magnets exhibit a complex, multiphase microstructure, which in fact controls besides the magnetocrystalline anisotropy the coercivity of the magnets. For the development of new hardmagnetic materials the exact knowledge of the microstructure is important for a better understanding of the coercivtiy mechanisms of the materials (nucleation or pinning). Metallography and transmission electron microscopy has widely been used to characterize the complex microstructure.

1. INTRODUCTION

Modern permanent magnets are based on rare earth-transition metal intermetallic compounds with hexagonal or tetragonal crystal symmetry and exhibiting rather large uniaxial magnetic anisotropy, such as SmCo5, Sm2Co17 and RE2Fe14B, with RE=Nd, Pr, Dy and Tb. The condition of high magnetocrystalline anisotropy is necessary, but not sufficient in order to achieve good permanent magnetic properties. The microstructure of the magnet is another factor controlling the hardmagnetic properties, i.e. the coercivity. Two different mechanisms, explaining the coercivity, are distinguished:

(a) Pinning of magnetic domain walls
(b) Nucleation and expansion of reversed magnetic domains

The occurance of nucleation or pinning depends on the microstructure of the magnet. In modern permanent magnets the values of the hardmagentic properties, such as the coercivity are in practice only 10 - 40 % of the theoretical limits. Several micromagnetic theories to explain the coercivity have been developed [1,2]. All of these theories are based on a two-dimensional "model-microstructure" and determine the equilibrium state of lowest free energy. Empirical microstructural parameters have been deduced from these theories, such as describing the magnetic decoupling and misalignment of hardmagnetic grains or describing the effect of inhomogeneity of the magnetocrystalline anisotropy on nucleation and pinning, or the local demagnetization factor, which has been partly correlated to the grain size of the material, and other parameters.

The real microstructure influences or in some cases determines the coercivity. Microstructural investigations of rare earth (RE) permanent magnets with a high energy density product are necessary for a better understanding of the contribution of the microstructure to the hardmagnetic properties. In fact, microstructural parameters and processing parameters, such as:

(a) distribution of phases
(b) chemical composition and crystal structures of phases
(c) grain size distribution
(d) size and shape of particles
(e) processing and annealing treatments

determine the value of the coercive field of each individual magnet.

The purpose of this paper is to show the difference of transmission electron microscopic (TEM) results of a pinning controlled $Sm(Co,Fe,Cu,Zr)_{7.5}$ magnet and a nucleation controlled Nd-Fe-B magnet. In the light of the historical development of permanent magnetic materials the improvment of the coercivity is closely related with a better microstructural understanding of the mechanisms leading to higher coercive forces.

2. MICROSTRUCTURE OF $Sm(Co,Fe,Cu,Zr)_{7.5}$ SINTERED MAGNETS

Copper containing RE-cobalt magnets with a nominal composition of $Sm(Co,Fe,Cu,TM)_{6-8}$ with TM=Zr,Ti or Hf show a fine scale, cellular microstructure [3-7]. Rhombic cells of the type $Sm_2(Co,Fe)_{17}$ rhomb. - phase A - are separated by a $Sm(Co,Cu,TM)_{5-7}$ cell boundary phase - phase B (Fig.1a). In magnets with high coercivities thin platelets - phase C - are found perpendicular to the hexagonal c-axis (Fig.1a). Our high resolution electron microscope investigations (Fig.1c) show that the crystal structure of the platelet phase C is close to the hexagonal Sm_2Co_{17} structure with a c-crystal parameter of 0.8 nm. This is in agreement with metallurgical considerations on the formation of various phases in sintered SmCo 2:17 magnets by A.E. Ray [8-10]. Remarkable for high coercivity SmCo 2:17 magnets is also the observed twinning within the rhombohedral 2:17-cell interior phase. Twin boundaries may coincide with the platelet phase but also occur within the rhomb. 2:17-phase (Fig.1.c).

From our investigations it is obvious that there are different reasons for low coercivities. Since in precipitation hardened SmCo 2:17 magnets the cellular precipitation structure acts as attractive pinning centre for magnetic domain walls during the magnetization reversal (Fig.2) [11,12], the size, the composition and the completeness of the continuus cellular precipitation structure control the coercivity. The platelet phase (C) predominately acts as diffusion path for the chemical redistribution process during the post-sintering heat treatments and is favourable for the formation of the cell boundary phase of the 1:5-ordered type or 1:7- disordered type. Figure 3 shows an electron micrograph of a magnet with 23.9 wt% nominal Sm-content. A high density of the platelet phase is shown, but due to the lack of samarium the formation of the cell boundary phase is poor leading to an intrinsic coercivity of 250 kA/m. Impurities, primarily such as oxygen and carbon, lead to the formation of macroscopic precipitates of Sm_2O_3, ZrC, TiC etc.. A high amount of these phases in the magnet impedes the formation of the platelet phase and the cellular precipitation structure. It has been shown [13] that small amounts of Zr, Ti or Hf are necessary for the formation of the platelet phase (C).

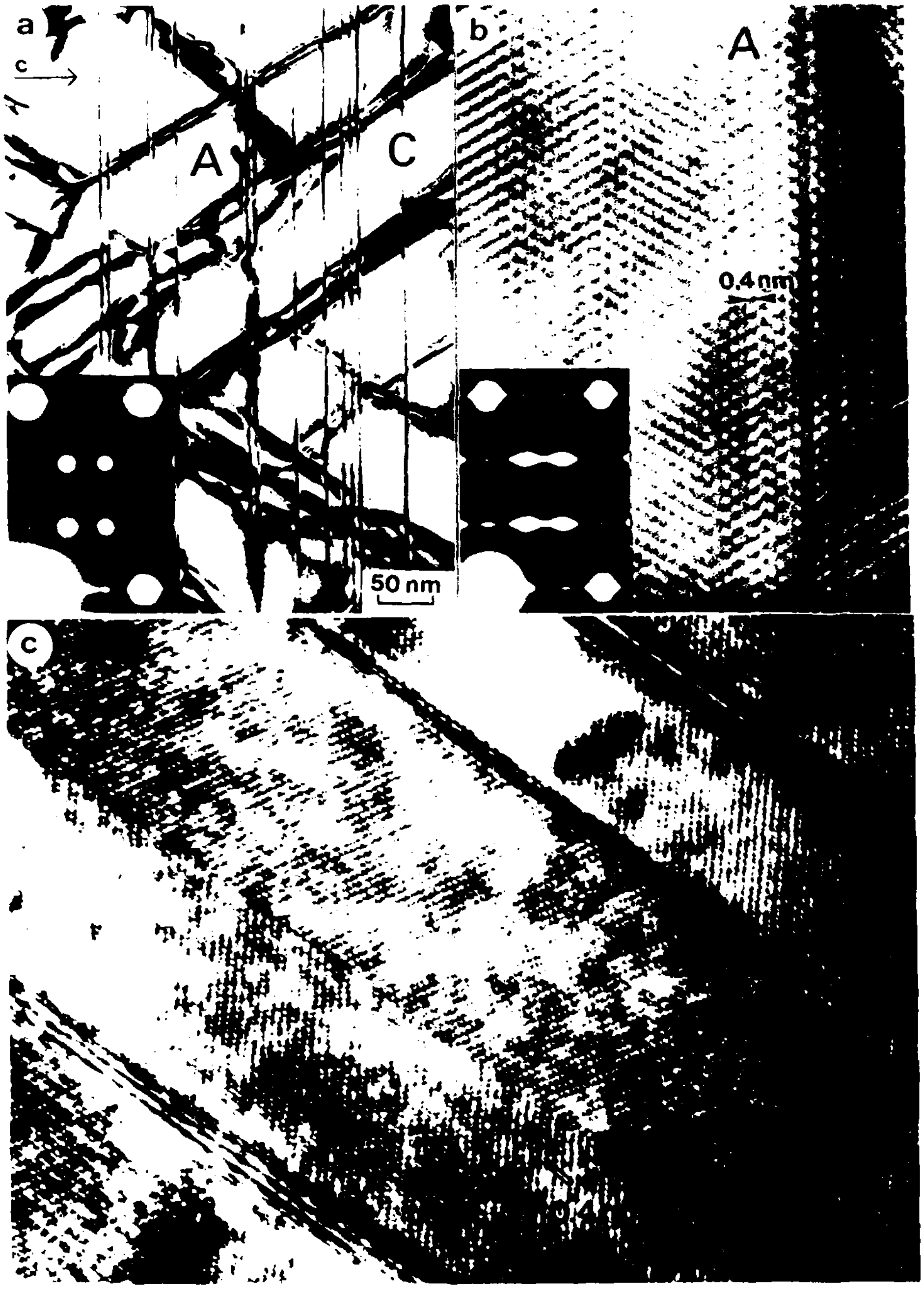


Fig.1: Electron micrographs showing the cellular precipitation structure of a $Sm(Co,Fe,Cu,Zr)_{7.5}$ magnet.

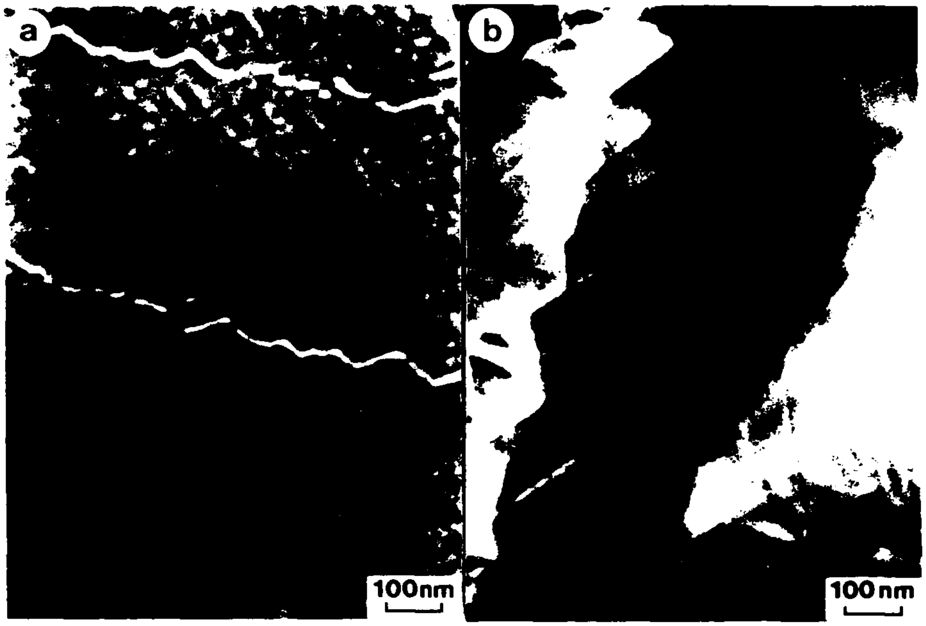


Fig.2: Lorentz electron micrographs showing the attractive domain wall pinning at the continuous cell boundary phase.

The high resolution electron micrograph of Fig.1b shows the cell interior of a magnet with an intrinsic coercivity of iHc = 600 kA/m. No platelet phase (C) is found and X-ray microanalysis shows that this region of the magnet is depleted from zirconium. The contrast of this image correspond to the atomic positions along the [1120]-zone axis. A high density of stacking faults, and therefore also microtwinning is observed. It should be noted that the distance between atomic layers in the basal plane varies, especially near stacking faults. The development and growth of the cellular precipitation structure occurs during the isothermal aging procedure and involves diffusion of samarium, whereas the chemical redistribution of the transition metals during the step aging procedure following the isothermal aging increases the coercivity. Possible diffusion paths for this diffusion process are the platelets of phase (C) and the disordered regions near planar stacking faults and twin boundaries in the basal plane as observed in Fig.1.

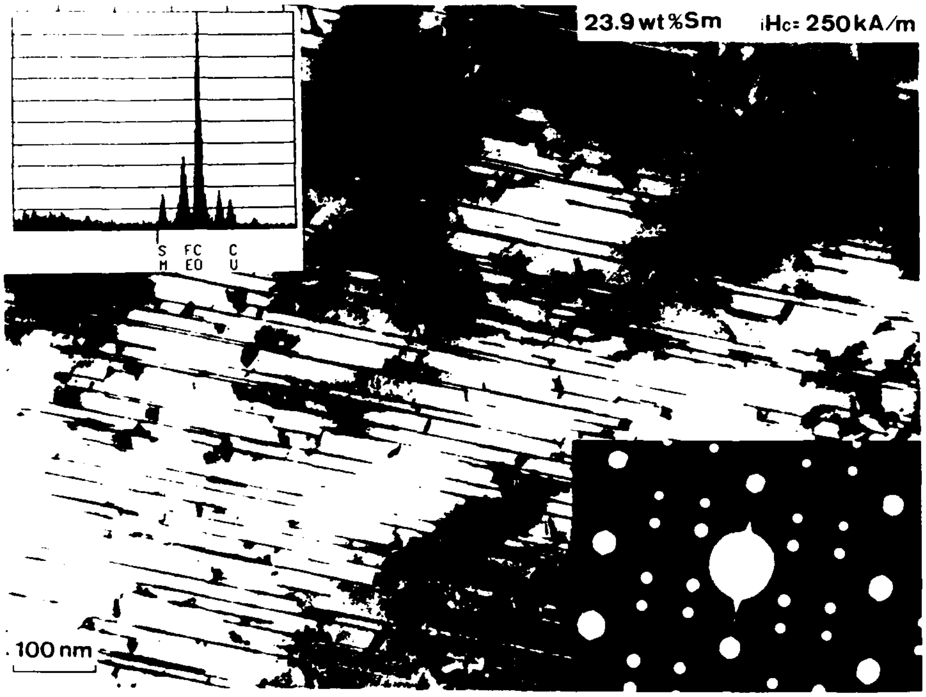


Fig.3: Due to the lack of samarium the cell boundary phase is only incompletely formed. A high density of the platelet phase is observed.

3. MICROSTRUCTURE OF ND-FE-B BASED MAGNETS

The application of RE-Fe-B based magnets has been limited by the low Curie temperature of the hard magnetic phase $RE_2Fe_{14}B$, which results in a high temperature dependence of the coercive field. The high irreversible thermal losses are reduced and the reversible temperature coefficient of the remanence Br is increased by partial substituting Co for Fe and Dy for Nd and adding small amounts of additional elements. The high magneto-crystalline anisotropy at room temperature of the $Nd_2Fe_{14}B$ (Φ)-phase primarily determines the intrinsic coercivity and substituents such as Dy, which increase the anisotropy field, effectively increase the coercive field. Another possibility to enhance the coercivity is to add a small amount (<1 wt.%) of dopants, such as Al, Nb, Zr, Mo, Ga or other refractory elements. The influence of the dopants on the coercive field is not fully understood, but it is aggreed that the increase of coercivity (up to 30%) is due to a microstructural effect, since the anisotropy field only sligthly changes (mostly decreases) [14,15]. Four different processing techniques for RE-Fe-B magnets are distinguished:

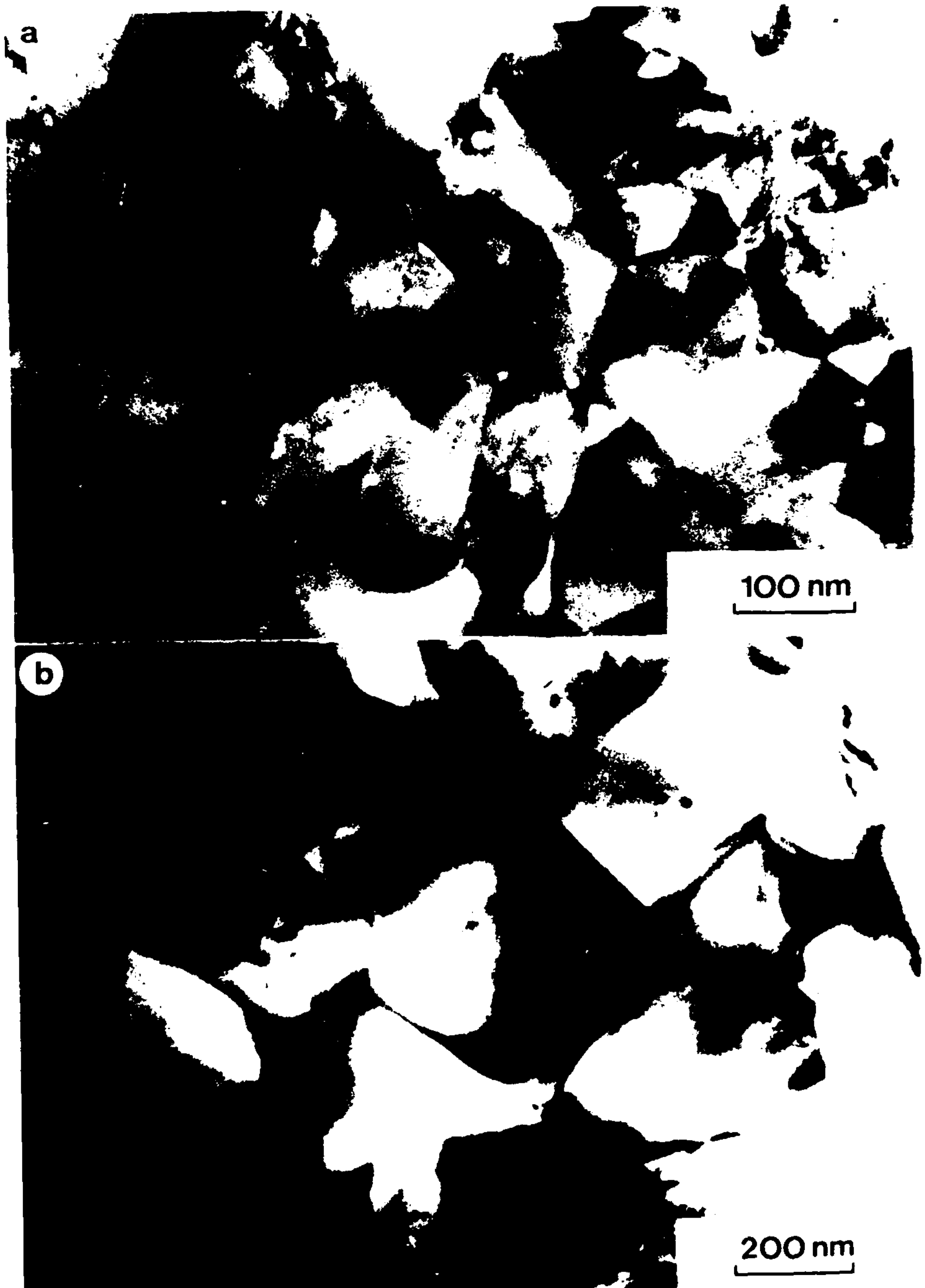


Fig.4: Transmission electron micrographs of a "melt-spun" (a) and a mechanically alloyed (b) Nd-Fe-B magnet.

(1) Powdermetallurgical sintering-process
large grain size (up to 15 m)
multiphase microstructure

(2) Process derived from melt-spun materials (MQ I, II, III)
small grain size (50 nm)
"two-phase microstructure"

(3) Mechanically alloyed magnets (MM I, II, III)
small and medium grain size (50 - 500 nm)
multiphase microstructure

(4) Cast, hot pressed or extruded magnets
grain size and microstructure similar to (1)?

Depending on the processing technique RE-Fe-B based permanent magnets exhibit a complex, multiphase microstructure. Optical metallography, microprobe analysis, transmission electron microscopy together with X-ray microanalysis and field ion microscopy have been used to characterize the complex multiphase microstructure of $Nd_2Fe_{14}B$ based permanent magnets so far. The grain size of the magnets also strongly depends on the processing technique. The electron micrographs of Fig.4 show the microstructure of fine-grained magnets, prepared by melt-spinning technique (Fig.4a) and prepared by the mechanically alloying process (Fig.4b). The microstructure of cast, hot pressed and extruded magnets is rather unknown, but first investigations show that the grain diameters are comparable with the one of sintered magnets [16]. Our study of sintered magnets revealed at least

Table 1: Phases found in $Nd_2Fe_{14}B$ - based permanent magnets

TYPE	PHASE	MARK	COMPOSITION/ STRUCTURE
(A)	$Nd_2Fe_{14}B$ (grains)	Φ	tetr.
(B)	$Nd_{(1+\epsilon)}Fe_4B_4$ (grains)	η	tetr.
(C)	Nd-rich (intergranular)	n1	$NdO_?$ - fcc
		n2	$NdO_?$ - hcp
	Nd-platelet (intergranular)	pl	$Nd_5Fe_2B_6O_?$
	Nd-oxide (precipitate)	no	Nd_2O_3 - hex
(D)	Fe-rich	fn	Fe_2Nd - an.or
	Fe-rich (Fe-Nd-Oxide)	fo	Fe/Nd≈4
	dopant-enriched (intergranular)	al	$Nd(Fe,Al)_2$
	dopant-enriched (precipitate)	nb1	$NbFe_2$
		nb2	NbFeB
		zr1-3	
		mo1	Mo_2FeB_2
(E)	α-Fe	f	bcc
(F)	"impurity" Nd-Cl phases	i1	
	"impurity" Nd-P-S phases	i2	

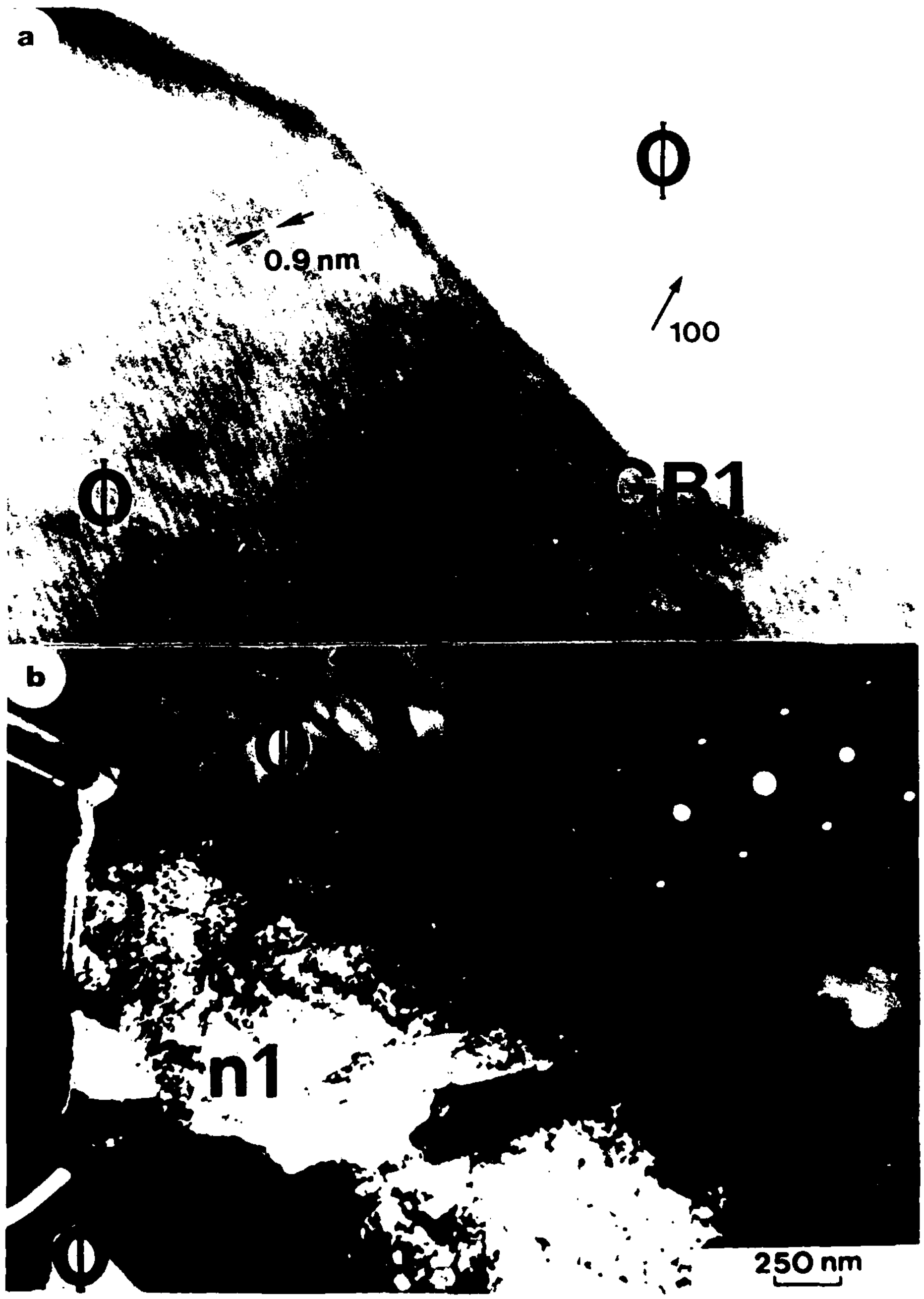


Fig.5: Electron micrographs of a sintered Nd-Fe-B magnet showing to different cases of grain boundaries between Φ-grains.

five different types of phases in addition to the hardmagnetic Φ-phase (see Table 1) [17]. Several Nd-rich phases with different Nd/Fe ratios are found preferentially as intergranular phases at grain boundary junctions and extending to grain boundaries. Previous TEM studies showed [17,18] that two types of grain boundaries occur in Nd-Fe-B sintermagnets: grain boundaries (GB1) without any intergranular phases and grain boundaries (GB2) composed of nonmagnetic Nd-rich phases. The micrographs of Fig.5 show the typical microstructure of found in Nd-Fe-B sintered magnets. In Fig.5.a the Φ-grains are separated by no intergranular phase and in Fig.5.b the Φ-grains are separated by an fcc Nd-rich (n1)-phase. Two types of Nd-rich intergranular phases with minor Fe-content are found. The phase (n1) with a high dislocation density (Fig.6) exhibits a fcc crystal structure with a=0.52 nm [12], whereas phase (n2) exhibits a hcp crystal structure with a=0.39 nm and c=0.61 nm which was determined by electron diffraction. Within the interior of the (n2) phase only individual dislocations are visible (Fig.6). Analytical TEM investigations reveal a remarkable difference of the X-ray spectra [19]. With decreasing Fe content (< 5 at.%) the Nd-rich phase changes from the fcc (n1) to the hcp (n2) crystal structure. Al-doped magnets contain an increased amount of the (n2) phase.



Fig.6: Different Nd-rich phases occur within the intergranular region between hardmagnetic Φ-grains.

Our TEM investigations occasionally revealed Nd-rich intergranular phases with a higher iron content than the (n1)-phase and an unknown crystal structure [20,17] and also a platelet shaped phase with an approximate composition of $Nd_5Fe_2B_6O_7$ (p1) embedded in the (n1)-phase [19]. Polycrystalline,

spherical Nd_2O_3-inclusions are found with diameters up to 500 nm within the hardmagnetic Φ-grains as well as embedded in the intergranular phase.

If dopants are added to the prealloy or before sintering in order to increase the coercive field, the microstructure is affected in the following way:

(1) the dopant is dissolved in the hardmagnetic Φ-phase (changing the magnetocrystalline anisotropy ?)

(2) precipitation within Φ-grains: Nb, Zr, Mo ....
(possibly domain wall pinning?)

(3) formation of new intergranular phases: Al, Nb, Mo ....
(influences wettability and therefore magnetic coupling of grains)

In the case where the solubility of the dopant is low at sintering temperature (Nb,Mo,Zr), precipitates are formed within the Φ-phase [21-23]. The electron micrograph and the inserted X-ray spectrum of Fig.7 show incoherent, spherical $NbFe_2$-precipitates with diameters in the order of 100 nm within a Φ-grain.

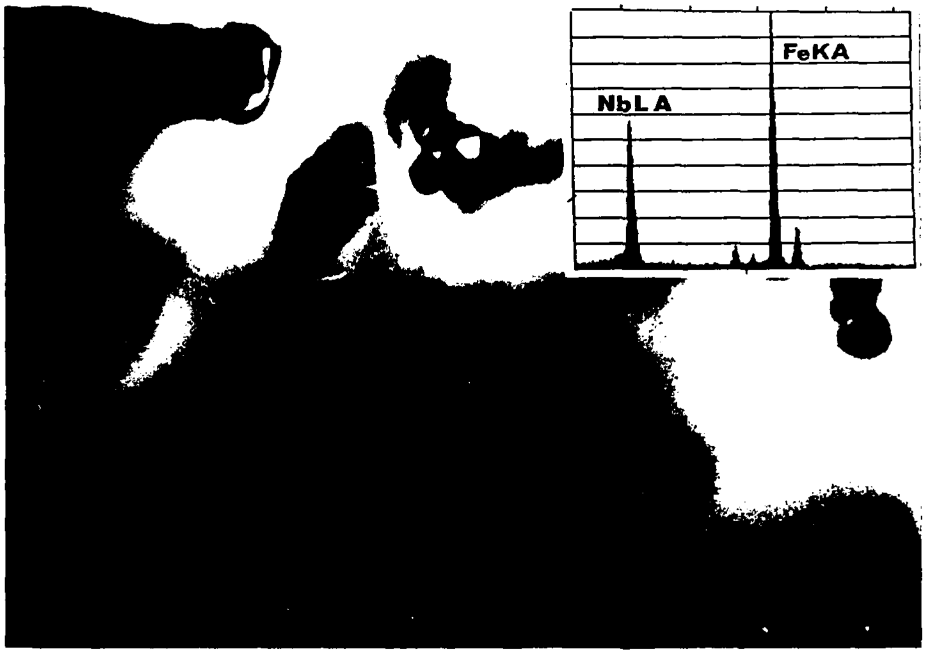


Fig.7: Electron micrograph and X-ray spectrum of incoherent spherical $NbFe_2$-precipitates within a Φ-grain in a Nb-doped sintered magnet.

Dopants also form new intergranular phases and influence the wetting of the liquid phase and the smoothness of the surface of the Φ-grains during sintering and therefore affect the coercivity [18,19]. In Al-doped Nd-Fe-B sintered magnets Al is always found to replace the Fe-sites in the hardmagnetic Φ-grains. Energy dispersive X-ray microanalysis shows an additional AlKα-peak in

the X-ray spectrum of the Φ-phase (Fig.8a). In order to decrease the dihedral angle and therefore to increase the amount of intergranular phases separating the hardmagnetic Φ-grains the formation of new intergranular phases positively influence the coercivity. The coercivity of Nd-Fe-B sintermagnets is increased

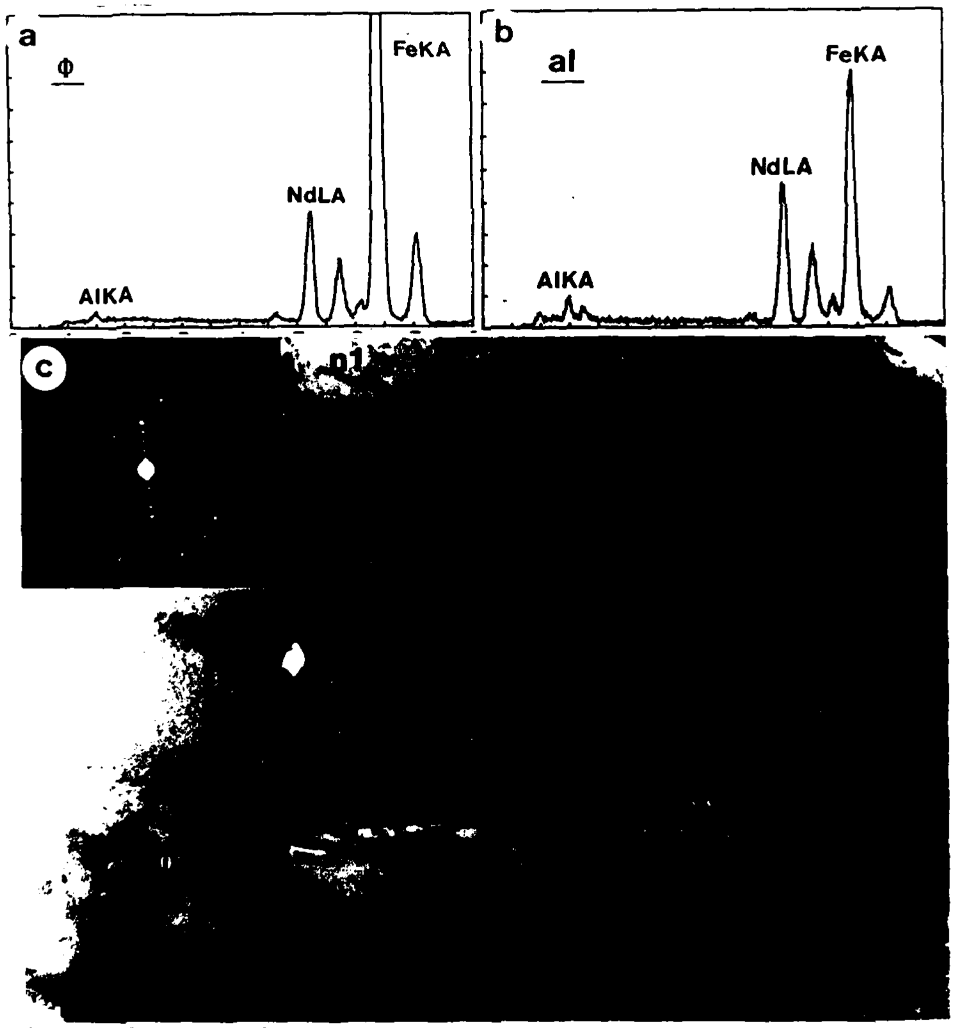


Fig.8: Electron micrograph and X-ray spectra of an Al-doped sintered magnet, showing the occurance of a $Nd(Fe,Al)_2$-phase (al) within the intergranular region between Φ-grains.

by adding small amouts of Al or Al_2O_3. Our study of such doped materials revealed a high amount of an Al-containing phase (al). From X-ray microanalysis (Fig.8b) we determined the composition of this phase as $Nd(Fe,Al)_2$, which is in accordance with Grieb et

al. [24], who detected this phase as stable phase in the ternary system Fe-Al-Nd. The electron micrograph of Fig.8c shows such an (al)-phase embedded between Φ-grains and (n1)-phases.The crystal structure and the crystal lattice parameters of this Al-containing phase are unknown at present. From the lattice fringe image of this phase a crystal lattice periodicity of about 1.2-1.4 nm was determined. It should be mentioned that our investigations never revealed any Al-enrichment of the Nd-rich phases (n1) and (n2). This result is in contrast with previously reported data, which showed a partial enrichment of Al in the Nd-rich intergranular phase [25,26].

In RE-Fe-B magnets a nonmagnetic layer phase between the Φ-grains is desirable in order to increase the expansion field of reversed domains and to decrease the coupling field between neighbouring grains. Individual large, softmagnetic phases in the form of precipitates or inclusions, such as α-Fe or Fe- rich phases, extremely deteriorate the coercive field and have to be avoided. In principle, small precipitates within the Φ-grains could act as domain wall pinning centres, if density and size of precipitates were optimized. In fact, no sintered RE-Fe-B magnet with effective domain wall pinning was reported so far.

4. CONCLUSION

As long as the coercivity of an individual magnet cannot be calculated or predicted by the micromagnetic theories, microstructural investigations are necessary to show the difference between the real, three-dimensional microstructure of the material and the "model-microstructure". The aim of all microstructural investigations is to get at least a qualitative characterization and, in the future, a quantitative description of the real microstructure. The main hindrance for the quantitative description is the inhomogeneity of the microstructure of rare earth permanent magnets.

Besides chemical analysis, X-ray analysis and magnetic measurements also metallography together with anaylitical electron microscopy (AEM) and high resolution electron microscopy (HREM) is necessary for a better understanding of the mechanisms leading to high coercivities in rare earth permanent magnet materials. These investigations are only useful if they are accompanied by phase-diagram and phase relation studies.

Acknowledgements

The partial financial support of this work by the Austrian Nationalbank (No. 3065), the Austrian Forschungsfonds FWF (P6935P) and the US Army European Research Office, London, UK, under contract No. DAJA-86-C-0010 is acknowledged.

References

[1] H. Kronmüller, K.D. Durst and M. Sagawa, J. Magn. Magn. Mat. 74, 291 (1988).

[2] D. Givord, E-MRS Fall Meeting, Nov. 1988, Strasbourg, France, J. Magn. Magn. Mat., to be published.

[3] J.D. Livingston and D.L. Martin, J. Appl. Phys. 48, 1350 (1977).

[4] R.K. Mishra, G. Thomas, T. Yoneyama, A. Fukuno and T. Ojima, J.Appl.Phys. 52, 2517 (1981).

[5]. J. Fidler and P. Skalicky, J. Magn. Magn. Mat. 27, 127 (1982).

[6]. J. Fidler, P. Skalicky and F. Rothwarf, IEEE Trans.Magn. MAG-19, 2041 (1983).

[7] J. Fidler, J. Bernardi and P. Skalicky, Mat. Res. Soc. Symp. Proc. Vol.96, 181 (1987).

[8]. A.E. Ray, Proc. of Soft and Hard Magnetic Materials with Applications, Lake Buena Vista, Florida, Oct.1986, published by ASM.

[9] A.E. Ray, J. Appl. Phys. 55, 2094 (1984).

[10] A.E. Ray, IEEE Trans. Magn. MAG-20, 1614 (1984).

[11] J. Fidler, J. Mag. Magn. Mat. 30, 58 (1982).

[12] H. Kronmüller, K.D. Durst, W. Ervens amd W. Fernengel, IEEE Trans.Magn. MAG-20, 1569 (1984).

[13] L. Rabenberg, R.K. Mishra and G. Thomas, J. Appl.Phys. 53, 2389 (1982).

[14] W. Rodewald and W. Fernengel, IEEE Trans.Magn. MAG-24, 1638 (1988).

[15] S. Hock and H. Kronmüller, Proc. on 5th Int. Symp. on Magn. Anisotropy and Coercivity in RE-Tránsition Metal Alloys, eds. C. Herget, H. Kronmüller and R. Poerschke, Bad Soden, FRG, Vol.2 (1987) p. 275.

[16] J.P. Noziers, R. Perrier del la Bathie and D.W. Taylor, E-MRS Fall Meeting, Nov. 1988, Strasbourg, France, J. Magn. Magn. Mat., to be published.

[17] J. Fidler, Proc. on 5th Int. Symp. on Magn. Anisotropy and Coercivity in RE-Transition Metal Alloys, eds. C. Herget, H. Kronmüller and R. Poerschke, Bad Soden, FRG, Vol.2 (1987) p. 363.

[18] J. Fidler and K.G. Knoch, E-MRS Fall Meeting, Nov. 1988, Strasbourg, France, J. Magn. Magn. Mat., to be published.

[19] J. Fidler, K.G. Knoch, H. Kronmüller and G. Schneider, J. Mat. Res. in press.

[20] J. Fidler, IEEE Trans.Magn. MAG-23, 2106 (1987).

[21] S.H.F. Parker, P. Grundy and J. Fidler, J.Magn.Magn.Mat. 66, 74 (1987).

[22] R.J. Pollard, P.J. Grundy, S.F.H. Parker and D.G. Lord, IEEE Trans.Magn. MAG-24, 1626 (1988).

[23] W. Rodewald and P. Schrey, IEEE Trans.Magn. in press (Proc. Intermag 89).

[24] B. Grieb, K.G. Knoch, E.-Th. Henig and G. Petzow, E-MRS Fall Meeting, Nov. 1988, Strasbourg, France, J. Magn. Magn. Mat., to be published.

[25] P. Schrey, IEEE Trans.Magn. MAG-22, 913 (1986).

[26] J.K. Chen and G. Thomas, Mat. Res. Soc. Symp. Proc. Vol.96, 221 (1987).

31

THE INFLUENCE OF DOPANTS ON MICROSTRUCTURE AND COERCIVITY OF Nd-Fe-B SINTERED MAGNETS

Josef Fidler and K.G. Knoch [1]

Institut für Angewandte Physik, TU Wien, Vienna, Austria
[1] Max-Planck-Institut für Metallforschung, Stuttgart, F.R.G.

ABSTRACT

The complex, multiphase microstructure and the coercivity of $Nd_2Fe_{14}B$ based sintered magnets is influenced by doping the magnet. In doped sintered magnets the dopant is dissolved in the hardmagnetic Φ-phase. If the solubility of the dopant is low, precipitates are formed within the Φ-phase. Dopants also form new intergranular phases and influence the wetting of the liquid phase and the smoothness of the surface of the Φ-grains during sintering. The increase of $_iH_c$ by dopants such as Al, Al_2O_3, Dy_2O_3, Nb, Mo, Zr and Ga will be discussed.

INTRODUCTION

In sintered Nd2Fe14B-based permanent magnets the coercivity is in practice only 20 - 40 % of the theoretical limits. Several micromagnetic theories to explain the coercivity have been developed [1,2]. All of these theories are based on a two-dimensional "model-microstructure" and determine the equilibrium state of lowest free energy. Empirical microstructural parameters have been deduced from these theories, such as describing the magnetic decoupling and misalignment of hardmagnetic grains or describing the effect of inhomogeneity of the magnetocrystalline anisotropy on nucleation and pinning, or the local demagnetization factor, which has been partly correlated to the grain size of the material, and other parameters.

Th application of RE-Fe-B based magnets has been limited by t.. low Curie temperature of the hard magnetic phase $RE_2Fe_{14}B$, which results in a high temperature dependence of the coercive field. The high irreversible thermal losses are reduced and the reversible temperature coefficient of the remanence B_r is increased by partial substituting Co for Fe

****

Paper No.___ at the 10th International Workshop on Rare-Earth Magnets and Their Applications, Kyoto, Japan, 16-19 May, 1989 (Proceeding Book: The Society of Non-Traditional Technology, 1-2-8, Toranomon, Minatu-ku, Tokyo, 105 Japan)

Address inquiries to: J. Fidler, Institut für Angewandte Physik, Technische Universität, Wiedner Hauptstr.8-10, A-1040 Vienna, Austria.

and Dy for Nd and adding small amounts of additional elements. The high magnetocrystalline anisotropy at room temperature of the $Nd_2Fe_{14}B$ (Φ)-phase primarily determines the intrinsic coercivity and substituents such as Dy, which increase the anisotropy field, effectively increase the coercive field. A high magnetocrystlline anisotropy is a necessary, but is not a sufficient condition in order to achieve high coercive fields. The real microstructure influences or in some cases determines the coercivity. Another possibility to enhance the coercivity is to add a small amount (<1 wt.%) of dopants, such as Al, Nb, Zr, Mo, Ga or other refractory elements. The influence of the dopants on the coercive field is not fully understood, but it is aggreed that the increase of coercivity (up to 30%) is due to a microstructural effect, since the anisotropy field only sligthly changes (mostly decreases) [3,4].

The present study was undertaken to show the influence of dopants, in particular of Al-dotation on the microstructure and coercivity of $Nd_2Fe_{14}B$ based sintered magnets.The real microstructure influences or in some cases determines the coercivity.

EXPERIMENTAL PROCEDURE

The samples investigated were optimized sintered magnets (in the peak aged condition) which were prepared by conventional powder metallurgical processing technique as described in detail in [5,6]. Three different types of sintered magnets were investigated by optical metallography and analytical TEM in order to identify the multiphase microstructure. The nominal composition of the magnet NFB without dotation was $Nd_{20}Fe_{73.5}B_{6.5}$. In magnet NFB-Al 0.99 wt.% aluminium was added to the prealloy and in magnet NFB-Al_2O_3 a small amount of Al_2O_3 (1.48 wt.%) was added to the powder before compacting. The coercive field H_{ic} was incresed by dodation from 776 kA/m (NFB) to 1380 ka/m (NFB-Al) and 1400 kA/m (NFB-Al_2O_3), respectively. The magnets were examined in a JEOL 200 CX scanning transmission electron microscope (STEM) fitted with a LaB_6 filament, a high take off-angle energy dispersive X-ray analyzer (EDS) and a GATAN electron energy loss spectrometer (EELS). A beryllium double tilt specimen stage was used to reduce background intensities. All X-ray spectra were analyzed using the quantitative software program for thin samples.

RESULTS

In Nd-Fe-B sintered magnets a nonmagnetic layer phase between the hardmagnetic Φ-grains is desirable in order to increase the expansion field of reversed domains and to decrease the coupling field between neighbouring grains originated by magnetic stray fields. Individual large, softmagnetic phases in the form of precipitates or inclusions, such as α-Fe or Fe-rich phases, extremely deteriorate the intrinsic coercive field and have to be avoided [7,8]. In principle, small softmagnetic precipitates within the Φ-grains

could act as domain wall pinning centres, if the density and size of precipitates were optimized.

Table 1: Phases found in $Nd_2Fe_{14}B$ - based permanent magnets

TYPE	PHASE	MARK	COMPOSITION/ STRUCTURE
(A)	$Nd_2Fe_{14}B$ (grains)	Φ	tetr.
(B)	$Nd_{(1+\varepsilon)}Fe_4B_4$ (grains)	η	tetr.
(C)	Nd-rich (intergranular)	n1	$NdO_?$ - fcc
		n2	$NdO_?$ - hcp
	Nd-platelet (intergranular)	pl	$Nd_8Fe_2B_6O_?$
	Nd-oxide (precipitate)	no	Nd_2O_3 - hex
(D)	Fe-rich	fn	$Fe_2NdB_?O_?$
	Fe-rich (Fe-Nd-Oxide)	fo	Fe/Nd≈4
	dopant-enriched (intergranular)	al	$Nd(Fe,Al)_2$
	dopant-enriched (precipitate)	nb1	$NbFe_2$
		nb2	NbFeB
		zr1-3	
		mo1	Mo_2FeB_2
(E)	α-Fe	f	bcc
(F)	"impurity" Nd-Cl phases	i1	
	"impurity" Nd-P-S phases	i2	

In fact, no sintered Nd2Fe14B-based magnets with effective domain wall pinning were reported so far.

We have extensively studied the microstructure of sintered Nd-Fe-B magnets and our investigations revealed at least five different types of phases in addition to the hardmagnetic Φ-phase (see Table 1) [7]. Several Nd-rich phases with different Nd/Fe ratios are found preferentially as intergranular phases at grain boundary junctions and extending to grain boundaries [9]. Previous TEM studies showed [7,10,11] that two types of grain boundaries occur in Nd-Fe-B sintermagnets: grain boundaries (GB1) without any intergranular phases and grain boundaries (GB2) composed of nonmagnetic Nd-rich phases. The electron micrograph of Fig. 1 shows a typical microstructure of the intersection of three hardmagnetic Φ-grains found in Nd-Fe-B:Al sintered magnet by TEM. The triple grain boundary junction is filled with a Nd-rich phase (n1). Two types of Nd-rich intergranular phases with minor Fe-content are found. The phase (n1) with a high dislocation density (Figs.1 and 2a) exhibits a fcc crystal structure with a=0.52 nm [12], whereas phase (n2) exhibits a hcp crystal structure with a=0.39 nm and c=0.61 nm which was determined by electron diffraction [6]. Within the interior of the (n2) phase only individual dislocations are visible (Fig.2). Analytical TEM investigations reveal a remarkable difference of the X-ray spectra (Fig.2b and 2c). With decreasing Fe content (< 5 at.%) the Nd-rich phase changes from the fcc (n1) to the hcp (n2) crystal structure.

Al_2O_3-doped magnets contain an increased amount of the (n2) phase.



Fig.1: Electron micrograph showing the grainboundary intersection of three Φ-grains filled by the (n1)-phase.

Our TEM investigations occasionally revealed Nd-rich intergranular phases with a higher iron content than the (n1)-phase and an unknown crystal structure [7,9] and also a platelet shaped phase (p1) with an approximate composition of $Nd_5Fe_2B_6O_7$ embedded in the (n1)-phase (Fig.2a) [6]. Polycrystalline, spherical Nd_2O_3-inclusions with diameters up to 500 nm are always present within the hardmagnetic Φ-grains as well as embedded in the intergranular phase [6,7,9].

If dopants are added to the prealloy or before sintering (in the form of oxides) in order to increase the coercive field, the microstructure is affected in a threefold way:

(1) the dopant is dissolved in the hardmagnetic Φ-phase (changing the magnetocrystalline anisotropy ?)

(2) precipitation within Φ-grains: Nb, Zr, Mo .... (possibly domain wall pinning?)

(3) formation of new intergranular phases: Al, Nb, Mo .... (influences wettability and therefore magnetic coupling of grains)

The dopant element is always found to replace the Fe-sites in the hardmagentic Φ-grains. Energy dispersive X-ray microanalysis shows an additional AlKα-peak in the X-ray spectrum of the Φ-phase (Fig.3a). A low solubility of the

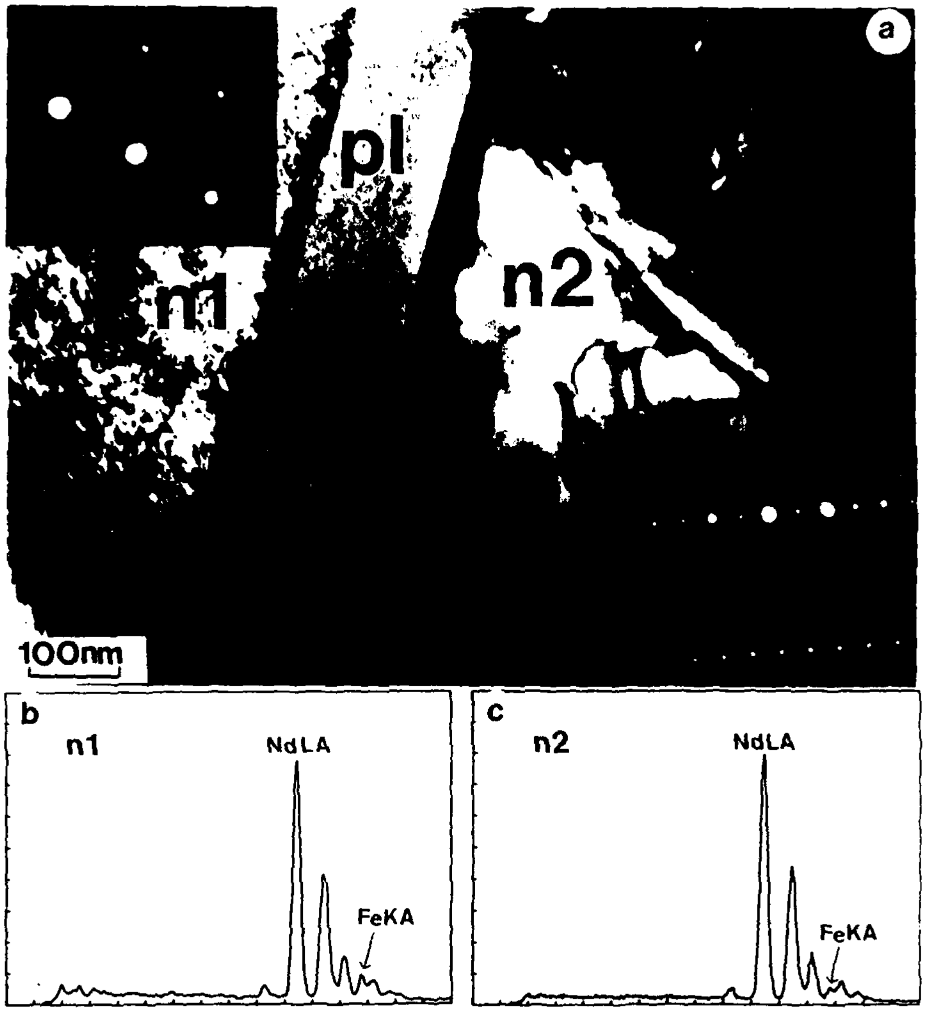


Fig.2: Different Nd-rich phases occur within the intergranular region between Φ-grains.

dopant element at sintering temperature leads to the formation of precipitates enriched by the dopant, such as in the case of Nb, Mo and Zr [13-15]. In Al-doped sintermagnets no such precipitation has been found. Parker et al.[13] reported on Nb-precipitation within the Φ-grains in Nb-doped (Nd,Dy)-Fe-B magnets. Two types of precipitates have been identified: the Laves phase type $NbFe_2$ having a $MgZn_2$ structure (a=4.82 nm and c=7.87 nm) and the FeNbB-phase. Zirconium additions result in three different, partly coherent Zr-rich or Zr-containing

precipitates within the Φ-grains [14]. A similar precipitation behaviour was reported in Mo-doped Nd-(Fe,Co)-B magnets [15].

Dopants also form new intergranular phases and influence the wetting of the liquid phase and the smoothness of the surface of the Φ-grains during sintering and therefore affect the coercivity [6,16]. The coercivity of Nd-Fe-B sintered magnets is increased by adding small amouts of Al or Al_2O_3. Our study of such doped materials revealed a high amount of an Al-containing phase (al). From X-ray micro-analysis (Fig.3b) we determined the composition of this phase

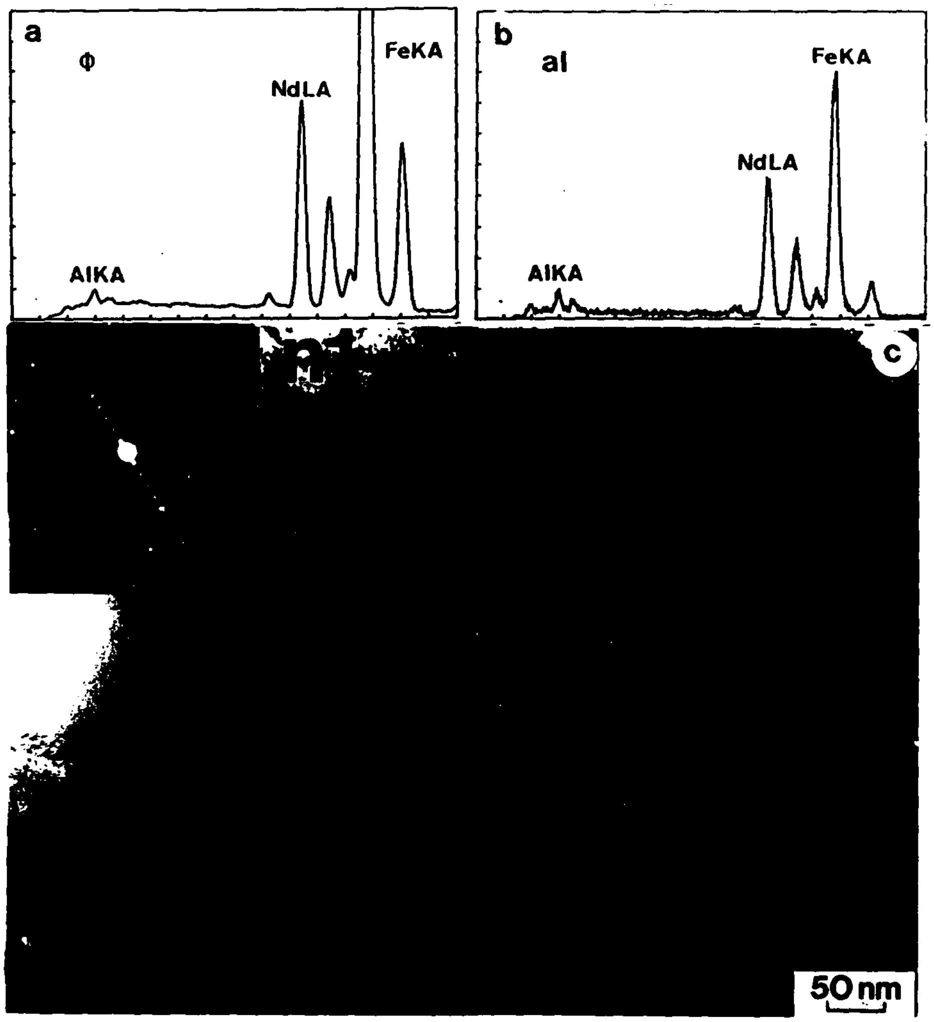


Fig.3: Electron micrograph and X-ray spectra of an Al-doped sintered magnet showing the occurance of a Nd(Fe,Al)2-phase (al) within the intergranular region between Φ-grains.

as $Nd(Fe,Al)_2$, which is in accordance with Grieb et al.[17], who detected this phase as stable phase in the ternary system Fe-Al-Nd. The high resolution electron micrograph of Fig.3c shows such an (al)-phase embedded between Φ-grains and (n1)-phases.The crystal structure and the crystal lattice parameters of this Al-containing phase are unknown at present. From the lattice fringe image of this phase a crystal lattice periodicity of about 1.2-1.4 nm was determined. It should be mentioned that our investigations never revealed any Al-enrichment of the Nd-rich phases (n1), (n2) and (p1) [6]. Figure 2b and 2c show the X-ray spectra of phases (n1) and (n2) of a Nd-Fe-B:Al sintered magnet. This result is in contrast with previously reported data, which showed a partial enrichment of Al in the Nd-rich intergranular phase [16,18].

Other Fe-rich phases and α-Fe precipitates within the $Nd_2Fe_{14}B$- grains as well as in Nd-rich intergranular regions were found in several magnets with decreased coercivity [7,9]. Such phases are probably byproducts of an oxidation process [19,20].

DISCUSSION

Sintering of Nd-Fe-B magnets is primary determined by the liquid phase type of sintering mechanism which involves the presence of a low melting, viscous Nd-rich eutectoid [21-23]. During sintering the driving force for densification of Nd-Fe-B magnets is the capillary pressure and the surface tension. Both, surface diffusion along grain boundaries and volume diffusion play also an important role during densification. Liquid phase sintering occurs most readily when the liquid thoroughly wets the solid particles at the sintering temperature. The liquid in the narrow channels between the particles results in substantial capillary pressure. The particle size, sintering temperature and time, the uniformity of particle packing, the particle shape and the particle size distribution are extremely important parameters. Fine particle size powder can be sintered more rapidly and at lower temperature than coarser powder. If particle packing is not uniform in the pressed "green" compact, it will be difficult to avoid porosity during sintering. Smaller particles exhibit a higher driving force for densification (higher capillary pressure and higher surface energy) than coarser particles. The rate of liquid phase sintering is strongly affected by the sintering temperature. A small increase in temperature results in a substantial increase in the amount of liquid present, but on the other hand this causes excessive grain growth, which deteriorates the magnetic hardness [24].

Densification during the liquid phase sintering process depends on two important parameters, the contact (wetting) angle and the dihedral angle. Generally, better liquid phase sintering is associated with smaller values of both angles [24]. The wetting angle is a characteristic parameter which describes the balance between the interfacial energies of liquid, solid and vapor phases. Knoch et al.[25] showed that the wetting angle is in the order of $< 8°$ and

decreased with increasing Al-content of the magnet. In order to get a high amount of intergranular phases good wetting between intergranular and Φ-phases is favourable. The dihedral angle is formed where a solid-solid grainboundary intersects the liquid and is important to the microstructure of polycrystalline grains and to the contact of Φ-grains in the liquid phase. In first approximation the dihedral angle is estimated from the two-dimensional section of the three phase junction (Fig.1) to be in the order of 20° at one corner. A high dihedral angle between the Φ-grains during the liquid phase sintering process retains the liquid phase from penetration into the grain boundaries. For a dihedral angle over 60° the liquid becomes isolated at the triple points between grains and forms a continuous network along the three grain junctions [24]. From our investigations we conclude that the constitution of the intergranular region is inhomogeneous and consists of several phases with different composition. This is in good agreement with our analytical TEM investigations with two types of grain boundaries (GB1) and (GB2) in a two dimensional section [11]. Depending on the cooling rate and post-sintering heat treatments various Nd-rich phases (n) occur in the magnet. The formation of new intergranular phases positively influence the coercivity, because the contact angle and the dihedral angle are decreased leading to a higher voulume fraction of intergranular phases, which separate the hardmagnetic Φ-grains [25]. In $Nd_2Fe_{14}B$ sintermagnets both Nd-rich phases, the one with fcc (n1) and the one with hcp (n2) crystal structure have been identified, so far [12,26-28]. The metastable (n1) phase is probably stabilized by additional elements. Our EELS investigations show an oxygen pick-up of this phase which is in accordance with Auger electron spectroscopic results of in situ fractured surfaces and EDS X-ray micronalytic results taken with an ultrathin window detector [29]. Our systematic investigations show that besides oxygen also a small amount of Fe must be considered as stabilizing factor. With decreasing Fe content (< 5 at.%) the Nd-rich phase changes from the fcc to the hcp crystal structure.

The increase of the coercive field of the doped magnets $Nd_2Fe_{14}B:(Al;Al_2O_3)$ is attributed to the presence of $Nd(Fe,Al)_2$ and hcp Nd-rich phases, because no change of the morphology and microstructure of the fcc Nd-rich phase (n1) is observed (no Al content). For the explanation of the increased coercivity two effects are essential: First, there is a better ***wettability*** of these phases compared to the fcc Nd-rich phase, thus the volume fraction of grain boundaries containing an intergranular phase is increased, which leads to a an increased magnetic decoupling Φ-grains. Second, the ***smoothness*** of the surface of the hardmagnetic Φ-grains during the liquid phase sintering process is influenced. A similar effect was found in Dy_2O_3-doped sintered magnets [30].

In conclusion our TEM analysis performed indicates that the increase of the coercive field of doped $Nd_2Fe_{14}B$-based sintered magnets, in particular of Al-doped magnets, has to be attributed to the change of the constitution and the wettability by the intergranular phases. Coercivity is increased by a higher contiguity of the

intergranular region (decoupling of hardmagnetic grains) and by suppression of nucleation sites for reversed domains (surface hardening of hardmagnetic grains).

Acknowledgments

The authors are grateful to Prof. H. Kronmüller and Dr. E.-Th. Henig for many helpful discussions. One of the authors (J.Fidler) acknowledges the partial financial support of this work by the Austrian Nationalbank (No. 3065), the Austrian Forschungsfonds FWF (P6935P), the US Army European Research Office, London, UK, under contract No. DAJA-86-C-0010 and the "Hochschuljubiläumsstiftung" of the city of Vienna.

References

1. H. Kronmüller, K.D. Durst and M. Sagawa, J. Magn. Magn. Mat., 74 (1988) p.291.
2. D. Givord, E-MRS Fall Meeting, Nov. 1988, Strasbourg, France, J. Magn. Magn. Mat., in press.
3. W. Rodewald and W. Fernengel, IEEE Trans.Magn., MAG-24 (1988) p.1638.
4. S. Hock and H. Kronmüller, Proc. on 5th Int. Symp. on Magn. Anisotropy and Coercivity in RE-Transition Metal Alloys, eds. C. Herget, H. Kronmüller and R. Poerschke, Bad Soden, FRG, Vol.2 (1987) p. 275.
5. G. Schneider , Thesis Univ. Stuttgart, FRG, 1988.
6. J. Fidler, K.G. Knoch, H. Kronmüller and G. Schneider, J. Mat. Res. in press.
7. J. Fidler, Proc. on 5th Int. Symp. on Magn. Anisotropy and Coercivity in RE-Transition Metal Alloys, eds. C. Herget, H. Kronmüller and R. Poerschke, Bad Soden, FRG, Vol.2 (1987) p. 363.
8. J.Fidler and Y. Tawara, IEEE Trans. Magn., MAG-24 (1988) p.1951.
9. J. Fidler, IEEE Trans.Magn., MAG-23 (1987) p.2106.
10. J. Fidler and P. Skalicky, Mikrochimica Acta [Wien] I, (1987) p.115.
11. J. Fidler and K.G. Knoch, E-MRS Fall Meeting, Nov. 1988, Strasbourg, France, J. Magn. Magn. Mat., in press.
12. M.Sagawa, S. Fujimura, H. Yamamoto, Y. Matsuura and K. Hiraga, IEEE Trans.Magn., MAG-20 (1984) p.1584.
13. S.H.F. Parker, P. Grundy and J. Fidler, J.Magn.Magn.Mat., 66 (1987) p.74.
14. R.J. Pollard, P.J. Grundy, S.F.H. Parker and D.G. Lord, IEEE Trans.Magn., MAG-24 (1988) p.1626.
15. W. Rodewald and P. Schrey, IEEE Trans.Magn. in press (Proc. Intermag 89).
16. P. Schrey, IEEE Trans.Magn., MAG-22 (1986) p.913 .
17. B. Grieb, K.G. Knoch, E.-Th. Henig and G. Petzow, E-MRS Fall Meeting, Nov. 1988, Strasbourg, France, J. Magn. Magn. Mat., in press.
18. J.K. Chen and G. Thomas, Mat. Res. Soc. Symp. Proc., Vol.96 (1987) p.221.
19. D. Cochet-Muchy and S. Paidassi, Proc. of ICM Conference, Paris, France (1988), J. Magn. Magn. Mat. in press.
20. J. Jacobson and K. Kim, J. Appl. Phys., 61 (1987) p.3763.

21. Y. Matsuura, S. Hirosawa, H. Yamamoto, S. Fujimura, M. Sagawa and K. Osamura, Jap. J. Appl. Phys., 24 (1985) p.L635.
22. G. Schneider, E.-Th. Henig, H.H. Stadelmaier and G. Petzow, Proc. on 5th Int. Symp. on Magn. Anisotropy and Coercivity in RE-Transition Metal Alloys, eds. C. Herget, H. Kronmüller and R. Poerschke, Bad Soden, FRG, Vol.2 (1987) p. 347.
23. D.S. Tsai, T.S. Chin, S.E. Hsu and M.P. Hung, IEEE Trans. Magn., MAG-23 (1987) p.3607.
24. R.M. German, "Liquid phase sintering", Plenum Press, 1985.
25. K.G. Knoch, G. Schneider, J. Fidler, E.-Th. Henig and H. Kronmüller, Proc. of Intermag 89, Washington, 1989, IEEE Trans.Magn., in press.
26. J. Fidler, and L. Yang, Proc. IV. Int. Symposium on magnetic Anisotropy and Coercivity in Rare Earth-Transition Metal Alloys, edited by K.J.Strnat (University of Dayton), Dayton, Ohio, USA, 1985, p.647.
27. G.C. Hadjipanayis, Y.F. Tao, and K.R. Lawless, IEEE Trans.Magn., MAG-22 (1986) p.1845.
28. Tang Weizhong, Zhou Shouzeng, Wang Run, J. Less-Common Met., 141 (1988) p.217.
29. R. Ramesh, J.K. Chen, and G. Thomas, J.Appl.Phys., 61 (1987) p.2993 .
30. M.H. Ghandehari and J. Fidler, Mat. Letters, 5 (1987) p.285.

IEEE Trans Mag, submitted

Al-DOPED Nd-Fe-B PERMANENT MAGNETS: WETTING AND MICROSTRUCTURAL INVESTIGATIONS

32

K.G. Knoch*, G. Schneider*, J. Fidler**, E.-Th. Henig*, H. Kronmüller*

*Max-Planck-Institut für Metallforschung, Heisenbergstr. 5, D-7000 Stuttgart 80

**Institut für Angewandte Physik, T.U. Wien, Wiedener Hauptstr. 8-10, A-1040 Wien

Abstract: The coercivity of Nd-Fe-B sintered magnets has been improved by Al additions. To study the microstructural effect of Al addition two types of investigation were performed: 1. The change in the wetting behaviour of the liquid phase, at the sintering temperature, was studied by measurements of the wetting angle. 2. The microstructural changes resulting from Al additions have been studied by TEM assisted by EDX and EELS. A systematic change was detected depending on the kind of Al addition, either metallic or as Al_2O_3.

Introduction

The outstanding magnetic properties of Nd-Fe-B permanent magnets are well known since their first development by Croat[1] and Sagawa[2]. Nevertheless the strong decrease in coercivity, H_{cJ}, with increasing temperature combined with the low Curie temperature, T_c (T_c=308°C), still makes these magnets inapplicable above 150°C. There have been several attempts to improve these properties by addition of different elements[3,4]. The most favourable elements are cobalt (Co) and aluminium (Al). The former increases T_c up to about 700°C[5] whereas the latter increases H_{cJ} by up to 60%[6]. In this paper our interest is focused on the Al additions and its influence on the microstructure. Since Al deteriorates the intrinsic magnetic properties of the hardmagnetic Φ phase ($Nd_2Fe_{14}B$)[3,7], the increase in H_{cJ} in these magnets is believed to result from Al-induced microstructural changes. Two microstructural changes are to be distinguished: morphological changes and the appearance of new phases. Common methods to investigate the microstructure are optical microscopy and transmission electron microscopy (TEM) assisted by energy dispersive X-ray analysis (EDX) and electron energy loss spectroscopy (EELS) which are reported here. Also reported here is about the influence of additives on the morphology which can be drawn from the wetting behaviour when correlated with the contiguity.

Wetting Behaviour

Experimental: The wettability was investigated in a special device where melting of the sample on a substrate was observed in situ. A sequence of photographically recorded silhouettes, either as a function of temperature, the amount of additives or as a function of time at a fixed temperature were evaluated. The substrate was a small disc of polycrystalline Φ phase (10 mm diameter and 0.5 mm thickness) which was ground and polished. The sample was a cube of about 2 x 2 x 2 mm^3 with the composition Nd45-Fe(48-x)-Alx-B7 (x = 0; 3; 5; 10). This is the approximate composition of the liquid at the sintering temperature. Substrate and sample were as free from oxides as possible.

Model and Discussion: For this study, contiguity refers to the contact area of adjacent grains of the same phase. This means the lower the contiguity the more grain boundaries are filled with nonmagnetic Nd-rich phase. Assuming that a third gaseous phase does not drastically alter the behaviour of the liquid, wetting is used as a model describing the contact behaviour of the liquid during sintering. The wetting angle Θ is defined in Fig.1 and is determined by the interface energies γ_{ss}, γ_{sl} and γ_{sv} (s=solid, l=liquid, v=vapour). The gaseous phase is given by the ambient atmosphere. The experiments were carried out in an Ar atmosphere of 840 hPa, the vapour pressure of the metals in the temperature range of measurement can be neglected. At the temperature of most interest (sintering temperature T_s=1050°C) Θ remained essentially constant for t ≥ 20 min, which defines the equilibrium wetting angle. Fig.2 shows the dependence of Θ on the Al content. For Al contents less than 5 at.%, Θ is reduced slightly while for Al contents in excess of 5 at.% the decrease is drastic. These measurements suggest that Al doping considerably reduces the number of Φ-Φ grain

contacts. The resulting microstructure approaches an ideal microstructure where all Φ grains are embedded in an Nd-rich phase.

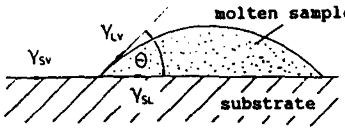


Fig.1 Definition of the wetting angle θ.

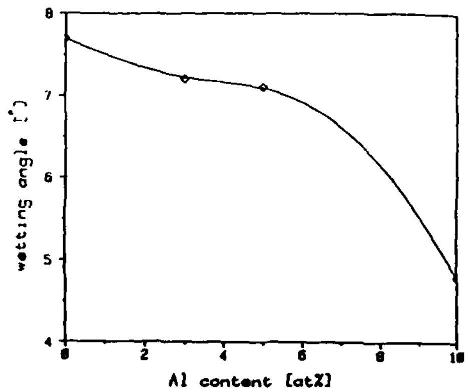


Fig.2 Wetting angle θ vs. Al content at 1050°C of the Nd-Fe-B-Al system.

Microstructural Investigations

Experimental Procedure: Three different sintered magnets of compositions Nd20-Fe71.5-B6.5 (NFB), Nd20-Fe71-B6.5-Al2.5 (NFB-Al) and Nd20-Fe71.2-B6.5-Al2.3 ($NFB-Al_2O_3$, Al_2O_3-doped) were investigated. They were all prepared by the conventional powder metallurgical process, sintered at 1050°C for 1 h and annealed at 600°C for 1 h. For TEM observations the samples were ground, polished, dimpled and ion-thinned. Metallographic studies were also performed in the polished state . The TEM observations were executed using JEM 200CX with EDX- and EELS-facilities.

Results and Discussion: A systematic study of the dependence of the microstructure on the kind and/or concentration of Al addition has not yet been completed. The ingot compositions studied yielded "two-phase" magnets[6]. The microstructure was comprised of the hard magnetic phase Φ and the Nd-rich phase; no B-rich phase η ($Nd_{1+\epsilon}Fe_4B_4$) was found, independant of whether Al was added or not. Table I gives the H_{cJ} values of the different samples. By optical microscopy, it was found that NFB mainly consists of the three phases: Φ, a Nd-rich phase (n1) and a platelet shaped phase (p1). The composition of the phases[8] (considering only elements with atomic number Z≥11 by the EDS) shows that n1 (fcc, a=0.52 nm) consists of ≈ 93 at.% Nd and 7 at.% Fe.

Table I: H_{cJ} of the samples

magnet	NFB	NFB-Al	$NFB-Al_2O_3$
H_{cJ} [kA/m]	776	1384	1400

The second intergranular phase, p1, contains ≈ 67 at.% Nd and 33 at.% Fe independent of the kind of Al addition. The crystal structure has not yet been determined. Fig.3 shows a micrograph of NFB containing all three phases. The platelets are about 0.1 μm thick and (1-5)μm long. Recent EELS results[9] show a considerable amount of B so that an overall composition of about $Nd_{37}Fe_{15}B_{48}$ can be estimated which matches with the T_3 phase reported by Matsuura[10] and Chaban[11], giving a composition of about Nd_2FeB_3. Related magnetic measurements remain somewhat ambiguous. The composition of the n1 phase does not change in the Al-doped magnets. This is contrary to Schrey[12]. With the addition of Al at least one additional phase appears. Unrelated to the kind of Al addition an Al containing phase, a1, occurs. A lattice periodicity of (1.2-1.4)nm was determined from lattice fringe image (Fig.4) and further crystallographic experiments are yet to be conducted. The composition is given by EDX as $Nd(Fe,Al)_2$ in accordance with Grieb[13] showing the existence of a stable phase $Nd(Fe,Al)_2$ in the Nd-Fe-Al system. Another most interesting result of these studies is the effect of Al_2O_3 addition leading to the occurrence of a second Nd-rich phase n2 which is extremely Fe-poor and much less faulted than n1 (Fig.5). EDX results give an Fe content down to 1.5 at.% (Table II). The crystal structure, determined by electron diffraction patterns, was found to be hcp with a=0.39nm, c=0.61nm[14]. Therefore the addition of oxygen by Al_2O_3 seems to stabilize a second Nd-rich phase. Whether the phases contain oxygen or

are stabalized by it, remains unknown because EELS results indicate that the samples inside the TEM are tarnished so much that the real oxygen content of the phases must be hidden under the oxide peak.

Conclusions

The wettability of Φ is enhanced by Al addition. TEM observations reveal that enhancement of H_{cJ} by Al addition is combined with the appearance of a new phase. The mechanism by which these phases could enhance H_{cJ} is still under discussion as well as the correlation with better wettability.



Fig.3 TEM micrograph of NFB shows the phases Φ, n1 (Nd-rich) and p1 (platelet shaped).

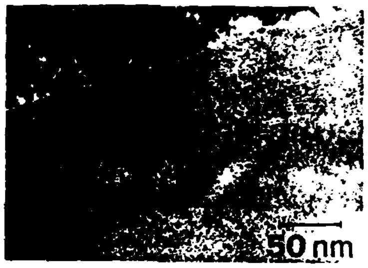


Fig.4 a1 phase in NFB-Al embedded in n1. Lattice fringes give a periodicity of (1.2-1.4)nm.

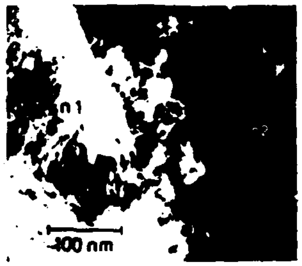


Fig.5 Both types of Nd-rich phases in NFB-Al_2O_3 are shown. The different defect densities are evident.

Table II: Approximate average composition of occurring phases determined by EDX (elements with Z < 11 (Na) not considered).

magnet	Φ	n1(fcc)	n2(hcp)	p1	a1
NFB					
Nd[at.%]	13.6	94.5-95.9	-	73.7	-
Fe[at.%]	86.4	4.1- 5.5	-	26.3	-
NFB-Al					
Nd[at.%]	12.8-13.9	90.4-93.2	-	64.9	29.5-39.5
Fe[at.%]	83.7-84.0	6.8- 9.6	-	35.1	51.9-63.6
Al[at.%]	1.6- 2.6	-	-	-	5.2-7.9
NFB-Al_2O_3					
Nd[at.%]	13.1-13.6	90.3-94.8	95.5-98.5	67.2-67.6	31.0-31.5
Fe[at.%]	84.3-84.4	5.2- 9.7	1.5- 4.5	32.4-32.8	58.1-59.5
Al[at.%]	2.0- 2.6	-	-	-	5.9- 8.5

References:

[1] J.Herbst, J.Croat, F.Pinkerton, W.Yelon, Phys.Rev.B1 29(1984)4176

[2] M.Sagawa, S.Fujimura, N.Tagawa, H.Yamamoto, Y.Matsuura, J.Appl.Phys. 55(1984)2083

[3] C.Abache, H.Oesterreicher, J.Appl.Phys. 60 (1986)3,1114

[4] M.Zhang, D.Ma, X.Jiang, S.Liu, Proc. 8th Int. Workshop on Rare-Earth Magnets and Their Applications, Dayton (USA) 1985,541

[5] E.Burzo, A.T.Pedziwiatr, W.E.Wallace, Sol. State Com. 61(1987)1,57

[6] G.Schneider, Thesis 1988, Universitat Stuttgart

[7] S.Hock, H.Kronmuller, Proc. 5th Int. Symp. on Magnetic Anisotropy and Coercivity in Rare Earth-Transition Metal Alloys, Bad Soden (FRG) 1987, 275

[8] J.Fidler, K.G.Knoch, H.Kronmüller, G.Schneider, J.Mat.Res. to be published

[9] K.G.Knoch, J.Fidler, E.Bischoff, E.-Th. Henig, Mat.Lett. to be submitted

[10] Y.Matsuura, S.Hirosawa, H.Yamamoto, S.Fujimura, M.Sagawa, K. Osamura, Jap.J. Appl.Phys. 24(1985)8,L635

[11] N.F.Chaban, Y.B.Kuz'ma, N.S.Bilonizhko, O.O.Kachmar, N.F.Petriv, Fiz.-Mat.Tekh. Nauki 10(1979)875

[12] P.Schrey, IEEE Trans.Mag. MAG-22(1986)913

[13] B.Grieb, K.G.Knoch, E.Th.Henig, G.Petzow, E-MRS Fall Meeting Nov.88 Strasbourg (France), JMMM to be published

[14] J.Fidler, K.G.Knoch, JMMM to be published

submitted to Materials Letters

33

Analytical TEM-Study of Cast Nd80-Fe15-B5 Alloys

K.G. Knoch, E. Bischoff, E.-Th. Henig
Max-Planck-Institut für Metallforschung, Heisenbergstr. 5, D-7000 Stuttgart 80
J. Fidler
Technische Universität Wien, Wiedner Hauptstr. 8-10, A-1040 Wien

Controversial results on the microstructure of cast Nd80-Fe15-B5 alloys have been reported. Our investigations revealed a microstructure consisting of three phases: the hardmagnetic Φ phase, the platelet shaped boride phase (ρ) $Nd_5Fe_2B_6$, identical with the one found in Nd20-Fe73.5-B6.5 sintermagnets which is embedded within the fcc-Nd phase. A new phase with a Nd:Fe ratio of 1:1.1 was found.

1. Introduction

TEM studies provide varied information about the different phases occurring in the microstructure of Nd-Fe-B permanent magnets. The most important items to know are their composition and morphology. In sintered magnets, besides the hardmagnetic Φ phase ($Nd_2Fe_{14}B$) and the nonmagnetic Nd-rich phase, other phases appear, depending on the ingot composition. In case of Nd20-Fe73.5-B6.5 the amount of η phase ($Nd_{1.1}Fe_4B_4$) is reduced so drastically that its influence on the magnetic properties can be neglected. However, a platelet shaped phase (pl) is observed which has not been reported before. First results revealed an Nd:Fe

ratio of 2.5:1 [1,2,3]. Further investigations have been performed on an as-cast Nd80-Fe15-B5 sample using EDX (energy dispersive X-ray analysis) and EELS (electron energy loss spectroscopy), preliminary results were given by Schneider et al. [4]. Our results, obtained by SEM-EDX (scanning electron microscopy), TEM-EDX and EELS confirm Schneider's et al. [5] recent interpretation of the microstructure.

2. Experimental

The cast sample was prepared from 99.8% pure iron, 99.9% pure neodymium and a ferro-boron master alloy in an arc furnace. It was remelted several times to assure homogeneity.

For the TEM investigations, thin slabs were produced by spark cutting, ground and polished to a thickness of about 100 μm and finally ion-thinned. The microstructure was observed by optical metallography. The TEM investigations were performed using a JEM 200CX (STEM) with an EDX spectrometer and an electron energy loss spectrometer (EELS). To reduce the background noise a beryllium double tilt specimen stage was used. The energy spectra were analysed by a Tracor Northern computer system.

3. Results and Discussion

In the optical micrograph of as-cast Nd80-Fe15-B5 three phases can be seen (fig.1): a matrix phase (dark), a platelet shaped phase and a eutectic phase. The existence of just three phases is confirmed by TEM observations as shown

in fig.2. The Nd:Fe ratios were determined by EDX, fig.3a to c show the spectra of the three detected phases and the concentration analysis is given in table 1. The three phases are:

- The heavily faulted matrix phase is composed of Nd merely, no Fe at all was detected (fig.3a).
- The platelet shaped phase pl, which has been of most interest because it was supposed to be the platelet shaped phase pl(NFB) [1,2,3] of pure and Al-doped Nd-Fe-B sintered magnets. The investigations reported here revealed the identity of these phases; both the striped contrast in the TEM micrograph (fig.2) and the ratio Nd:Fe = 2.5:1 are the same as observed in the magnets. An EDX spectrum of this pl phase in the as-cast sample of this investigtion is shown in fig.3b.
- The eutectic phase (mi) shows a fine grained structure observed by TEM (fig.2). The EDS (fig.3c) gives a ratio Nd:Fe = 1:1.1, which can not be related to any known phase.

To obtain information about the B distribution and the influence of oxygen EELS was performed. Figures 4a to c give the typical electron energy loss spectra of the described three phases. Concerning the B content, the pl phase was determined to be the only B-containing phase with a ratio Nd:B ≈ 1:1.2 to 1.3, a composition which was calculated by EDS and EELS analysis to correspond to $Nd_5Fe_2B_6$ [6] or Nd_2FeB_3 [7]. Figure 5a gives the B concentration scaled to Nd versus the relative thickness t/λ (λ = mean free path of plasmons) of the pl phase. The slight dependence of the B

content on the sample thickness may result from the analysis method. Figure 5b gives the O concentration scaled to Nd versus t/λ of all the three phases, the Nd matrix, the pl phase and the mi phase. However, the oxygen content decreases much more strongly with increasing analysed sample thickness than the B concentration of the pl phase. Bulk oxygen would give a constant Nd:O ratio. So we can conclude that an oxidation process starts at the surface diminishing into the bulk. This oxidation may result from the sample preparation and/or the oxygen of the ambient atmosphere during handling. The oxidized material does not reflect the situation inside the bulk of a magnet which presumably might be studied at the surface of an in situ fractured sample e.g. by AES.

4.Conclusions

Schneider[4] reports of a ferromagnetic phase with the approximate composition $NdFe_4O_x$ in as-cast Nd80-Fe15-B5 which could be contained in permanent magnets. Our studies revealed three phases within this as-cast composition. One of them is pure nonmagnetic Nd, possibly oxidized. The second one could be identified as the pl phase ($Nd_5Fe_2B_6$) of the Nd-Fe-B sintered magnets. There is a third phase unknown hitherto, so it is not possible to attribute the magnetism of the as-cast sample to one phase only. Further investigations are being undertaken.

References:

[1] Fidler J., K.G. Knoch, H. Kronmüller, G. Schneider, J.

Mat. Res., submitted

[2] Fidler J., K.G. Knoch, J.M.M.M., in press

[3] Knoch K.G., G. Schneider, J. Fidler, E.-Th. Henig, H. Kronmüller, IEEE Trans.Mag., submitted

[4] Schneider G., G. Martinek, H.H. Stadelmaier, G.Petzow, Mat.Let. 7(1988)215

[5] Schneider G., F.J.G. Landgraf, F.P. Missell, J.Less-Com.Met., submitted

[6] Mooij D.B. de, K.H.J. Buschow, Philips J.Res. 43(1988)1

[7] Matsuura Y., S. Hirosawa, H. Yamamoto, S. Fujimura, M. Sagawa, K. Osamura, Jap.J.Appl.Phys. 24(1985)L635

202

Table 1: Composition (in at.%) determinded by EDX of the Nd-phase, the pl phase, and the mi phase found in as-cast Nd80-Fe15-B5 and the pl phase in Nd-Fe-B sinter magnets (pl(NFB)) [1,2,3]. (Fe + Nd set to 100%; light elements such as B and O are not considered.)

	Nd	pl	mi	pl(NFB)
Nd[at.%]	100	65.4-75.0	47.6-48.8	68.9-73.7
Fe[at.%]	0	25.0-34.6	52.2-54.4	26.3-31.1

203

Figure Captions:

Fig.1. Optical micrograph of Nd80-Fe15-B5 (as-polished) showing three phases: matrix phase (dark), platelet shaped phase, bright phase

Fig.2. TEM micrograph of Nd80-Fe15-B5 showing the same three phases as Fig.1:

- Nd matrix phase, heavily faulted
- platelet shaped phase pl, striped contrast, Nd:Fe = 2.5:1
- phase mi with fine grained structure, Nd:Fe = 1:1.1

Fig.3. EDX spectra of the Nd matrix phase (a), the platelet shaped pl phase (b) and the mi phase (c)

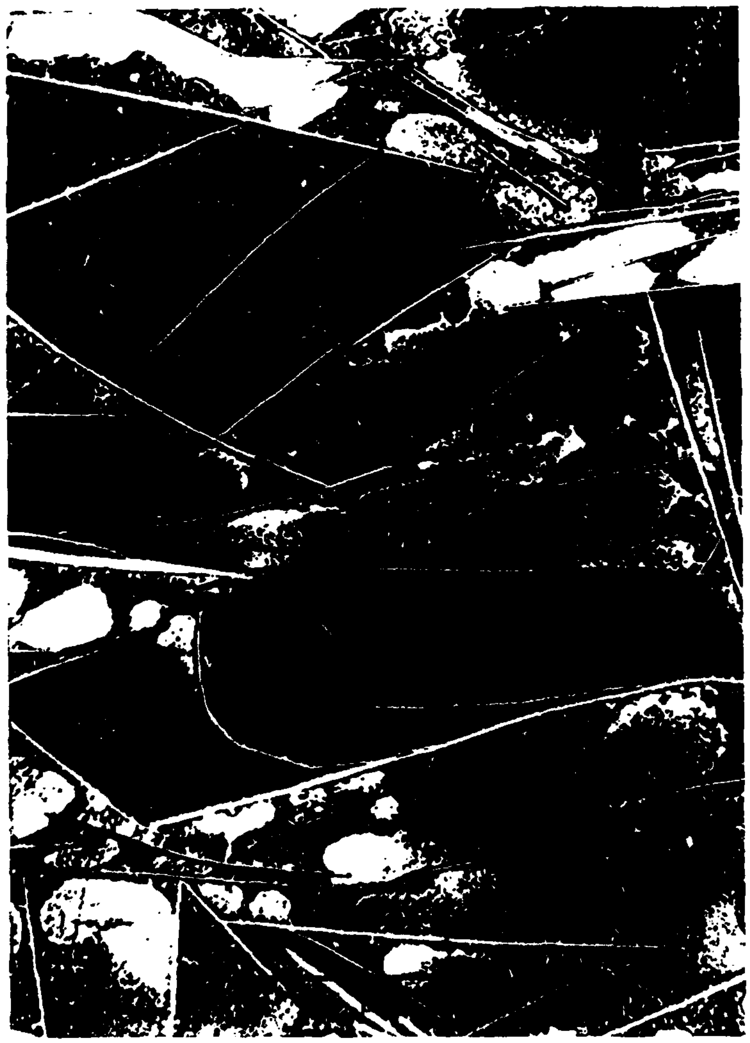
Fig.4. EELS spectra of the Nd phase (a), the pl phase (b) and the mi phase (c).

Fig.5. (a) B concentration of the pl phase vs relative thickness

(b) O concentration of Nd, pl, mi phase vs. relative thickness

The concentrations are scaled to the Nd content, the relative thickness t/λ is scaled to the free mean path plasmons λ.

204

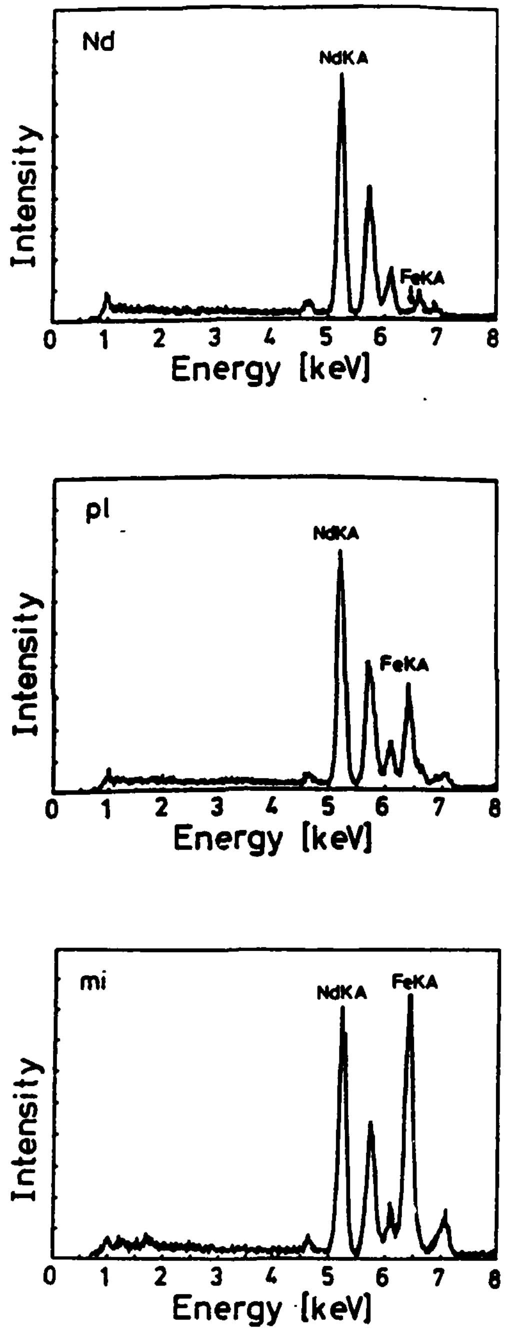


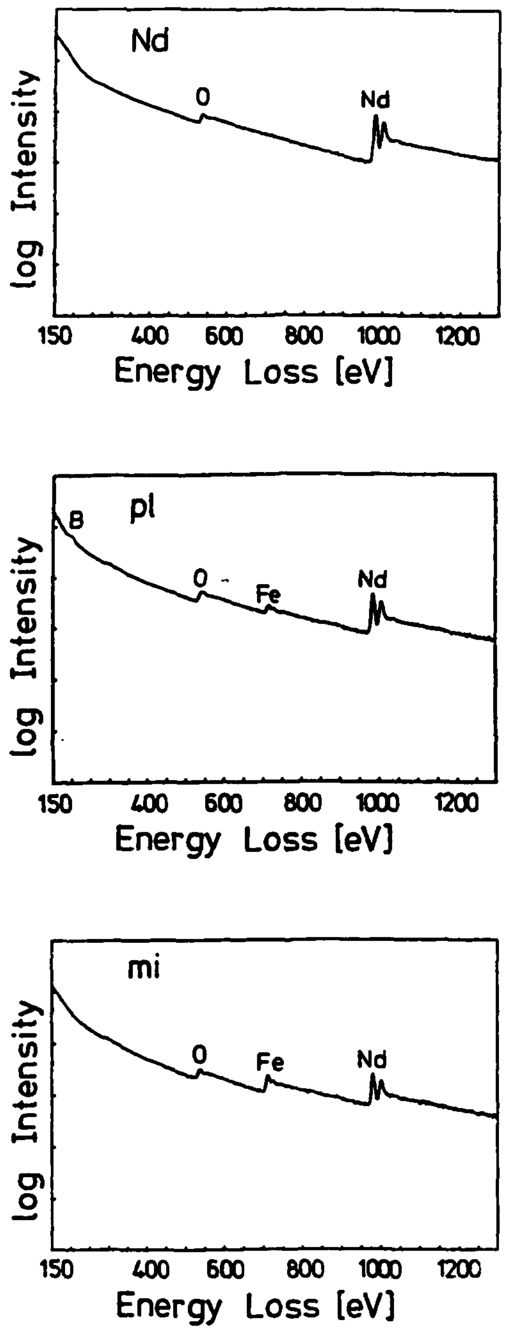

200 nm

a

b

c


Nd
NdKA
FeKA
Intensity
Energy [keV]
pl
NdKA
FeKA
Intensity
Energy [keV]
mi
NdKA
FeKA
Intensity
Energy [keV]



Nd
log Intensity
O
Nd
150
400
600
800
1000
1200
Energy Loss [eV]
pl
B
O
Fe
Nd
log Intensity
150
400
600
800
1000
1200
Energy Loss [eV]
mi
O
Fe
Nd
log Intensity
150
400
600
800
1000
1200
Energy Loss [eV]

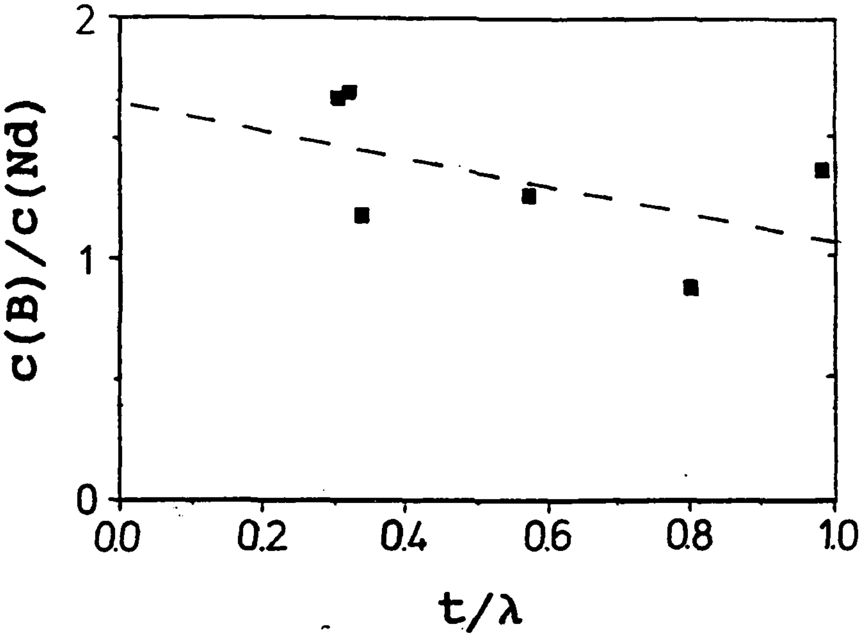
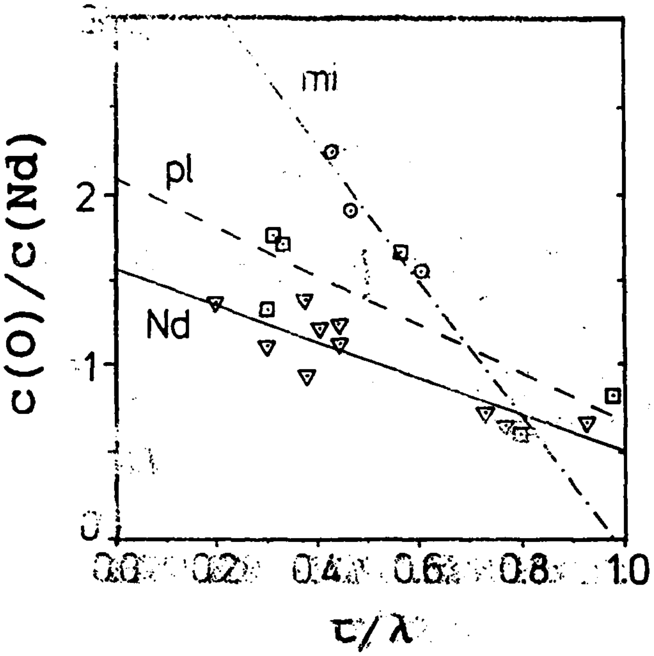


Fig. 5a.


mi
pl
Nd
c(O)/c(Nd)
τ/λ
0
1
2
3
0.0
0.2
0.4
0.6
0.8
1.0